A MULTI-UNIT, POLYMER-BASED, PROLONGED-RELEASE, INTRAUTERINE DEVICE FOR THE RELIEF OF THE GENITOURINARY SYNDROME OF MENOPAUSE

AHMED ABDALLA BAKHEIT ABDELGADER

A thesis submitted to the Faculty of Health Sciences, University of the Witwatersrand, in fulfillment of the requirements for the degree of Doctor of Philosophy

Supervisor:

Professor Yahya E. Choonara

Department of Pharmacy and Pharmacology, Faculty of Health Sciences, University of the Witwatersrand, Johannesburg, South Africa

Co-Supervisors:

Doctor Mershen Govender

Department of Pharmacy and Pharmacology, Faculty of Health Sciences, University of the Witwatersrand, Johannesburg, South Africa

Professor Pradeep Kumar

Department of Pharmacy and Pharmacology, Faculty of Health Sciences, University of the Witwatersrand, Johannesburg, South Africa

Johannesburg

2024

DECLARATION

I, Ahmed Abdalla Bakheit Abdelgader, declare that this thesis is my own work. It is being submitted for the degree of Doctor of Philosophy in the Faculty of Health Sciences, University of the Witwatersrand, Johannesburg. It has not been submitted before for any degree or examination at this or any other University.

……

Signature

This 29 day of August, 2024

DEDICATION

This thesis is dedicated to my inspiration, to my motivation, to my parents,

Abdalla Bakheit and Amnah Elterifi

To my family and friends

RESEARCH OUTPUTS, GRANTS AND FUNDING

A. Publications

1. Ahmed Abdelgader, Mershen Govender, Pradeep Kumar, and Yahya E. Choonara (2023). Intravaginal Drug Delivery Systems to Treat the Genitourinary Syndrome of Menopause: Towards the Design of Safe and Efficacious Estrogen-Loaded Prototypes. Journal of Pharmaceutical Sciences, 112(6), p. 1566-1585. (Abstract in Appendix A1).

2. Ahmed Abdelgader, Mershen Govender, Pradeep Kumar, and Yahya E. Choonara (2024). A Novel Intrauterine Device for the Spatio-Temporal Release of Norethindrone Acetate as a Counter-Estrogenic Intervention in the Genitourinary Syndrome of Menopause. Pharmaceutics, 16(5), 587. (Abstract in Appendix A2).

3. Ahmed Abdelgader, Mershen Govender, Pradeep Kumar, and Yahya E. Choonara (2024). Development and Optimization of a Hormone-loaded Polymer-Based Intrauterine Device as a Cutting-Edge Intervention for the Genitourinary Syndrome of Menopause. To be submitted to Journal of Drug Delivery Science and Technology.

4. Ahmed Abdelgader, Mershen Govender, Pradeep Kumar, and Yahya E. Choonara (2024). Fabrication and *In Vitro* Evaluation of a Novel Estradiol-Loaded Intrauterine-Intravaginal Delivery System: A Promising Approach for the Treatment of the Genitourinary Syndrome of Menopause. To be submitted to International Journal of Pharmaceutics.

B. GRANTS AND FUNDING

1. Postgraduate Merit Award (PMA), University of the Witwatersrand, South Africa, 2021-2023.

2. Clinical Training Grant (CTG), Faculty of Health Sciences, University of the Witwatersrand, South Africa, 2022-2023.

3. Faculty Research Committee Individual Research Grants (FRC), Faculty of Health Sciences, University of the Witwatersrand, South Africa, 2022-2023.

SUMMARY

The genitourinary syndrome of menopause (GSM) is a prevalent condition affecting millions of women globally, with a large number of drug delivery systems currently available for the treatment of this condition.

A critical examination of these contemporary delivery modalities for addressing GSM underscores a recurring issue: therapeutic shortcomings frequently arise due to suboptimal patient adherence to prescribed regimens, a consequence attributed to the inefficacy and unsuitability of delivery systems employed. The current therapeutic strategies for GSM management additionally commonly involve oral or vaginal administration of estrogens, yet these methodologies are also affected by inherent limitations and the associated risk of endometrial hyperplasia.

Thus, in an effort to address these GSM formulation challenges, an implantable, multi-unit, polymer-based, prolonged release platform (MUPP) has been designed, formulated and evaluated for the site-specific delivery of two hormonal drugs in a prolonged release manner, ultimately easing complicated treatment regimens, and improving patient compliance. The MUPP has been designed as two variants, each comprising three units: The first variant is a fully intrauterine device composed of an estradiol hemihydrate (E2) unit and a norethindrone acetate (NETA) unit, while the second variant is an advancement on the first variant and is composed of a NETA-loaded intrauterine unit and a E2-loaded intravaginal unit. These variants have been prepared to ascertain the effect of site-specific delivery of the active ingredients in both the uterine and vaginal cavities. In the fabrication of both variations an additional intrauterine indomethacin (IND)-loaded unit has been included to alleviate the pain and inflammation associated with the administration of intrauterine devices (IUDs).

The MUPP employs a combination of polymer blends to tailor the drug release and weight loss profiles of the individual units. These polymeric blends, which comprises of polycaprolactone (PCL) and ethyl cellulose (EC), were employed to fabricate the E2- and NETA-loaded uterine units, as well as E2-loaded vaginal unit. Meanwhile, the unit loaded with IND employed a polymeric blend of PCL and polyethylene glycol (PEG). The intrauterine units were prepared as hollow cylindrical devices using a simple molding technique, while the intravaginal unit was prepared as a donut-shaped tablet through direct compression. The influence of the drug load and the ratio of each polymer on the key attributes of the intrauterine units were evaluated and thereafter these units were optimized using a design of experiments (DoE) methodology. In addition, the effect of polymer ratio in the polymer blend and the compression force on the E2-loaded intravaginal unit characteristics was studied using a 2^2

factorial design. The incorporation of E2 aims to achieve adequate hormonal levels to effectively manage GSM symptoms, while NETA serves to alleviate the potential adverse effects due to estrogen monotherapy, such as endometrial hyperplasia. Additionally, through addressing the potential challenges associated with intrauterine device usage, pharmacologically effective concentrations of IND were included to enhance the therapeutic profile and potential acceptability of the MUPP.

In both configuration variants, the *in vitro* drug release and weight loss profiles of NETA- and IND-loaded units were assessed in simulated uterine fluid (SUF, pH 7, 37°C), while the E2-loaded unit was assessed in SUF in the first configuration (variant) and in simulated vaginal fluid (SVF, pH 6 and 4.2, 37°C) in the second configuration. The prepared units were noted to erode gradually and released the drugs in a controlled sustained manner. The fabrication processes were also noted to be simple and reproducible. Furthermore, when regarding the critical attributes of the prepared units such as drug release and erosion patterns, it was found that through the selection of optimal formulation variables (employed polymers concentrations) and processing factors such as a compression force (for the intravaginal unit), there was the potential to fabricate a platform capable of sustaining the release of E2 and NETA for an extended period of time (variant one releasing E2 up to 22 weeks and NETA up to 19 weeks, with variant two further increasing the release of E2 up to 140 weeks), while also delivering IND for two weeks to alleviate the initial pain and inflammatory response due to IUD insertion. Furthermore, the implementation of the design of experiments emerges as a significant methodology, enabling the statistical elucidation of crucial experimental factor combinations and interactions that influence the characteristics of the fabricated units of the MUPP. The produced units furthermore exhibited heightened hardness and resistance to indentation. Moreover, the fabricated units demonstrate commendable cytocompatibility, both individually and when integrated as a unified platform.

Overall, the MUPP presents a promising solution to address the challenges of current GSM treatment regimens, potentially revolutionizing drug delivery in the genitourinary tract by providing a versatile platform for the sustained and targeted delivery of multiple drugs in a site-specific manner.

ACKNOWLEDGEMENTS

My utmost gratitude goes to the ALLAH, the author of life who has enabled me and provided the opportunity to embark on this journey of acquisition of knowledge.

My heartfelt appreciations and deepest thanks go to my supervisor, Professor Yahya Choonara, whose guidance and mentorship have been valuable throughout this journey. I am also grateful for the conducive research environment he created, which includes highly equipped advanced laboratories, where I was able to learn various pharmaceutical science techniques. Your dedication to the field is truly inspiring, and I am grateful for your encouragement and support in my growth as a researcher.

I further wish to extend my heartfelt gratitude to my esteemed and amiable co-supervisor, Dr. Mershen Govender, for his critical analysis and input into my research work. His dedication, time, and commitment invested in guiding me and my research are gratefully appreciated. The knowledge and skills he has imparted to me are immeasurable, and without his support, this research would not have been possible.

I would also like to express my heartfelt gratitude to my co-supervisor, Professor Pradeep Kumar for his time and commitment invested in guiding me and my research, the knowledge and skills that you have imparted on to me is immeasurable, without your support this research also would have not been possible.

My deepest gratitude to my parents, Abdalla Bakheit and Amnah Elterifi, for their unwavering love, endless sacrifices, and unwavering support. Your prayers and blessings have shaped me into the person I am today, and I am profoundly grateful for the privilege of having you as my parents. I am determined to continue striving to make you proud.

To my sisters and brothers, I would like to thank you for your constant support and words of encouragement. I am very fortunate to have siblings like you.

I would especially like to thank my lovely Fiancée, Amani Osman for her support and belief in me and for her motivation, laughs and encouragement over the years.

To my uncles, aunties, and cousins in the Abdelgader's and Elterifi's families, for keeping me in your prayers and the constant support you have given me over the years.

To all my colleagues at Wits Advanced Drug Delivery Platform (WADDP) Research Unit for their continuous assistance, support and encouragement and definitely friendship.

I extend my sincere appreciation to all the staff at WADDP for their invaluable support in running the laboratories. Their unwavering assistance, accommodation, and expertise have been indispensable throughout my research endeavors.

The financial assistance of the National Research Foundation (NRF) of South Africa and the University of the Witwatersrand towards this research is hereby acknowledged and greatly appreciated.

Thank you very much,

Ahmed Abdelgader

TABLE OF CONTENTS

TABLE OF CONTENTS

LIST OF FIGURES

LIST OF TABLES

LIST OF ABBREVIATIONS

2D:	Two-Dimensional
3D:	Three-Dimensional
ABS:	Acrylonitrile Butadiene Styrene
ACN:	Acetonitrile
Adjusted-R^2:	Adjusted Coefficient of Correlation
AESC:	Animal Ethics Screening Committee
AIC:	Akaike's Information Criterion
Alg:	Alginate
ANOVA:	Analysis of Variance
API:	Active Pharmaceutical Ingredient
AUC:	Area Under the Curve
CAD:	Computer Aided Design
CCD:	Central Composite Design
C_{max}:	Maximum Plasma Concentration
CO_2:	Carbon Dioxide
DCM:	Dichloromethane
DMEM:	Dulbecco's Modified Eagle Medium
DMSO:	Dimethyl Sulfoxide
DoE:	Design of Experiments
DVDS:	Doughnut-shaped Vaginal Delivery System
E2:	Estradiol Hemihydrate
EC:	Ethyl Cellulose
EPHCD:	Estradiol-loaded Polymer-based Hollow Cylindrical Device
EUVM:	Engineered Uterine-Vaginal Cellular Model
FBS:	Fetal Bovine Serum
FD:	Factorial Design
FDA:	Food and Drug Administration
FDC:	Franz Diffusion Cell

FTIR:	Fourier Transform Infrared
GEL:	Gelatin
GSM:	Genitourinary Syndrome of Menopause
HCL:	Hydrochloric Acid
HPLC:	High Performance Liquid Chromatography
IDDS:	Implantable Drug Delivery System
IUD:	Intrauterine Device
IUS:	Intrauterine Systems
IND:	Indomethacin
IV:	Intravenous
KCl:	Potassium Chloride
MeOH:	Methanol
MSC:	Model Selection Criterion
M_w:	Molecular Weight
MUPP:	Multi-unit Polymer-based Prolonged Release Platform
n:	Sample Size
NaCl:	Sodium Chloride
NaOH:	Sodium Hydroxide
NETA:	Norethindrone Acetate
NIH/3T3:	Mouse Fibroblast Cells
NLPM:	Norethindrone Loaded Polymeric Matrix
PBS:	Phosphate Buffered Saline
PCL:	Polycaprolactone
PDMS:	Polydimethyl Siloxane
PEG:	Poly(Ethylene Glycol)
Ph. Eur.:	The European Pharmacopeia
PLA-CA:	Polylactic Acid-based Custom Architecture
PRESS:	Prediction Error Sum of Squares
PVDF:	Polyvinylidene Fluoride
QoL:	Quality of Life

R^2:	Correlation Coefficient
RMSE:	Square Root Mean Squared Error
rpm:	Revolutions per Minute
RSD:	Relative Standard Deviation
RSM:	Response Surface Methodology
SD:	Standard Deviation
SEM:	Scanning Electron Microscopy
Sqrt:	Square Root
STL:	Stereolithography
SVF:	Simulated Vaginal Fluid
SUF:	Simulated Uterine Fluid
UV:	Ultraviolet-Visible
WRAF:	Wits Research Animal Facility
XRD:	X-Ray Diffraction

LIST OF EQUATIONS

CHAPTER 1

1 Introduction

1.1 Background to this study

Menopause is the physiologic shift that occurs in women when menstruation ceases (Hill et al. 2016, Kaur et al. 2019), with the average age of onset of menopause being approximately 51.4±3.8 years (Kaur et al. 2019). Several women undergo menopause asymptomatically, while many experience genitourinary and vasomotor symptoms. Statistics show that nearly 70% of women suffer from hot flashes during menopause, with obese women, those with a lower economic status, smokers and those of African origin being at greater risk (Hill et al. 2016). The genitourinary syndrome of menopause (GSM), on the other hand, depicts the wide range genitourinary changes that occur during menopause and affects millions of women worldwide (Angelou et al. 2020, Gandhi et al. 2016, Hill et al. 2016, Palacios et al. 2015). These changes, which are due to the decreased level of estrogen, includes anatomical and physiological effects such as decreased blood flow, less elasticity, thinning of the vaginal tissue, and increased vaginal pH, with additional symptoms including vaginal dryness, itching or burning, dysuria, recurrent urinary tract infections and dyspareunia (Hill et al. 2016, Nappi et al. 2020). GSM was introduced for the first time in a 2014 consensus conducted by the International Society for the Study of Women's Sexual Health and the North American Menopause Society, replacing the terms vulvovaginal atrophy, vaginal atrophy, and urogenital atrophy (Hill et al. 2016, Nappi et al. 2020).

Both postmenopausal and premenopausal women can be affected by GSM, however, the condition is more prevalent in postmenopausal women (Angelou et al. 2020, Santoro and Komi 2009). Most of the GSM symptoms differ in frequency and intensity according to the time passed since menopause. Approximately 65% of women suffer from these symptoms within one year post-menopause, increasing to 84% within six years, with these symptoms highly affecting and significantly impacting the quality of life (QoL) of the affected women (Angelou et al. 2020). The initial aim of treating GSM symptoms is therefore to lessen and eliminate the experienced symptoms (Angelou et al. 2020). Numerous treatment options are currently available for GSM and can be classified into non-hormonal therapy and hormone replacement therapy. The non-hormonal therapy is considered the first-line recommended treatment for mild symptoms and includes vaginal lubricants and moisturizers. Hormonal and estrogen-containing medications are mainly used for severe and persistent symptoms and are considered the "gold standard'' and most effective therapy since they act directly to the cause of the GSM, the lack of estrogen (Angelou et al. 2020, Hill et al. 2016).

Estrogen therapy functions well to relieve GSM symptoms because it momentarily restores the body to its normal physiological state. While both local and systemically delivered dosage forms successfully relieve GSM symptoms (Gandhi et al. 2016), the latest trends toward treating GSM symptoms have focused on low dose estrogen due to fears regarding the prolonged use of estrogens (Santoro and Komi 2009). Several routes of administration are additionally used for delivering estrogen-containing medications, such as the vaginal, oral, and transdermal routes (Angelou et al. 2020, Palacios et al. 2015). Orally and transdermally delivered estrogens, however, face numerous problems. Estrogens delivered through oral administration may undergo metabolism via the first-pass metabolism, while transdermal systems may require frequent administration and is associated with an unsteady plasma estrogen concentration, topical irritation, and patient unacceptability (Woolfson et al. 1999). Systemic products may additionally induce breast tenderness, vaginal bleeding, nausea, and modest weight gain with other adverse effects including headaches, back pain, abdominal discomfort, and vaginal yeast infections (Abdelgader et al. 2023, Angelou et al. 2020, Elsokkary et al. 2016, Hill et al. 2016). Extended estrogen monotherapy may furthermore lead to the proliferation of the uterine lining, with this excessive growth resulting in endometrial hyperplasia, development of carcinoma, and alterations in bleeding patterns (Elsokkary et al. 2016).

Due to these adverse effects associated with the systemic administration of estrogen, the vaginal route has been effectively used for the treatment of GSM. The vaginal route exhibits superior outcomes due to the vagina possessing a mucous membrane with a large surface area, an abundance of blood vessels, bypassing first-pass hepatic metabolism, and the ability to retain a high amount of drug locally (Abidin et al. 2020, Angelou et al. 2020, Ndesendo et al. 2008). Various vaginal low dose estrogenic preparations are currently on the market and in use, including creams (Premarin®), tablets (Vagifem®), and vaginal rings (Estring® and Femring®). These vaginal cream and tablet preparations, however, have several limitations and drawbacks, such as messiness, increased vaginal secretion, the need for an applicator, low retention time due to the self-washing out mechanism of the vagina, frequent insertions for tablets and creams, as well as the administered tablets remaining intact for days or not completely dissolving (Albertini et al. 2009, de Araújo et al. 2019, Gavini et al. 2002, Hassan et al. 2018, Hiorth et al. 2014, Hussain and Ahsan 2005, Pacheco-Quito et al. 2020, Vermani and Garg 2000, Yang et al. 2021). Vaginal rings have thus been designed to release loaded estrogen controllably over several months (Lynch 2009). As with the other interventions, vaginal rings however also have several drawbacks, such as difficulty during insertion and removal, alteration of their location, and issues related to the release of estradiol due to an initial burst release (Pickar James H et al. 2016b). These factors and limitations associated

with the currently available locally estrogenic therapies therefore make them inconvenient, resulting in a decreased level of comfort (Hassan et al. 2018, Vermani and Garg 2000). As a consequence of this decreased patient compliance, treatment adherence reduces over time and symptoms thus recur. Therefore, the choice of the delivery system is highly dependent on the patient's preferences and needs (Minkin et al. 2013). In addition to the aforementioned concerns, all the presently available local hormonal dosages for the treatment of GSM contain only one active agent, mainly the estrogen. There is therefore the need for the development of alternative advanced hormonal treatment platforms that allow for the prolonged effective treatment of GSM, while promoting compliance and increasing patient QoL.

1.2 Rationale and Motivation for this study

An optimal drug delivery system seeks to precisely target a designated anatomical site, ensuring controlled and sustained release of the therapeutic agent over a defined temporal window. Traditional delivery modalities often yield fluctuating plasma drug concentrations characterized by peaks surpassing therapeutic thresholds, followed by troughs with suboptimal levels. These fluctuations, coupled with frequent dosing regimens, can pose challenges to patient compliance and treatment adherence, critical for therapeutic efficacy (Stamatialis et al. 2008). To address these challenges, implantable drug delivery systems (IDDS) have emerged as compelling alternatives to conventional modalities, offering the potential for localized or systemic drug delivery. Predominantly composed of polymeric biomaterials, IDDS devices or formulations are designed for implantation at various anatomical sites. They offer advantages such as reduced dosing frequency, prolonged duration of action, minimized systemic side effects, and enhanced patient adherence (Korelidou et al. 2022, Wsoo et al. 2021). Thus, a delivery system, free of the limitations associated with the conventional systems used for treatment of GSM (as discussed in section 1.1.), administered less frequently through the prolonged release of drug can ensure increased patient acceptability and greater control and treatment of GSM.

Intrauterine drug administration is a crucial method for delivering medications, particularly for long-term contraception, local anesthesia before biopsy or surgery, and terminating pregnancies. The uterus, a pear-shaped hollow organ, naturally provides sufficient space for various device shapes to be comfortably retained for extended periods with minimal to no user discomfort. Its highly vascularized wall facilitates efficient blood and lymphatic drainage, while bypassing the hepatic first-pass effect. While the intrauterine route is ideal for potent drugs with prolonged effects over months to years, drugs such as progestogens have garnered significant attention due to their tendency to accumulate in the uterus, as demonstrated by *ex vivo* human perfusion models (das Neves et al. 2021).

Intrauterine devices (IUDs) are IDDS administered directly into the uterine cavity and are the most commonly used long-term reversible contraceptive dosage form because they are effective in terms of safety and efficacy, and can be retrieved (Bao et al. 2020, Wang Ying-Ying et al. 2019). These systems are mainly composed of a T-shaped frame and a hollow tubular reservoir containing either copper (non-hormonal IUD) or progesterone (hormonal IUD). The reservoir in hormonal IUDs is coated with a release-controlling membrane, and the physical configuration of the IUD components is designed to manage the release behavior of the incorporated active agent. The properties of polymers used in the fabrication of the intrauterine device largely determine the release behavior of that system. The most used polymers are silicone polymers due to their biocompatibility, inertness, good stability, and non-degradability (Bao et al. 2020). It should be noted that despite diminished safety concerns regarding intrauterine systems (IUS), continuous research on potential toxicity and clinical monitoring remains warranted, given the nature of IUSs housing large amounts of potent drugs for extended uterine residence. In addition, IUS administration requires skilled physicians and can be achieved by various methods including through transvaginal access with catheters for liquids or insertion devices for solids (das Neves et al. 2021).

A prominent hormonal IUD extensively utilized in clinical settings is exemplified by levonorgestrel-releasing IUDs. Despite the limited availability of information regarding their manufacturing processes and *in vitro* characterization methods, these devices have gained recognition for their contraceptive efficacy. Moreover, they have been utilized as a viable alternative to progestogens in perimenopausal and postmenopausal women undergoing estrogen therapy (das Neves et al. 2021, Rose et al. 2009, Somboonporn et al. 2011). Beyond IUDs, alternative approaches seek to enhance drug distribution within the uterus for specific medical conditions. Thermosensitive gels, transitioning to a gel state at body temperature, ensure controlled distribution and prevent leakage, while composite porous scaffolds loaded with growth factors promote endometrial healing, highlighting innovative strategies for intrauterine drug delivery (das Neves et al. 2021). However, these IUD products only deliver a single API, usually, levonorgestrel, which has limited efficacy and there is no available marketed hormonal intrauterine dosage targeting GSM. Moreover, many IUDs are further associated with prostaglandin and leukocyte release upon their insertion, resulting in side effects such as pain, inflammation, and bleeding during the initial few weeks of their administration. These limitations are considered as the leading cause for the discontinuation of IUD use (Jinying et al. 2008, Yang et al. 2009). There is therefore the need for the development of a hormone loaded IDDS for the treatment of GSM, designed to overcome the currently experienced concerns with localized GSM treatment, as well as the adverse effects

associated with IDDSs. These IDDSs should therefore fulfill several criteria, as summarized below:

- The IDDS should overcome the limitations inherent in conventional delivery systems, such as messiness, leakage, low retention time at the application site, pain during application, frequent administration, and unpredictable release behavior.
- Deliver multiple drugs to specific sites for a predetermined duration while maintaining controlled release patterns.
- Demonstrating simplicity and ease of fabrication, reproducibility, and scale-up attributes.
- Enabling control over formulation and processing parameters during fabrication, which directly influence critical attributes. Therefore, the ideal delivery system should be customizable to achieve the desired drug release and erosion profiles.
- Display a favorable cytocompatibility to minimize side effects upon administration and over the intended treatment period.

In this research, a novel multi-unit polymer-based prolonged release platform (MUPP) IUD has been designed, developed, optimized, and evaluated for the local delivery of hormone active agents in a controlled manner, over an extended period, with primary aim of alleviating the GSM symptoms associated with decreased estrogen levels. This MUPP device has been loaded with estradiol hemihydrate (E2), as well as the progesterone norethindrone acetate (NETA) in separate units. The use of progesterone with estradiol has been noted to overcome the endometrial effects of prolonged exposure to estrogen (Elsokkary et al. 2016). Incorporating systemic progestogens as part of hormone therapy regimens however has the potential for adverse effects in various organs, including an elevated risk of cardiovascular diseases and breast cancer. Contrary, direct delivery of progestogens to the uterus has the potential to overcome the problems of systemic administration due to both the avoidance of first pass metabolism and the lower circulating concentrations of hormones. This localized approach may retain the beneficial effects on the endometrium and could be beneficial in treating dysfunctional uterine bleeding and menopausal sequelae (Ostad et al. 1998, Somboonporn et al. 2011).

In addition to the units containing NETA and E2, to increase the adherence to treatment and reduce the removal rate of the platform as a consequence of pain and bleeding due to IUD insertion (Jinying et al. 2008, Yang et al. 2009), a third unit offering sustained-release of indomethacin (IND) has been fabricated, evaluated, and incorporated to the platform. The controlled release of IND has previously been developed and applied in Cu-IUDs, which are

used as a contraceptive (Qi et al. 2012, Tian et al. 2013). Herein, the IND was controlled to be released for the first two weeks of treatment.

The developed novel MUPP therefore synergistically incorporates E2 and NETA, the main active agents, into biocompatible and biodegradable polymer-blends-matrices, which comprise of polycaprolactone (PCL), ethyl cellulose (EC). These matrices have been modified and optimized to achieve controlled drug release and to facilitate each unit's biodegradation. Additionally, IND was incorporated within a matrix comprising of PCL and polyethylene glycol (PEG). This collective strategy demonstrates a sophisticated approach to delivering multiple agents for prolonged periods, addressing the challenges associated with the systemic administration of hormones for the treatment of GSM, focusing on improving patient compliance and treatment outcomes.

In the design of the MUPP system, two variants have been developed and evaluated in this study (as depicted in Figure 1.1). The first variant is an IUD containing both the NETA and E2-loaded units on a T-frame for delivery of the respective actives to the uterine cavity. The second variant, which is an advancement of the first variant, consists of an IUD consisting of a NETA-loaded unit on a T-frame for delivery of NETA to the uterine cavity with the E2-loaded unit suspended into the vaginal vault. These variants were developed to elucidate the potential of localized delivery in both the uterine and vaginal cavities for the treatment of GSM (a further discussion on the MUPP architecture has been provided in section 1.3).

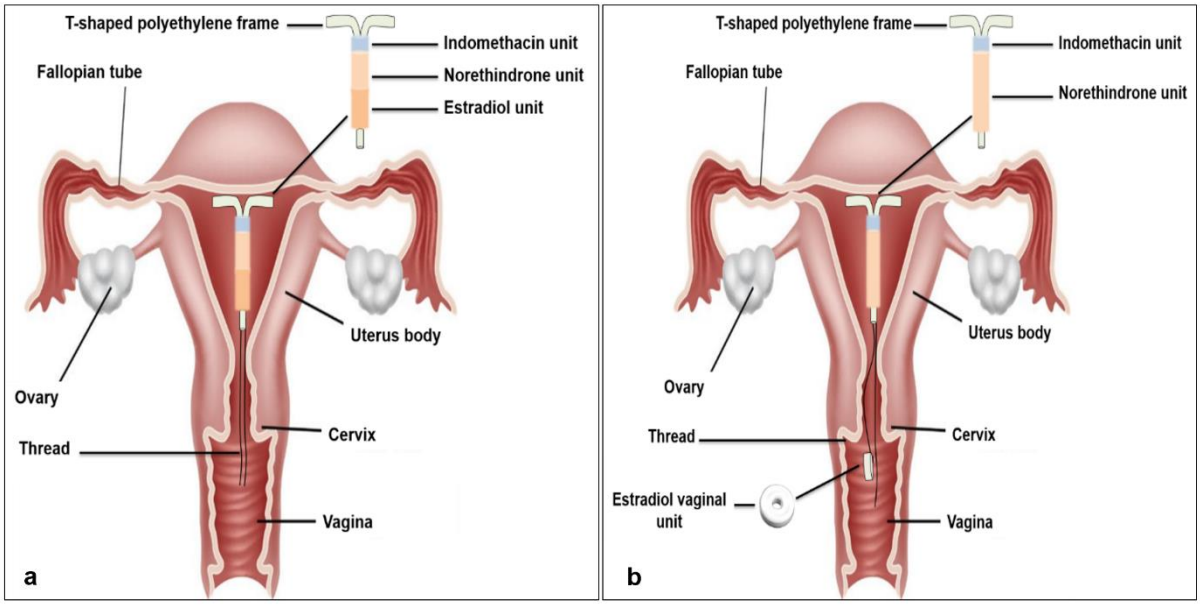

Figure 1.1: Schematic representation of the MUPP with (a) depicting the IUD with the E2-loaded enveloped on the T-shape frame inside the uterine cavity (variant one) and (b) depicting the E2-loaded unit suspended into the vaginal vault (variant two).

1.3 Architectural strategy employed for fabricating the novel MUPP

Despite the availability of numerous estrogen- and progestogens-loaded drug delivery systems (DDSs) in today's market, such as vaginal rings and IUDs, which feature advanced technologies for controlled release, these systems mainly accommodate and release one active agent and are localized to specific anatomical compartment, either the vaginal or uterine cavity. The novel MUPP proposed in this thesis, as depicted in Figure 1.1, considers the anatomical aspects of the genitourinary tract and offers possibilities to overcome such shortfalls of these DDSs. This novel MUPP is configured in a way that enables the simultaneous administration of multiple agents within a single platform, while promoting the controlled sustained release of the drugs payload for an extended period of time.

To assemble the MUPP, the E2-loaded unit was integrated into the novel platform using two distinct configurations (variants). In the first configuration, E2 was loaded into a cylindrical layer encased to the vertical stem of the T-shaped IUD frame (Figure 1.1a). Additionally, the upper part of this T-shaped frame housed the NETA- and IND-loaded units. This arrangement aimed to localize the E2-loaded unit near the cervix and consequently the vaginal tissues, thereby minimizing the exposure of the upper uterine tissues to the released E2. In the second configuration, E2 was loaded into an intravaginal unit suspended within the vaginal vault (upper space of the vagina). This unit was attached via a polyethylene string to the intrauterine unit comprising a T-shaped frame made of low-density polyethylene, which enveloped the NETA- and IND-loaded units (Figure 1.1b). For the first configuration, the E2-, NETA-, and IND-loaded units were fabricated as hollow cylindrical rods using a simple molding technique. In the second configuration, both NETA- and IND-loaded units were prepared using the same simple molding technique, while the E2-loaded intravaginal unit was prepared as a donut-shaped tablet using direct compression employing a specialized set of punches fitted with a central metal rod.

1.4 Novelty of this Study

The novelty of this study represented in this introduction is based on a novel approach in the delivery of a combined regimen comprising the hormonal agents E2 and NETA, along with the anti-inflammatory analgesic agent IND, within a single extended-release platform. This is achieved through the utilization of optimized polymer blends to attain the desired drug release kinetics for the management of GSM. Additionally, a three-unit design was adopted, wherein either all three units are encased within the T-frame of the intrauterine device (configuration one) or an E2-loaded intravaginal unit is attached to the intrauterine device, with NETA- and IND-loaded units enveloped alongside (configuration two). These designs offer versatility by allowing for the modification and tuning of each individual unit’s features without necessitating an increased number of experimental runs or excessive quantities of polymers and drug

substances. Furthermore, the fabrication methodologies utilized for the production of the MUPP units, molding and direct compression techniques, are characterized by their simplicity, ease of implementation, and reproducibility. These methods do not necessitate the use of complex or expensive equipment, thereby enhancing their accessibility and practicality for large-scale production of the MUPP.

This platform, upon its use, is expected to be superior to the conventional commercially available systems and will ensure that there will be improved control of GSM symptoms, biodegradation, and release of the drugs over the treatment period. This will additionally enhance patient compliance and acceptance. Furthermore, this platform is expected to have the potential to be a marketable product and to be used in further applications other than GSM, including contraception for child-bearing women and for uterine adhesions.

1.5 Aim and Objectives of this Study

The aim of this study was therefore to develop, fabricate and optimize a novel multi-unit, polymer-based device for the sustained release of E2, NETA, and IND into uterine and vaginal tissues for localized pharmacological effects in the treatment of GSM. This platform seeks to be superior and overcome the shortfall associated with current commercially available systems used in managing the symptoms of GSM. The specific objectives of this research are as follows:

1. Fabrication of a E2-, NETA-, and IND-loaded intrauterine units through the incorporation of the respective drugs into matrices formulated using different ratios of polymers such as PCL, EC, and PEG.

2. 3D printing of a T-shaped plastic frame for the loading of the drug-loaded units.

3. Determination of the effects and optimization of different drug loads and polymer (PCL, EC, and PEG) ratios on key attributes, such as the erosion and release kinetics of the prepared units through a statistical design of experiments and analysis of the optimized drug-loaded units for the fabrication of MUPP variant one.

4. Formulation and evaluation of E2-loaded donut-shaped intravaginal unit through incorporations of drug into matrices formulated using different ratios of PCL and EC, as well as different compression forces.

5. Employment of a statistical design of experiment, particularly the 2^2 factorial design, to evaluate the effect of polymers and compression force variations in the hardness, release, and erosion characteristics of the prepared E2-loaded intravaginal unit for the fabrication of MUPP variant two.

6. Evaluation of the physicochemical, physicomechanical, and morphological properties of the starting materials and formulated hormonal and analgesic anti-inflammatory units, through the use of Fourier-transform infrared spectroscopy and scanning electron microscopy, as well as determination of hydration capacity and drugs flux through the uterine and vaginal membranes.

7. Determination of the cytotoxic potential of the prepared hormonal and the analgesic anti-inflammatory units through cell studies.

8. Engineering of a cellular model of uterine-vaginal membranes to mimic the *in vivo* environment, using cultured NIH/3T3 cells in a gelatin/alginate hydrogel mounted in a 3D printed custom-designed model frame.

9. Determination of the cytotoxic potential of the configured platforms in the engineered cellular model.

1.6 Overview of this Thesis

Chapter 1 of this thesis furnishes a succinct background and introduction to GSM, shedding light on the existing challenges within current drug delivery methods targeting the GSM and establishing the rationale for undertaking the presented research. An innovative solution to address these challenges is subsequently outlined. Furthermore, the chapter provides a summary encompassing the aims and objectives, as well as the approach and methodology adopted in the current research.

Chapter 2 of this thesis presents an extensive literature survey on vaginally administered estrogen-containing delivery systems designed for the treatment and management of GSM, with a table containing a comprehensive summary of clinical trials performed. The survey categorizes and contrasts the diverse estrogen-containing platforms, emphasizing their performance in terms of systemic absorption, efficacy, safety, and patient satisfaction and acceptance. Furthermore, the chapter outlines crucial considerations in the design of estrogen-containing platforms for GSM and offers insights into future research perspectives in this domain.

Chapter 3 of this thesis outlines the process of fabricating an intrauterine NETA-loaded polymeric matrix units, utilizing a blend of PCL and EC, in the distinctive form of hollow cylindrical rods. Statistical optimization of the NETA-loaded unit using a 2^2 factorial statistical design is further presented in this chapter, which was implemented to assess the impact of

varying formulation variables on key characteristics of the drug-loaded unit and to optimize these characteristics. In the factorial design, the drug load, and the EC-to-PCL ratio for the NETA unit, served as independent variables, while weight loss and drug release percentages were designated as responses. The study analyzed the effects of the independent variables on the responses and determined the optimal combination. Additionally, the degradation of the formulated units under accelerated alkaline conditions and their hardness in terms of resistance to indentation were thoroughly evaluated. Moreover, the optimized formulation was analyzed using various analytical techniques such as FTIR, hydration capacity, and SEM, prior to the evaluation of its cytocompatibility using NIH/3T3 cells.

Chapter 4 of this thesis details the fabrication process of the hollow cylindrical E2-loaded polymeric matrix intrauterine unit, employing a blend of PCL and EC, as well as formulation IND-polymeric matrix units using PCL and PEG. Assessment of the impact of varying E2 load and EC-to-PCL ratio on weight loss and drug release profiles and optimization of these features has been undertaken using a rotatable CCD of experiment and presented in this chapter. Moreover, a 2^2 factorial design (FD) is further presented in this chapter to assess the impact of varying formulation variables on key characteristics of the IND-loaded polymeric matrix and to optimize these characteristics. In the factorial design, the drug load and the PEG content served as independent variables, while weight loss and drug release percentages were designated as responses. Additional investigations in this chapter include a comprehensive evaluation of the degradation of the formulated E2- and IND-loaded units under accelerated alkaline conditions and their resistance to indentation. The compositions interaction was further determined using FTIR with the optimal formulations undergoing assessment for both its hydration capacity and cytocompatibility with NIH/3T3 cells. Moreover, provided in this chapter is the assembly of the intrauterine device from the three units incorporating the E2, NETA and IND (MUPP variant one as described in section 1.3) and thereafter, the cytocompatibility studies of this variant were performed on NIH/3T3 cell line using a MTT assay.

Chapter 5 of this thesis presents the fabrication of the E2-loaded polymer-based intravaginal unit, designed in the form of a donut-shaped tablet. A 2^2 FD of experiment was employed to optimize the donut-shaped unit, using the PCL-to-EC ratio and compression force as independent parameters, with drug release and unit hardness considered as responses. The optimal combination was determined and subjected to further characterization, including textural and weight loss profiling, determination of release mechanism through fitting to different kinetic models, and compatibility evaluation using cell studies on NIH/3T3 cell line. Further provided in this chapter is the assembly of the intrauterine-intravaginal device

incorporating the NETA and IND intrauterine units and the E2-loaded intravaginal unit (MUPP variant two as described in section 1.3) and thereafter the cytocompatibility studies of this variant were performed on the NIH/3T3 cell line using a MTT assay.

Chapter 6 of this thesis delineates the pivotal steps taken in engineering a sophisticated 3D printed cellular model representing the uterine and vaginal tissues. The establishment of this model serves as a crucial component in comprehensively assessing the cyto-compatibility of the prepared intravaginal-intrauterine polymeric platform. The chapter encompasses the methodologies employed in constructing the cellular model, including the 3D printing optimum setup, cell types, culture conditions, and the integration of physiological parameters to emulate the *in vivo* environment. Additionally, the chapter outlines the systematic approach adopted to conduct extensive cyto-compatibility evaluations, providing insights into the interaction between the engineered cellular model and the fabricated MUPP. This integrated analysis aims to elucidate the platform impact on cellular viability, proliferation, and overall compatibility.

Chapter 7 serves as the conclusion and recommendations section of this thesis, presenting a thorough summary of the diverse aspects investigated in the dissertation pertaining to intravaginal-intrauterine hormonal delivery using polymeric matrices. The chapter presents recommendations for future research in the domain of localized hormonal delivery as well as future applications of the developed MUPP system, with a particular focus on rectifying the identified shortcomings of implantable polymeric delivery systems.

CHAPTER 2

2 A Review of the Currently Developed Intravaginal Drug Delivery Systems to Treat the Genitourinary Syndrome of Menopause: Towards the Design of Safe and Efficacious Estrogen-Loaded Prototypes

2.1 Introduction

The genitourinary symptoms experienced during menopause are broad and include a number of physiological processes that often result in dryness of the vagina, pain during intercourse, urinary inconsistency and recurrent urinary tract infections (Hill et al. 2016). Both postmenopausal and premenopausal women are affected by GSM. However, GSM has been noted to be more prevalent in postmenopausal women (Angelou et al. 2020, Santoro and Komi 2009) with more than 50% of postmenopausal women experiencing at least one of these symptoms (Archer et al. 2018, Hirschberg et al. 2021, Ilhan et al. 2021, Marino 2021). Despite the high prevalence and availability of treatments for GSM, these conditions are often under-diagnosed and under-treated for several reasons including: the unwillingness of women to discuss the symptoms with their healthcare provider, a lack of education regarding the condition and its treatment, women not recognizing that their experienced symptoms relate to estrogenic deficiency, and many healthcare practitioners not assessing their patients for GSM symptoms (Kagan et al. 2019, Portman et al. 2015, Steele and Ledbetter 2016).

Using estrogen-containing medications, mainly through the vaginal route, leads to the restoration of the vaginal cytology with increased superficial cells, raised vaginal blood flow and fluid secretions, microbiological balance of the vagina, reduced pH, increased resistance of the vaginal cell to infection and inflammation, and as a consequence improvement in GSM symptoms (Al-Baghdadi and Ewies 2009, Pinkerton et al. 2017, Portman et al. 2015).

Drug distribution throughout the vaginal tissue differs noticeably with the attributes of the delivery system (e.g., tablet demonstrates less absorption than the cream). The selection of vaginal delivery system relies on the intended effect of treatment. Drug retention at the mucosal surface with even distribution and low mucosal penetration is favored for local effects, while a systemic effect could be obtained via controlled extended drug absorption through the vaginal epithelium. Semi-solid systems are desirable for local effects because they distribute evenly in the vaginal cavity and are bio-adhesive, while vaginal ring systems are more suitable for topical effects (Srikrishna and Cardozo 2013, Thapa et al. 2022).

Estradiol vaginal delivery systems have been demonstrated to be efficient, yet variations in their composition raise concerns regarding their properties. These systems exhibit several limitations and drawbacks, including messiness, the necessity of an applicator, short retention

times, and the need for frequent insertion of tablets and creams (Albertini et al. 2009, de Araújo et al. 2019, Gavini et al. 2002, Hassan et al. 2018, Hiorth et al. 2014, Hussain and Ahsan 2005, Pacheco-Quito et al. 2020, Vermani and Garg 2000, Yang et al. 2021). Furthermore, vaginal rings, while effective, present invasiveness during insertion and removal, potential dislodgement, and issues associated with initial burst release (Pickar et al. 2016b). Although the performances of the vaginally-administered estrogen platforms in terms of efficacy, safety, and tolerance have been thoroughly researched, there is limited data correlating this performance to their inactive constituents and design attributes. Therefore, the purpose of this chapter is to define the pathophysiology of GSM, the factors influencing effective GSM treatment, describe and compare the various vaginal E2 formulations based on their design specification, loaded amount of estradiol, and carrier, as well as to evaluate their performance in terms of systemic absorption, efficacy, safety, and patient satisfaction. An extensive review of this subject matter has been undertaken to inform the development of the multi-unit, polymer-based, prolonged-release, implantable devices for the relief of the GSM, and further highlights the shortcomings of the currently developed treatment for GSM, for which the developed MUPP device has been designed to overcome.

2.2 Pathophysiology of GSM

The genitourinary syndrome of menopause depicts the wide range of changes that occur due to the decreased level of estrogen associated with menopausal transition (Angelou et al. 2020, Gandhi et al. 2016, Hill et al. 2016, Palacios et al. 2015, Sritonchai et al. 2020) or due to iatrogenic estrogen deficiency during reproductive age, which can relate to external factors, such as drug use, oophorectomy, and cancer treatment (Weber et al. 2015). This decreased level of estrogen leads to a breakdown of collagen and elastin fibers, resulting in genital changes such as the loss of elasticity, labia minora fading, labia majora shortening, narrowing of the introital opening, vaginal shrinkage and a narrowing and thin-pale vaginal epithelium (Al-Baghdadi and Ewies 2009, Weber et al. 2015). Also, the decline of estrogen level is associated with the reduction of blood flow to the vagina, causing less exudation and lubrication during sexual arousal and consequently results in dyspareunia and postcoital bleeding (Al-Baghdadi and Ewies 2009, Nappi et al. 2020). In addition, glycogen production decreases with the diminished estrogen level, leading to increased pH and imbalance of the normal vaginal microflora, resulting in increased risk of urinary tract infections (Al-Baghdadi and Ewies 2009, Nappi et al. 2020). The GSM gynecological, urological, and sexual signs and symptoms are illustrated in Figure 2.1. In general, GSM develops later than the other symptoms of menopause and does not begin until the amount of endogenously produced estrogen is significantly lower than that is essential for endometrial stimulation (Samsioe 1998, Woods 2012). At this phase of menopause, there is a therapeutic index (Figure 2.2) during

which it is probable to combat genitourinary atrophy by using lower doses of estrogen than that normally prescribed, without hazardous endometrial hyperplasia (Samsioe 1998, Woods 2012).

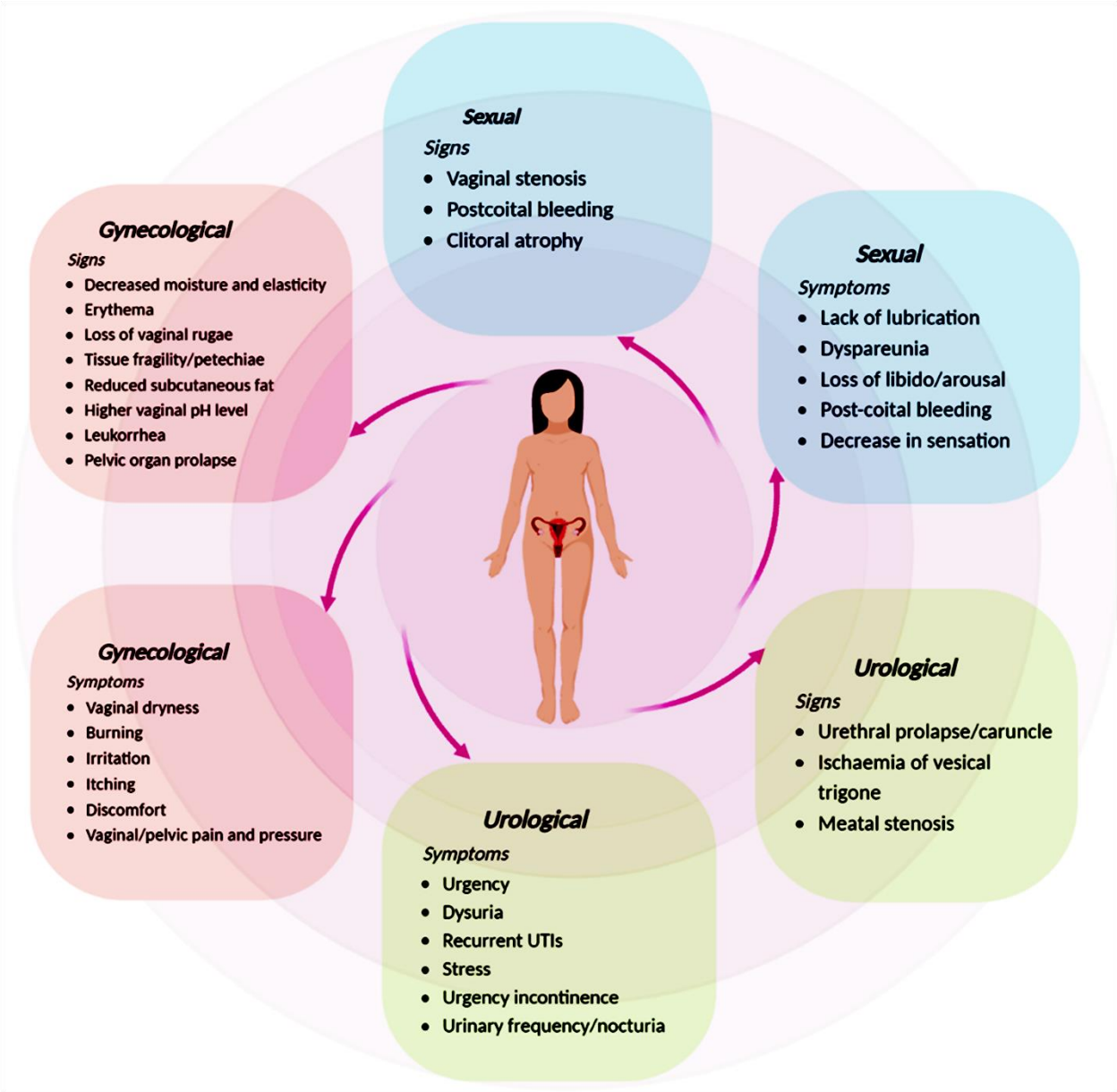

Figure 2.1: The common clinical manifestations of GSM.

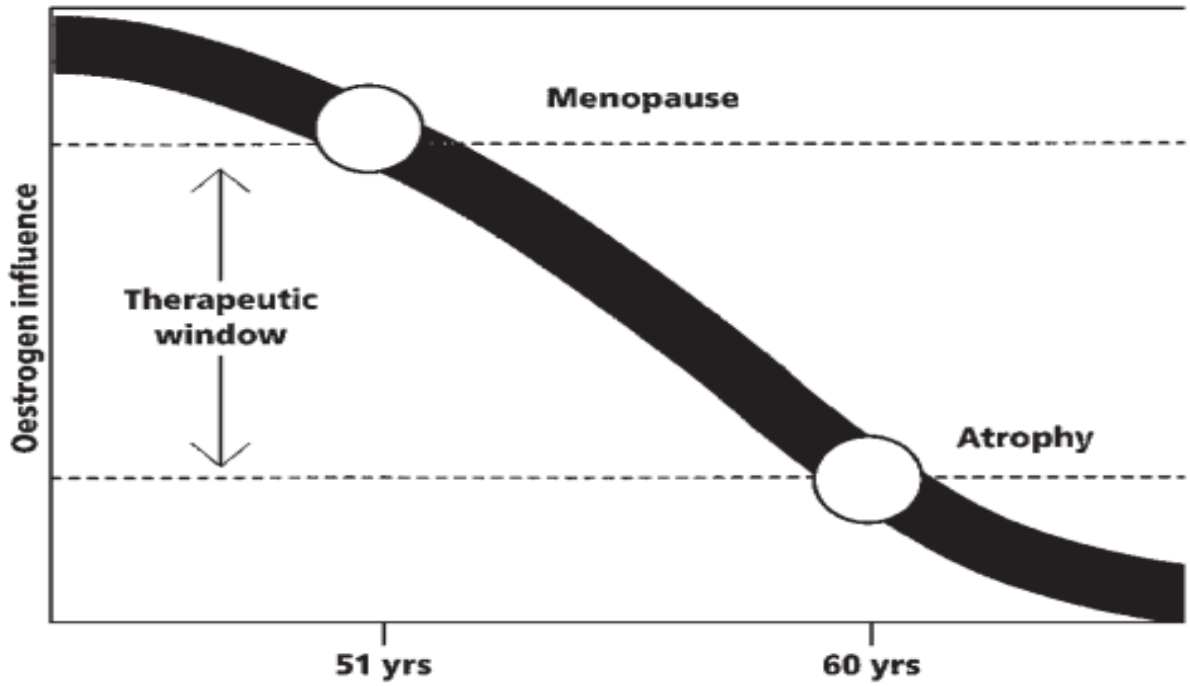

Figure 2.2: Therapeutic index during which it is probable to combat GSM using lower doses of estrogen. Reproduced with permission from (Samsioe 1998, Woods 2012) © 1998 Mosby, Inc.

2.3 Factors Affecting the Drug Absorption from the Vagina during Menopause

The onset of menopause has numerous effects on the absorption of drugs, not only in the treatment of menopause. Drug absorption from the vagina occurs in two major steps: i) drug dissolution within the vaginal cavity, and ii) permeation through the vaginal membrane, which occurs by transcellular or paracellular pathways. Thus, elements that influence these steps may impact drug absorption patterns from the vagina (Srikrishna and Cardozo 2013, Thapa et al. 2022). These elements could be the formulation characteristics, physicochemical properties of the drug and the excipients used, as well as the physiological features of the vagina (Cicinelli 2008, Thapa et al. 2022).

2.3.1 Physicochemical Properties of Drug and Excipients

The vaginal absorption of a drug can be affected by its properties such as its hydrophobicity, molecular weight, surface charge, and ionization. Hydrophilic steroids (such as hydrocortisone) show lower absorption through the vaginal mucosa compared to lipophilic steroids (progesterone/estrone). Also, high molecular weight lipophilic therapeutic agents are less likely to be absorbed trans-vaginally than those with a lower molecular weight (Srikrishna and Cardozo 2013). Additionally, weakly basic drugs with a pKa of 8.5-10.5 are readily ionized in the low pH vaginal fluid of productive-age women, while weakly acidic drugs with a pKa of

less than 5.5 remain unionized. Nonetheless, the oscillating vaginal pH can directly influence the ionization of a drug, and consequently drug solubility and absorption (Thapa et al. 2022).

The excipients and delivery system characteristics can also greatly influence drug absorption (e.g., vaginal rings and tablets exhibit less systemic drug exposure than creams). The intended therapeutic outcome could therefore be achieved through the appropriate design of delivery system (Cicinelli 2008, Thapa et al. 2022). Through the proper selection of excipients and dosage form design, it is possible to control the hydrophilic-lipophilic balance and the extent of the absorption as a consequence, making the pKa of drug of more importance than the molecular weight of drug for the obtaining a formulation with the desired characteristics (Thapa et al. 2022).

17β-estradiol belongs to Class II in the Biopharmaceutical Classification System with a poor water solubility (0.2– 5 µg/mL) and a high permeability (Xiong et al. 2017). It is sparingly soluble in vegetable oil, well absorbed orally (Hariharan et al. 2006, Wang et al. 1999) and undergo broad first pass metabolism, leading to poor bioavailability, and as a consequence, large and frequent oral dose is required, leading to greater side effects (Hariharan et al. 2006, Prakapenka et al. 2020, Zaghloul et al. 2005). 17β-estradiol also exists commercially in different dosage forms including oral, vaginal, and transdermal formulations (Križman et al. 2021b, Prakapenka et al. 2020, Turek et al. 2016). However, the physicochemical properties of the drug can be hindered by the dynamic changes in the vaginal environment, hence, it is critical to evaluate these physiological conditions prior to developing a delivery system (Thapa et al. 2022).

2.3.2 Physiologic Features

Drug absorption through the vaginal mucosa is influenced by the physiological conditions of the vagina including the mucosal thickness, vaginal fluid pH and viscosity, hormonal levels changes and the presence of enzymes (Cicinelli 2008).

2.3.2.1 Vaginal Fluid Volume and pH

The vaginal fluid volume and pH are both important parameters that influence the absorption of vaginally administered drugs (Bernkop-Schnürch and Hornof 2003). Because the vaginal epithelium lacks secretory glands, vaginal fluid is primarily a mixture of several components sourced from blood vessel transudates and contributions from the upper reproductive tract fluids, Bartholin's and Skene's glands, and exfoliated epithelial cells (Bernkop-Schnürch and Hornof 2003, Owen and Katz 1999, Srikrishna and Cardozo 2013, Tietz and Klein 2018, Willhite and O'Connell 2001). The reported amount of vaginal fluid over 24 hours is highly variable with studies reporting 1-3g, 6g and 7.92g per day, with 0.5–0.75 mL continuously present in the vagina at any given time (Owen and Katz 1999, Tietz and Klein 2018). The

aqueous nature of vaginal fluid is essential for drug solubilization (Bernkop-Schnürch and Hornof 2003), and large amounts of vaginal fluid can alter the muco-adhesive and rheological properties of the drug formulation, resulting in low retention time and consequently washout of the dosage form (Bernkop-Schnürch and Hornof 2003, Thapa et al. 2022).

In healthy reproductive-aged women, estrogen induces glycogen production, which is converted by *Lactobacilli* into lactic acid, leading to the maintenance of an acidic vaginal pH (3.5-4.5). During menopause and decreased estrogen levels, vaginal glycogen and *Lactobacilli* decrease, leading to a rise of vaginal pH (>5) (Nilsson et al. 1995, Weber et al. 2015). This change in vaginal pH directly affects the degree of drug ionization, affecting drug absorption (Thapa et al. 2022). In addition, the microbiome imbalance in the vagina during menopause can lead to formation of a layer of pathogenic bacteria on the vaginal mucosa, which can act as an obstacle to the absorption and/or local action of a drug (Thapa et al. 2022).

2.3.2.2 Vaginal Membrane

The vaginal wall comprises of three layers; the adventitia, muscularis, and mucosa, which is composed of non-secretory epithelium (Bernkop-Schnürch and Hornof 2003, Srikrishna and Cardozo 2013). The maturation and thickness of vaginal epithelium is controlled by sex hormones. In adult premenopausal women, the normal thickness of epithelium ranges between 200-300 mm (Bernkop-Schnürch and Hornof 2003). After menopause and other hypo-estrogenic status, the thickness of vaginal epithelium layer decreases, with the vagina also becoming narrower and shorter (Turcan et al. 2022, Woods 2012). The absorption of drugs administered via the vaginal route is directly affected by the alteration of vaginal mucosa characteristics (Thapa et al. 2022). The thinner atrophic vaginal mucosa demonstrates a higher absorption rate for estrogen and steroids when compared to non-atrophic mucosa (Bernkop-Schnürch and Hornof 2003, Srikrishna and Cardozo 2013).

2.3.2.3 Enzymatic Activity

Drug absorption and stability of a delivery system can be influenced by the activity of the enzymes that exist within the vagina (Bernkop-Schnürch and Hornof 2003, Thapa et al. 2022). A broad range of enzymes exist in the vagina despite the fact that the activity of the enzymes is lower compared to that of the gastrointestinal tract. Vaginal fluid contains enzymes, such as lysozyme, nucleases, aldolase, β-glucuronidase, and esterase. Phosphatases, β-glucuronidase, aminopeptidase, and lactate dehydrogenase furthermore exist in the vaginal mucosa, all of which have the potential to influence drug stability and absorption (Bernkop-Schnürch and Hornof 2003).

2.4 Factors Influencing GSM Severity and Response to Therapy

Demographic factors have been noted to potentially influence the degree of GSM symptom severity, as well as age and body mass index. It is recognized that the proceeding in age leads to lessening estrogen levels, in contrast to an increase of body mass index which leads to an increase in circulating estrogen. Hence, alteration in such factors would expect a change in the severity of GSM symptoms and their response to treatment (Constantine et al. 2017a).

In the 12 week, multi-center, phase 3 REJOICE trial carried out by Constantine *et al.*, assessment of the influence of age, body mass index, pregnancy and uterine status on the clinical efficacy and safety of 4, 10, 25 µg doses of TX-004HR was evaluated (Constantine et al. 2017a). The vaginal pH, dyspareunia severity, superficial cells and parabasal cells percentages were analyzed to measure the efficacy outcomes from baseline to week 12 of different doses, in comparison with a placebo within pre-specified subgroups (age: ≤56, 57 to 61, and ≥62 years, body mass index: ≤24, 25 to 28, and ≥29 kg/m^2, pregnancy history and the number of vaginal births, uterine status: intact or not intact uterus). The findings showed that the three doses significantly lessened dyspareunia, the pH of the vagina and parabasal cells, and increased superficial cells, with an improvement in dyspareunia severity noted as early as Week 2 with a constant effect through the 12 weeks of study.

The frequency and intensity of most GSM symptoms differ according to the time passed since menopause. Sixty five percent of women suffer from GSM symptoms within one-year post-menopause, increasing to 84% within six years (Angelou et al. 2020). The British Menopause Society and the International Menopause Society recommended that vaginal atrophy treatment be commenced early to obtain the best response (Derzko et al. 2021). Recently, Derzko *et al.* analyzed data obtained through a multi-center, randomized, double-blind, parallel-group, placebo-controlled trial and detailed the influence of postmenopausal women age at the start of treatment, using 10 µg Vagifem® as the treatment response. The participants were classified according to their age, younger (≥ 45 - < 60 years) or older (≥ 60 years) and the change from baseline to Week 52 in pH, vaginal maturation index, with the most problematic symptoms evaluated and analyzed. Although a more robust response had been observed in younger women, the findings demonstrated that starting the treatment at any age can improve GSM symptoms (Derzko et al. 2021). Another study by Simon *et al.* looked at the effects of body position, supine and ambulatory or seated, after 25 µg TX-004HR dosing on the bioavailability of the estradiol. C_{max}, AUC_{0-24}, and T_{max} were measured by high-performance liquid chromatography-tandem mass spectroscopy. The findings demonstrated there is no significant difference in bioavailability due to body position after TX-004HR dosing (Simon et al. 2020).

2.5 Estradiol-Loaded Vaginal Drug Delivery Systems

The vagina is an important site for local and systemic drug delivery and is considered an effective alternative route to deliver drugs with poor oral bioavailability (Hiorth et al. 2014, Tosca et al. 2021). Vaginal delivery further reduces systemic adverse effects and offers local drug accumulation (Tuğcu-Demiröz et al. 2021). It also demonstrates numerous other benefits such as self and easy administration, high permeability, and a large perfusion surface area (Abidin et al. 2020, Abilova et al. 2020, Tuğcu-Demiröz et al. 2021). One clinical challenge associated with vaginal dosage forms, however, is patient perspective, as many patients fear that the formulation will be washed out (Krause et al. 2009). Traditionally, the vaginal route has been employed to deliver hormones and anti-infective agents such as antivirals, antifungals, and anti-bacterial, in the form of different dosages (Abilova et al. 2020, Vermani and Garg 2000). Currently, various delivery systems for both local and systemic action are available on the market or in clinical development. These systems include classical dosage forms such as creams, ointments, pessaries, tablets, and capsules. Recently, novel formulations such as films and vaginal rings have also been developed (Abidin et al. 2020, Tanmahasamut et al. 2020, Yang et al. 2021). Low dose vaginal estrogen-loaded formulations have also been extensively used due to its avoidance of hepatic metabolism and the more respond-ability of vaginal tissues to locally applied estrogen, and are considered more efficient than systemic delivery in the alleviation of urogenital symptoms of menopause (Nilsson and Heimer 1992, 1995, Notelovitz et al. 2002). Estradiol-based pessaries and creams are the first vaginal formulations effectively used in relieving the urogenital symptoms, but they are rarely used for an extended treatment duration.

The choice of the delivery system is therefore highly dependent on the patient's preferences and needs (Minkin et al. 2013). The dose regimen for the rings is that one ring is inserted vaginally for three months, while the dose regimens for creams and tablets consist of starting with daily application for two weeks, as a loading dose, followed by applications twice per week as a maintenance dose for the period needed to control symptoms (Da Silva et al. 2021, Hirschberg et al. 2021). The underlying rationale for this schedule is that during the initial days of therapy, the vaginal epithelium is atrophic leading to high estradiol absorption. The vaginal epithelium subsequently matures with estradiol use and time, resulting in decreased absorption; hence, smaller doses are usually required to provide adequate estradiol accumulation to avoid vaginal atrophy recurrence (Da Silva et al. 2021). Table 2.1 shows the FDA approved vaginal estradiol delivery system, their excipients, estradiol load, release rate, and their dose regimens, while Table 2.2 summarizes studies that compare estradiol vaginal formulations versus placebo, or other vaginal estrogen, formulations.

Table 2.1: FDA approved vaginal estradiol delivery systems.

Delivery system	Active	Generic	Additives	Company	Strength/ Release rate	Dosing	Reference
Cream	17β-estradiol	Estrace	A non-liquefying base containing propylene glycol, stearyl alcohol, white ceresin wax, mono- and di-glycerides, hypromellose 2208 (4000 cps), sodium lauryl sulfate, methylparaben, edetate di-sodium, tertiary butylhydroquinone and purified water	Warner Chilcott Laboratories Rockaway, NJ. Allergan USA, Inc., Irvine, CA	0.01%	2-4 g/daily for 1-2 weeks followed by 1-2 g for 1-2 weeks; 1 g maintenance dose 1-3 times weekly.	(Archer et al. 2018, Chism 2012, Chollet 2011, Estrace Cream , Jiang et al. 2021, Marino 2021, Minkin et al. 2013)
Tablet	Estradiol	-Vagifem -Yuvafem (generic)	Lactose, starch, hydroxyl propyl methyl cellulose (HPMC), magnesium stearate, polyethylene glycol	Novo Nordisk Pharmaceuticals, Princeton, NJ	10 µg/ Tablet 25 µg/ tablet (discontinued)	10 µg inserts daily for 2 weeks then 2 per week	(Abramowicz et al. 2019, Chism 2012, Chollet 2011, Jiang et al. 2021, Marino 2021, Minkin et al. 2013, Vagifem Tablet)
Softgel capsules	17β-estradiol	Imvexxy	MIGLYOL 812 N, gelatin, polyethylene glycol stearate, lecithin, propylene glycol, FD&C Red #40, titanium dioxide, glycerine, polyvinyl acetate phthalate	Therapeutics MD, Inc., Boca Raton, FL.	4, 10 µg/ insert	4 µg-10 µg inserts daily for 2 weeks then 2 per week	(Abramowicz et al. 2019, Constantine et al. 2017b, Marino 2021, Paton 2018, Simon et al. 2017b)
Ring	17β-estradiol	Estring	Silicone polymers and barium sulfate	Pharmacia & Upjohn Pfizer, New York, NY	2 mg 7.5 µg/day	One ring inserted every 3 months	(Abramowicz et al. 2019, Boyd et al. 2019, Chism 2012, Chollet 2011, Estring , Jiang et al. 2021, Marino 2021, Minkin et al. 2013, Rafiei et al. 2021)
Ring	17β-estradiol-3-acetate	Femring	Cured silicone elastomer composed of dimethyl polysiloxane silanol, silica (diatomaceous earth), normal propyl orthosilicate, stannous octoate; barium sulfate	Warner Chilcott Laboratories, Rockaway, NJ Millicent Pharma	12.4, 24.8 mg 50,100 µg/day	One ring inserted every 3 months	(Boyd et al. 2019, Chollet 2011, Femring , Jiang et al. 2021, Rafiei et al. 2021)

Table 2.2: Summary of studies that compared Estradiol vaginal formulations versus placebo or other vaginal estrogen formulations.

Study	Treatment	Comparator	Duration of treatment	Design of the study	Objective	Location and No of centers
(Rioux et al. 2018)	25 µg Vagifem (n= 80) Withdrawal (8)	1.25 mg Premarin (n= 79) Withdrawal (25)	24 weeks	Multicenter, open-label, randomized, parallel-group study	Compare the efficacy safety and acceptability	Canada (6 centers)
(Ekin et al. 2011)	25 µg Vagifem (n= 24) Withdrawal (3)	5 mg hyaluronic acid tablet (n= 24) Withdrawal (3)	8 weeks	Randomized, controlled study	Compare the efficacy	Turkey (1 center)
(Dugal et al. 2000)	25 µg Vagifem (n= 48) Withdrawal (6)	0.5 mg estriol vagitories (n= 48) Withdrawal (5)	24 weeks	Randomized, parallel-group, single blind, multicenter trial	Compare the acceptability, efficacy and safety	NA
(Ilhan et al. 2021)	10 µg Vagifem (n= 30)	2 g Cicatridina ovule (n= 31) And 10 mg Colpotrophine ovule (n= 30)	12 weeks	Prospective and open-label study	Compare the efficacy	Turkey (centers=NA)
(Hosseinzadeh et al. 2015)	25 µg Vagifem (n= 80) Withdrawal (NA)	Vaginal estrogen cream (n= 80) Withdrawal (NA)	12 weeks	Simple randomized clinical trial	Compare the efficacy, acceptability, and safety	Iran (1 center)
(Labrie et al. 2009)	25 µg Vagifem (n= 10) Withdrawal (NA)	0.625 mg Premarin (n= 10) Withdrawal (NA)	1 week	A prospective, randomized trial	Evaluation of the systemic bioavailability and the pharmacokinetics	NA NA
(Nilsson and Heimer 1992)	10 µg Vagifem	24 participants*	25 µg Vagifem	2 weeks	Randomized, double-blind, cross-over study	Determination of the systemic absorption	NA
(Notelovitz et al. 2002)	10 µg Vagifem (n= 30) Withdrawal (7)	25 µg Vagifem (n= 28) Withdrawal (9)	12 weeks	Double-masked, randomized, parallel group study	Determination of the systemic absorption	USA (1 center)

* Participants randomized between the treatment and the comparator.

Table 2.2: (Continued)

(ClinicalTrials.gov)	Generic 10 µg estradiol tablet	10 µg Vagifem Placebo	2 weeks	An investigator-blind, randomized, parallel-group, placebo-controlled, multicenter study	Compare the safety and efficacy	USA (25 Centers)
(Minkin et al. 2013)	10 µg Vagifem tablet	79 Participants* Estring ring Estrace cream Premarin cream	5 weeks	Online survey of postmenopausal local estrogen therapy users	Study of patient satisfaction with estradiol vaginal tablets in postmenopausal women previously treated with another local estrogen therapy	USA NA
(Eriksen Poul Sindberg and Rasmussen 1992)	25 µg Vagifem (n= 81) Withdrawal (6)	Placebo (n= 83) Withdrawal (4)	12 weeks	Double-blind randomized placebo-controlled study	Compare the efficacy	Denmark (centers=NA)
(Diem et al. 2018)	10 µg Vagifem + placebo vaginal gel (n= 102) Withdrawal (NA)	Placebo vaginal tablet + vaginal moisturizer (n= 100) Withdrawal (NA) Placebo tablet + placebo gel (n= 100) Withdrawal (NA)	12 weeks	A randomized, double-blind, placebo-controlled trial	Compare the effects of a Vagifem tablet and a vaginal moisturizer to placebo on menopause-related quality of life and mood	USA (2 centers)
(Mashingaidze 2014)	4 µg TX-004HR (n= 18) 10 µg TX-004HR (n= 19) 25 µg TX-004HR (n= 18)	Placebo (n= 17) Withdrawal (1)	12 weeks	Multicenter, double-blind, placebo-controlled, phase 3	To evaluate the pharmacokinetics parameters	United States Canada (11 centers)

* Participants randomized between the treatment and the comparator.

Table 2.2: (Continued)

(Pickar James H et al. 2016b)	10 µg TX-004HR (n= 24) Withdrawal (0)	Placebo (n= 26) Withdrawal (2)	2 weeks	Single-center, double-blind, placebo-controlled phase 2 pilot trial	To evaluate the safety and efficacy	NA (1 center)
(Constantine et al. 2017b)	4 µg TX-004HR (n= 191) Withdrawal (11) 10 µg TX-004HR (n= 191) Withdrawal (14) 25 µg TX-004HR (n= 190) Withdrawal (9)	Placebo (n= 192) Withdrawal (10)	12 weeks	Multicenter randomized, double-blind, placebo-controlled, phase 3 study	Safety and efficacy	USA Canada (89 centers)
(Simon et al. 2019)	4 µg TX-004HR (n= 191) Withdrawal (NA) 10 µg TX-004HR (n= 191) Withdrawal (NA) 25 µg TX-004HR (n= 190) Withdrawal (NA)	Placebo (n= 192) Withdrawal (NA)	12 weeks	Post hoc analyses for data obtained from a multicenter, double-blind, randomized, placebo-controlled, phase 3 trial	To evaluate improvement of dyspareunia and associated vaginal dryness with a TX-004HR softgel vaginal insert	USA Canada (Centers=NA)
(Mirkin et al. 2021)	4 µg TX-004HR (n= 22) Withdrawal (NA) 10 µg TX-004HR (n= 25) Withdrawal (NA)	Placebo (n= 25) Withdrawal (NA)	12 weeks	Post hoc analysis for data obtained from a phase 3, prospective, randomized, double-blind, placebo-controlled, multicenter study	To evaluate endometrial progesterone receptor expression in menopausal women	USA Canada (89 Centers)

Table 2.2: (Continued)

(Casper et al. 1999)	Estring (n= 174) Withdrawal (31)	Estriol vaginal pessaries (n= 72) Withdrawal (17)	12 weeks	Randomized open-label comparative trial with parallel groups	Compare the efficacy, safety and acceptability	Austria Switzerland Germany (14 centers)
(Barentsen et al. 1997)	Estring (n= 83) Withdrawal (11)	Estriol vaginal cream (n= 82) Withdrawal (16)	12 weeks	Open-label, change-over, randomized parallel group trial	Compare the efficacy and evaluation of treatment preference	Netherland (12 centers)
(Weisberg et al. 2005)	Estring (n= 126) Withdrawal (32)	25 µg Vagifem (n= 59) Withdrawal (7)	48 weeks	Open-label, randomized, parallel-group study	Endometrial safety	Australia (4 centers)
(Henriksson et al. 1994)	Estring (n= 112) Withdrawal (11)	0.5 mg estriol vaginal pessary (n= 53) Withdrawal (8)	12 weeks	An open, randomized, parallel-group, comparative trial	Efficacy, safety, and acceptability	Sweden Finland Denmark (9 centers)
(Ayton et al. 1996)	Estring (n= 131) Withdrawal (11)	0.625 mg Premarin (n= 63) Withdrawal (7)	12 weeks	An open, randomized, parallel, comparative multicenter trial	To compare the safety, efficacy and acceptability	Australia (3 centers)
(Casper et al. 1999)	Estring (n= 43) Withdrawal (10)	Placebo (n= 41) Withdrawal (7)	24 weeks	Double-blinded randomized placebo-controlled in parallel groups	Compare the efficacy	Germany (10 centers)
(Eriksen Bjarne C 1999)	Estring (n= 53) Withdrawal (17)	No treatment (control group) (n= 55) Withdrawal (6)	36 weeks	A multicenter, randomized, open, parallel-group study with an untreated control group	To detect the preventive effect of the Estring) on recurrent urinary tract infections in postmenopausal women	Norway (15 centers)
(Smith et al. 1993)	2 mg estradiol vaginal ring (n= 222) Withdrawal (56)	NA	54 weeks	The study was designed as a multiple independent trial	To study the efficacy, safety and acceptability	Sweden (7 centers)

Table 2.2: (Continued)

(Speroff and Group 2003)	50 µg Femring (n= 113) Withdrawal (14) And 100 µg Femring (n= 112) Withdrawal (11)	Placebo (n= 108) Withdrawal (29)	13 weeks	Double-blind, randomized, placebo-controlled trial	To assess the efficacy, tolerability, and acceptance for vasomotor and GSM symptoms	USA (35 centers)
(Buckler et al. 2003)	50 µg Menoring + placebo tablet (n= 84)	1mg oral estradiol tablets (Elleste Solo) + placebo ring (n= 75)	24 weeks	Prospective, multi center, randomized, double-blind, comparator-controlled, parallel group study	Evaluate the efficacy and acceptability	United Kingdom (21 centers)
(Antoniou et al. 1997)	50 µg vaginal ring + progesterone suppository (n= 28)	50 µg estradiol patch + levonorgestrel IUD (n= 28)	12 months	NA	To compare the efficacy, safety and acceptability	Greece (1 center)
(Hamada et al. 2003)	Vaginal ring deliver *in vitro* estradiol 160 µg/day and progesterone 20 mg/day (n= 8) Withdrawal (1) Vaginal ring deliver *in vitro* estradiol 160 µg/day and progesterone 10 mg/day (n= 12) Withdrawal (2)	NA	16 weeks	NA	To investigate whether vaginal rings delivering estradiol and progesterone could prevent endometrial hyperplasia and relieve climacteric symptoms	NA

Table 2.2: (Continued)

(Martin et al. 1979)	Estrace vaginal cream (n= 20) Withdrawal (0)	1.25 mg Premarin (n = 10) Withdrawal (1)	2 weeks	NA	To evaluate systemic absorption and sustained effects of two estrogen vaginal cream preparations	NA NA
(ClinicalTrials.gov)	Generic 0.01% estradiol cream (n= 268) Withdrawal (5)	0.01% Estrace cream (n= 262) Withdrawal (5) Placebo (n= 133) Withdrawal (2)	9 days	A randomized, double-blind, placebo-controlled, parallel-design, multiple-site study	To evaluate the therapeutic equivalence and safety	USA (44 centers)
(Archer et al. 2018)	0.003% estradiol vaginal cream (n= 287) Withdrawal (22)	Placebo cream (n= 289) Withdrawal (28)	12 weeks	Phase 3, randomized, double-blind, placebo controlled, multicenter study	To examine the efficacy and safety	NA
(Kroll et al. 2018)	0.003% estradiol vaginal cream (n= 277) Withdrawal (22)	Placebo cream (n= 273) Withdrawal (31)	12 weeks	Phase 3, randomized, double-blind, placebo controlled, multicenter study	To compare the safety and efficacy	NA
(Tanmahasamut et al. 2020)	25 µg estradiol gel (n= 40) Withdrawal (2)	Placebo (K-Y® Jelly) (n= 40) Withdrawal (3)	8 weeks	A randomized double-blind controlled trial	To evaluate the efficacy and safety	Thailand (1 center)

2.5.1 Vaginal Tablets

Vaginal tablet dosage forms are characterized by their ease of manufacture and ease of administration, making them more convenient for patients (Bhat and Shivakumar 2010). Vaginal estradiol tablets are approved and marketed commercially for the treatment and alleviation of symptoms associated with atrophic vaginitis and include Vagifem® tablets (Novo Nordisk, Baegsvard, Denmark) (Nygaard et al. 2004). Vagifem® tablets are a film-coated hydrophilic cellulose matrix with the ability of adhesion into the vaginal mucosa and offer controlled in site, pH-independent release with no significant systemic absorption of estradiol (Sindberg and Rasmussen 1992, Notelovitz et al. 2002, Weisberg et al. 2005). Vagifem® is present in two strengths: 10 µg and 25 µg. In 1988 the Vagifem® tablet with the 25 µg 17β-estradiol load was introduced for the first time (Chollet 2011). In July 2010, the manufacturing company stopped trading the 25 µg Vagifem® tablet in the USA (Hosseinzadeh et al. 2015).

Additionally, the Food and Drug Administration approved the 10 µg Vagifem® tablet as a treatment for vulvovaginal atrophy in November 2009 (Chollet 2011, Hosseinzadeh et al. 2015). The Vagifem® 10 µg tablet is the lowest approved dose, which has only 1.14 mg estradiol exposure throughout a twelve month period (Lindahl 2014, Panay and Maamari 2012, Simon and Maamari 2013). The dose schedule for Vagifem® consists of an application of one tablet per day during the initial two weeks of treatment, followed by one tablet twice a week as a maintenance dosage (Chollet 2011). Each one Vagifem® tablet is located in a prefilled single-use applicator (Brunner and Theodor 2020, Sindberg and Rasmussen 1992) positioned deeply in the vagina; where the tablet adheres to the vaginal mucosa forming a gel layer from which the estradiol is slowly released by diffusion (Chollet 2011, Dugal et al. 2000, Hosseinzadeh et al. 2015). The main advantages of the estradiol vaginal tablet dosage form over other vaginal estradiol dosage are represented in the efficacy in local alleviation of symptoms, ease of use, a more hygienic administration, increased patient acceptability and a low estradiol loading-dose, which leads decreased systemic adverse events (Hosseinzadeh et al. 2015, Notelovitz et al. 2002, Portman et al. 2015, Zolghadri et al. 2014). Yuvafem is a generic 10 µg estradiol vaginal tablet manufactured by Amneal Pharmaceuticals (Bridgewater, NJ) (Rosenblum 2020).

A crucial concern regarding the delivery of estrogen through locally administered dosage forms is the amount that enters systemic circulation, which is clinically important with regards to probable adverse events such as breast cancer and venous thromboembolism (Da Silva et al. 2021, Santen RJ 2015). Several pharmacokinetic studies showed that local vaginal estradiol formulations are associated with lower systemic exposure compared to oral formulations, implying

that the probability of adverse events incidence is also minimum (Ilhan et al. 2021, Paton 2018). The analysis and determination of estrogen levels are also more complicated in postmenopausal than premenopausal women, due to the reduced sensitivity of many assays to detect low estrogen levels. Several methods are in use for the determination of estradiol such as gas chromatography-mass spectrometry, radio-immunoassays, and ultra-sensitive bioassay.

Two studies investigated and compared the systemic absorption of 17β-estradiol from 10 and 25 µg Vagifem® tablets in postmenopausal women (Nilsson and Heimer 1992, Notelovitz et al. 2002). Both of these studies showed low systemic absorption (within normal postmenopausal range) for both doses, with higher absorption associated with the 25 µg dose, confirming that the extent of the absorption was dose dependent. Interestingly, the absorption patterns in one study initially showed significant estradiol absorption at both doses, which decreased significantly by day fourteen (Nilsson and Heimer 1992), while Notelovitz *et al.* reported a steady absorption pattern at the beginning and end of the 12-week study period (Notelovitz et al. 2002). Both studies used a radioimmunoassay technique to detect systemic estradiol. The number of participants and the study period were 58 women and 12 weeks, respectively, for the study undertaken by Notelovitz *et al.* with serum estradiol <20 pg/ml as the enrolment criterion, compared to 24 participants, a 2-week study period, and no specification for the baseline serum estradiol levels in the other study (Nilsson and Heimer 1992). In contrast, a study by Labrie *et al.* used a sensitive and accurate mass spectrometry assay (chromatography/mass spectrometry), evaluating the systematic bioavailability of estradiol and estrone during the 24 hours following a one week application of 25 µg Vagifem® and 0.625 mg Premarin® cream (Labrie et al. 2009). Although the study had a small number of participants (10 patients in each group), the findings demonstrated that serum estradiol was increased five-fold during the first 24 hours period after administration of 25 µg Vagifem® or 1 g Premarin®, and that serum estrone increased 150% with Vagifem® and 500% with Premarin® cream after daily administration. The results indicate that systemic events are likely to occur following administration of these dosage forms.

GSM is also characterized by the incidence of numerous events, such as increased parabasal cells, decreased superficial cells, vaginal epithelium thinning, and an increased pH to more than 5; thus, improvement in these factors and other vaginal symptoms could be used as indicators for vaginally-delivered estradiol system effectiveness in treating the symptoms of GSM (Liu et al. 2020, Rioux et al. 2018). The efficacy of an estradiol vaginal tablets were evaluated and compared to other estrogen-containing dosage forms in numerous studies, with an improvement in subjective and objective signs and symptoms, without major safety concerns demonstrated

(Dugal et al. 2000, Ekin et al. 2011, Hosseinzadeh et al. 2015, Ilhan et al. 2021, Rioux et al. 2018, Weisberg et al. 2005). A study undertaken by Dugal *et al.* followed 96 postmenopausal women for 24 weeks to evaluate and compare the efficacy of 25 µg Vagifem® tablets to estriol vagitories (Dugal et al. 2000). The results showed that the efficacy of both treatments is equivalent. However, the endometrial thickness was increased more in the Vagifem® group during the initial two weeks, but the base line thickness was restored when the dosing schedule reduced to two applications per week. In a study by Hosseinzadeh *et al.*, 160 postmenopausal women were randomized into two groups for treatment with Vagifem® or with a vaginal estrogen cream for 12 weeks (Hosseinzadeh et al. 2015). Both treatments significantly improved symptoms of atrophic vaginitis without significant difference between the two groups. Similarly, Rioux *et al.* conducted a multicenter, open-label, randomized, parallel group study on 159 menopausal women to compare the efficacy of Vagifem® and a vaginal estrogen cream (Rioux et al. 2018). The authors concluded that the efficacy of both the tablet and cream was equivalent in relieving symptoms of atrophic vaginitis. In addition, Vagifem® demonstrated localized effects with no significant increase in the systemic estradiol level or estrogenic side effects.

With the increased prevalence of GSM, there is also a need for cheap therapeutic options, especially in developing countries, where combined oral contraceptive tablets are less expensive compared to vaginally-administered estrogenic-medications (Chompootaweep et al. 1998). One study compared the efficacy of easily obtainable and less expensive combined oral pills (250 µg levonorgestrel and 30 µg ethinyl estradiol) with conjugated equine estrogen cream for the treatment of urogenital symptoms in 40 postmenopausal Thai women (Chompootaweep et al. 1998). Twenty participants applied one tablet every week vaginally for 8 weeks, while the other 20 participants applied the cream in a decreasing dosage of 1 gram three times per week to 1 gram once per week by Week 3. All tablet users had a marked improvement in vaginal dryness, dyspareunia, urinary urgency, and urinary frequency, with no statistically significant differences between the groups. Also, in both groups, pH decreased and maturation and karyopyknotic indexes were improved compared to baseline.

2.5.1.1 Safety of vaginal tablets

With the vaginal administration of estrogens offering reduced systemic absorption compared to orally delivered estrogens, the occurrence of serious side effects are expected to be minimal (Abramowicz et al. 2019, Mirkin et al. 2021). The safety of vaginally estradiol dosages are mainly screened through the occurrence of adverse events, laboratory markers findings, and endometrial biopsies using ultrasonography (Rioux et al. 2018). The most common adverse events associated

with vaginal estrogens administration are vaginal bleeding, candidiasis and discharge, in addition to the risks associated with systemic estrogen exposure, which may lead to venous thrombosis and endometrial hyperplasia (Marino 2021). The risk of endometrial proliferation associated with the use of unopposed estrogen furthermore remains a crucial concern. The serum estradiol levels which can lead to endometrial proliferation are approximate more than 70 pmol/liter, which is the higher limit of the normal postmenopausal range, with some inter-individual difference (Weisberg et al. 2005). Several studies demonstrated that transdermal and oral estrogen treatment results in 1-28% and 0.2-3% of all endometrial hyperplasia and neoplasia cases, respectively, while locally applied estrogen causes 0-2% of all cases. Thus, no categorical association between vaginal estrogen and endometrial hyperplasia has been established (Kovachev and Kovachev 2022). However, the lack of evidence on long term estrogenic adverse events makes the systemic exposure from vaginal delivery of great concern and may be the foundation to contraindicate vaginal formulations for some postmenopausal women (Jonasson et al. 2020). In a study to evaluate the endometrial safety of the administration of a 10 µg estradiol vaginal tablet for 52-weeks, Simon *et al.* evaluated the incidence rate of endometrial hyperplasia and carcinoma in two joint studies with 541 total participants (Simon et al. 2010). The biopsy data revealed that the incidence rate of hyperplasia and carcinoma is only 0.52% per year from 386 evaluable samples, and thus indicated there is no increased risk of endometrial hyperplasia and carcinoma in postmenopausal women using 10 µg estradiol vaginal tablets for 1 year under the same study conditions. The impact of the Vagifem® dosage regimen on the endometrial tissues was further evaluated by Mettler and Olsen. During the first two weeks, all participants with GSM were treated with one 25 µg Vagifem® tablet daily. Thereafter the participants were randomized in an open controlled, two parallel groups, receiving either Vagifem® two times per week (34 participants), or once weekly (17 participants), for 50 weeks. After one year of treatment, no endometrial hyperplasia was observed in 45 patients who completed the one-year study period. Nine of the patients (two of the once weekly and seven of the twice weekly maintenance therapy groups) continued treatment for a further 12 months, with the application of one tablet twice per week. From this group, one patient of the once weekly and two patients of the two weekly maintenance therapy groups showed weak endometrium proliferation. All nine patients who completed two years of treatment showed atrophic endometrium (Mettler and Olsen 1991). These findings indicate that the twice weekly administration of 25 µg Vagifem® is the lowest safe and effective dose for the long-term treatment of urogenital symptoms in postmenopausal women.

The guidelines of North American Menopause Society and the International Society for the Study of Women's Sexual Health recommend the use of non-hormonal therapies as the treatment of

choice for women at high risk of breast cancer and low dose vaginal formulations as second-line for women whose symptoms persist with non-hormonal therapies (Kagan et al. 2019). Recently, breast cancer survivors increasingly use aromatase inhibitors more than tamoxifen, leading to more induction of GSM symptoms (Kendall et al. 2006). To study the concomitant use of vaginal estrogen with aromatase inhibitors, Kendall *et al.* analyzed the serum level of estradiol in seven women, where six of them used 25 µg Vagifem® tablets and one used Premarin® cream (Kendall et al. 2006). The serum estradiol was found to be ≤5 pmol/l at baseline and increased to an average of 72 pmol/l at Week 2, then decreasing to less than 35 pmol/l in most participants, although significant further increases were seen in two participants. The authors found that the 25 µg Vagifem® tablet significantly increased systemic estradiol exposure and stated that it is contraindicated in women with breast cancer undergoing aromatase inhibitors treatment, unless there is ability for regular screening for serum estradiol. This study, however, included a small number of participants and used a radioimmunoassay to determine estradiol levels.

2.5.1.2 Acceptability

Patient acceptability is a vital feature in GSM treatment as therapy is mostly often for an extended period (Dugal et al. 2000). Additionally, the selection of vaginal estrogen formulations is highly based on the user's preferences and needs, due to most formulations having been demonstrated to be effective with a high safety profile (Minkin et al. 2013). Many studies have shown higher acceptance rates for estradiol tablets compared to other vaginal delivery systems and placebo formulations (Daneshmand et al. 2014, Diem et al. 2018, Dugal et al. 2000, Hosseinzadeh et al. 2015). This high acceptance rate was primarily attributed to the minimal or absence of leakage and messiness, low pain during application, ease of use and high hygienic value, in addition to a higher improvement of mood and quality of life compared to the placebo. From a design and formulation perspective, advantages are attributed to the small tablet size, tablet muco-adhesion, and deep positioning during administration. In a study conducted by Minkin et al., an online survey was used to study the reason for changing to vaginal estradiol tablets from other estradiol preparations such as creams, rings, and conjugated estrogen creams (Minkin et al. 2013). The respondents demonstrated that the tablets are preferable to the ring or cream. The factors for shifting from vaginal cream to vaginal tablet are depicted in Figure 2.3. Efficacy, ease of use, and longer adherence to treatment were the main reasons behind the preference of tablets. However, in addition to the small number of the population included in this study (79 participants), only 9% of the participants had previously used an estradiol ring, which may reduce the evidence of the tablet preference over vaginal ring. Furthermore, in clinical practice settings, patients using

vaginal tablets demonstrated a significantly longer treatment duration and adherence to treatment than those using vaginal creams ($p<0.01$) (Shulman et al. 2008).

Little data and information exist on the efficacy, safety and acceptance of the generic 10 µg estradiol vaginal tablets, however, two phase 3 clinical studies (NCT01779947 and NCT02668796) compared the safety and efficacy of two generic 10 µg estradiol vaginal tablets to the FDA approved 10 µg Vagifem® tablet in postmenopausal women with moderate to severe vaginal atrophy (ClinicalTrials.gov, ClinicalTrials.gov). Even though both trials have been completed, the results data from the NCT01779947 study have been submitted to ClinicalTrials.gov but is not yet publicly available, while there are no results posted for the NCT02668796.

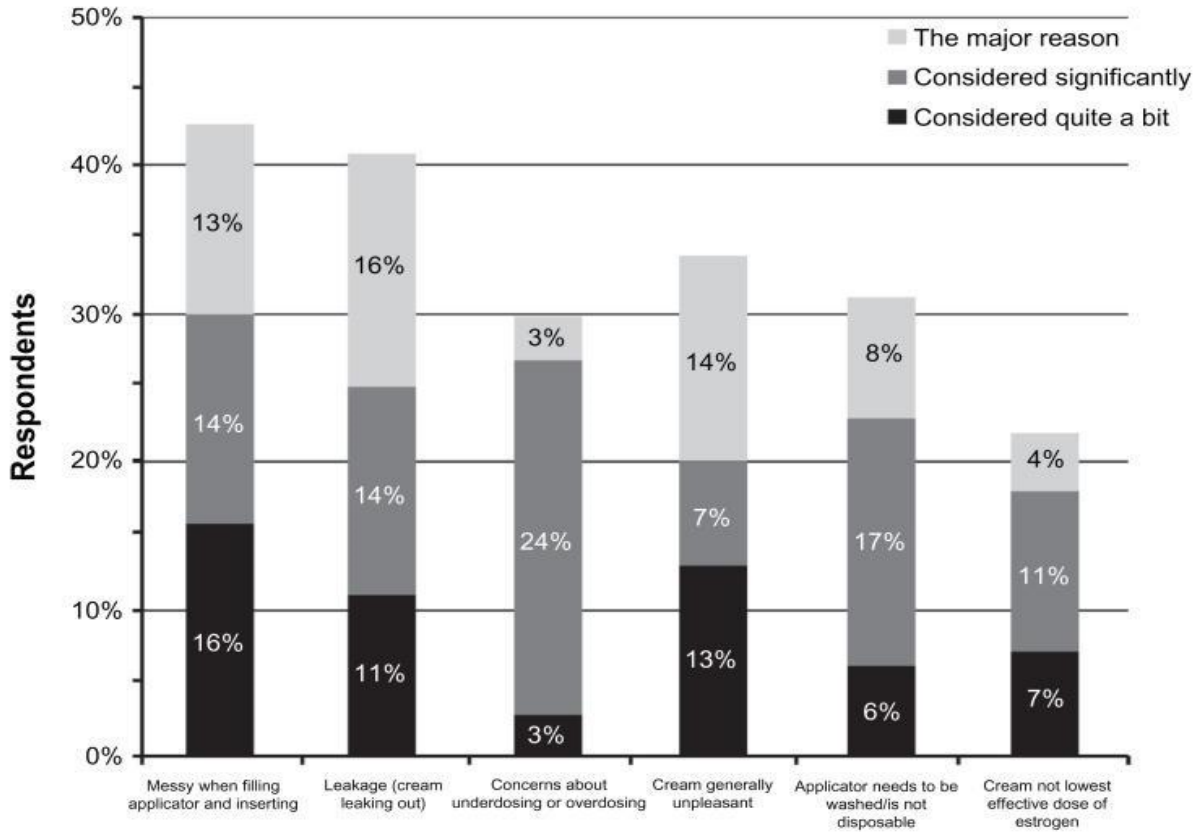

Figure 2.3: Reasons for switching from vaginal cream to vaginal tablet. Reproduced from (Minkin et al. 2013), © 2013 Minkin et al, publisher and licensee Dove Medical Press Ltd.

2.5.2 Softgel Capsules

TX-004HR, commercially traded as Imvexxy® (TherapeuticsMD, Inc., Boca Raton, FL), is 17β-estradiol low dose softgel capsule which adheres to the vaginal epithelium after manual insertion

to provide a rapid improvement in vulvovaginal atrophy symptoms in postmenopausal women with negligible to deficient systemic absorption (Constantine et al. 2017a, Kingsberg et al. 2017, Liu et al. 2020, Simon et al. 2017a). In 2018, the FDA approved two dosages (4 µg and 10 µg) of TX-004HR for the treatment of moderate to severe dyspareunia (Constantine et al. 2018, Liu et al. 2020, Mirkin et al. 2021, Simon et al. 2020). TX-004HR products are tear-shaped, small softgel capsules with about 1.58 cm length, encased by gelatin as the capsule shell (Liu et al. 2020, Paton 2018). The dosing schedule of TX-004HR includes the application of one capsule daily for the first two weeks, followed by one capsule twice per week (Abramowicz et al. 2019, Constantine et al. 2017a, Paton 2018). It is recommended to commence the treatment regimen with the lowest 4 µg capsule dosage (Abramowicz et al. 2019, Paton 2018).

The main advantages of TX-004HR capsules lies in its ability to afford local efficacy, with low systemic absorption, ease of administration, avoidance of messiness, and convenience (Pickar et al. 2016a). The TX-004HR contrasting to Vagifem®, is contraindicated in the case of suspected breast cancer, active arterial or history of venous thromboembolism, idiopathic vaginal bleeding, and estrogen-dependent neoplasia (Abramowicz et al. 2019).

The TX-004HR softgel capsule was designed to offer local estrogenic effect without escalating the systemic absorption of estradiol (Pickar et al. 2016a). The position at which the dosage form is inserted in the vaginal cavity could also have an influence in the degree of systemic estradiol absorption from vaginal formulations. The lower one third of the vaginal cavity absorbs estradiol less systemically than the upper one third, with the vulva less absorptive than the vaginal epithelium (Marino 2021). Also, the delivered dose could affect the amount of estradiol that reaches the systemic circulation. The low dose estradiol (4, 7.5, and 10µg) results in the lowest systemic absorption, while the intermediate dose (25 µg) provides to some extent higher systemic exposure (Santen 2015, Shim et al. 2021). Additionally, other factors influencing systemic absorption include the carrier used to deliver the estradiol, and the type of delivery system (Nilsson and Heimer 1992, 1995, Santen 2015). In a 12-week sub-study of the REJOICE trial, the pharmacokinetics parameters of 4, 10, and 25 µg TX-004HR softgel capsules were assessed compared to a placebo. The findings showed that the softgel capsules exhibited minor to very low systemic absorption. Additionally, there were no significant differences in estradiol measures of AUC, C_{max}, C_{avg}, C_{min}, and T_{max} between the 4 µg softgel capsules dose and the placebo. The 10 µg dose showed C_{max} was significantly higher than the placebo on Day 1 with no difference on Day 14. The pharmacokinetic parameters of the 25 µg softgel capsules dose were also

significantly higher than the placebo, but the amount of absorbed estradiol remained within the normal range for postmenopausal women (Archer et al. 2017).

Pickar *et al.* assessed the pharmacokinetics and safety of 10 and 25 µg doses of TX-004HR softgel capsules (applied to lower part of the vagina) compared to the corresponding Vagifem® tablet doses (inserted deeply in the vagina) in two randomized, single-dose, two-way cross-over, relative bioavailability trials in postmenopausal women (Pickar JH et al. 2016a). In both studies, the degree of systemic estradiol, estrone, and estrone sulfate exposure with softgel capsules were significantly lower than that of Vagifem®. Also, both doses of softgel capsules exhibited a faster systemic absorption pattern and a rapid return to baseline serum estradiol levels compared to Vagifem® (Figure 2.4). This faster absorption pattern probably reflects a more rapid release of estradiol from the oil carrier in the softgel capsules than that from the cellulosic base of the Vagifem® tablets.

The TX-004HR softgel capsules at all doses compared to placebo has also been noted to have a strong positive influence on vaginal physiology, resulting in improvement of the subjective and objective symptoms of GSM (Constantine et al. 2017a, Simon et al. 2017a). This improvement in symptoms is dose-dependent and observed as earlier as Week 2 of starting the treatment, compared to Week 12 reported with conjugated estrogens (Simon et al. 2017a). Two 12-week studies also evaluated the efficacy of 4, 10, and 25 µg doses of TX-004HR softgel capsules in treating severe to moderate dyspareunia. All three doses of TX-004HR significantly improved dyspareunia and vaginal dryness compared to a placebo (Constantine et al. 2017b, Simon et al. 2019).

2.5.2.1 Safety of softgel capsules

The topical vaginal administration of estrogens has been shown to have a lower systemic absorption compared to oral administration. Thus, vaginal administration of estrogen is expected to exhibit lower adverse events. Nonetheless, all FDA-approved local estrogen dosages prescribing information enclose a black-box warning concerning the risk of endometrial and breast cancer, cardiovascular disorders, and probable dementia (Woods 2012). To assess the safety of 10 µg TX-004HR softgel capsules, Pickar *et al.* conducted a 2-week double-blind, placebo-controlled, single center study. Results showed that 28% of participants experienced adverse events. However, all side effects were mild, and no deaths or serious events were reported (Pickar et al. 2016b). Another recent study used endometrial progesterone receptor expression as a biomarker for estradiol exposure after administration of 4 and 10 µg softgel capsules (Mirkin et al. 2021). The findings indicated that there is no significant difference in endometrial progesterone

receptor expression between the baseline and Week 12. This indicates that both doses are not expected to pose a potential endometrial safety concern (Mirkin et al. 2021). It is however noted that both studies had a relatively small sample size, with none directly measuring endometrial thickness. Additionally, neither included a safety evaluation of TX-004HR at strength of 25 µg and had short study times.

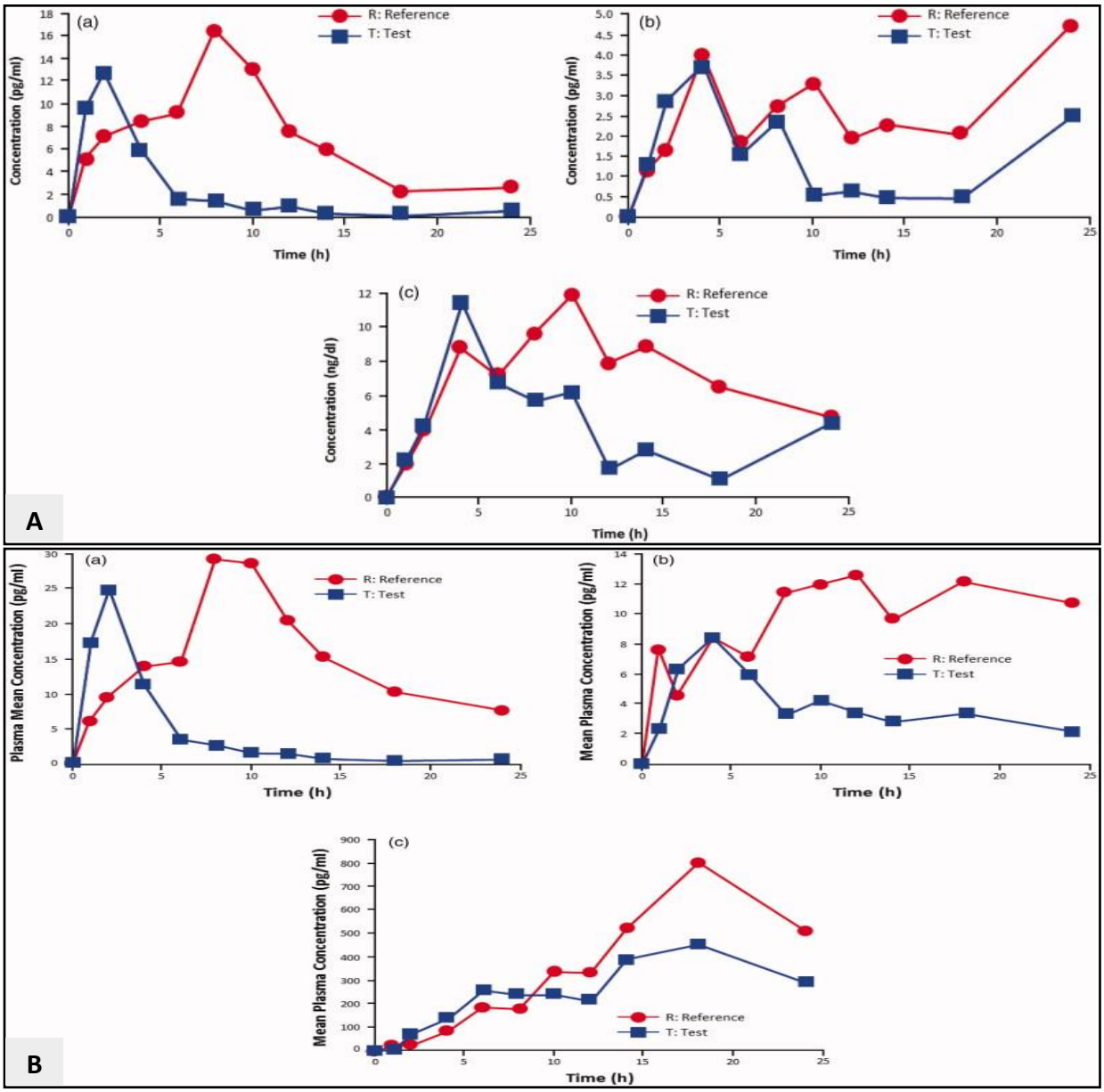

Figure 2.4: Linear plot of baseline-corrected mean plasma concentration versus time for (a) estradiol, (b) estrone, and (c) estrone sulfate after treatment with the test and reference preparations, each at (A) 10 µg and (B) 25 µg. Test product: TX-004HR; TherapeuticsMD, Inc., Boca Raton, FL. Reference product: Vagifem®; Novo Nordisk, Plainsboro, NJ. Reproduced from (Pickar JH et al. 2016a) © 2016 J. H. Pickar.

2.5.2.2 Acceptability

The TX-004HR was designed with some features to increase its acceptance by users, such as features to be used without an applicator, designed to be less messy and the dose could be

applied at any time of the day to start the treatment (Simon et al. 2017a). A survey of five questions was employed to assess the acceptability of TX- 004HR at the three strengths. Most of the participants rated the ease of product insertion as good to excellent (75% to 82.6%), and about 90% of participants found it was easy to use. The majority of participants rated the product as very satisfied or satisfied, compared to the placebo. Also, most patients very much or somewhat preferred TX- 004HR over other treatments they had used previously (Figure 2.5) and would probably or definitely use TX- 004HR again. The satisfaction, ease of insertion, and possibly reuse of TX-004HR were correlated with improved dyspareunia, vaginal pH, and vaginal dryness (Kingsberg et al. 2017). The increased patient acceptance and satisfaction may therefore lead to a higher adherence to prescribed medication regimens and lower treatment failure rates. This high level of acceptance may be due to several features of softgel capsules such as the ability to administer without an applicator in a more hygienic manner, no need to measure individual doses, less concern about systemic absorption, rapid dissolution after application, and the muco-adhesive properties of the capsules, which can decrease the rate of messiness. However, one of the limitations of this study is the need for a direct comparison with other intravaginal estradiol delivery systems.

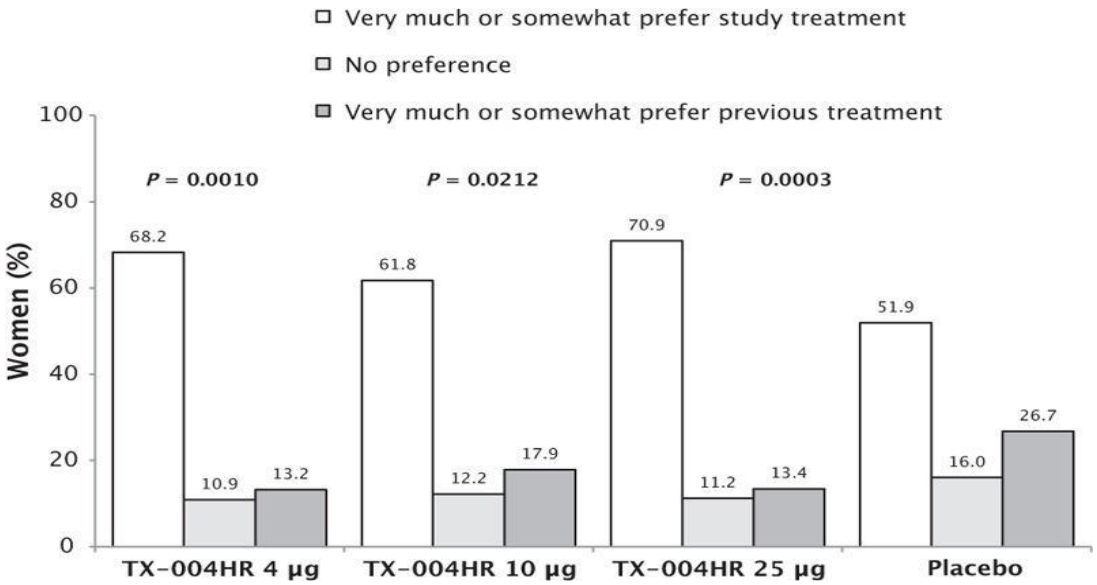

Figure 2.5: Treatment preference over previously used vulvar and vaginal atrophy treatments. P value versus placebo. Reproduced from (Kingsberg et al. 2017), © 2017 The Author(s).

2.5.3 Vaginal Rings

The vaginal ring is a drug delivery system affording the controlled release of therapeutic agents for localized or systemic effects over an extended period of time (Ridgeway et al. 2022). Vaginal rings can also be utilized for contraception and the relieving the symptoms of GSM (Ridgeway et al. 2022, Weisberg et al. 2005). The intravaginal ring, in addition to its prolonged duration of action, can overcome many of shortfalls associated with other vaginal delivery systems, such as inadequate retention time inside the vaginal cavity and difficulty of use, thus raising the effectiveness and patient acceptance (Karl et al. 2002, Speroff and Group 2003). Vaginal rings, however, have some disadvantages, such as an increased vaginal discharge and the possibility of expulsion (Rafiei et al. 2021).

FDA approval has been granted for the use of estradiol vaginal rings in the treatment of GSM and offers additional options for this condition (Bachmann 1998). Several 17β-estradiol vaginal rings are currently in commercial use, including a ring which minimally increases the level of estradiol in plasma, however not more than the normal menopausal range (Ballagh 2004). The second ring increases systemic estradiol to 40.6 pg/mL and 76 pg/mL at doses of 50 µg/day and 100 µg/day, respectively, with this ring used to treat both GSM and the systemic symptoms of menopause. Other rings for combination hormonal therapy have been described in the literature but are not commercially available (Ballagh 2004).

One of the approved products is the Estring® vaginal ring. Estring® is a soft, flexible device with an outer 55 mm diameter and 9 mm thickness, comprised of an inner core containing 2 mg of 17β-estradiol as a reservoir and covered with a release rate controlling membrane made of a silicone elastomer to release about 7.5 µg of 17β-estradiol per day for a period of 90 days (Bachmann 1998, Casper et al. 1999, Eriksen 1999, Henriksson et al. 1996, Sarkar 2003). This consistent release provides mean steady plasma concentrations of 5.7 and 7.6 pg/mL, which is suitable for the treatment of GSM (Speroff and Group 2003).

Due to its relatively high polarity, 17β-estradiol cannot be clinically delivered at a rate of at least 50 µg per day from a hydrophobic vaginal ring with a reservoir design. Therefore, the use of a suitable estradiol ester with a sufficient balance of hydrophobic and aqueous property, such as estradiol acetate, may enable effective sustained delivery at suitable rates for the treatment of the vasomotor symptoms of menopause (Woolfson et al. 1999). Estradiol-3-acetate has improved solubility in ring-forming polymer and is rapidly hydrolyzed to active estradiol in plasma and tissues. These properties enable it to provide release rates of 100 or 50 µg per day for 90 days, offering average serum concentrations of about 280 and 150 pmol/L, respectively. These serum

concentrations resemble that achieved by estradiol transdermal patches and is adequate to control the vasomotor symptoms of menopause (Al-Azzawi and Buckler 2003, Buckler et al. 2003).

A novel estradiol acetate vaginal ring of a reservoir system was approved for use in the UK in 2001 and marketed as Menoring®. In 2002, it was approved by the US FDA under the name of Femring® (Al-Azzawi et al. 2005, Ballagh 2004). This novel vaginal ring is approved for the alleviation of both vulvovaginal atrophy and the vasomotor symptoms of menopause (Chollet 2011, Kagan et al. 2019, Speroff and Group 2003). Femring® is a flexible, soft, off-white ring, composed of estradiol acetate embedded in a central core shielded with a release-rate controlling membrane. The amount of estradiol acetate load is either 12.4 mg or 24.8 mg to consistently release 50 or 100 µg of estradiol acetate per day, respectively, for a period of 90 days (Lynch 2009). The released estradiol acetate is rapidly hydrolyzed and converted to naturally occurring estradiol. The release of 50 or 100 µg estradiol per day results in average daily plasma concentrations of 40-76 pg/mL (Santen 2015, Speroff and Group 2003). Due to this systemic absorption of estradiol, women with an intact uterus need to use concomitant progestogen therapy to oppose the estradiol effect and avoid endometrial stimulation (Kagan et al. 2019, Santen 2015). Figure 2.6 illustrates the diameter and cross-sectional diameter of Femring® and Estring®.

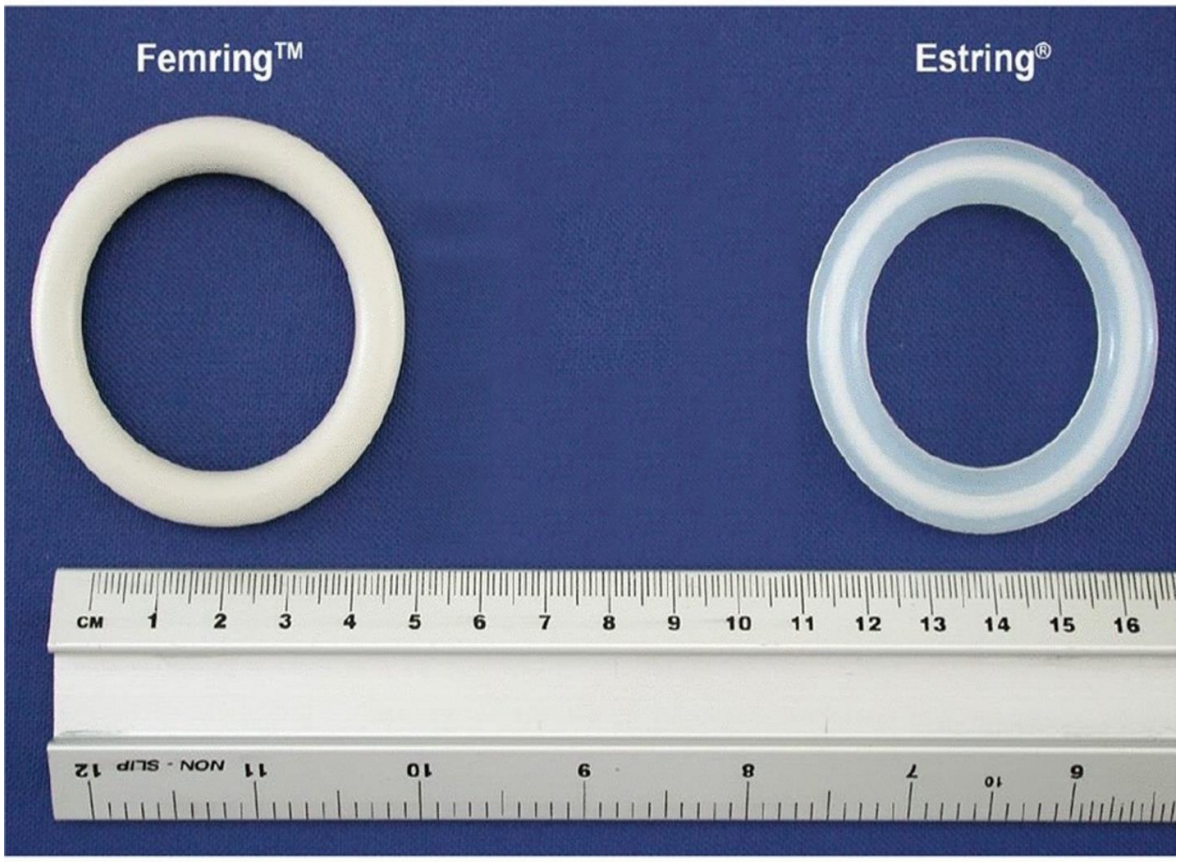

Figure 2.6: Images of the FDA approved vaginal rings for hormone replacement therapy (Estring® and Femring®) adapted from (Zhao et al. 2022) © 2022, The Author(s).

Akcess Medical Products Inc. of King of Prussia, PA, prepared rings comprising of a core of 4% 17β-estradiol in a dimethylsiloxane/vinylmethylsiloxane matrix. These rings have an *in vitro* release rate of 100, 150, 200 µg/day according to the breadth of the outside silicone membrane: 0.47, 0.28, and 0.21 mm, respectively. The dipping process was utilized in order to coat the rings with the outside release rate controlling membrane (Nash et al. 1997). Also, FEI Technologies (Plainsboro, NJ) have developed two models of toroidal shape vaginal rings with an inner core containing 4% of 17β-estradiol. One version was designed to release average of about 140 µg per day *in vitro* with the other designed to release about 60 µg per day. Both models are approximately 56 mm in overall diameter and 8 mm in cross-sectional diameter (Nash et al. 1999). Other rings composed of toroidal silicone elastomer tubing loaded with estradiol and low or high dose progesterone include the rings manufactured by FEI Technologies, designed with a 55 mm diameter and a 9 mm cross-sectional diameter. Both versions contain 0.36 g of 17β-estradiol, and 3.6 g or 1.8 g of progesterone, respectively. The low-dose and high-dose rings have *in vitro* drug release patterns of 7, 5, and 4 mg of progesterone per day and 13, 8, and 6.5 mg of progesterone

per day at 30, 90, and 180 days, respectively. Corresponding to that, both rings release estradiol at rates of 160 µg, 150 µg, and 140 µg per day. These rings provide a promising method for hormone replacement therapy with effective endometrial proliferation prevention (Maruo et al. 2002).

The development of ethylene vinyl acetate-based vaginal rings that release a combination of estradiol and progesterone may provide additional therapeutic options to those currently available. A novel ethylene vinyl acetate vaginal rings that can deliver a combination of estradiol at a rate of 160 µg and progesterone at 4 µg or 8 µg per day, were prepared by employing ethylene vinyl acetate fibers of various length and drug loading (Weiss et al. 2019). The administration of the estradiol vaginal ring by insertion into the upper third of the posterior vault of the vagina only once every three months for a maximum uninterrupted treatment period of 24 months (Al-Baghdadi and Ewies 2009, Bachmann 1998, Speroff and Group 2003), in addition to a rare expulsion rate, might lead to increased patient acceptability (Ridgeway et al. 2022).

One of the most vital issues during the designing and development of vaginal rings is the selection of the appropriate polymers, which have a significant influence on drug release patterns. The solubility and diffusivity of the drug in the polymer, and the polymer's biocompatibility and stability, are the most important factors that should be considered. The intravaginal rings are made mainly from three polymers, silicone, polyethylene-co-vinyl acetate, and polyurethane (Rafiei et al. 2021). The most common silicone is polydimethylsiloxane which is formed by the attachment of methyl groups to the siloxane backbone and is employed extensively in drug delivery and medical devices due to its biocompatibility and flexibility (Rafiei et al. 2021); also, polydimethylsiloxane, is recognized by its hydrophobicity and permeability to diffuse of different substances (Racles 2013). In addition, the polydimethylsiloxane matrices are characterized by their ability to release the steroid in a steady rate fashion for an extended period of time (Saleh et al. 2003). Two common silicone elastomers are used to manufacture estradiol vaginal rings, additive-cured and condensed-cured type silicone elastomers. Additive-cured silicone elastomers are also used in the formulation of Estring®, while Femring® is manufactured using condensed-cured silicone elastomers (Carson et al. 2021). Vaginal rings were also initially developed as homogenous systems with a steroidal drug evenly distributed in polysiloxane matrix. This resulted in a high immediate burst release, and to overcome that shortfall, the rings were coated with drug-free release-controlling membrane (Ballagh 2004).

In a study by Woolfson *et al.*, reservoir design, intravaginal rings, loaded with 17β-estradiol or its acetate ester were prepared by employing an injection molding method (Woolfson et al. 1999). A

similar method was described by Malcolm *et al.* to prepare matrix-type vaginal rings loaded with 17β-estradiol or estradiol acetate, except by coating the rings with a release rate-controlling membrane (Malcolm et al. 2003). Also, Weiss *et al.* reported a method for preparation of novel vaginal ring of 17β-estradiol and progesterone loaded ethylene vinyl acetate (Weiss et al. 2019).

Generally, all the investigational or commercially available estradiol vaginal rings are either a reservoir system, in which there is a release rate controlling membrane surround the drug core, or of a matrix system, in which the estradiol is dissolved or dispersed in a polymeric carrier. In the reservoir type, the estradiol diffuses through the membrane due to concentration gradient and the release rate usually remains constant over time. Interestingly the release of estradiol from one reservoir type ring designed to release 160 µg/day demonstrated initial burst release during the first 4 days, followed by a steady release to 100 days (Nash et al. 1999).

During pharmaceutical product development is important to understand the relation between the *in vitro* and *in vivo* release which allows the prediction of *in vivo* performance. A study by Nash *et al.* determined the relation between the *in vitro* release of three ring releasing 200, 150, and 200 µg/day and the *in vivo* release in 21 postmenopausal participants over 22 days. The authors reported that all three doses showed identical plasma estradiol levels to *in vitro* estradiol release, with plasma estradiol levels sufficient to control menopausal symptoms (Nash et al. 1997).

2.5.3.1 Safety of vaginal rings

The uncontrolled continuous release of the estrogens associated with most local vaginal estrogens delivery dosages may result in increased plasma estrogen and vaginal tissues. The estradiol vaginal ring was designed to avoid this problem (Holmgren et al. 1989). The Estring® vaginal ring is designed to release about 0.8 mg of estradiol during the first 90 days of insertion, with a systemic absorption of about 8% of the total daily estradiol released. This reduced systemic absorption of the estradiol minimizes the possibility of endometrial proliferation. The initial burst release is also not incremental and the amount of systemic absorption of the estradiol is lower in the insertion of the second and following rings. This effect is most likely due to the vaginal epithelium maturation following the initial ring (Bachmann 1998). In a multi-center, randomized, open-label, parallel-group study carried out by to evaluate and compare the systemic absorption of estradiol released from Estring® and Vagifem®, the results showed increased serum levels of estradiol and estrone in both groups throughout the treatment period, but within the normal range of postmenopausal women. The mean levels of serum estradiol in the Estring® and Vagifem® groups were found to be 16±22 pmol/l and 15±33 pmol/l at baseline and increased to 49±64 pmol/l and 36±51 pmol/l at Week 24, respectively, lessening to 20±19 pmol/l in the Estring® group and

approximately steady in the Vagifem® group at Week 48. Similarly, the mean levels of serum estrone in the Estring® group were found to be 1±0.67, 1.4±0.86, and 1.57±0.89 nmol/l at baseline, Week 24, and Week 48, respectively, while the Vagifem® group mean serum estrone levels were 1.14±1.76, 1.39±0.82, and 1.69±1.48 nmol/l at baseline, Week 24, and Week 48, respectively (Weisberg et al. 2005).

Some vaginal rings have however been constructed to provide systemic levels of estradiol. Femring® intravaginal rings allow accurate, controlled administration of drug for up to 1 year. Woolfson *et al.* demonstrated that an almost constant level of estradiol could be provided in healthy postmenopausal human volunteers for several months using an intravaginal ring (Woolfson et al. 1999). Another early study reported the preparation of two forms of vaginal rings; one as matrix ring loaded with 400 mg of estradiol and the other as a three-layer ring, in which the middle layer was loaded with 100, 200, or 400 mg estradiol. The ability of the ring to deliver systemic estradiol was examined in 14 castrated and postmenopausal women. Both ring designs resulted in burst release after insertion, with the three layer design returning to base line levels within one day, while the matrix type maintained estradiol levels for a minimum of one week above 300 pg/ml, and thereafter at 109-159 pg/ml for a period of 90 days (Stumpf et al. 1982).

The controlled continuous release vaginal ring delivery systems employed for hormonal replacement therapy have been shown to be effective for GSM compared to a placebo and other vaginal estrogen-medications. Casper *et al* evaluated the efficacy and safety of Estring® in comparison to a placebo and 0.5 mg estriol pessaries in two trials (Casper et al. 1999). The Estring® group showed significant improvement in dyspareunia, maturation value, and reduced pH value compared to the placebo group. On the other hand, even though the participants treated with Estring® exhibited higher cure rates than the pessaries group, both dosages showed equivalent efficacy at Weeks 3 and 12. Additionally, the occurrence of adverse events was not significantly different between the groups. Few participants reported non-serious adverse effects such as local irritation of the vagina, while the Estring® group showed a minimal increase of endometrial thickness by 0.3 mm. A similar study evaluated and compared the efficacy of Estring® with 0.5 mg estriol pessaries (Henriksson et al. 1994). The subjective and objective symptoms were improved excellently in both treatment groups. The vaginal cytology assessment showed significant vaginal epithelium maturation in the Estring® group, compared to the pessary group. In addition, at Week 12, 20% of the Estring® group demonstrated vaginal mucosa atrophy, compared to 58% of the estriol pessaries group.

A study by Weisberg *et al.* also compared the efficacy of Estring® versus Vagifem® in the alleviation of GSM (Weisberg et al. 2005). The results demonstrated that the urogenital symptoms were improved greatly in both groups, with the pH of the vagina reduced to 5 at three months, and the signs of atrophy decreased from about 90% to about 15% at Week 48. In addition, 8% of the Vagifem® group had fully mature vaginal epithelium, compared to about 26% of the Estring® group. Another study by Smith *et al.* evaluated the effect of a vaginal ring containing 2 mg 17β-estradiol in a silicone core (E2-IVR; US Pat 4888074-A and 4,871,543) on the atrophic vaginal mucosa (Smith et al. 1993). The hormone dosage was controlled by changing the surface area of the ring. The vaginal atrophy symptoms were improved with a dosage of 5-10 µg/day when used for 90 days without endometrial proliferation.

The effectiveness of vaginal rings that deliver high doses of estradiol have also been evaluated in many studies. These novel vaginal rings produce a constant plasma concentration of estradiol over an extended period of time, sufficient to effectively treat both vasomotor and genitourinary symptoms of menopause. A study by Nash *et al.* evaluated vaginal rings delivering 60 and 140 µg per day, *in vitro*, for the relief of menopausal symptoms (Nash et al. 1999). The mean estradiol levels were 123 and 307 pmol/l for the 60 and 140 µg estradiol releasing rings, respectively, and the estrone levels were higher than estradiol levels by 2.6 and 1.7 fold for the low and high dose ring respectively. The authors found that the rings were effective in correcting genitourinary symptoms and reducing hot flashes by 80% over 6 months. Another double-blind, randomized, multicenter study evaluated and compared the efficacy and safety of a 50 µg/day Menoring® to a 1 mg per day oral estradiol formulation in 159 postmenopausal women. The Menoring® demonstrated significant reduction in vasomotor symptoms severity and frequency similar to that of oral dosage forms. Moreover, Menoring® showed excellent acceptability and was well tolerated by participants (Buckler et al. 2003).

In addition to its effectiveness in controlling GSM, estradiol vaginal rings have shown beneficial effects in controlling urinary tract infections associated with decreased estrogen levels during menopause. Eriksen evaluated the ability of Estring® to prevent the recurrence of urinary tract infections in postmenopausal women (Eriksen 1999). The findings demonstrated that Estring® was valuable in delaying the recurrence and reduced the recurrence of urinary tract infections per year, with the ability to improve the other urogenital symptoms among the postmenopausal women significantly. In addition, Estring® is well tolerated and has exhibited a safe profile.

The risk of endometrial stimulation associated with the use of long term use of unopposed estrogens therapy is, however, considered a major concern (Henriksson et al. 1994, Weisberg et

al. 2005). The estradiol release pattern from the vaginal ring is consistent at a level of about 7.5 µg/day after a short period of initial burst release. This release pattern is expected to result in minimized systemic estradiol absorption, resulting in a decreased probability of serious events occurrence. Many studies have evaluated the safety profile of estradiol vaginal rings compared to other estrogens delivery systems. Two relatively short-term studies (Ayton et al. 1996, Henriksson et al. 1994) compared the safety of Estring® to 0.625 Premarin® cream and estriol pessaries. The findings showed that there is no significant difference between the ring and cream in the incidence of bleeding or endometrial response following a progestogen challenge test. Additionally, the events reported by the Estring® group were vagina burning sensation, breast enlargement, migraines, edema, and urinary incontinence. On the other hand, the estriol-treated patients reported vaginal itching, breast enlargement and pain, with one patient reporting severe bleeding on days two through five. Another study in 2005 looked at the potential for a local effect on the endometrium with the longer-term use (48-weeks total) of Estring® and Vagifem® (Weisberg et al. 2005). The safety of treatment on the endometrium was evaluated by measuring the endometrial thickness and the progestogen challenge test at baseline and Week 48. The findings demonstrated that there was no significant difference in the change in endometrial thickness between the two groups ($p=0.81$). After the progestogen challenge test, bleeding was uncommon, although there is a statistically significant difference between the two groups, where no Estring® group participants had bleeding, while four participants of the Vagifem® group reported this event.

In postmenopausal women with an intact uterus, the use of estrogen containing products with high doses, further increases the risk of endometrial stimulation. To reduce this risk, it is recommended to add a progesterone with the aim to oppose the effect of estrogens on the uterus. Maruo *et al.* studied estradiol vaginal rings loaded with low doses of progesterone for hormonal replacement and endometrial proliferation (Maruo et al. 2002). The vaginal rings, which delivered estradiol at a rate of about 150 µg/day and progesterone of about 9 mg/day or 5 mg/day, were used continuously for 4 and 6 months by postmenopausal women. The results showed an improvement in vasomotor and vaginal symptoms and a decreased incidence of bleeding relative to the pre-treatment status. Also, the authors concluded that the used doses of progesterone were adequate to prevent endometrial proliferation.

A similar study by Hamada *et al.* evaluated two models of vaginal rings to relieve menopausal symptoms in postmenopausal women with an intact uterus and prevent endometrial hyperplasia during a four month study period (Hamada et al. 2003). The models were designed to release 10 mg and 20 mg of progesterone per day *in vitro*, respectively. Both rings were also designed to

release 160 µg estradiol per day *in vitro*. There was a significant reduction in the incidence of hot flashes and night sweats, and a noticeable improvement in mood. Participants in both groups reported an increase in vaginal discharge during the first 6 weeks. The incidence of vaginal bleeding was more common among participants in the high progesterone ring group. Endometrial assessments in both groups showed endometrial thickness of less than 3 mm throughout the treatment period. Hence, the combined estradiol-progesterone vaginal ring could potentially be used for long-term hormone replacement therapy with effective protection of the endometrium.

2.5.3.2 Acceptability

The acceptance of the vaginal ring to deliver low dose estrogens to the vaginal tissues remains of high interest as the ring may dislodge and requires a health care practitioner to insert a new ring every 90 days. A systemic review (Ridgeway et al. 2022) demonstrated that the acceptability of the vaginal rings varied according to the intended indication, accessibility of other dosage forms, and expected risk. Generally, the acceptance of vaginal ring is highest when indicated for the treatment of GSM compared to contraception. Also, many studies compared the acceptability of estradiol vaginal rings to other estrogen dosages or a placebo. One study found that there is no statistically significant difference in the acceptability between Estring® and Vagifem®. The finding showed that 85% and 83% of Vagifem® and Estring® treated patients, respectively, reported the products as excellent or good, while only 4% Vagifem® treated patients and 3% Estring® treated patients reported the products as bad or unacceptable (Weisberg et al. 2005). Other studies (Ayton et al. 1996, Barentsen et al. 1997, Casper et al. 1999, Henriksson et al. 1994) showed more significant acceptability for Estring® compared to Premarin® cream, estriol cream, and estriol vaginal pessaries. This high acceptance over creams and pessaries may be attributable to the leakage and messiness associated with these dosage forms. The acceptability of Femring® was also assessed by Speroff and coworkers in a multi-center, double blind, randomized, placebo-controlled phase 3 trial. The vaginal ring showed significant improvement in urogenital and vasomotor symptoms, mild-moderate adverse events, and was well tolerated. The majority of women found the ring was easy to remove and reinsert and only a small number of participants reported discomfort during intercourse (Speroff and Group 2003). Although the estradiol vaginal rings are associated with a high acceptance rate, more research is needed to clarify the impact of the ring's physical features such as flexibility, outer diameter, and cross-sectional diameter on patient acceptability.

2.5.4 Vaginal Creams

Vaginal creams as a delivery system are associated with several limitations and drawbacks, such as being messy, dosage leaks, and sometimes not offering the precise dose (Rahman and Ahmed 2016). Estrace® is a 0.01% estradiol vaginal cream and was approved by the FDA in 1984 for the treatment of vulvovaginal atrophy in postmenopausal women (Archer et al. 2018). The recommended dose schedule for Estrace® cream is 2-4 grams applied daily for the first two weeks with a gradual decrease of the dose to half over 1-2 weeks. Afterwards, one gram is applied once to three times per week as a maintenance dose (Lindahl 2014). Little data and information exist on the acceptability and systemic absorption of estradiol after using Estrace® cream. However, several phase 3 clinical studies (NCT03294538 (ClinicalTrials.gov), NCT03332303 (ClinicalTrials.gov), NCT02995694 (ClinicalTrials.gov), and NCT02195986 (ClinicalTrials.gov)) were performed to evaluate and compare the therapeutic equivalence and safety of generic 0.01% estradiol vaginal creams to the FDA listed Estrace® vaginal cream.

A study by Rigg *et al.* evaluated and compared the systemic estradiol absorption of two cream concentrations (2 mg or 0.2 mg estradiol per 2g cream) with Premarin® cream (Rigg et al. 1978). The products were evaluated in six women with the sequence determined by a latin square design and the serum estradiol and estrone levels measured using a radioimmunoassay. In the 2 mg dose, the serum estradiol concentrations were significantly raised ($p<0.05$) within 15 minutes and the C_{max} (527pg/ml) was reached at 4 hours after application. The levels thereafter decreased gradually but remained 19 times greater than the baseline level at 24 hours. The 0.2 mg dose increased serum estradiol level ($p<0.01$) within 30 minutes and the C_{max} (80pg/ml) was reached at 4 hours, with the concentration decreasing to 34pg/ml at 24 hours. Contrary, Premarin® resulted in a slow rising in systemic estradiol and the C_{max} (33pg/ml) was observed 6 hours after application, with the concentration decreasing at 24 hours to levels similar to the baseline level. Another study measured and compared the systemic absorption of estradiol and estrone following application of 0.01% Estrace® cream and 1.25 mg Premarin cream in 29 postmenopausal women for two weeks. The Estrace® cream showed increased serum estradiol estrone levels to about 4-fold and 2.5-fold, respectively, within 12 hours of first application. The levels of both estradiol and estrone after two weeks of daily application were found to be the same levels as 12 hours after initial application. Additionally, the levels of estradiol and estrone in Premarin treated group at 12 hours and after two weeks were found to be significantly lower than that of the Estrace® cream. These findings indicated that the topical vaginal estradiol cream is rapidly absorbed into the systemic circulation and can result in appreciable blood levels of estrogen (Martin et al. 1979).

2.5.4.1 Safety of vaginal creams

With the vaginal tablet and ring dosing regimens, patients receive approximately 1.14 mg and 2.74 mg of estradiol over a one-year treatment period, respectively, while vaginal cream exposes the patient to higher doses of estrogen (Chism 2012), with the use of 0.01% estradiol cream (considered as high-strength) associated with high systemic exposure. Consequently, the European Medicines Agency in 2020 recommended that the use of the 0.01% estradiol cream be limited to a 4-week period (European Medicines Agency 16.January.2020, Hirschberg et al. 2021). In addition, FDA guidance recommends the use of appropriate low doses of estrogens in order to reduce systemic estrogen exposure (Archer et al. 2018, Kroll et al. 2018). Two randomized, double-blind, placebo-controlled studies from the same working group (Archer et al. 2018, Kroll et al. 2018) examined the efficacy and safety of investigational very low dose 0.003% estradiol creams (three times lower than Estrace®). Both trials found that the 0.003% cream is effective and well tolerated. The authors further identified that the daily application of estradiol cream for two weeks followed by three times per weeks, resulted in a significant improvement on superficial cells, decreased parabasal cells, reduced vaginal pH, decreased vaginal dryness severity, and improvement in dyspareunia. In terms of safety, there is no significant difference between estradiol and the placebo groups except for vulvovaginal mycotic infections, which were more frequent with the estradiol group. The 0.003% estradiol cream also provides very low doses (15 µg per application), which ensures effectiveness and minimize systemic absorption. The cream is also compatible with FDA recommendation and similar to that provided by the 10-25 µg approved tablets (Archer et al. 2018, Kroll et al. 2018). It was noted that in this study, the majority of participants were of a single demographic, therefore the results of both studies may not be generalized to all ethnic groups. Additionally, the systemic absorption of estradiol was also not measured in any of the studies, although the creams tested contained small amounts of estradiol and systemic exposure would be expected to be negligible. Furthermore, both studies did not report the incidence of messiness and leakage, which may highly impact the acceptance rate, and the safety of the creams, which should be evaluated in long-term studies. Another study, more recently in 2020, evaluated the efficacy of a 25µg estradiol gel on postmenopausal patients with vaginal atrophy (Tanmahasamut et al. 2020). Although the findings demonstrated significant improvement in laboratory markers between participants of the estradiol group compared to the placebo group, the most bothersome symptoms of GSM were improved equally with no significant difference between both groups. This may be due to the lubricant effect of K-Y® Jelly, which was used as placebo in the study. Also, in this study, the analysis of serum estradiol level showed no higher concentration of estradiol than the reference level in postmenopausal women. In addition,

there was no increase in endometrial thickness and no adverse events reported at Week 4 or Week 8. Another 12-weeks study evaluated the efficacy of various doses of estradiol cream (10, 5, 2.5, and 1.25 µg) for the alleviation of GSM symptoms. The 10 µg dose demonstrated reduced pH and improved vaginal cytology. The systemic estradiol remained within the postmenopausal range and there was no effect on the endometrium (Santen et al. 2002).

The lower urinary tract is rich with estrogens receptors; hence, the application of estrogen is expected to have a useful outcome on urinary tissue, function and symptoms. Several studies have therefore examined the efficacy of estrogen in treatment of overactive bladder and urinary incontinence. The intravaginal estrogen treatment was shown to be more beneficial for the lower urinary tract than oral formulations (Ellington et al. 2016). Ellington *et al.* compared the efficacy of Estrace® cream with an oral tolterodine formulation for the treatment of overactive bladder symptoms in a 12-week single-site randomized, open-label trial. The authors found that there is significant improvement in overactive bladder symptoms in both groups from baseline to 12-weeks, with no difference between the two groups of treatment (Ellington et al. 2016).

2.5.4.2 Acceptability

The effectiveness of local estrogen therapy is greatly affected by the adherence to the treatment. Breakdown of the recommended dosing schedule increases the probability of treatment failure. The treatment adherence may also be attributable to a fixed dosing schedule, the formulation being less messy, and the convenience of the system (Portman et al. 2015). Locally-administered vaginal estrogens creams however are associated with many limitations including being messy, uneven application intervals, with many patients finding the cream difficult to apply, especially in the elderly (Ayton et al. 1996, Smith et al. 1993). In a retrospective study, comparing adherence of postmenopausal women with vulvovaginal atrophy to vaginal estrogen therapy, it was found that women who used Premarin® or Estrace® cream terminated treatment earlier than those on the 10 µg Vagifem® tablet (Portman et al. 2015). The investigators followed 30,197 women, 40.4% of them who started the treatment with Premarin® cream, 38.3% initiated with Estrace® cream, and 21.3% with Vagifem® tablets. Throughout a one-year follow-up, 57.8% of Vagifem® users terminated the therapy after the first prescription fills in contrast to 86.2% - 89.4% of the cream users ($p<0.0001$). The average treatment period was 44.6 to 48.1 days for the creams compared to 103.4 days for Vagifem® ($p<0.0001$).

2.6 Advanced Estradiol Drug Delivery Systems for Menopausal Symptoms

With the large number of developed and marketed oral tablets, vaginal rings and creams, advanced platforms have been researched to enhance patient treatment, safety, and acceptability. Hormonal replacement therapy has also been investigated to be delivered through various routes such as orally, nasally, dermally, vaginally, and intramuscularly, where the dose regimen could be customized to each patient (Águas et al. 2020).

The availability of versatile polymers and their incorporation into drug delivery systems has been made a remarkable advance in this field of research. Several of these polymers have been employed in the formulation of vaginal delivery systems to address practical challenges such as leakage and imparting sustained controlled release (Thapa et al. 2022). Other systems have been developed for the delivery of estradiol topically. Estradiol transdermal spray solutions are considered appropriate delivery systems for the alleviation of menopausal symptoms, especially for women with diabetes mellitus hypertriglyceridemia and those with altered liver function. These delivery systems offer better bioavailability, steady estrogen levels and estradiol/estrone ratio over extended periods of time and are associated with low adverse events compared to oral estrogen (Águas et al. 2020). Additionally, the transdermal spray delivery systems are free of shortfalls related to traditional transdermal estradiol delivery systems (Buster 2009). One novel transdermal spray solution is Lenzetto® (Gedeon Richter Plt., Hungary) which contain 1.53 mg of estradiol per 90 µl one spray dose (Águas et al. 2020, Buster 2009). The Lenzetto spray container contains 95% ethanol, octisalate (as skin penetrating agent), in addition to the 17β-estradiol. The application of the dose is controlled to the specific area by using a plastic housing, which is controlling the angle and distance of the sprier from surface of the skin (Buster 2009).

Additionally, in a study by Križman *et al.*, the practicability of silk fibroin xerogels as an implantable drug delivery system for continuous controlled-released estradiol delivery in hormone replacement therapy was investigated (Križman et al. 2021b). The system exhibited sustained *in vitro* release for more than four months (Figure 2.7) and a biodegradation pattern suitable for the extended term delivery of estradiol. The system could also offer an attractive alternative to conventional systems and could be useful in future clinical applications.

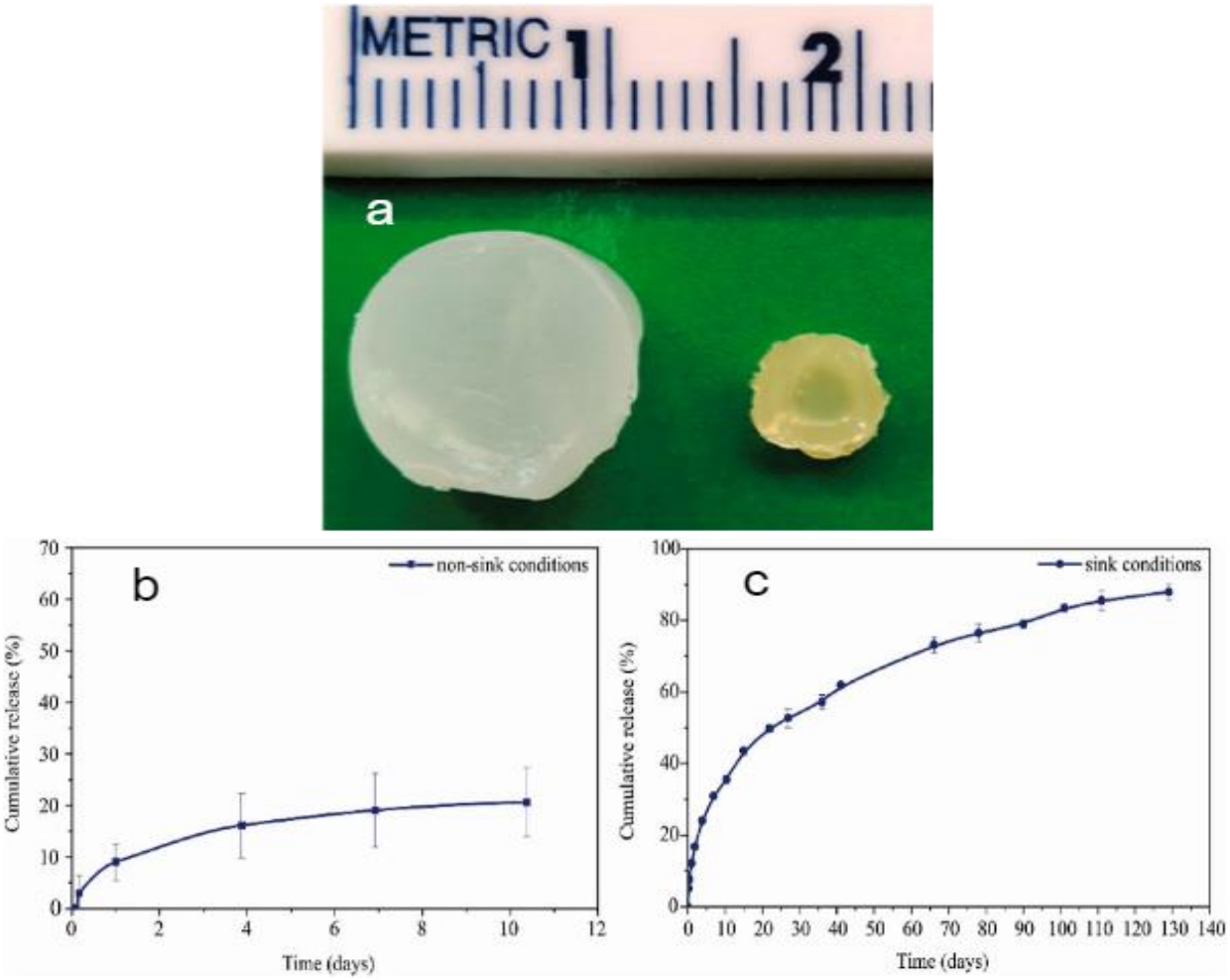

Figure 2.7: (a) Morphology of silk fibroin hydrogel (left) and xerogel (right) samples with estradiol; *in vitro* release profiles of estradiol from xerogel delivery systems in (b) non-sink and (c) sink conditions (arithmetic means and standard deviations of n = 3). Adapted with permission from (Križman et al. 2021b) © 2021 Elsevier B.V.

2.7 Concluding remarks

GSM is a common, chronic, under-diagnosed, and under-treated condition due to decreased estrogen levels throughout menopause. The treatment of GSM should be continued for extended periods of time as long as the condition persists. Local vaginal low dose estrogen therapies are employed for treatment of mild to severe GSM when over-the-counter therapies fail to control symptoms. A variety of pharmaceutical delivery systems of low dose estradiol in the form of tablets, softgel capsules, creams, and rings are approved and available and in use for the site-specific release of estradiol into vaginal tissues. These products, with the exception of the vaginal rings which are applied every three months, are administered locally in a complicated dose

regimen, where multiple administrations are often required per week. All forms are effective and provide rapid improvement in the subjective and objective symptoms of the GSM, but not the vasomotor symptoms, except when using the high dose Femring®. Additionally, all local estradiol containing formulations exhibit negligible to low systemic estradiol exposure in levels that do not exceed the normal postmenopausal range. This low absorption of estradiol, associated with non-significant differences compared to a placebo in the incidence of endometrium stimulation, is free of the risk of serious side effects of systemic estrogen treatment. However, vaginal estradiol formulations often have side effects such as bleeding, discharge, and breast pain. The choice of a particular local estradiol delivery system is highly determined by the patient's acceptability and preference, and this should be considered in the development of pharmaceutical systems for the treatment of GSM.

An effective strategic approach to address the challenges highlighted in this chapter involves the development of intrauterine implantable delivery systems capable of sustaining hormone release over extended duration. Such advancements aim to enhance patient adherence and maintain optimal hormone levels while mitigating the drawbacks of frequent dosing, thereby improving treatment efficacy. However, the long-term use of estrogenic medications such as in an intrauterine implantable device may raise concerns regarding the endometrial hyperplasia and risk of endometrial cancer. To mitigate these risks, incorporating progestogens like NETA which can act as a counter-estrogenic intervention can be beneficial. Hence, the subsequent chapter (Chapter 3) will explore the formulation and assessment of an intrauterine polymeric delivery system loaded with NETA to address the risks associated with prolonged estrogen therapy. This NETA-loaded unit has thereafter been included with an E2-loaded and an IND-loaded unit on a single IUD for the treatment of GSM, which has been provided in Chapter 4.

CHAPTER 3

3 A Novel Intrauterine Device for the Spatio-Temporal Release of Norethindrone Acetate as a Counter-Estrogenic Intervention in the Genitourinary Syndrome of Menopause

3.1 Introduction

In context of hormonal management of GSM, a crucial consideration is the physiological consequences associated with unopposed estrogen therapy. This regimen may trigger uterine endometrial thickening, a consequence of a disrupted estrogen-progesterone balance, fostering endometrial hyperplasia, carcinoma, polyps, and fibroids (Abdelgader et al. 2023, Angelou et al. 2020, Elsokkary et al. 2016, Hill et al. 2016). The concurrent utilization of progestogens therefore offers a means to counteract the effects of estrogen on the endometrial tissues, thereby reducing the risk of endometrial hyperplasia (Abdelgader et al. 2023, Elsokkary et al. 2016). The oral route is the most common method for administering progestogens in postmenopausal hormone therapy. However, oral administration is associated with first-pass hepatic metabolism, with the extent of metabolism varying based on the chemical structure of each progestogen. To circumvent first-pass hepatic metabolism, alternative routes have been explored, including the intra-muscular, vaginal, percutaneous, intranasal, sublingual, and rectal routes (Caufriez 2007, Palacios and Mejía 2016). The drawback of systemic progesterone administration, however, is its potential to interact with various steroid receptors, leading to stimulation or blockage of estrogen, androgen, glucocorticoid, and mineralocorticoid receptors, in addition to its action on progesterone receptors, while the most common adverse effect of vaginally administered progestogens is irregular vaginal bleeding. Furthermore, continuous estrogen-progestogen therapy typically results in amenorrhea for most women (Palacios and Mejía 2016). Moreover, progestogen administration through transdermal delivery using creams or gels, may not achieve sufficient endometrial effects due to lower circulating hormone concentrations. It is also noteworthy that systemic progestogen administration can additionally influence lipid profiles in the bloodstream, dependent on the progestogen type and co-administered estrogen dosage (Ostad et al. 1998).

The adoption of site-specific, sustained-release progestogens, delivered by an IDDS, presents a strategic approach to counteracting the proliferative effects of estrogen on endometrial tissues. This intervention holds promise for mitigating the undesirable side effects related to existing

progestogen treatments and may additionally serve as a viable option for addressing dysfunctional uterine bleeding and menopause-related complications (Ostad et al. 1998).

IDDSs have, in recent times, garnered significant research interest, with a predominant focus on the utilization of polymeric biomaterials in their development (Stewart et al. 2020, Wsoo et al. 2021). IDDSs are specifically designed to be placed within the body, providing continuous release of a targeted drug, at a controlled rate, over an extended duration. The primary advantages of IDDSs over conventional delivery methods, such as oral and parenteral approaches, include an increased effectiveness and reduced side effects associated with the lower drug doses, thereby promoting superior patient compliance, as well as substantial economic savings within healthcare systems (Bassand et al. 2023, Karunakaran et al. 2021, Korelidou et al. 2022, Muhindo et al. 2022, Penhasi et al. 2020, Varela-Fernández et al. 2021).

IDDSs can be classified into two main types: standalone implants employed for therapeutic purposes (e.g., delivering of contraceptives or treating periodontal and ophthalmic diseases) and secondly as part of a functional implant to enhance the success of the overall implantation procedure by preventing complications like rejection, infection, and inflammation (e.g., in the use of drug-eluting stents or orthopedic implants). Additionally, certain IDDSs combine features of both types, as observed in biodegradable stents and scaffolds used in tissue engineering (Penhasi et al. 2020). IDDSs can be further categorized as either biodegradable or non-biodegradable, depending on the type of polymer employed. Non-biodegradable implants are typically crafted using non-biodegradable polymers, necessitating removal from the body upon drug depletion, with drug release mechanisms being easily predictable due to the stable structure of these polymers. Conversely, biodegradable implants, fabricated from polymers that undergo degradation, have their drug release primarily governed by the rate of polymer degradation (Wsoo et al. 2021).

Intrauterine devices (IUDs) are implantable platforms used for a variety of applications including for contraception, as well as for the treatment of various ailments within the female genitourinary system (Nelson and Massoudi 2016). The manufacturing methods employed for IUDs have involved extrusion, 3D printing, and injection molding (Holländer et al. 2016). The selection of suitable polymers for IUDs is however limited due to the requirements of non-swell-ability and non-biodegradability, or alternatively, a very slow degradation rate. Commercially available IUDs thus primarily employ non-degradable polymers, such as polydimethylsiloxane (PDMS). Mirena®, a widely used long-lasting contraceptive IUD, exemplifies this category and is composed of a

polyethylene backbone, a drug delivery cylinder, and is enveloped by a rate-controlling PDMS membrane (Holländer et al. 2016)

Norethindrone, a synthetic progestin categorized within the 19-nortestosterone derivatives family, is utilized synergistically with oral contraceptive formulations or as a standalone progestin-only pill. It is efficacious in treating various conditions, including premenstrual syndrome, irregular or painful menstruation, abnormal heavy bleeding, menopausal syndrome, and period postponement. Additionally, it has applications in preventing uterine hemorrhage in complex non-surgical or pre-surgical gynecologic cases and for the management of nonresponsive cyclical mastalgia. Oral norethindrone is characterized by a half-life of approximately 10 hours and is administered orally once per day (Al-Nimry et al. 2019).

PCL, an aliphatic polyester polymer synthesized via the ring-opening polymerization of ε-caprolactone (Lam et al. 2008, Lu et al. 2012, Luo et al. 2021), stands at the forefront of drug delivery system exploration, manifesting in various forms such as films, nano and microparticles (Pathak et al. 2014). Esteemed by the US FDA for medical application, PCL finds utility in implantable devices for sustained drug release, spanning contraceptives among other various medications (Annuryanti et al. 2023, Cheng et al. 2009, Elbjorn et al. 2023, Manini et al. 2021, Puga et al. 2012). Its commendable attributes encompass solubility across a spectrum of organic solvents, a robust drug-loading capacity, non-toxicity, ready availability, and cost-effectiveness (Ma et al. 2006, Muhindo et al. 2022, Pan et al. 2019). Furthermore, PCL exhibits bio-resorbability, coupled with excellent biocompatibility (Boia et al. 2019, Kalva et al. 2023, Lebourg et al. 2008, Li Shu et al. 2021), and a gradual biodegradation rate relative to other polymers, rendering it an optimal choice for prolonged implantation setups (Kemala et al. 2012, Wsoo et al. 2021). PCL degrades harmlessly while preserving its primary structure when exposed to biological fluids (Elbjorn et al. 2023, Khalili et al. 2022). Hydrolysis-induced random chain scission of the ester group dictates degradation timelines, ranging from 2 to 4 years contingent upon molecular weight (Annuryanti et al. 2023, Lyons et al. 2008). The controlled release of drugs from the PCL matrix primarily aligns with water sorption and hydrolytic degradation mechanisms (Boia et al. 2019). PCL further exhibits remarkable permeability to low molecular species and different drug array under physiological temperatures (Lyons et al. 2008, Muhindo et al. 2022). Its distinctive thermoplastic attributes, delineated by lower melting (60°C) and glass transition temperatures (-60°C) (Kaluzynski et al. 2022, Lei et al. 2010), coupled with a high decomposition temperature of 350°C, underscore exceptional processability, customizable physical and mechanical properties, and stability under elevated temperatures (Lam et al. 2008, Pan et al. 2019, Varela-Fernández et

al. 2021). PCL sustains structural integrity long-term within the body before eventual metabolization and complete excretion (Li Shu et al. 2021, Ma et al. 2006). All these features positioning PCL as an exemplary candidate for the development of implant-based drug delivery systems. Recent strides in technology offer a pathway to tailor and tune PCL's degradation kinetics and drug release rates, attained through the creation of copolymers or physical blends with compatible agents (Kemala et al. 2012, Puga et al. 2012). In this regard, the preference for blending PCL with biocompatible polymers, over the development of entirely new copolymers, is driven by considerations of cost-effectiveness and enhanced safety predictability, although research in this domain remains relatively limited (Kemala et al. 2012, Puga et al. 2012). The adaptability of PCL to form miscible blends with a diverse range of polymers further emphasizes the practical utility of blend formulations (Khalili et al. 2022, Li et al. 2010, Pan et al. 2019). Additionally, the intrinsically low steroid permeability of PCL dictates specific modifications when contemplating steroid delivery (Ma et al. 2006). This nuanced understanding contributes to the evolving landscape of controlled drug release systems and holds significance for applications in various biomedical contexts.

EC is a cellulose derivative known for its versatility, achieved through the conversion of hydroxyl groups in glucose units to ethyl ether groups. Recognized for its water-insolubility, good solubility in organic solvents, low biodegradability, biocompatibility, nontoxicity, cost-effectiveness, thermoplasticity, inert nature, stability, ease of processing, and mechanical strength, EC proves to be an ideal choice across various applications (Beikzadeh et al. 2021, Maji et al. 2012, Mohebian et al. 2022). Particularly notable in the pharmaceutical industry, EC excels in sustained-release systems, earning its place as a valuable component in drug delivery systems due to its controlled-release characteristics (Abbaspoor et al. 2018). These attributes are demonstrated in sustaining the effects of anticancer, anti-inflammatory, and anti-infective agents, as well as serving as a film-forming agent and a binding agent in controlled-release solid dosage units (Ahmed et al. 2020). EC films and microspheres exhibit excellent extended drug release properties, especially for highly water-soluble drugs (Liu et al. 2010). Additionally, its unique properties make EC suitable for formulating hybrid composites with various materials. Moreover, the physico-chemical attributes of EC, including compressibility, passivity, and hydrophobic characteristics, heighten its appeal in the preparation of lipophilic pharmaceutical dosage forms (Mohammad et al. 2017).

This chapter therefore provides for the fabrication, optimization, and evaluation of NETA-loaded, hollow, cylindrical polymer-based device for implantation in the uterine cavity as a counter-

estrogenic intervention in the treatment of GSM. The developed system, which is adaptable to patient-specific estrogen therapy, is prepared from a polymer blend comprising PCL and EC and has been designed for the sustained release of NETA. The device has been statistically optimized using a two-factor, two-level factorial design (2^2), with the mechanical properties, degradation, swelling, and *in vitro* drug release of NETA from the device evaluated. The morphological characteristics of the platform were further investigated through scanning electron microscopy in addition to cytocompatibility studies using NIH/3T3 cells. Figure 3.1 represents the schematic representation of the polymer-based IUD loaded with NETA.

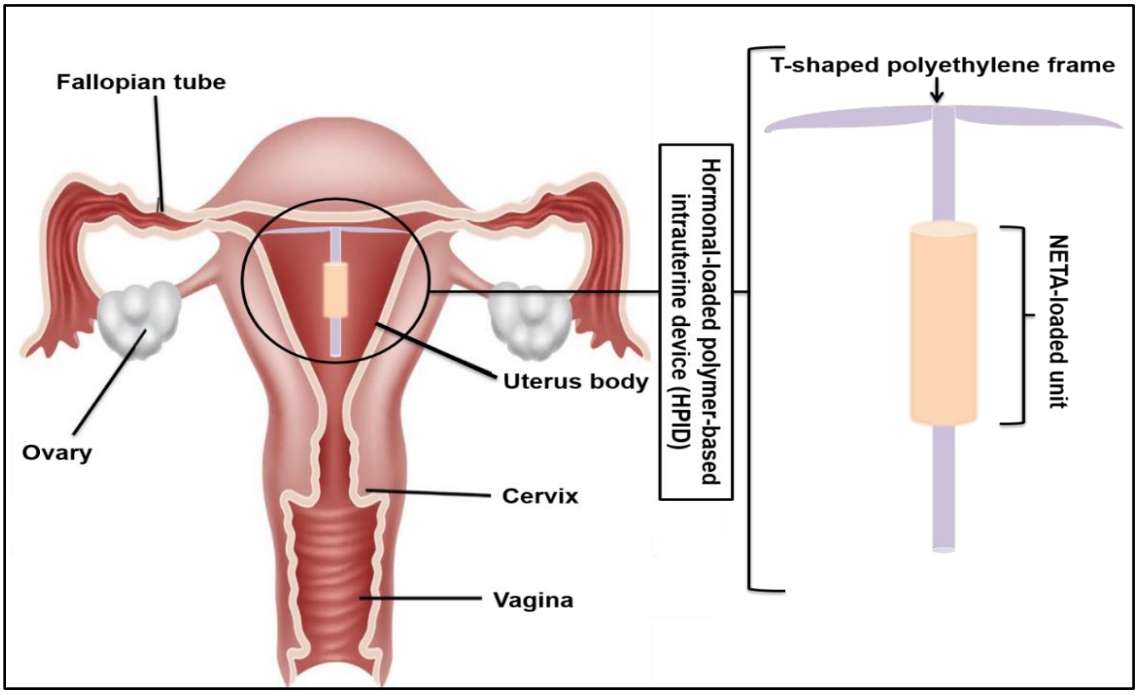

Figure 3.1: Schematic representation of the polymer-based IUD depicting the NETA-loaded unit placed on an implantable T-shape frame.

3.2 Materials and Methods

3.2.1 Materials

PCL Mn = 80,000 was purchased from Sigma-Aldrich (Tokyo, Japan), ethyl cellulose from Sigma-Aldrich Chemie GmbH (St Louis, MI, USA), Norethindrone acetate from Leap Chem (Hong Kong, China) and sodium hydroxide pellets from Merck Chemicals (Modderfontein, South Africa). NIH/3T3 mouse fibroblast cells (ATCC CRL-1658) were obtained from the ATCC (American Type Culture Collection, Manassas, VA, USA), Dulbecco's Modified Eagle Medium (DMEM) from Life Technologies Limited “Gibco” (Paisley, UK), Fetal bovine serum from PAN Biotech (Aidenbach,

Germany), and MTT solution and solubilizing buffer from Roche Diagnostic GmbH (Mannheim, Germany). All other chemicals were of analytical grade and used without further purification.

3.2.2 Methods

3.2.2.1 3D printing of the plastic T-shaped frame of the IUD

Tinkercad® software, a computer-aided design (CAD) tool, was utilized to design the T-shaped frame, which was then exported in .stl file format. Subsequently, Ultimaker Cura software (version 4.10.0, USA) was employed to slice the design prior to printing. The dimensions of the T-shaped frame included a diameter of 1 mm and arm lengths, as well as the vertical stem, each measuring 32 mm. For 3D printing, the Ultimaker2 printer (Ultimaker, Geldermalsen, Netherlands) was employed, utilizing Acrylonitrile Butadiene Styrene (ABS) filaments as the printing material. The printer nozzle was preheated to a printing temperature of 240°C until the ABS feed reached its melting point. The build plate was heated to 90°C, with a printing speed of 40 mm/sec and a flow rate set at 100.

3.2.2.2 Fabrication of the NETA-loaded polymeric matrix (NLPM)

The NLPM was prepared utilizing the method as described by Pathak *et al.*, with modifications. Briefly, a binary polymer mixture was prepared as per the DoE formulations and dissolved in acetone at 45 °C using an oil bath (Pathak et al. 2014). NETA (5, 7.5 or 10% w/w) was thereafter added as a fine powder to the molten polymers prior to mixing until a homogenous mixture was achieved. The resultant malleable drug/polymer blends were then fed manually into a customized mold comprising of a 1 mL polypropylene syringe body, equipped with 1mm central metal rod serving as a centering device (Figure 3.2). Subsequently, the blends were rapidly cooled at -80 °C to induce polymers crystallization. After 4 h, the hardened segments were removed from the molds and stored at -80 °C overnight. The prepared segments were thereafter dried under ambient conditions in a fume hood for a further 72 h. After drying, the regular hollow cylindrical segments were cut using a scalpel and capped from both ends using 5% PCL solution in acetone (Figure 3.3). For comparative purposes, drug-free formulations corresponding to the design formulations were also prepared. Statistical optimization of the prepared NLPM was undertaken using a Design Expert ® DOE software (Version 8, StatEase, Inc, Minneapolis MN 55413, USA) factorial design (FD), with the design formulations prepared as provided in Table 3.1.

Molding techniques play a crucial role in the fabrication of complex and precise drug delivery systems. However, their industrial application is limited by several challenges, including the time-

consuming nature of the processes and the requirement for extensive manual intervention, which complicates scalability. The scale-up of molding processes is further hindered by technical difficulties such as variability in surface morphology and final product quality. In contrast, direct compression offers a more straightforward, cost-effective alternative with fewer processing steps, making it more favorable for large-scale production. Despite these limitations, recent advances in molding technologies, such as hot-melt extrusion (HME) and 3D printing, are being actively researched to enhance process efficiency, reproducibility, and scalability, thereby improving the industrial feasibility of molding methods in drug delivery system production (Parhi and Jena 2022).

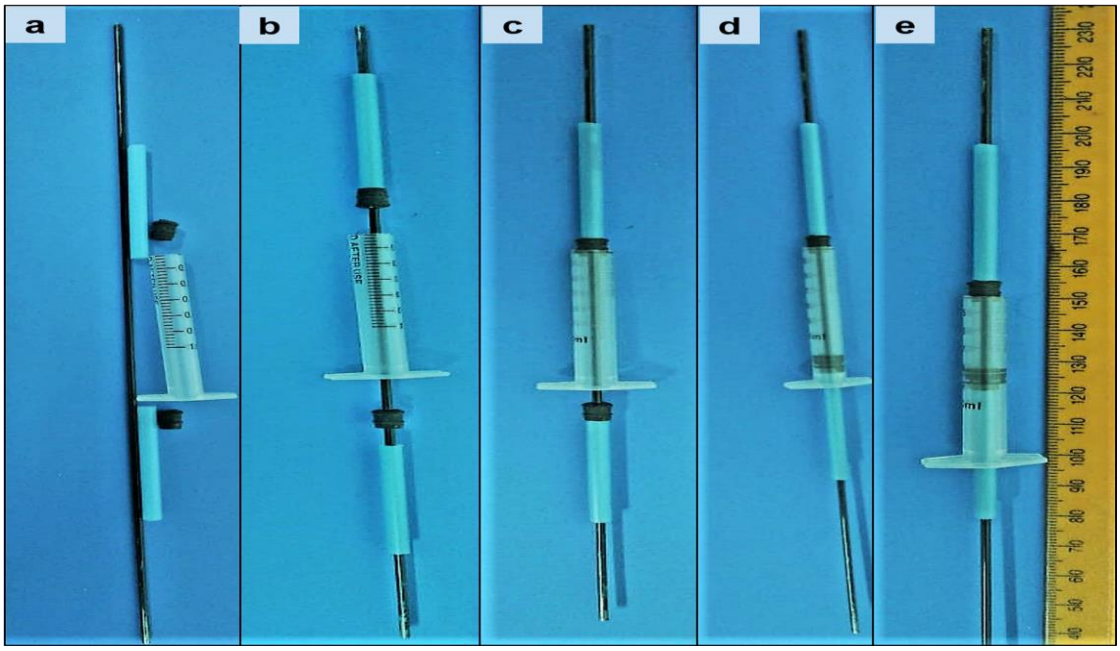

Figure 3.2: Illustrates the customized mould (a) and technique employed in constructing the platform segments (b-e).

Table 3.1: Formulation compositions as generated by the 2^2 FD.

Point type	Formulation Code	Drug to polymer ratio	EC-to-PCL ratio
Factorial	N1	5%	10%
Factorial	N2	10%	10%
Factorial	N3	5%	50%
Factorial	N4	10%	50%
Center	N5	7.5%	30%
Center	N6	7.5%	30%
Center	N7	7.5%	30%

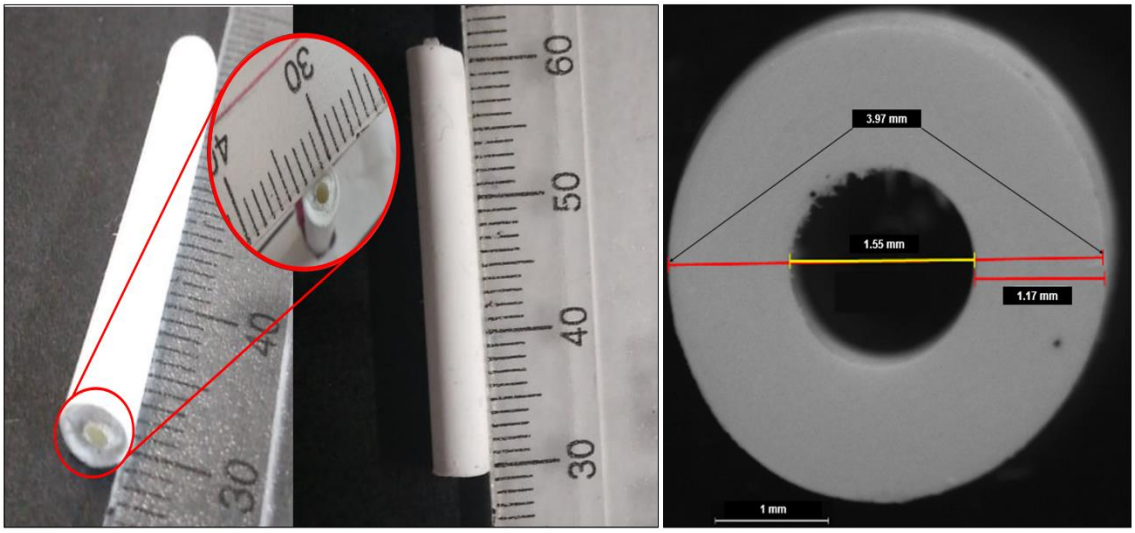

Figure 3.3: Digital Images of the formulated drug free PCL/EC hollow cylindrical matrix.

3.2.2.3 Experimental design and optimization

3.2.2.3.1 Diameter and drug content uniformity

Prior to the evaluation of each design formulation, the diameter of each hollow cylindrical matrix was determined utilizing a digital vernier caliper. For the accurate delivery of dose and to ensure uniform drug distribution within the segment, percent content uniformity was assessed using a slightly modified method as described in the literature (Cheng et al. 2009, Li et al. 2010). Briefly, sample pieces of 2 mm-length were carefully dissected using a scalpel from three regions of randomly selected matrices from each formulation. Specifically, the pieces were taken from the middle and from a quarter from each edge. Each piece was thereafter weighed accurately and dissolved in 2 ml acetonitrile in a 20 ml test tube placed in a 40 °C oil-bath. Methanol (8 ml) was thereafter added to the mixture to precipitate the polymers. The resultant suspension was then subjected to centrifugation for 10 min at 12000 rpm (Centrifuge 5810R, Eppendorf, Germany), with the supernatant filtered through a 0.45 µm PVDF filter and analyzed using an Implen NanoPhotometer® NP80 (Implen GmbH, Germany) at 240 nm (ε = 0.0471; R^2 = 0.999, Figure 3.4). All experiments were conducted in triplicate, with the drug loads determined as the detected mass of drug relative to the total mass of the piece, expressed as mean values with standard deviation (SD).

Validation of the UV-spectroscopy quantification method for specificity to NETA was undertaken utilizing a wavelength scan spanning 200-800 nm conducted on a 40 µg/ml NETA in acetonitrile

(ACN) and methanol (MeOH) (20:80) solution and at the maximum wavelength (λmax) of NETA (240 nm). Following this, a solution of a 1:1 ratio of EC-to-PCL matrix (melted in acetone at the same processing temperature) was prepared at a concentration of 632 µg/ml, centrifuged, and filtered to remove any undissolved polymer, and thereafter analyzed over 200-800 nm and at 240 nm. The higher concentration of EC/PCL was analyzed due to the high polymer to drug ratio utilized in the experimental design. Analysis of the EC/PCL solution wave-scan revealed no discernible peak at 240 nm, indicating the absence of interference between NETA and the employed polymers at this wavelength with the absorbance of the polymer solution (0.021) determined to be negligible when compared to that of the NETA solution (2.004).

The validation protocol was repeated using a 40 µg/ml NETA and a 632 µg/ml EC/PCL in simulated uterine fluid (SUF; biodegradation and *in vitro* drug release media) solution, with no detectable peak similarly determined for EC and PCL at 240 nm. The absorbance of the EC/PCL-SUF solution was further determined to be negligible (0.082) when compared to the NETA-SUF solution (2.030). This analysis therefore determined that the utilized UV-spectroscopy method was specific to NETA and that there was no interference between NETA and the employed polymers at the analysis wavelength of 240 nm, even at higher polymer concentrations. The wavelength scans of the NETA and EC/PCL ACN:MeOH and SUF solutions have been provided in Figure 3.5.

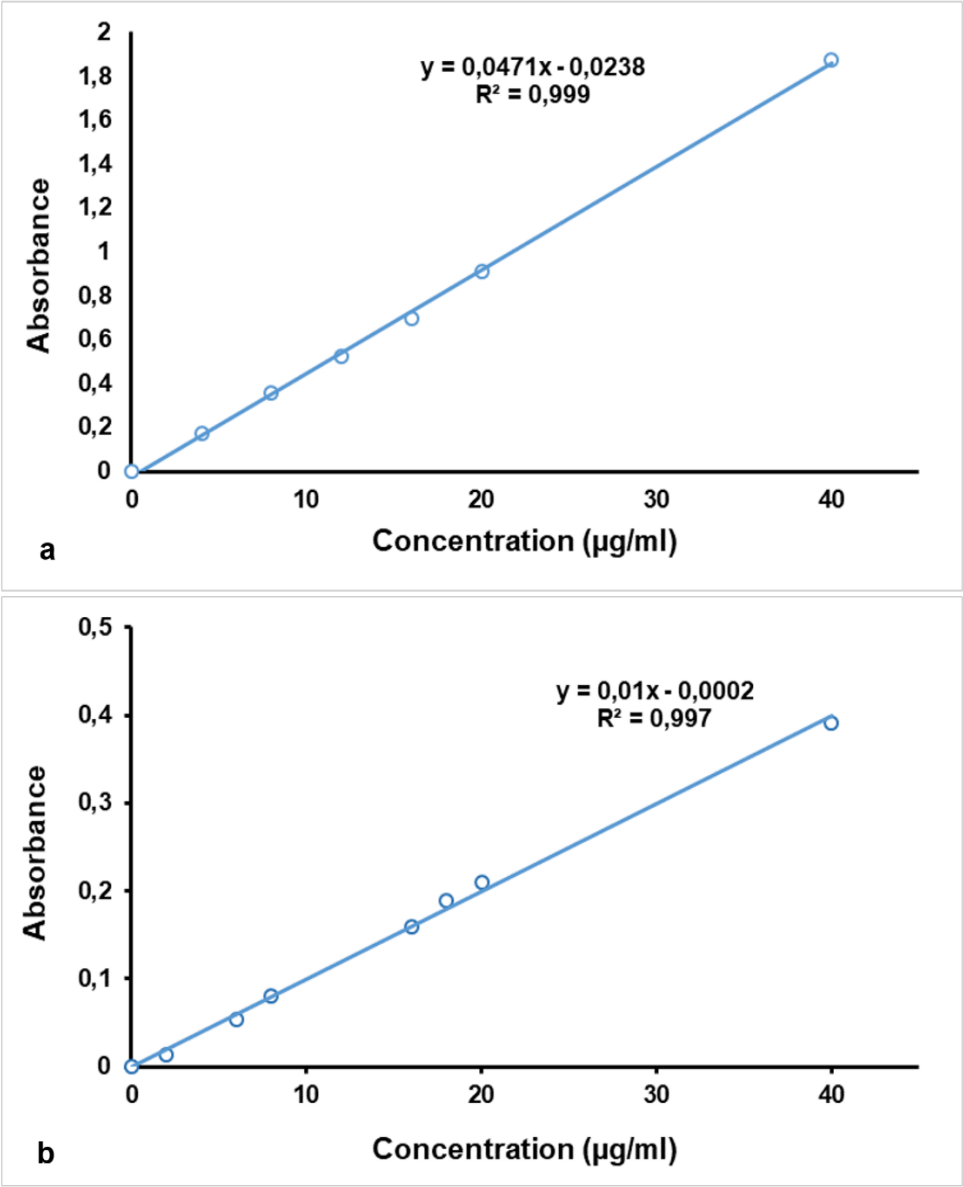

Figure 3.4: Calibration curve of NETA in (a) ACN:MeOH and (b) SUF.

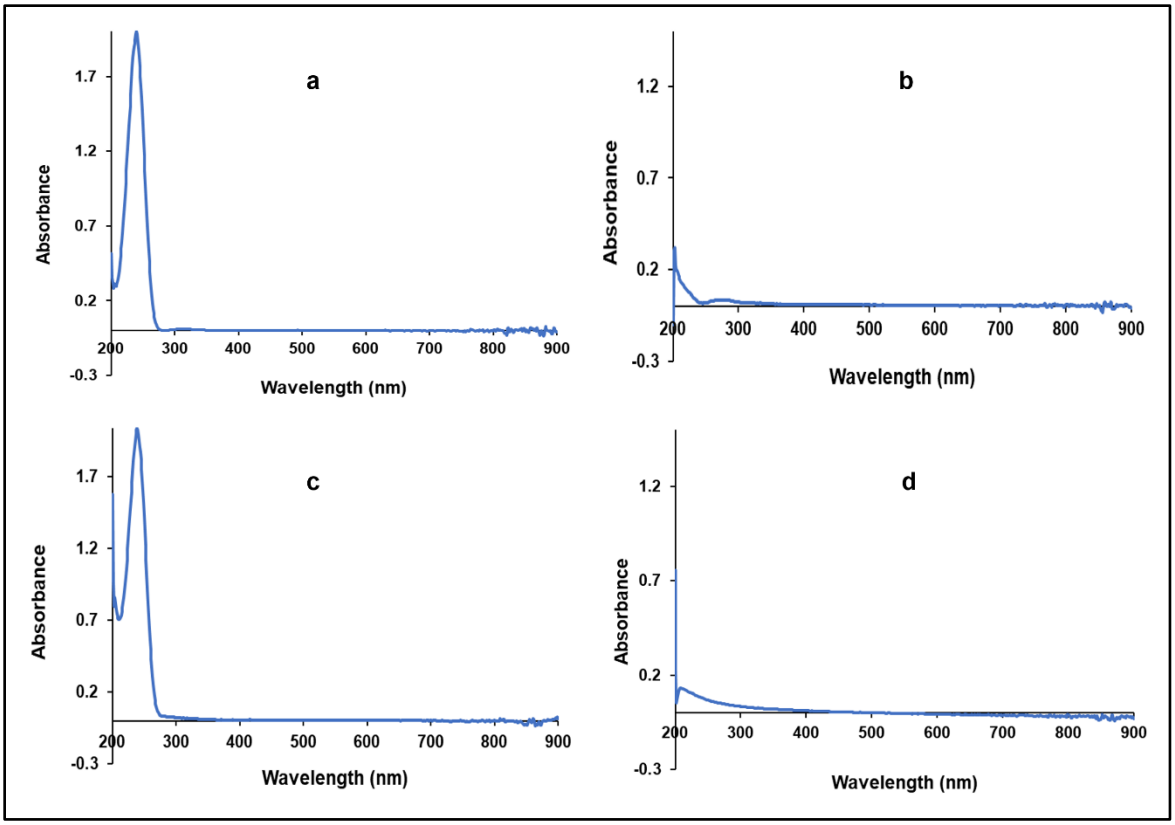

Figure 3.5: Wave-scan of (a) NETA in ACN:MeOH at 40 µg/ml, (b) EC/PCL in ACN:MeOH at 632 µg/ml, (c) NETA in SUF at 40 µg/ml, (d) EC/PCL in SUF at 632 µg/ml.

3.2.2.3.2 Biodegradation and accelerated alkaline degradation studies

The biodegradation of the NLPM in SUF was determined by placing a 5 mm length of accurately weighed segment (W_i) in 15 ml SUF (pH 7.0; 37 °C) rotating in an orbital shaker at 25 rpm for 8 weeks. SUF (pH 7.0) was prepared based on the method as described by Jinying *et al.* (Jinying et al. 2008). The degradation medium was changed and replaced with fresh SUF every 7 days. At a predefined time (8 weeks), the NLPMs were removed from the degradation medium, rinsed with double-distilled water to eliminate any residual solutes adhering to the matrix surface and allowed to air-dry for 72 h in a fume hood before being weighed (W_F).

Similarly, the *in vitro* hydrolysis degradation patterns of NLPM and drug-free matrix were studied at accelerated alkaline conditions by adapting the method previously developed by Boia *et al.* (Boia et al. 2019). For this study, three samples of 2 mm length for each iteration were weighed accurately and kept immersed overnight in bi-distilled water. Subsequently, the samples were immersed in 3 mL of NaOH solution (5 M) for 10 min at room temperature, gently wiped with filter paper and weighed to obtain the initial weight (W_i). The samples were thereafter placed in an

orbital shaker (37 °C; 25 rpm), removed at predefined time intervals (4, 24, 48, 72, and 96 h), wiped with filter paper to remove excess media, and thereafter weighed (W_F) at each time point. Biodegradation and accelerated alkaline degradation were thereafter calculated in terms of percentage weight loss using Equation 3.1.

$$\%\ Weight\ loss = \frac{(W_i - W_F)}{W_i} X\ 100 \qquad \text{Equation 3.1}$$

where W_i is the dry initial weight of the NLPM, and W_F is dry weight of the NLPM after "t" incubation in SUF or NaOH. All the experiments were performed in triplicate with all values expressed as the mean ± SD.

3.2.2.3.3 Textural analysis

Textural profiling was employed to investigate the hardness of the design formulations (n=3). To achieve this, a calibrated textural analyzer (TA.XT.plus; Stable Micro Systems, Surrey, UK) equipped with a 5 mm diameter ball probe indenter was employed to press the surface of horizontally mounted hollow cylindrical matrix with an average 4 mm diameter, pre-cut to a length of 5 mm (Figure 3.6). Data acquisition was accomplished using the Texture Exponent Software (Version 6.1.16.0). The specific parameter configurations employed for the analysis are provided in Table 3.2. Moreover, the maximum force generated during the indentation of the segment matrix at a depth of 0.3 mm was determined and regarded as the matrix hardness or indentation resistance. As a comparison, the hardness of the corresponding drug-free formulation was determined.

Table 3.2: Textural configurations for determining device hardness.

Parameters	**Settings**
Test mode	Compression
Test speed	0.5 mm/s
Post-test speed	5 mm/s
Indentation depth	0.3 mm
Target mode	Distance
Trigger type	Button
Load cell	50 kg

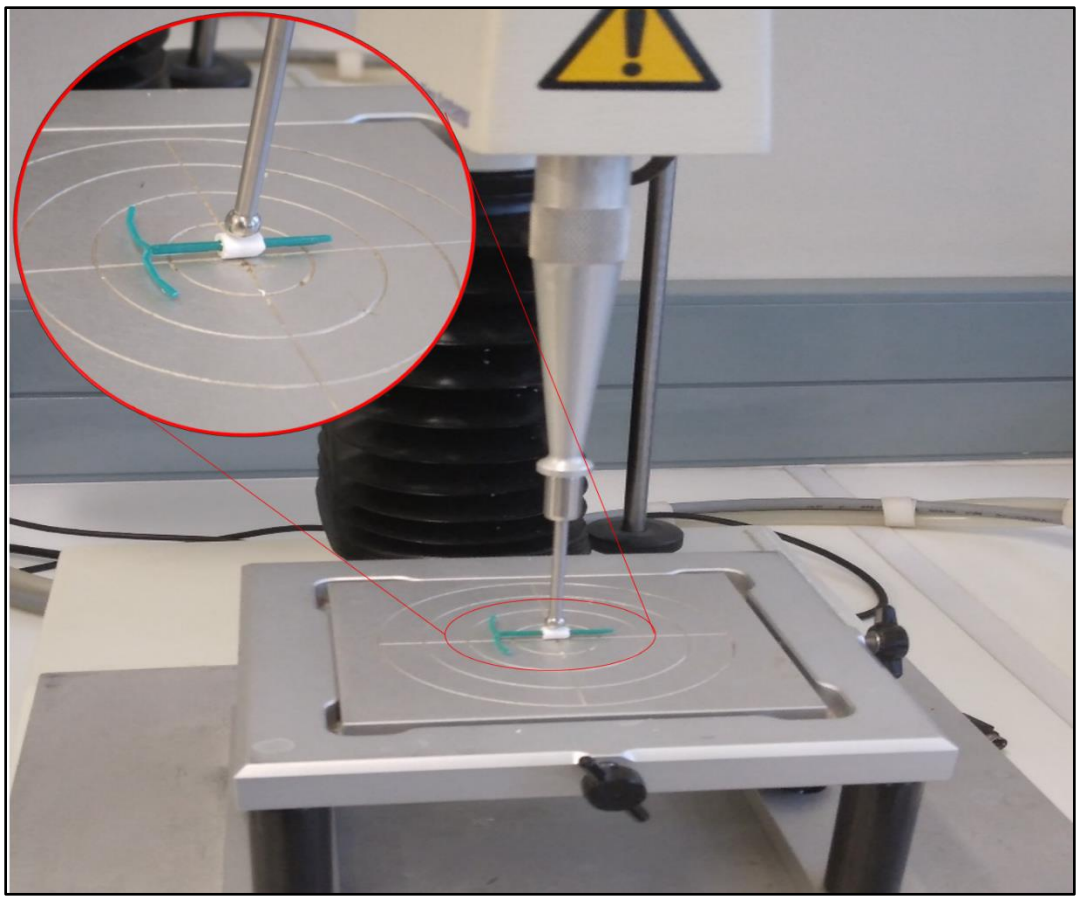

Figure 3.6: Experimental setup for indentation testing using a textural analyzer machine.

3.2.2.3.4 *In vitro* drug release analysis

In vitro drug release studies were carried out on the design formulations (n=3) at 37 °C in SUF over a 4-week period. For the analysis, each NLPM was enveloped on a 3D printed T-shaped plastic frame (Figure 3.7 a-c). All *in vitro* release analyses were carried in 15 mL SUF, placed in an orbital shaker rotating at 25 rpm to facilitate release conditions. At 24-hour periodic intervals, 12 mL of the release medium (representing 80% of total release medium) was withdrawn and replenished with an identical volume of fresh medium to maintain sink conditions. All extracted samples were thereafter filtered analyzed by UV spectroscopy at 240 nm, as previously stated.

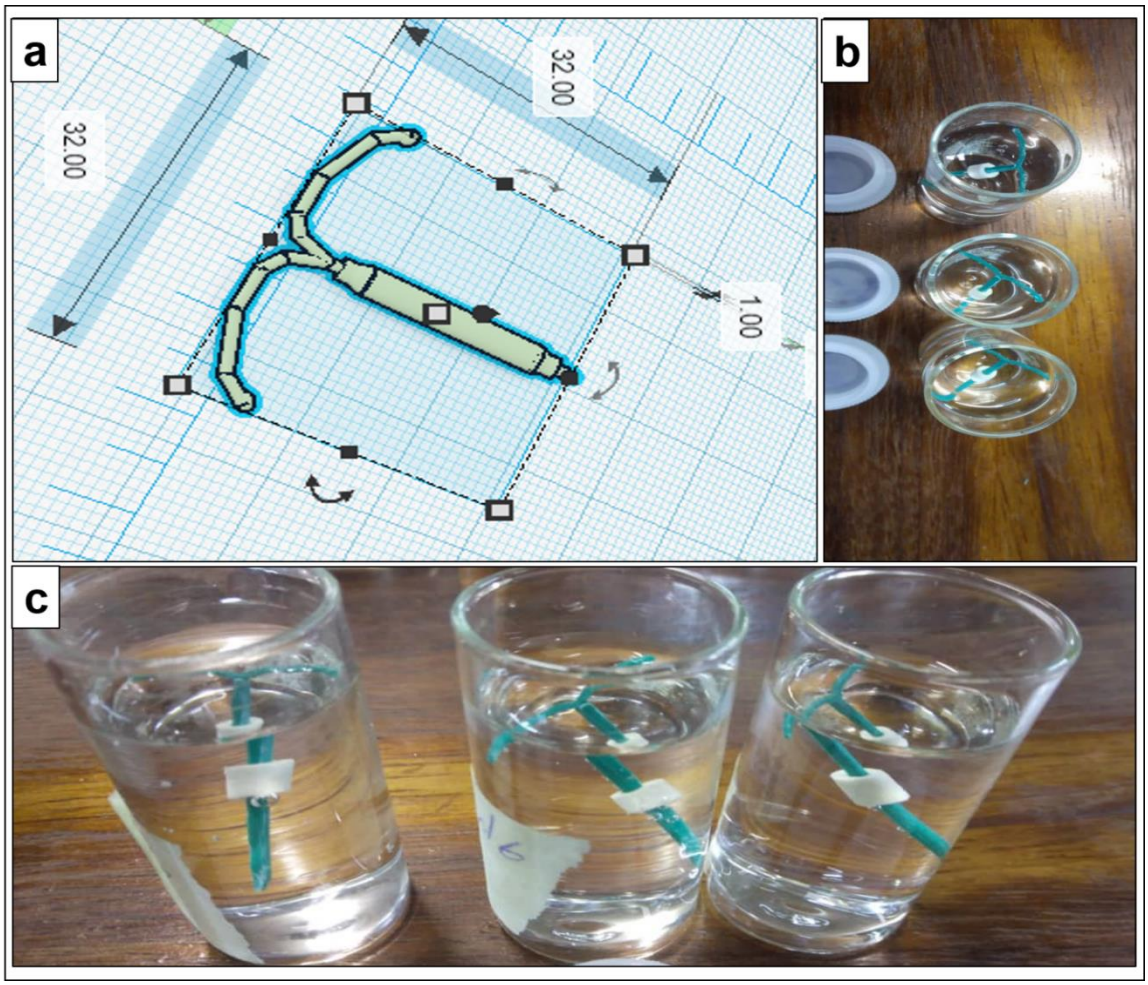

Figure 3.7: Representation of the design and dimensions of the T-shaped frame (a); NLPM enveloped on a 3D printed T-shaped plastic frame, top view (b), side view (c).

3.2.2.3.5 Statistical optimization of NLPM

Statistic optimization of the NLPM was achieved utilizing the data generated in the evaluation of design formulations. The parameters utilized for the optimization were the “in range” for the NETA load and EC-to-PCL ratio. In addition, the minimized release and weight loss were set as desirable. Statistic optimization through the DOE generated an optimal formulation of high NETA load (10%) and EC-to-PCL ratio (50%). The optimal formulation was thereafter subjected to content uniformity studies, textural profiling in the wet state (incubated in SUF at pH 7.0, 37 °C for 24 h), and *in vitro* drug release analysis, as described previously, with hydration studies, structural profiling, morphological analysis, release kinetic modeling and cytocompatibility studies undertaken as described below.

3.2.2.4 In vitro characterization of the optimal NLPM

3.2.2.4.1 Water retention capacity

The hydration properties of both the drug-free and optimal NLPM were assessed using a gravimetric method. Initially, the samples were weighed in their dry state on a digital balance (Mettler Toledo, Switzerland). Subsequently, all samples were placed in petri dishes containing purified water maintained within a constant temperature environment at 22°C. After incubation, the samples were removed, with the excess water extracted using filter paper. The hydration percentage was thereafter calculated using Equation 3.2.

$$Hydration\ \% = \frac{W_F - W_i}{W_i}\ X\ 100 \qquad \text{Equation 3.2}$$

where W_F represents the weight of the samples after incubation in water with W_i denoting the weight of the initial dry samples.

3.2.2.4.2 Structural profiling

FTIR analysis was performed on the optimal NLPM formulation, a drug-free formulation, pure NETA drug, and the pure polymer components (EC and PCL) using an FTIR spectrophotometer (PerkinElmer spectrum 100 FT-IR Spectrometer, Perkin Elmer, Waltham, Massachusetts, USA). All FTIR analyses were undertaken over a range of 4000–650 cm^{-1} at room temperature for 20 scans.

3.2.2.4.3 Morphological analysis

The surface morphology and the cross-section of the drug-free and optimal NLPM before and after an 8-week incubation in SUF was analyzed under scanning electron microscope (ZEISS SEM, Carl Zeiss Microscopy Ltd., Cambridge, UK). Prior to imaging, the surface and cross-section of each sample were mounted on SEM stubs and sputter coated with gold-palladium (Li et al. 2010, Muhindo et al. 2022). SEM images were thereafter obtained at an accelerated voltage of 3 kV at varying magnifications.

3.2.2.4.4 Mathematical modeling of the release kinetics

Mathematical modeling of the *in vitro* release data of the optimized NLPM formulation was undertaken to gain a comprehensive understanding of its drug release mechanism. Consequently, five mathematical kinetic models, implemented with DDSolver® software, an add-in integrated program for Microsoft Excel® (Microsoft, Santa Rosa, CA, USA), were employed to model the experimental release data. For this analysis, the release data was fitted using the zero-order, first-order, Higuchi, Korsmeyer-Peppas, and Peppas-Sahlin models. After successful

modeling, the coefficient of correlation (R^2), adjusted coefficient of correlation (adjusted-R^2), Square Root Mean Squared Error (RMSE), Akaike Information Criterion (AIC), and Model Selection Criterion (MSC) were determined, and the kinetic parameters obtained.

3.2.3 Cytocompatibility Studies

3.2.3.1 Cell culture and experimental setup

In vitro cytocompatibility studies were undertaken by determining the cell viability of NIH/3T3 mouse fibroblast cells. At its core, the primary objective of this assessment was to discern any potential cellular detriment induced by the prepared NLPM. The utilization of a cell line differing from those originating from the uterus, was rooted in the study's emphasis on elucidating the drug cytotoxicity and its interactions with the polymeric matrix, rather than assessing any uterine-specific effects (Calvo et al. 2019). Additionally, previous studies for the treatment of endometriosis have utilized NIH/3T3 cells to probe the cytotoxicity of their respective delivery systems (Jana et al. 2014, Siddiqa et al. 2019, Siddiqa et al. 2021), accordingly highlighting the role of NIH/3T3 cells in elucidating the cytotoxicity of various delivery modalities.

For the cytocompatibility study, NIH/3T3 cells (ATCC CRL-1658) were cultured in Dulbecco's modified Eagle's medium (DMEM) containing 10% (v/v) fetal bovine serum (FBS) and 1% (v/v) penicillin/streptomycin. All cells were thereafter incubated in a humidified incubator (NUAIRE, Radobio, China) at 37 °C with 5% CO_2, with the cell media changed every 2 days until reaching ≈ 90% confluency.

3.2.3.2 Device sterilization and sample preparation

Prior to the performance of the cytocompatibility studies, the drug-free and optimal NLPM was exposed to source UV light on a continuous path for 5 min (UV-C 254 nm, UV EQUIP, South Africa), washed in 70% ethanol for 15 sec, dried, and thereafter handled under aseptic conditions in a Class II biological safety cabinet (ESCO, Singapore) (Korelidou et al. 2022). Sample preparation consisted of extraction of leachates from the prepared drug-free and NLPM. Briefly, under sterile conditions the devices were incubated in 10 mL sterile SUF (pH 7) at 37°C and 25 rpm for 5 days. The supernatant was thereafter filtered through sterile 0.45 µm syringe filters under sterile conditions and were then diluted 1:5 with culture media.

3.2.3.3 MTT assay

Cytocompatibility of the drug-free and NLPM was evaluated (n=5) using a MTT assay (3-(4,5-dimethylthiazol-2-yl)-2,5-diphenyl-2H-tetrazolium bromide dye). For this assay, a cell suspension with density of 2×10^4 cells/well in 100 µL was seeded on 96 well plates and incubated for 24 h at

37 °C and 95% relative humidity containing 5% CO_2. Afterward, the growth medium was aspirated and replaced with a growth medium consisting of the extracted leachates, with the cells thereafter grown for an additional 1, 3, 5 and 7 days. Throughout the 7-day testing period, the growth medium containing the extracted leachates was replenished every 2 days. At the end of each designated time point (1, 3, 5, and 7 days), MTT solution (10 µL) was added to each well plate, followed by an addition of 100 µL solubilizing buffer after 4 h, and incubation overnight under the standard culture conditions. The absorbance's reading of each treatment sample was thereafter taken in triplicate at 570 nm against a 690 nm background using a VICTORTM X3 Multilabel Plate Reader (PerkinElmer, USA). In addition to the treatment arms (the NLPM and drug-free segments), NIH/3T3 cells in culture medium and cells in culture medium with DMSO were used as negative and positive controls, respectively.

3.2.4 Statistical Analysis

This study employed Design Expert® 8 for the construction of FD matrix and to investigate the influence of independent variables on the selected response parameters of the fabricated segments. The obtained results were presented as mean values ± SD, calculated utilizing Microsoft Excel 2010 software. Statistical analysis was further conducted using SPSS version 16.0 for Windows. The Shapiro test was additionally used to evaluate the normal data distribution. Two-sample t-tests were employed to determine significance between the two experimental groups and the analysis of variance (ANOVA) was employed, followed by the application of the Tukey HSD and Games-Howell post hoc tests for result comparisons between three and more experimental groups, with all results at a 95% confidence interval.

3.3 Results and Discussion

3.3.1 Evaluation of the Experimental Design

3.3.1.1 Diameter and drug content uniformity

The assessment of drug content uniformity offers valuable insight regarding drug loads across the various batches and the drug distribution within each device. Table 3.3 provides the average diameter and drug content of the drug-loaded devices. The findings exhibited that the drug content in all formulations closely matched the initial feed ratios for the different batches, with a very low SD, suggesting that NETA was uniformly distributed within their respective polymer matrices, and that there was no substantial drug decomposition that took place during the fabrication process. The uniform distribution of the drug within the matrix is likely a consequence of the rapid cooling of the molten blend, facilitating instant crystallization and polymer phase solidification. This process likely hinders the sedimentation of drug particles, ensuring their uniform dispersion

throughout the matrix. These observations align with the results reported by Asvadi *et al.* in a previous study (Asvadi et al. 2013a). Also, from the drug content present, it is evident that the loaded drug is affected by the amount of the drug used for device preparation. Furthermore, it is observable that the hydrophobicity of the drug facilitates the incorporation within the matrix of the corresponding hydrophobic polymer blend. Moreover, the fabricated devices exhibited quite minimal variation in diameter, with values below 3%. This slight variability is likely attributable to variances in the density and viscosity of the malleable blends utilized across the various formulations. Consequently, when considering the diameter and content uniformity results, it can be deduced that the fabrication technology and processing conditions meet the criteria for reproducibility and are deemed suitable and acceptable (Lu et al. 2012).

Table 3.3: Diameter and drug content in the fabricated NLPM (n=3).

Formulation code	Diameter (mm)	Theoretical loading%	Drug content (%±SD)	Incorporation efficiency (%±SD)
N1	3.84±0.006	5	4.99±0.07	99.81±1.36
N2	3.73±0.020	10	9.98±0.1	99.77±1.01
N3	3.79±0.080	5	5.00±0.12	100.01±2.33
N4	4.11±0.050	10	10.03±0.22	100.36±2.15
N5	3.99±0.076	7.5	7.51±0.13	100.07±1.75
N6	4.03±0.021	7.5	7.50±0.39	99.98±5.24
N7	4.02±0.012	7.5	7.48±0.23	99.74±3.01

3.3.1.2 Biodegradation and accelerated alkaline degradation studies

The structural alterations linked to degradation could potentially impact the drug release patterns of the prepared hollow cylindrical segments (Frank et al. 2005). Consequently, it is crucial to track the *in vitro* erosion by assessing the percentage weight loss as a function of time. PCL, which is contained within the segment, exhibits a total *in vivo* degradation time frame spanning from 2 to 4 years, which is primarily driven by the random hydrolytic cleavage of ester linkages, leading to a reduction in its molecular weight to below 3000, and subsequently, intracellular degradation takes place (Boia et al. 2019, Woodruff and Hutmacher 2010).

The findings pertaining to the percentage weight loss throughout the 8 weeks incubation in SUF of formulations N1 to N7 exhibited a range from 1.92±0.06 to 4.51±0.21%, as depicted in Figure 3.8. Notably, at 50% EC-to-PCL, as exemplified by formulations N3 and N4, it was noted that this polymer ratio was associated with a significant increase in weight loss with the transitioning of the drug load from 5% (N3) to 10% (N4). In addition, maintaining the drug load at a higher level (10%) with a decrease in the EC level led to a significant increase of weight loss as evidenced when comparing formulation N4 and N2. Furthermore, at 10% EC-to-PCL levels, altering the drug load from 5% to 10% led to an increased weight loss, as observed when comparing N1 and N2 formulations. Moreover, it is worth noting that the combinations of intermediate levels for both independent variables resulted in an intermediate weight loss.

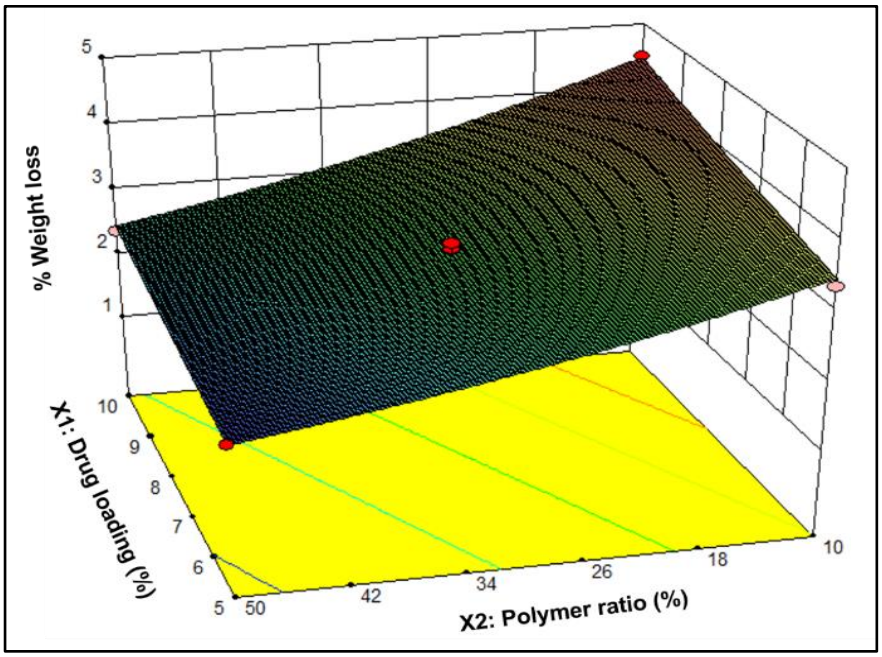

Figure 3.8: 3D surface plot depicting the influence of drug load (%) and EC-to-PCL ratio (%) on the weight loss percentage of the NLPM.

Alkaline degradation studies were additionally conducted on both drug-free and optimal NLPM devices under high pH conditions (5 M NaOH), with the influence of EC-to-PCL ratios and drug loads on the degradation rates examined and compared. Figure 3.9 illustrates the results in terms of percentage weight loss. Notably, formulations drug-free 1 (DF1) and N1 exhibited the highest degree of degradation, while formulations DF4 and N4 displayed the least degradation over the same duration. These results highlighted a decrease in the degree of weight loss with an increase in the EC-to-PCL percentage. Regarding drug load, a distinct trend emerged when comparing the

degradation of DF formulations with low EC-to-PCL ratios (DF1 and DF2) after 96 hours to their corresponding formulations loaded with drug. The NLPM formulations (N1 and N2) demonstrated a significant increase in weight loss% when compared to the drug-free counterparts ($p < 0.05$). Conversely, when examining the DF formulation with high EC content (DF4) in comparison to its counterpart with both high EC content and high drug load (N4), the findings reveal no significant differences in weight loss percentage after 96 h ($p > 0.05$).

From these results, it can be inferred that the compositions used in the preparation of the segments exert a significant influence on the weight loss profile and erosion characteristics. EC, characterized by its hydrophobic nature, high molecular weight, and chain stiffness, plays a crucial role in these observations. As the content of EC increases within the matrix, there is a concurrent rise in hydrophobicity. This heightened hydrophobicity establishes a protective barrier that restricts the penetration of water or other degrading agents into the matrix, consequently decelerating the degradation process. Moreover, the augmentation of EC content can enhance the interfacial adhesion between EC and PCL. This improved adhesion fosters a more compact and uniform structural arrangement, resulting in fewer micro-voids or weak points within the segments. As a result, it reduces the availability of sites for water ingress and, consequently, hinders the initiation and progression of the degradation processes. The combined effects of heightened hydrophobicity and improved interfacial adhesion contribute to the observed reduction in weight loss and erosion characteristics in the segments.

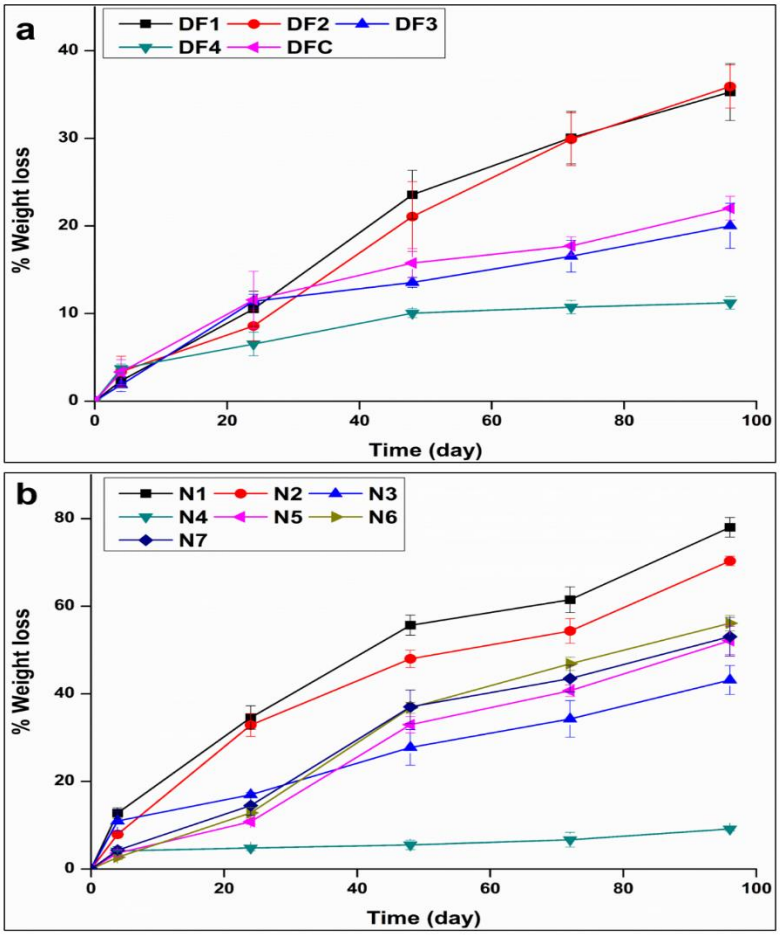

Figure 3.9: Accelerated weight loss (%) in alkaline media as a function of time: (a) Drug-free segment and (b) NLPM. DFC represents the drug free formulation with a 30% EC to PCL ratio.

3.3.1.3 Textural profiling

In the context of long-term loading, it is imperative for implants to exhibit robust mechanical properties, enabling them to effectively withstand persistent stress and mitigate the risk of undesirable deformations (Penhasi et al. 2020). In this regard, the hollow cylindrical devices, tailored for intrauterine deployment, necessitate adequate strength and flexibility to endure internal uterine environment without detrimental effects on surrounding tissues, as well as to expedited removal during emergency scenarios. Consequently, an assessment of the mechanical properties of the fabricated segments in dry state as well as for the optimal formulation in wet state was conducted by quantifying the externally applied stress required to induce deformation in the prepared segments.

Figure 3.10 illustrates the force values (N) generated from the penetration of the probe into the various segment matrices. The findings from the drug-free segment reveal a statistically

significant impact of the increasing level of EC on the force (Figure 3.10a). This effect becomes evident when contrasting formulations DF4 with the formulations featuring 30% and 10% of EC-to-PCL ($p < 0.05$). Furthermore, formulation DFC, characterized by a medium level of EC-to-PCL (30%), demonstrated a slight, albeit non-significant, increase in force compared to DF1 and DF2 (low level of EC) ($p > 0.05$).

In the context of NLPM (Figure 3.10b), the findings indicate a noteworthy influence of escalating EC content on the indentation force, as evidenced by a statistically significant increase observed in formulations N4 and N3 in comparison to N1, as well as when contrasting N4 with other formulations ($p < 0.05$). An elevation in drug load further demonstrated a slight, non-significant, increase in force, exemplified in the comparison between N1 and N2, as well as in formulations at center points, and the comparison between N3 and N4 ($p > 0.05$).

The hydrated optimal NLPM formulation and the corresponding drug free formulation, after 24 h incubation in the SUF, exhibited resistance to indentation of 14.3±0.8 and 11.44±1.4 N. These results demonstrate statistically significant increase of hardness due to the hydration of the drug free formulation ($p=0.041$), while there is no difference between the dry and hydrated NLPM formulation ($p=0.078$), with only a slight increase in the hardness seen. The observed heightened resistance to indentation, as deduced from the preceding results, may be attributed to the uniform dispersion of drug and EC within the PCL matrix. This uniform dispersion likely contributes to improved interfacial adhesion between the polymers and drugs, specifically pertaining to their hydrophobic nature, thereby resulting in a reduction of micro-voids in the interphase region.

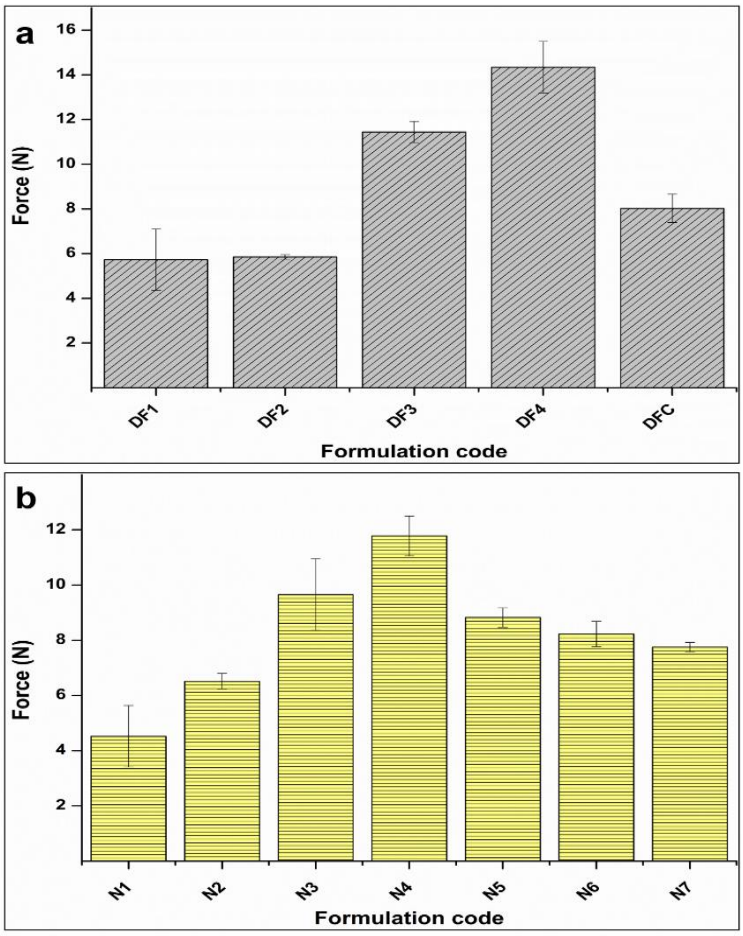

Figure 3.10: Analysis of indentation force of the drug-free matrix (a) and NLPM (b).

3.3.1.4 In vitro drug release

In vitro measurements necessitate the replication of an environment mirroring human uterine conditions. The intricate composition of human uterine fluid, encompassing inorganic compounds, carbohydrates, lipid factors, amino acids, peptides, and proteins, displays dynamic variations across different menstrual cycle phases and among individuals (Tietz and Klein 2018, Zhang et al. 1996). These intricacies, arise from its metabolic origin, pose formidable challenges for precise simulation. Several endeavors have been undertaken to develop an experimental system capable of simulating this complex milieu such as employing synthetic media as Ringer solution, Hanks medium, and amino acid solutions (Zhang et al. 1996). In alignment with the current study's objectives, the SUF was formulated by drawing insights from pertinent literature (Jinying et al. 2008). This fluid was tailored to encompass compounds predominantly found in human uterine fluid, offering a methodologically robust approach to emulate the complex uterine environment (Zhang et al. 1996). Additionally, the pH level in uterine fluid exhibits high variability with reported

pH values ranging from ~6 to 8 (Mora et al. 2002, Zhang et al. 1996). In study by Jinying et al, the release behavior of cupric ion and indomethacin from Cu-IUDs was investigated in SUF with a pH value adjusted around 6.8-7.4 (Jinying et al. 2008). The postmenopausal period is characterized by microbiota imbalance (Abdelgader et al. 2023), potentially leading to an elevated pH in the upper genital tract (Lykke et al. 2021). In our study, a constant pH value of 7 was maintained throughout the experimentation. This standardization was implemented to align with our primary objective, focusing on determining the impact of the EC-to-PCL ratio and drug load on the release weight loss profiles of the prepared platform. Furthermore, the volume of uterine fluid exhibits inter-individual variation and undergoes fluctuations across different menstrual phases, with the reported volumes of 83 µl-180 µl, 105±92 µl, 40±32 µl, and less than 5-35 µl for mid-cycle, follicular phase, luteal phase, and mid-luteal phase, respectively (Zhang 2021). Herein, we standardized the volume to the lowest value to maintain sink conditions consistently throughout the assessments of drug release and platform weight loss. Moreover, the dynamics of fluid movement within the uterus are predominantly governed by myometrial contractions. However, quantifying the uterine movement and establishing a correlation with the rotational speed in the release assessment remains a methodological challenge. To ensure a reproducible laminar flow and prevent turbulence, agitation should be maintained at a relatively low rate (Zhang 2021). The choice of 25 rpm was therefore grounded in the need for consistency in our experimental conditions.

The cumulative NETA release percentages of the prepared formulations (N1 to N7) over a 4-week period (Y4) exhibited a considerable range, spanning from 37.95±1.62 to 83.67±1.84. Notably, formulations N4, characterized by high drug load (10%) in combination with high EC-to-PCL ratio (50%), exhibited comparatively low release percentages. In contrast, formulation N1, featuring the lowest level of drug load and EC percentage (5% and 10%, respectively), displayed the highest release. Additionally, when examining formulations with the drug load levels at 5%, a distinct pattern emerged as the percentage of drug release increased from 58.6±0.7 (N3) to 83.67±1.84 (N1) with a corresponding transition in the EC percentage from 50% to 10%. Furthermore, formulations distinguished by medium levels of both independent variables (7.5% and 30%, for drug load and EC ratio, respectively) displayed intermediate release percentages, as evidenced in formulations N5, N6, and N7. These findings underscore the profound impact of variations in both independent variables on the percentage of drug release, elucidated in Figure 3.11a-c, which portrays the main effects of drug load and EC-to-PCL ratio on the cumulative NETA release percentage over a 4-week evaluation period. The drug release profiles of NETA (Figure 3.11d) revealed sustained release characteristics from the polymer blend-based matrices.

Over the 4-week observation period, it is evident that the N1 formulation achieved the highest release, followed by N2, whereas N4 exhibited the lowest release percentage. These results are consistent with observations from a study by Desai *et al.*, which demonstrated that an increased amount of EC led to a reduction in drug release (Desai et al. 2006). This reduction was attributed to the increased hydrophobicity of the prepared granules with higher amounts of EC, which impeded the penetration of the release media into the matrix and decreased the diffusion of the drug into the release media. Moreover, these trends were observed in a study investigating progesterone release from PCL matrices, where despite a similar release pattern across varied drug loads, formulations with higher drug concentrations exhibited elevated release quantities, while those with lower drug loads revealed higher cumulative drug release percentages (Chang et al. 2005).

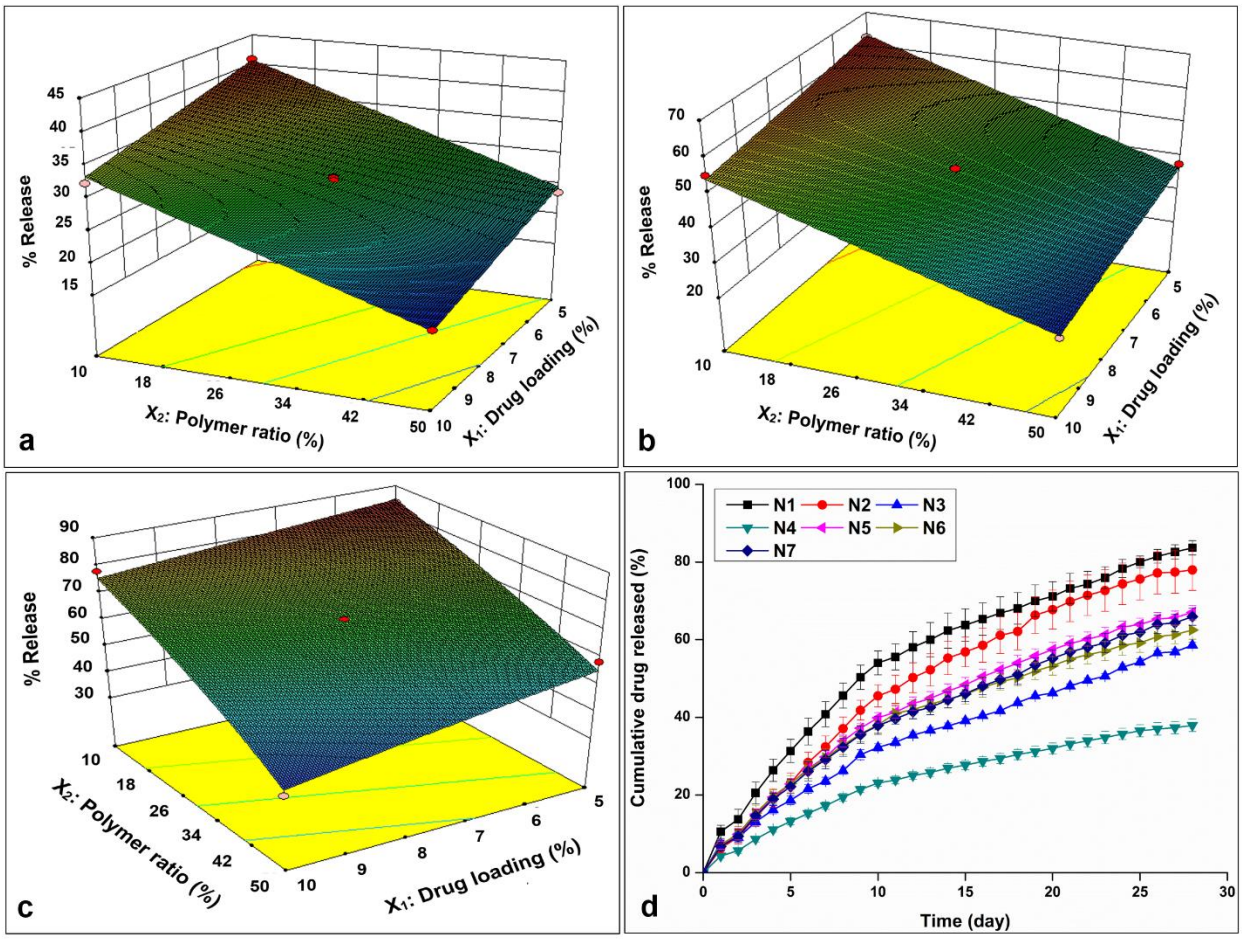

Figure 3.11: 3D Surface plots depicting the influence of Drug load (%) and polymer ratio (%) on the cumulative drug release at (a) week 1, (b) week 2, and (c) week 4, with (d) displaying the release profiles of the prepared design formulations.

3.3.1.5 Data analysis and optimization of the statistical design

Applying the principles of experimental design, a 2^2 FD was employed to generate seven formulations of NLPM. An overview of the design matrix, which encompasses two independent factors, and the corresponding responses is presented in Table 3.4. The experimental data pertaining to percentages release after 1, 2, 3 and 4 weeks and weight loss percentage after 8 weeks (denoted as Y1, Y2, Y3, Y4, and Y5, respectively) underwent mathematical transformations, involving the power transformation for Y3 and Y4, as well as the natural logarithm transformation for Y5. Linear regression models were then established and assessed based on the ANOVA results. Notably, the low probability values (p <0.0001, <0.0001, =0.001, =0.0009, and = 0.0001, for Y1, Y2, Y3, Y4 and Y5, respectively) highlight the robust statistical significance of the constructed models for responses, verified with a 95% confidence interval. The lack of significant lack-of-fit, as indicated by Lack of Fit p-values of 0.0764, 0.4647, 0.2569, 0.3269, and 0.3004 for Y1, Y2, Y3, Y4, and Y5 respectively, further underscores the models' high predictive capability, suggesting that the lack-of-fit has minimal influence in comparison to random error. The results reveal that the variation of EC-to-PCL ratio (X_2) exert a significant influence on both drug release throughout the 4 weeks and weight loss (Y5) percentages. Likewise, the drug load variation (X_1) has been determined to have a statistically significant impact on weight loss and drug release (%), albeit without exerting a statistically significant influence on drug release during week 3, as well as less influences on the responses compared to the EC-to-PCL ratio.

In Table 3.5, a comprehensive set of fitness statistics is presented. The similarity between the anticipated and observed responses is manifested in the high values of R^2, denoting more than 0.96. Furthermore, all responses evidenced remarkable levels of precision, surpassing a threshold of 4, and the predicted R^2 values closely mirrored the adjusted R^2 values. Additionally, model selection considerations were directed towards the minimization of Prediction Error Sum of Squares (PRESS) values, reinforcing the efficacy of the selected models. Moreover, the analysis of factorial design results led to the derivation of the following first-order linear equations, expressed in terms of coded factors:

$$Y1 = +28.95 - 3.68\,X_1 - 8.08\;X_2 \qquad \text{Equation 3.3}$$

$$Y2 = +45.47 - 4.48\,X_1 - 13.24\;X_2 \qquad \text{Equation 3.4}$$

$$(Y3)^3 = +2.05 \times 10^5 - 31487.37\, X_1 - 1.462 \times 10^5\, X_2 \qquad \text{Equation 3.5}$$

$$(Y4)^2 = +4386.46 - 727.93\, X_1 - 2051.98\ X_2 \qquad \text{Equation 3.6}$$

$$ln\ ln\ Y5\ = +1.07 + 0.13\, X_1 - 0.30\ X_2 \qquad \text{Equation 3.7}$$

In Equation 3.3 and 3.4, it is evident that both the main effect terms X_1 and X_2 exhibit statistically significant negative influences on the obtained release responses during week 1 and 2 as well as negative effect of X_2 on the cube of the release responses during week 3 as demonstrated in Equation 3.5. In addition, both main effect terms display significant negative effect on the squared of release responses during week 4 (Equation 3.6). Furthermore, as indicated in Equation 3.7, the main effect term X_1 displays a significant positive effect on the natural logarithm of weight loss percentage, whereas the term X_2 demonstrates a statistically significant negative association with the natural logarithm of weight loss percentage.

Table 3.4: 2^2 FD matrix and responses results for NLPM (n=3, SD).

Formulation	1-week drug release (%)	2-week drug release (%)	3-week drug release (%)	4-week drug release (%)	8-week weight loss (%)
N1	40.79±3.22	62.37±4.55	73.17±3.87	83.67±1.84	3.37±0.29
N2	32.42±2.79	55.28±4.24	69.84±5.19	77.99±5.33	4.51±0.21
N3	23.61±0.99	37.77±0.79	48.09±0.55	58.60±0.70	1.92±0.06
N4	17.26±0.90	26.93±1.19	33.14±1.56	37.95±1.62	2.38±0.03
N5	29.80±1.56	46.76±1.85	59.02±1.90	67.04±1.77	2.91±0.05
N6	29.62±2.25	44.67±2.31	55.02±2.46	62.50±2.41	2.98±0.08
N7	29.15±2.37	44.50±2.01	56.85±2.36	65.95±2.21	3.07±0.02

Table 3.5: Model statistical fit parameters.

Formulation	1-week drug release (%)	2-week drug release (%)	3-week drug release (%)	4-week drug release (%)	8-week weight loss (%)
R^2	0.9907	0.9913	0.9679	0.9706	0.9883
Adj R^2	0.9860	0.9870	0.9519	0.9558	0.9825
Pred R^2	0.9515	0.9587	0.8845	0.8501	0.9497
Adeq precision	41.740	41.403	19.932	22.399	36.771
C.V. %	2.97	2.87	13.28	8.64	3.31
PRESS	15.44	32.52	1.068×10^{10}	2.928×10^{6}	0.022

3.3.2 Characterization of the optimized NLPM

3.3.2.1 Water retention capacity

The *in vitro* hydration studies of the optimized drug-free and NLPM formulations in water were conducted over 24 h. The drug-free formulation displayed a significantly higher hydration percentage compared to the NLPM formulation (34.63% ± 2.2 vs 17.52%± 0.32, respectively; $p<0.05$). This observation could be attributed to the increased hydrophobicity, reduced porosity (Amini et al. 2021), and hindered water diffusion resulting from drug depositions on micro-voids and the surface of the NLPM.

3.3.2.2 Structural Profiling

Evaluation of the FTIR spectrum of PCL revealed key absorption bands at 2943 cm^{-1} and 2867 cm^{-1} related to asymmetric and symmetric stretching vibrations of CH_2 groups, respectively, and 1721 cm^{-1} attributed to the stretching vibrations of the ester carbonyl group (C=O) (Figure 3.12). Additionally, the signal located at 1294 cm^{-1} is corresponding to C-O and C-C stretching vibrations in the crystalline phase. Furthermore, distinct signals at 1240 cm^{-1} and 1165 cm^{-1} were detected, associated with the asymmetric and symmetric stretching of C-O-C bonds, respectively (Abdelrazek et al. 2016, Javaid et al. 2021). The EC spectrum revealed a prominent absorption band at 1054 cm^{-1}, and a peak at 1376 cm^{-1} attributed to CH_2 bending vibrations. The presence of OH groups was confirmed by a less pronounced but discernible peak at 3486 cm^{-1}. Furthermore, the spectrum exhibited small yet sharp peaks at 2977 cm^{-1} and 2872 cm^{-1}, corresponding to CHO stretching vibrations, which in alignment with results reported previously

in literature (Horvat et al. 2022, Phadke et al. 2014). The FTIR spectrum of pristine NETA exhibited two distinct peaks. The initial peak at 3235 cm^{-1} corresponds to the O–H stretching of the unbound hydroxyl group, while the subsequent peak at 1650 cm^{-1} corresponds to the C=O stretching of the ketone. These findings align with previous reports in the literature (Somboonporn et al. 2011). The NLPM's spectrum revealed the primary bands of NETA, albeit with lower intensities, and bands related to the PCL and EC structures were detected, suggesting no significant changes or shifts in major characteristic peaks. Identical characteristic peaks and the absence of discernible new peaks in the prepared device compared to the pure drug and polymers indicated homogeneous mixing of the drug and polymers, affirming physical interaction and further supporting the absence of strong chemical interaction. The FTIR spectra data validated the compatibility of matrix-forming polymers with the drug, indicating that performance characteristics were not altered.

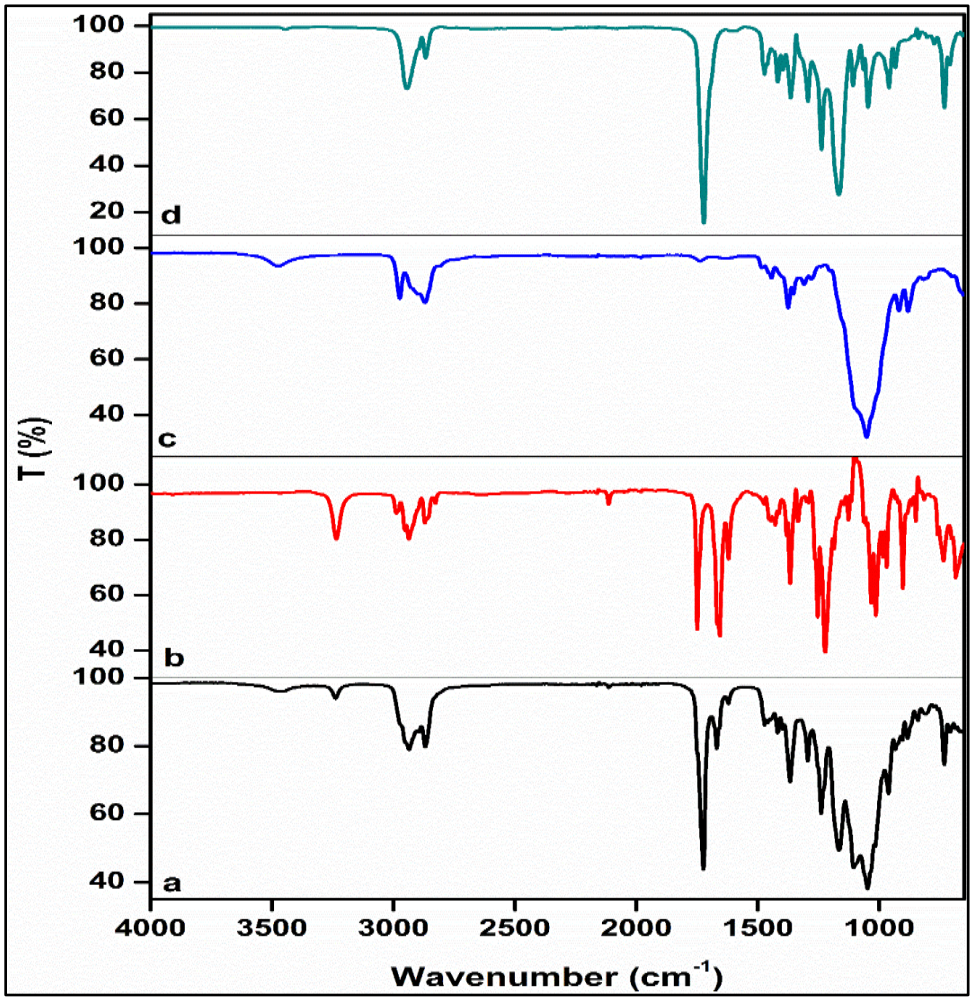

Figure 3.12: FTIR spectra of (a) the optimized NLPM, (b) NETA, (c) EC, and (d) PCL.

3.3.2.3 Morphological analysis

Assessments of morphological features were conducted using SEM to investigate the surface structural changes in the optimized drug-free and drug-loaded matrices, as well as the alterations observed due to the erosion during an 8-week incubation in SUF (Figure 3.13). SEM analysis revealed that prior to drug loading, the drug-free EC/PCL matrix exhibited a slightly roughened surface and cross-section with a sea-wave-like structure, characterized by fewer cavities, voids, and pores (Figure 3.13a1-a2). These surface irregularities and cavities lessened in the NLPM without any apparent signs of drug migration on the matrix surface (Figure 3.13b1-b2). Following an 8-week degradation period in SUF, the NLPM exhibited cracked and rough surfaces (Figure 3.13c1-c2). Furthermore, the cross-section contained closed-type pores that were not interconnected and lacked channel-like structures, which may limit the diffusion of the dissolution medium into the matrix. In an interesting observation, nano-crystalline structure, measuring in the range of 170 to 210 nm, appeared uniformly distributed within the cavities of the NLPM's cross-section (Figure 3.13d). This observation can be attributed to the rapid cooling of the NLPM from the molten state to -80 °C during the fabrication process, promoting the formation of these nano-structures (Poletaev et al. 2023).

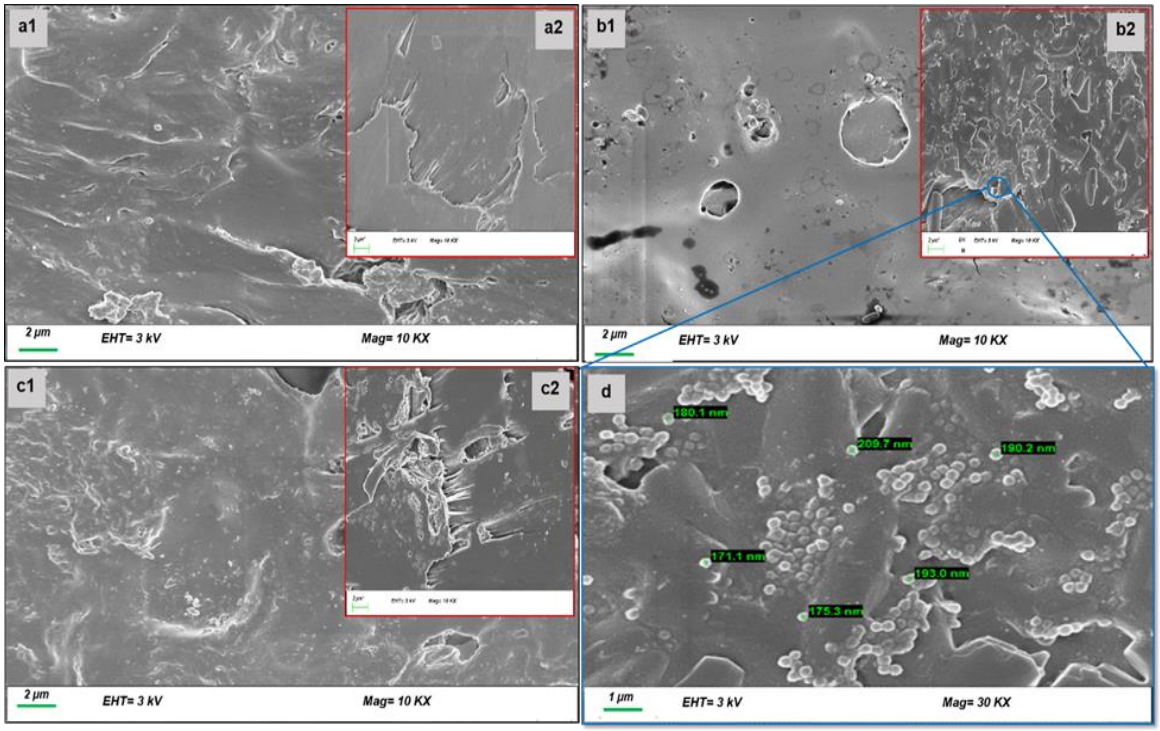

Figure 3.13: SEM analysis of surface and cross-sectional views for (a1 and a2) the drug-free PCL/EC-based matrix; (b1 and b2) the NLPM; (c1 and c2) 2-month degraded NLPM; and (d) precipitated nano-crystalline structure in the cross-section of the NLPM.

3.3.2.4 Drug release and release kinetics of optimal formulation

The efficacy of a pharmaceutical dosage form crucially relies on the processes of drug release and dissolution within biological fluids. The dissolution of a drug is a complex interplay of factors, including drug and excipient wettability and solubility. The predominant mechanisms governing drug release from polymeric matrices typically comprise diffusion, erosion, and swelling, with the prevalence of a particular mechanism contingent upon the nature of the polymer employed (Maderuelo et al. 2011, Paolini et al. 2019). Hydrophilic polymer-based matrices enable liberation of the drug load through the ingress of water into the system (Azhdari et al. 2020), a process often sensitive to temperature variations and transitions from a glassy to a matrix relaxation state. Consequently, in such matrices, the phenomena of swelling and diffusion frequently manifest. Conversely, in the case of hydrophobic polymer-based matrices, drug release predominantly occurs via diffusion or erosion, with one mechanism prevailing over the other based on the properties of the drug and the utilized excipients (Freire et al. 2017).

The drug release profiles of NETA revealed sustained release characteristics from the polymer blend-based matrices with the optimal formulation displaying a favorable drug release profile,

featuring a relatively low cumulative release percentage of approximately 38% over the 4-week testing period. However, it is noteworthy that there is an initial burst release on day 1, amounting to 178 µg, followed by a gradual decrease in daily drug release up to day 10 and thereafter extended release up to day 28 (Figure 3.14). The occurrence of burst release can be attributed to various chemical, physical, and processing factors. Factors such as drug migration during the cooling and drying processes resulted in non-uniform drug distribution, thereby promoting burst release. Additionally, the development of surface cracks is another factor contributing to burst release, as it facilitates surface erosion (Unagolla and Jayasuriya 2018).

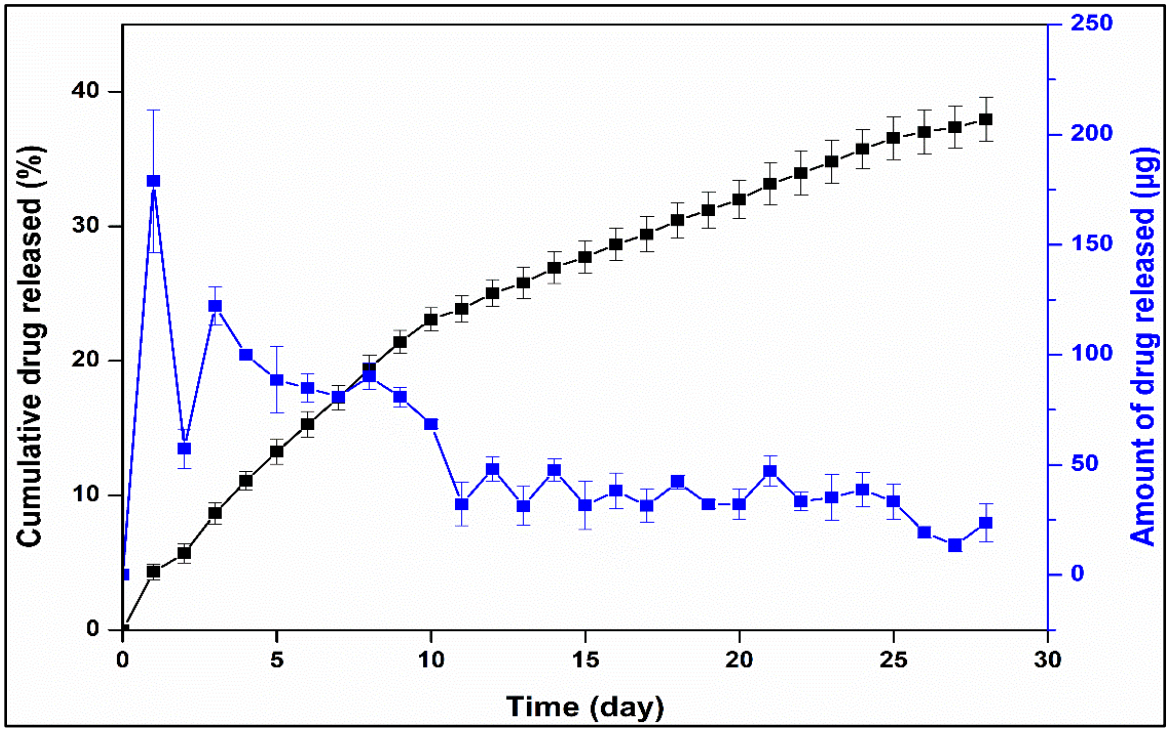

Figure 3.14: NETA release profile from the optimal NLPM formulation.

The pharmaceutical field places significant emphasis on the quantitative assessment of drug release from delivery systems. To gain a deeper understanding of this process, various mathematical models have been developed to fit experimental data. These models are designed to depict release profiles by comparing released drug fractions over time (Freire et al. 2017). To elucidate the drug release mechanism from the developed NLPM, the release kinetics of the optimized formulation were assessed through fitting the data to several release kinetic models. Table 3.6 presents the goodness of fit outcomes, including R^2, adjusted R^2, RMSE, AIC, and MSC values, applied to the averaged release profiles.

Among the mathematical models applied to describe the drug release behavior of the optimal formulation, the Peppas-Sahlin model exhibited the best fit, followed by the Korsmeyer–Peppas model. Peppas-Sahlin model demonstrates a satisfactory fit, owing to its ability to integrate both diffusional behavior and case II relaxation behavior. When the relaxation mechanism is negligible, the equality of the "n" value in the Korsmeyer-Peppas model and the "m" value in the Peppas-Sahlin model is expected (Unagolla and Jayasuriya 2018). Hence, the disparity between n (0.592) and "m" (0.801) exponents underscores that the mechanism governing NETA release is contingent on both diffusion and case II relaxation. Moreover, the obtained release exponent n from the Korsmeyer–Peppas model was 0.592 further confirms that the mechanism of NETA release exhibits an anomalous behavior or non-Fickian transport, implying that the release kinetics are characterized by a degree of complexity with several internal collective processes possibly interplay beside the diffusional mechanism, including polymer erosion, relaxation and swelling. In addition, the high value of Korsmeyer–Peppas kKP parameter (5.465) suggests that a burst release occurred during the initial phase of the release (approximately 178 µg of NETA being released on Day 1).

Table 3.6: Statistical assessment of fitting mathematical kinetic models to release data from the optimal NLPM.

Model	R^2	Adj-R^2	RMSE	AIC	MSC
Zero-order	0.7914	0.7914	4.5828	179.53	1.496
First-order	0.8985	0.8985	3.1962	159.35	2.217
Higuchi	0.9745	0.9745	1.6015	120.66	3.599
Korsmeyer-Peppas	0.9897	0.9893	1.0374	97.2838	4.4332
Peppas-Sahlin	0.9970	0.9967	0.5753	65.1683	5.5802

3.3.3 Cytocompatibility Studies

The *in vitro* cytocompatibility of the optimal NLPM and its corresponding drug-free counterpart was assessed by determining the cell viability of the NIH/3T3 cells. The cell culture medium served as a negative control, with resulting cell viability set at a value of 100% for comparison with the test samples.

On Days 1, 5, and 7, both NLPM and drug-free devices exhibited non-significant impact on the cellular viability, when compared to the negative control [p=0.092, p=0.09 (Day 1), p=0.863, p=0.966 (Day 5), p=0.602, p=0.146 (Day 7) for NLPM and drug-free matrices, respectively]. On

Day 3, matrices exhibited significant differences compared to the negative control (p=0.005, p=0.009, for NLPM and drug-free matrices, respectively). Additionally, the results showed that there are no statistically significant differences (p>0.05) between the NLPM and drug-free matrices on the cellular viability throughout the 7 days study period. Adhering to regulatory guidelines, a relative cell viability exceeding 70% compared to the control group (100%) implies non-cytotoxicity of the materials (Arany et al. 2021, Prasadh et al. 2022a). The MTT assay results on the NIH/3T3 cell line, as illustrated in Figure 3.15, affirms the cytocompatibility of the prepared optimal NLPM and drug-free matrices. Figure 3.16 further represents microphotographs of NIH/3T3 on Day 7 after treatment for the negative control, NLPM extract, and drug-free matrix extract, which further demonstrates the cytocompatibility of the optimal NLPM formulation.

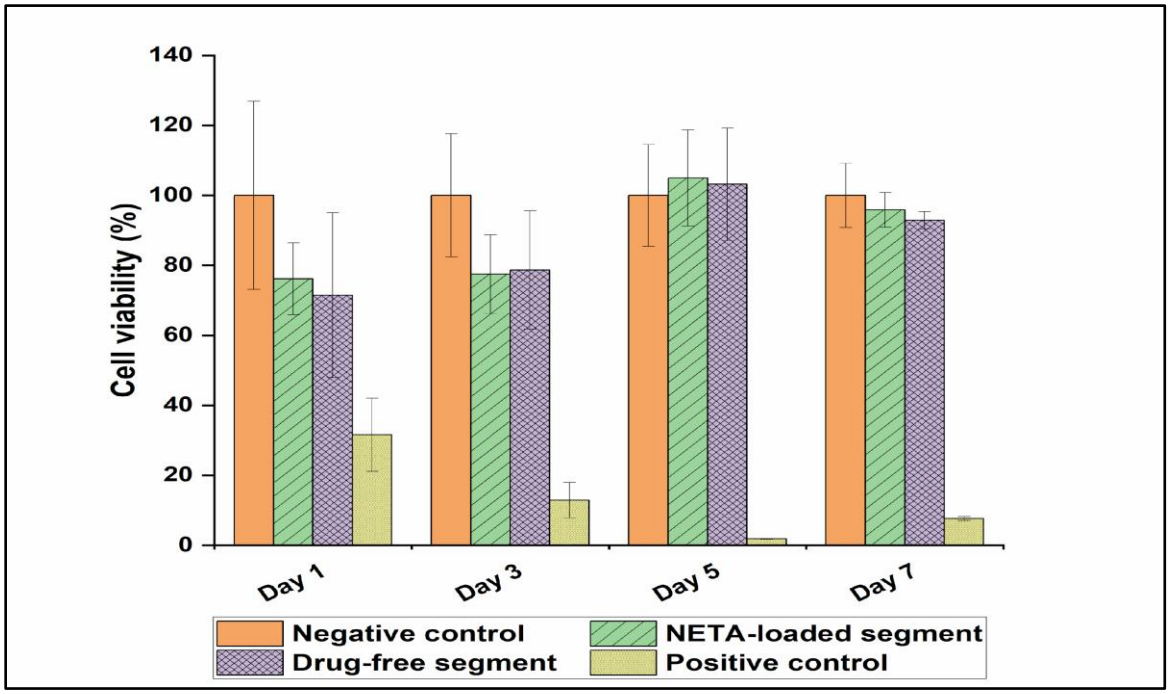

Figure 3.15: Viability of NIH/3T3 cells by MTT assay in the presence of the optimal drug-free and NLPM formulations.

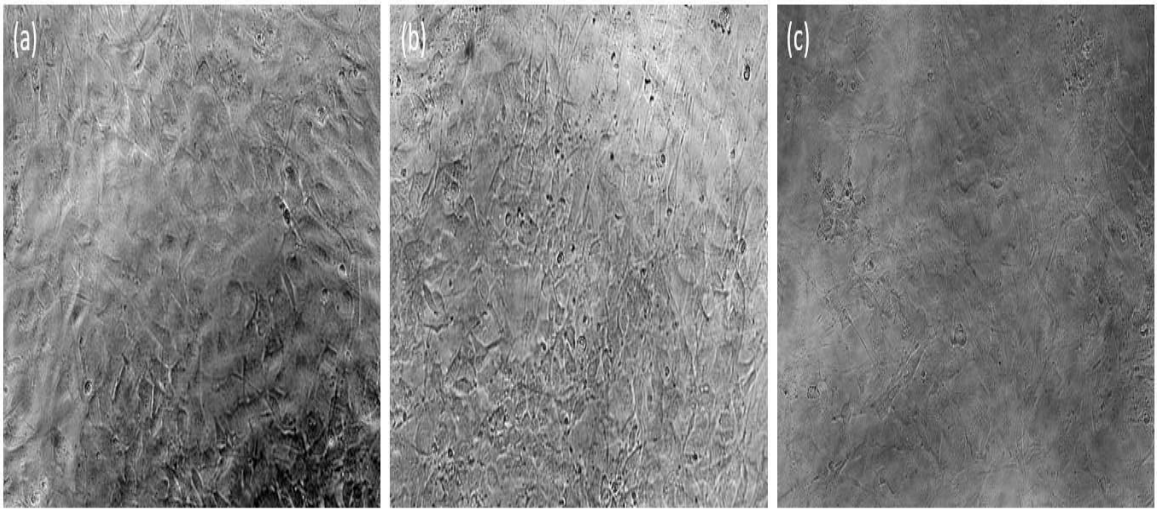

Figure 3.16: Micrographs of NIH/3T3 cells after 7 days treatment at 20X for (a) the negative control in cell culture media, (b) the NLPM extract, and (c) drug-free matrix extract (scale: 1 cm = 100 µm).

3.4 Concluding remarks

In this Chapter, polymer-based hollow, cylindrical platforms loaded with NETA were fabricated using solvent-assisted melting processing for use as a counter-estrogenic intervention in the treatment of GSM. The intricate interplay between drug loading and the proportion of matrix-forming polymers emerged as a key factor governing the kinetics of drug release and the weight loss profile in these platforms. The application of factorial experimental design stands out as an exceptional methodology, allowing for the statistical identification of experimental factor combinations and interactions critical to the attributes of the prepared platform, while the incorporation of the drug and an augmentation in the EC-to-PCL ratio significantly improved the matrix strength and resistance to indentation. Moreover, the drug release mechanism from the optimal formulation revealed a sophisticated interplay between diffusion and polymer relaxation behaviors, with the fabricated platform demonstrating commendable cytocompatibility, further emphasizing its potential application as a biocompatible and implantable intrauterine device in the management of GSM. Overall, these compelling findings therefore position the developed platform as a promising candidate for the sustained release of NETA within the uterine cavity to act as a counter-estrogenic intervention in the treatment of GSM, as well as potentially for other advanced biomedical applications.

With the positive results noted in this chapter, further research has been undertaken on the developed platform to enhance the treatment of GSM by incorporating a sustained-release

estrogenic matrix, addressing the concerns outlined in Chapter 2 regarding patient compliance and adherence. A viable approach for this involved designing an estrogen-loaded delivery system, comprising PCL and EC blend as a matrix-forming polymers. The proposed polymers were selected for their capacity to undergo controlled degradation, enabling the gradual sustained release of estrogen load within the uterine milieu, with subsequent transport to the vaginal tissues via uterine fluids. To translate these concepts into a novel delivery system, a polymeric delivery system has been formulated, tested, and statistically optimized in the subsequent chapter (Chapter 4). This developed system aims to effectively address GSM and overcome the aforementioned challenges.

CHAPTER 4

4 Development and Optimization of a Hormone-loaded Polymer-Based Intrauterine Device as a Cutting-Edge Intervention for the Genitourinary Syndrome of Menopause

4.1 Introduction

The pharmaceutical industry struggles with challenges such as lessened annual introduction of new chemical entities and heightened competition from generic drugs, necessitating inventive approaches for product manufacturing. The development of novel formulations and delivery modalities for existing drugs present opportunities to protract the product lifespan and ameliorate the financial landscape of the pharmaceutical industry (Holländer et al. 2016).

In response to the long-term treatment demands of GSM, the imperative development of a controlled release formulation for estrogenic medication emerges. This formulation is designed to facilitate sustained drug release over an extended duration, thereby diminishing the requirement for frequent dosing. The anticipated advantages encompass prolonged therapeutic effects, improved cost-effectiveness, and enhanced patient compliance (Hu et al. 2013).

Recently, substantial attention has been directed towards IDDSs, with a primary focus on the intricate incorporation of polymeric biomaterials (Desai et al. 2006, Wsoo et al. 2021, Zhou et al. 2015). These systems serve as platform for the extended release of therapeutic agents, spanning temporal scales from weeks to months and, in some instances, extending to years. The paramount objective of these systems is to maintain therapeutic drug concentrations within a desirable range. Moreover, IDDSs serve as an instrumental strategy for localized drug administration, ensuring heightened drug concentrations at specific anatomical sites while minimizing systemic exposure and consequent adverse effects (Bansal et al. 2011, Bassand et al. 2023, Karunakaran et al. 2021, Korelidou et al. 2022, Muhindo et al. 2022, Penhasi et al. 2020, Varela-Fernández et al. 2021).

While biodegradable polymers have played a pivotal role in drug delivery over recent decades (Li et al. 2010), the selection of polymers suitable for designing such delivery systems is considerably constrained, requiring stringent adherence to prerequisites such as biocompatibility, biodegradability, control over release kinetics, and specific mechanical attributes like high modulus, strength, and elongation at break, all while adhering to regulatory standards (Holländer et al. 2016, Penhasi et al. 2020). A polymer blend, formed by combining two or more polymers,

exhibits distinct physical properties that differ from those of its individual components. This approach holds promise for augmenting the intrinsic properties of polymers and provides an opportunity to develop composite structures with customized mechanical and biological characteristics (Kemala et al. 2012, Saini et al. 2016). The thermodynamic behavior of the polymer blend permits its molecular-level classification into either miscible or immiscible blends. The interfacial phenomena that emerge between the polymer phases play a pivotal role in determining the overall properties and level of compatibility observed in the blend (Penhasi et al. 2020).

In alignment with these concepts, this study endeavors to investigate a system structured using a polymer blend comprising PCL and EC, aiming to deliver a pharmacologically effective dose of E2 into the uterine cavity.

Estradiol, the essential estrogen (Farmer et al. 2021, Steffi et al. 2018), also recognized as 17 β-estradiol, E2, or chemically as estra-1,3,5(10)-triene-3, 17 β-diol, is released from women's ovaries and is functioning in several physiological processes as the maturity of breast, bones development, and appearance of various female puberty characteristics (Carter and Sluss 2013, Kireç et al. 2021). According to the menstruation phase, the daily amount of secreted Estradiol from the ovaries ranges between 70 to 500 µg (Naunton et al. 2006), resulting in plasma estradiol levels ranging between 40 to 250 pico-gram per ml in reproductive-age women. This level falls to about 15 pico-gram per ml in menopausal women (Prakapenka et al. 2017). Estradiol is highly administered alone or in combination with progestins to relieve the symptoms of severe and moderate menopause, contraception, osteoporosis, used as hypo-cholesteremic agent (Hariharan et al. 2006, Križman et al. 2021a, Mittal et al. 2007, Steffi et al. 2018, Zaghloul et al. 2006), and has known for its beneficial effects in the central nervous system (CNS) (Enayati et al. 2012, Prakapenka et al. 2017, Turek et al. 2016). Due to the severe side effects and risks of estradiol use, which depend on the duration of time and amount to be used, the slightest efficient dose of Estradiol is recommended when long regimen treatment is indicated (Hariharan et al. 2006, Steffi et al. 2018). Estradiol belongs to class II biopharmaceutical classification system with poor water solubility (0.2– 5 µg/mL), high permeability (Xiong et al. 2017), sparingly soluble in vegetable oil, and well absorbed orally (Hariharan et al. 2006, Wang Jue et al. 1999) and undergoes broad first pass metabolism leading to poor bioavailability, and as a consequence for that large and frequent oral dose is required which lead to more chance for side effects (Hariharan et al. 2006, Prakapenka et al. 2020, Zaghloul et al. 2005). 17β-estradiol exists and is marketed in different dosage forms as tablets to be taken orally or inserted via the vagina and as transdermal

formulations (Križman et al. 2021a, Turek et al. 2016). The currently marketed intravaginal tablet contains 10 µg of estradiol per tablet, intended for daily use for 2 weeks followed by 2 tablets per week. Estrace cream, containing 0.01% estradiol, is used daily for 2 weeks, followed by a maintenance dose of 1 to 3 times weekly. Imvexxy softgel capsules are available in ultra-low doses of 4 µg per insert, along with a dose of 10 µg per insert. Additionally, Estring and Femring are intravaginal rings available with different estradiol load, such as 2 mg per ring for Estring and 12.4 or 24.8 mg per ring for Femring, to GSM (Abdelgader et al. 2023). Detailed information regarding the additives, production methods, safety, and acceptance of these delivery systems can be found in Chapter 2.

The unopposed exposure to estrogenic medication for prolonged period of time may leads to uterine endometrial proliferation, potentially leading to endometrial hyperplasia and carcinoma (Elsokkary et al. 2016). The targeted delivery of progestogens such as NETA to the genitourinary tract tissues may preserve the beneficial effects and counteract the estrogenic effects on endometrial tissues (Ostad et al. 1998, Somboonporn et al. 2011). Direct delivery of E2 and NETA using modalities as IUD may associated with pain and bleeding as a consequence of device insertion (Jinying et al. 2008, Yang et al. 2009). However, controlled-release formulations of indomethacin (IND) developed for use in medicated IUDs could serve as a viable option to improve treatment adherence and reduce device removal rates (Qi et al. 2012, Tian et al. 2013).

Non-steroidal anti-inflammatory drugs (NSAIDs) are widely recognized for their efficacy in alleviating pain and inflammation. While various administration routes are available, oral delivery is considered the most preferable. However, oral delivery of NSAIDs is associated with a significant range of adverse effects. Among these, IND stands out as a frequently utilized NSAID for the management of inflammation and pain associated with rheumatic diseases, and, to a lesser extent, in postoperative pain management. Nevertheless, the clinical utility of indomethacin is tempered by its elevated incidence of gastrointestinal side effects (Dupeyrón et al. 2013).

The development of controlled release formulations necessitates a comprehensive approach, involving the meticulous adjustment and optimization of multiple parameters, including the composition of the polymer matrix and the ratio of drug to the matrix-forming polymer. Conventional trial-and-error approaches impose a substantial burden in terms of experimental resources, as they demand an escalating number of trials to ascertain a satisfactory solution. This inefficiency becomes particularly pronounced when dealing with a multitude of factors. In light of this, novel strategies for formulation optimization are warranted to enhance efficiency and precision in the development of controlled release systems (Barmpalexis et al. 2010). However,

these challenges have been surpassed by the statistical Design of Experiments (DoE) methodologies. Statistical DoE not only streamlines conventional optimization tasks but also effectively addresses the intricate challenges inherent in the formulation development process. DOE has gained widespread adoption in industrial settings, owing to its capacity to deliver statistically robust insights and economically efficient solutions throughout the formulation development process (Acharya et al. 2012, Barmpalexis et al. 2010).

In pharmaceutical research, the Central Composite Design (CCD) and the Box–Behnken design (BBD) are predominantly RSMs employed in pharmaceutical research to optimize independent variables (Kumar et al. 2022). The CCD, introduced by Box and Wilson in 1951, involves a set of two-level factorial design points, star points to extend the design area and estimate quadratic terms, and central points for evaluating experimental error (Ahmed et al. 2022). CCD, by its offering an additional rotatable star points with extreme values, holds an advantage over BBD in providing more flexibility and accurate predictions (Kumar et al. 2022).

In this Chapter, we developed, assessed, and optimized E2-loaded polymer-based hollow cylindrical device (EPHCD) based on PCL and EC polymeric blend. The primary objective of this system is to achieve sustained release of E2, targeting the GSM. The fabrication of EPHCDs was achieved via the solvent-assisted melting technique. Rotatable CCD was employed to optimize formulation parameters such as the drug-to-total polymer ratio and the EC-to-PCL ratio to achieve desired drug release kinetics and weight loss profiles. Subsequently, the optimized EPHCD underwent characterization to assess its morphology, hydration capacity, FTIR spectra, and mechanical properties under wet conditions. Furthermore, the release behavior and flux of E2, along with the biocompatibility of the optimized EPHCD, were thoroughly investigated and elucidated. Additionally, this Chapter presents the fabrication and performance assessment of an IND-loaded polymeric matrix (IND-LPM). This unit is based on a PCL and PEG polymer-blend, and evaluated, optimized and fabricated using the 2^2 FD. Furthermore, in conjunction with the EPHCD, the optimal NLPM discussed in Chapter 3 and the IND-LPM were assembled together to form a novel intrauterine polymer-based platform (Variant 1 as described in section 1.3) tailored to address GSM. The long term cytocompatibility of the combined delivery system was further elucidated. Figure 4.1 illustrates the schematic architecture of the intrauterine delivery system, showcasing the integration of the three-drug-loaded units designed to release E2, NETA, and IND.

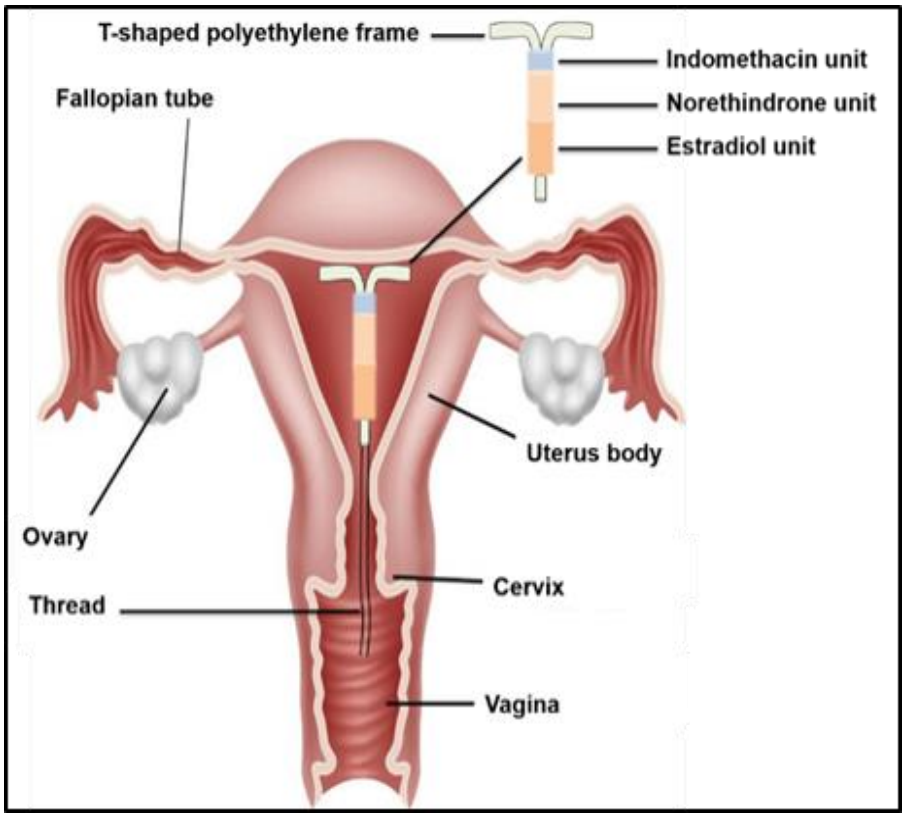

Figure 4.1: Schematic representation of the MUPP depicting the E2, NETA, and IND components placed on the T-shape frame.

4.2 Materials and Methods

4.2.1 Materials

Estradiol hemihydrate purchased from Leap Chem (Hong Kong, China), Indomethacin, PCL Mn = 80,000 was purchased from Sigma-Aldrich (Tokyo, Japan), ethyl cellulose from Sigma-Aldrich Chemie GmbH (St Louis, MI, USA) and sodium hydroxide pellets from Merck Chemicals (Modderfontein, South Africa). NIH/3T3 mouse fibroblast cells (ATCC CRL-1658) were obtained from the ATCC (American Type Culture Collection, Manassas, VA, USA), Dulbecco's Modified Eagle Medium (DMEM) from Life Technologies Limited “Gibco” (Paisley, UK), Fetal bovine serum from PAN Biotech (Aidenbach, Germany), and MTT solution and solubilizing buffer from Roche Diagnostic GmbH (Mannheim, Germany). All other chemicals were of analytical grade and used without further purification.

4.2.2 Methodology

4.2.2.1 Fabrication of EPHCD

The EPHCDs were fabricated as per methodology detailed in Chapter 3, Section 3.2.2.1. For the EPHCD, the impact of varying levels of independent formulation variables on key attributes of EPHCD and determining optimized combinations were assessed and explored. Statistical DoE techniques utilizing Design Expert® version 8 (StatEase, Inc, Minneapolis MN 55413, USA) were employed, generating a rotatable CCD template with α=1.414 and then used to produce EPHCD formulations involving combinations of PCL, EC, and E2. Two formulation variables, E2 load (X_1) ranging from 5% to 10%, and the ratio of EC-to-PCL (X_2) ranging from 10% to 50%, were chosen (Table 4.1). The effects of these variables were studied on key EPHCD outputs, including drug release percentages after 1, 2, 3, and 4 weeks (Y1, Y2, Y3, and Y4, respectively), and weight loss percentage after 8 weeks incubation in SUF (Y5). Fourteen experimental runs (EH1 – EH14) were conducted, encompassing factorial formulations at low (-1) and high (+1) levels, axial formulations, and central points, as outlined in Table 4.1. The runs were allocated in two blocks as all the runs could not be performed at once. Moreover, the order of experiments was fully randomized for all instances. In order to facilitate comparative analyses, control formulations devoid of the drug were prepared in correspondence to the E2-loaded formulations (Table 4.1).

The optimal mathematical models were selected based on an assessment of statistical parameters such as, p-value, R^2, adjusted R^2, predicted R^2, CV, and predicted residual sum of squares (PRESS). Second-order polynomial equations were derived to express the relationship between responses and input parameters, presented as follow (Equation 4.1):

$$Y = b_0 + b_1X_1 + b_2X_2 + b_{12}X_1X_2 + b_{11}X_1^2 + b_{22}X_2^2 \qquad \text{Equation 4.1}$$

where X_1, X_2 represent the main effects, X_1^2 and X_2^2 the quadratic effects, and X_1X_2 is the interaction effect. Y represents responses, b_0 is an intercept representing the arithmetic average of all quantitative outcomes, and b_1, b_2, b_{12}, b_{11}, b_{22} represent the regression coefficients.

The 3D and contour plots were generated from these equations to visualize the impact of formulation factors on measured responses. Response optimization was performed using numerical and graphical techniques, employing the desirability approach and overlay plots, respectively, to achieve an optimized solution with desirable drug load and polymeric proportions.

Table 4.1: Experimental design domain of the CCD and compositions of NLPM and drug-free devices.

EPHCD			Point type	Drug free device	
F Code*	E2	EC-to-PCL		F Code*	EC-to-PCL
EH1	5% (-1)	10% (-1)	Factorial	DF1	10% (-1)
EH2	10% (1)	10% (-1)	Factorial	DF2	10% (-1)
EH3	5% (-1)	50% (1)	Factorial	DF3	50% (1)
EH4	10% (1)	50% (1)	Factorial	DF4	50% (1)
EH5	7.5% (0)	30% (0)	Center	X	X
EH6	7.5% (0)	30% (0)	Center	X	X
EH7	7.5% (0)	30% (0)	Center	X	X
EH8	3.96% (-1.414)	30% (0)	Axial	DF5	30% (0)
EH9	11.04% (1.414)	30% (0)	Axial	DF6	30% (0)
EH10	7.5% (0)	1.72% (-1.414)	Axial	DF7	1.72% (-1.414)
EH11	7.5% (0)	58.28% (1.414)	Axial	DF8	58.28% (1.414)
EH12	7.5% (0)	30% (0)	Center	DF9 (C)**	30% (0)
EH13	7.5% (0)	30% (0)	Center	X	X
EH14	7.5% (0)	30% (0)	Center	X	X

* Formulation code ** Center point formulation

4.2.2.1.1 Analytical method for E2 quantification and the construction of calibration curves

The validation of E2 quantification method was conducted following the protocol outlined in Chapter 3, Section 3.2.2.2.1. The E2 was quantified in the formulations using UV-spectrophotometry at λmax 280 nm. Calibration curves for E2 were generated in SUF (pH 7) and ACN:MeOH mixture (20:80), using a known series of E2 concentrations ranging from 0 to 40 µg/ml. The calibration curves were subjected to linear regression analysis, with absorbance of E2 as the dependent variable and E2 concentration as the independent variable. The R^2 was computed to assess the linearity and goodness of fit for each calibration curve (Figure 4.2).

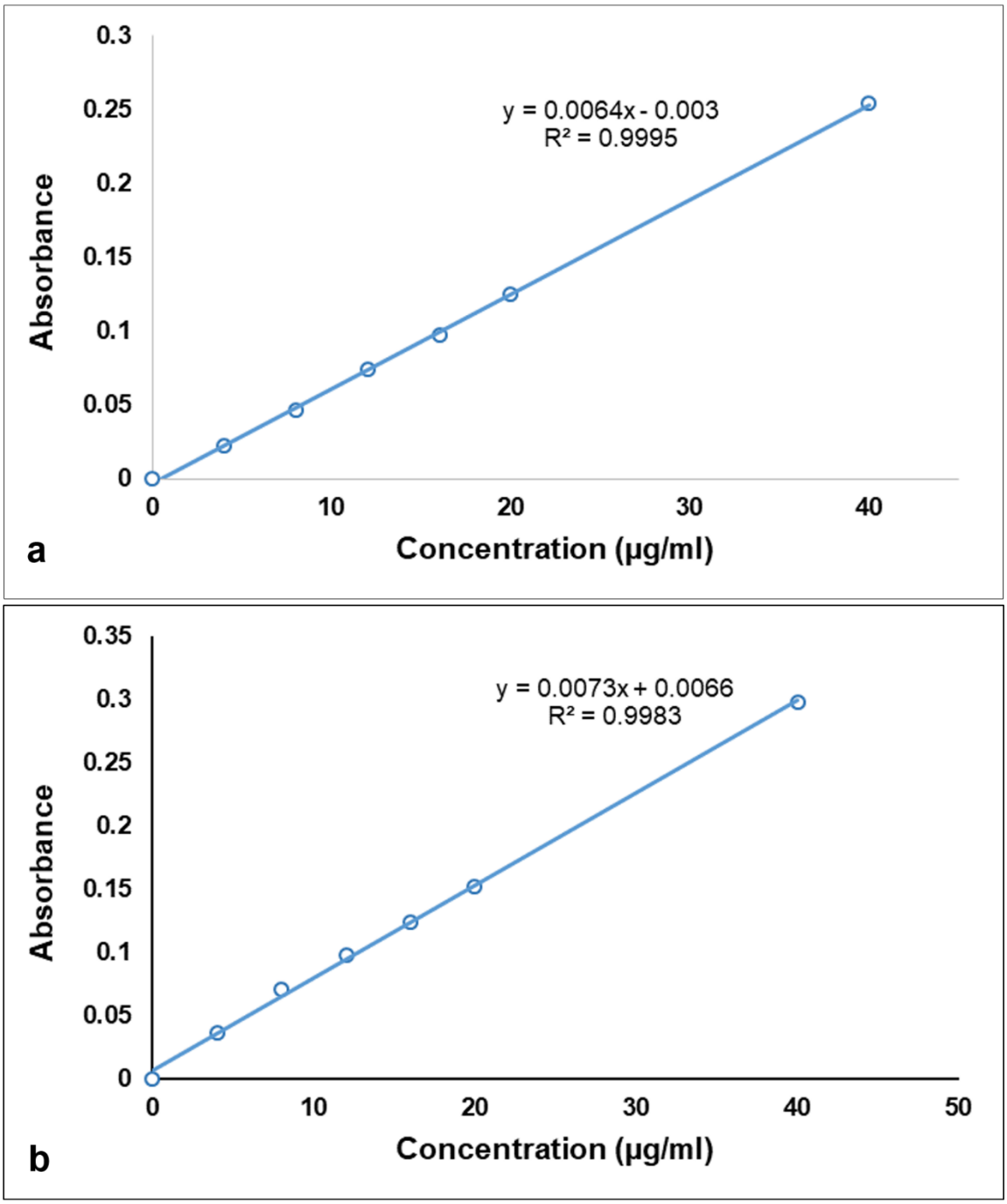

Figure 4.2: Calibration curve of E2 in (a) SUF and (b) ACN:MeOH.

4.2.2.1.2 Determination of diameter and drug content uniformity

The measurement of the diameter for each individual EPHCD was performed employing a digital vernier caliper. In addition, an assessment of percent content uniformity was conducted, to ascertain accurate dose delivery and ensure homogeneous drug distribution throughout the

device. This assessment was performed using the method detailed in Chapter 3, Section 3.2.2.2.1.

4.2.2.1.3 Biodegradation in SUF and accelerated alkaline degradation assessment

Specimens of EPHCD and drug-free devices underwent biodegradation analysis in SUF and assisted alkaline degradation as per the procedures described in Chapter 3, Section 3.2.2.2.2.

4.2.2.1.4 Textural analysis

Physico-mechanical characteristics of the EPHCD and drug-free formulations, particularly their hardness, were examined through the determination of resistance to indentation employing a calibrated textural analyzer (TA.XT.plus; Stable Micro Systems, Surrey, UK) and following the methodology reported in Chapter 3, Section 3.2.2.2.3. All experiments were conducted in triplicate and at a room temperature of 22°C.

4.2.2.1.5 *In vitro* drug release

The *in vitro* drug release patterns of EPHCD in SUF were investigated as detailed in Chapter 3, Section 3.2.2.2.4. The SUF was prepared according to method published by (Yang et al. 2009) and contained (gram per liter of purified water); 4.97 g NaCl, 0.224 g KCl, 0.025 g $NaHCO_3$, 0.072 g NaH2PO4.2H_2O, 0.167 g $CaCl_2$, and 0.5 g glucose. The release profiles were determined using cumulative percentage drug release based on the average triplicate experimental values populated.

4.2.2.1.6 Constrained statistical optimization of the EPHCD

Statistic optimization of the prepared EPHCD was achieved utilizing the data generated in the evaluation of design formulations. The parameters utilized for the optimization were the “in range” for the E2 load and EC-to-PCL ratio. In addition, the minimized release and weight loss were set as a desirable. The selected optimal formulation was thereafter subjected to hydration studies, structural profiling, morphological analysis, release kinetic modelling, *ex vivo* permeation studies, and cytocompatibility studies undertaken as described below.

4.2.2.2 In vitro characterization of the optimal EPHCD

4.2.2.2.1 Water retention capacity

The hydration characteristics of optimized EPHCD and its corresponding drug-free formulations were evaluated gravimetrically as per method outlined in Chapter 3, Section 3.2.2.3.1.

4.2.2.2.2 Determination of chemical integrity using FTIR spectroscopy analysis

FTIR spectra serves as a valuable tool to elucidate the drug-excipient interactions by monitoring alterations in the vibrational or stretching bands associated with key functional groups. The FTIR spectroscopy was acquired for the optimal formulation, pure drug, and pristine polymer components and was carried out as detailed in Chapter 3, Section 3.2.2.3.2.

4.2.2.2.3 Morphological analysis

Surface and cross-sectional imaging of optimal EPHCD, pre- and post-8-week incubation in SUF were executed following the procedures reported in Chapter 3, Section 3.2.2.3.3.

4.2.2.2.4 Mathematical modeling of the release kinetics

The mechanisms of drug release of optimized EPHCD were elucidated through the application of mathematical models, encompassing zero-order, first-order, Higuchi, Korsmeyer-Peppas, Hixson-Crowell, and Peppas-Sahlin models.

4.2.2.3 Fabrication of IND-LPM

The IND-LPM was fabricated as per methodology detailed in Chapter 3, Section 3.2.2.1. A 2^2 FD was employed to investigate the effect of the IND and PEG amount (mg) on the critical attributes of the IND-LPM, which contain constant quantity (mg) of PCL throughout the formulations (Table 4.2). The dependent variables chosen were the percentage drug release and degradation for 2 weeks. The 2^2 FD involved 7 runs, fully randomized, with 4 factorial formulations at low (-1) and high (+1) levels (F1 – F4) and 3 central points (F5 – F7), as indicated in Table 4.2.

Table 4.2: Experimental design domain of the 2^2 FD and compositions of IND-LPM.

F Code*	Point type	IND (mg)	PEG (mg)	PCL (mg)
IND1	Factorial	125 (-1)	500 (-1)	1000
IND2	Factorial	250 (1)	500 (-1)	1000
IND3	Factorial	125 (-1)	750 (1)	1000
IND4	Factorial	250 (1)	750 (1)	1000
IND5	Center	187.5 (0)	625 (0)	1000
IND6	Center	187.5 (0)	625 (0)	1000
IND7	Center	187.5 (0)	625 (0)	1000

* Formulation code

4.2.2.3.1 Determination of diameter and drug content uniformity

The measurement of IND-LPM diameter was achieved using a digital vernier caliper. Furthermore, the percent content uniformity assessment was conducted using the method detailed in Chapter 3, Section 3.2.2.2.1.

4.2.2.3.2 Biodegradation in SUF and accelerated alkaline degradation assessment

Specimens of IND-LPM underwent biodegradation analysis in SUF as per the procedures described in Chapter 3, Section 3.2.2.2.2.

4.2.2.3.3 Textural analysis

The resistance to indentation of IND-LPM were evaluated using a calibrated textural analyzer (TA.XT.plus; Stable Micro Systems, Surrey, UK) and following the procedures detailed in Chapter 3, Section 3.2.2.2.3.

4.2.2.3.4 *In vitro* drug release

The *in vitro* drug release patterns of IND-LPM in SUF were investigated as detailed in Chapter 3, Section 3.2.2.2.4, at 320 nm ($\varepsilon = 0.0189$; $R^2 = 0.999$).

4.2.2.3.5 Statistical optimization of the IND-LPM

Statistic optimization of the IND-LPM was achieved utilizing the data generated in the evaluation of design formulations. The parameters utilized for the optimization were the “in range” for the content of IND and PEG, while the release after 2 weeks and weight loss percentages were set to be maximized. Statistic optimization of IND-LPM through the DOE generated an optimal formulation closely similar to IND3 which featured low drug content (125 mg) and PEG content of 750 mg. The selected optimal formulation was thereafter subjected to FTIR (Chapter 3, Section 3.2.2.3.2.), morphological analysis (as described in Chapter 3, Section 3.2.2.3.3), and cytocompatibility studies undertaken as described below in Section 4.2.6.

4.2.3 Fabrication of and analysis of MUPP variant one

The MUPP variant one was assembled by envelopment of the optimized EPHCD, NLPM, and IND-LPM on the 3D printed T-shaped plastic frame, which was thereafter characterized for its drug release kinetics. Further cytotoxicity studies have been undertaken on the MUPP variant one and have been described in Section 4.2.6.

4.2.4 Drug release of MUPP variant one

The *in vitro* drug release pattern of MUPP variant one in SUF over one week period was investigated as detailed in Chapter 3, Section 3.2.2.2.4. Drug quantification was performed using

high-performance liquid chromatography (HPLC) method, adapted from a previously reported protocol (Dorantes and Stavchansky 1994), enabling for simultaneous detection of E2 and NETA. The HPLC system comprised a Flexar Binary LC pump and a Flexar UV/VIS LC detector (PerkinElmer Inc., Waltham, MA, USA) paired with a Brownlee Analytical C18 column (150 mm length, 4.6 mm diameter, 5 µm particle size; PerkinElmer, USA) operating at ambient temperature (22^{o}C). Chromatographic separation was achieved via isocratic elution with a mobile phase consisting of ACN: water (60:40), a flow rate of 0.8 ml/min, and a total run time of 12 min for each 20 µL injection volume. The retention times for E2 and NETA were 3.26 and 8.66 min, respectively, with both drugs detected at a wavelength of 240 nm. Standard solutions of E2 and NETA were prepared by dissolving the drugs in SUF and diluting to appropriate concentrations. The peak areas exhibited a linear relationship with E2 and NETA concentrations ranging from 1.56–50 µg/ml. Data acquisition and analysis were performed using Chromera software (Version 4, PerkinElmer, USA). Cumulative drug release was calculated from the HPLC data and normalized to the total drug content in the MUPP. All experiments were conducted in triplicate.

4.2.5 *Ex vivo* Drug Permeation Studies

Porcine uterine tissues were procured from the Wits Research Animal Facility (WRAF, Faculty of Health Sciences, University of the Witwatersrand, Johannesburg, South Africa) under an approved waiver from the Animal Research Ethics Committee of the University of the Witwatersrand (Waiver 16-11-2023-O; Appendix B1). The tissues were sourced immediately after the sacrifice of pigs and transported to the laboratory in phosphate-buffered saline (PBS). Upon arrival, the uterine body was longitudinally opened, washed with PBS, and the mucosa was meticulously separated from the underlying muscular layer. Circular pieces were then punched out, washed in PBS, and subsequently stored at -80 °C until use.

To assess E2 and NETA permeation across the pig uterine membrane, permeation studies were conducted using a Franz diffusion cell (FDC) apparatus (PermeGear Inc., Bethlehem, PA, USA) (Figure 4.3). The apparatus was equipped with a 12-mL receptor compartment, clamp, and stirrer-bar. The uterine tissue was positioned between the donor and receptor compartments of the FDC apparatus, with the endometrial part facing the donor compartment. The receptor compartment contained 10.5 mL of PBS (pH 7.4) at 37°C, maintained at a constant temperature with a water bath and stirred continuously using a magnetic stir bar. The uterine tissue thickness was approximately 1.8 ± 0.04 mm, with a permeation area of 1.039 ± 0.01 cm^{2}. In the donor compartment, a piece of the NLPM or EPHCD (certain weight) was placed, covered with 1 ml

simulated uterine fluid (SUF, pH 7), and assessed for drug permeation across the pig uterine tissue into the PBS in the donor compartment.

Samples of 0.2 ml were withdrawn from the receptor compartment at predetermined intervals over 8 hours. Quantitative drug analysis was performed using an Implen NanoPhotometer. Fresh PBS was replaced in the receptor compartment to maintain sink conditions. The permeation study was conducted in triplicate, and the drug flux (mg cm^{-2} h^{-1}) across the tissue was calculated at steady-state per unit area using linear regression analysis of the permeation data with the Equation 4.2:

$$J_s = \frac{Q_r}{A\,t} \qquad \text{Equation 4.2}$$

where J_s is the drug flux (mg cm^{-2} h^{-1}), Q_r is the drug quantity in mg that diffused through the pig tissue into the receptor compartment, A (cm^{-2}) is the effective cross-sectional area available for drug permeation, and t (h) is the time of drug exposure to the tissues.

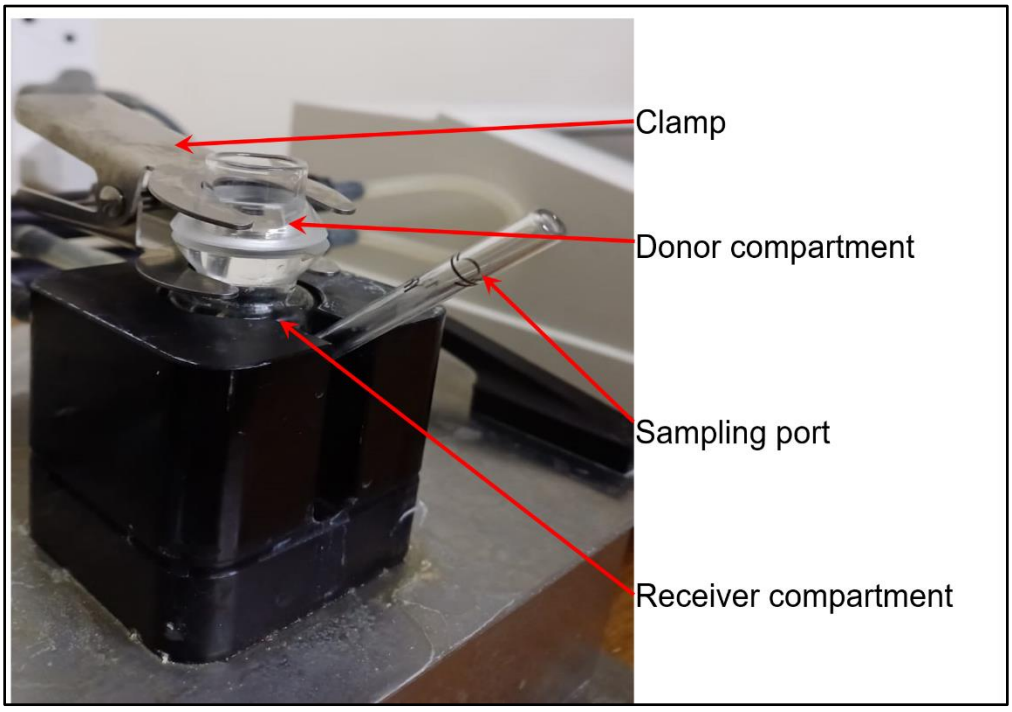

Figure 4.3: Franz diffusion cell apparatus used for permeation study.

4.2.6 Cytocompatibility Studies

The cytocompatibility over 7 days period of the optimal EPHCD and its corresponding drug-free formulation was assessed on NIH/3T3 cells (mouse fibroblast cells) as described in Chapter 3, Section 3.2.3.

Furthermore, the cells viability in the presence of mixture extracts of the three drug-loaded segments was evaluated. Sample preparation for this study consisted of extraction of leachates from the EPHCD, optimal NLPM, and optimal IND-LPM. The extracts leachates after 5 days in *in vitro* release media as well as that after 28 days were mixed together in a ratio of 1:1:1 (EPHCD:NLPM:IND-LPM) to obtain the cytocompatibility of the variant one of the MUPP device at varying drug concentrations. Thereafter, the cytocompatibility of the MUPP variant one device was studied over 7 days as described in Chapter 3, Section 3.2.3.

4.2.7 Statistical Analysis

The study utilized Design Expert® 8 software to construct the DOE matrices, aimed at elucidating the influence of independent variables on selected response parameters of the fabricated EPHCD and IND-LPM units and executing optimization strategies. All other statistical analysis were performed as detailed in Chapter 3, Section 3.2.4.

4.3 Results and Discussion

4.3.1 Fabrication of the EPHCD

Formulation variables and process employed to prepare the EPHCD were selected based on preliminary studies and the literature review. Different researchers have reported PCL as a base for matrices to be inserted via the female genitourinary tract either intravaginal or intrauterine (Asvadi et al. 2013b, Dang et al. 2013, Fernando et al. 2019, Holländer et al. 2016, Li et al. 2021, Pathak et al. 2014, Pathak et al. 2018). The proportion of polymers can influence various aspects of the manufacturing process, including demolding, which might result in uneven and fractured segment surfaces, potentially leading to sub-optimal release profiles. The range of polymer ratios considered herein, was identified based on ratios explored during the preliminary studies phase, which yielded the smoother segment surfaces, primarily attributed to improved ease of processing.

Several factors played a crucial role in determining the feasibility of the early prototypes' preparation process for this design. These factors included the melting duration and the selection of a suitable solvent. It was observed that the optimal time required to completely melt the binary polymer blend and drugs at the specified temperature (45 °C) is 30 minutes. Also, when acetone

is utilized as a solvent to accelerate the melting process, the blend's consistency and adaptability for processing are notably improved, in contrast to chloroform and DCM, which result in a blend with low consistency, making it challenging to mold and prone to a delayed hardening process during the cooling phase of preparation. Additionally, careful consideration should be paid to the time required to introduce the malleable blend into the mold. It was noted that the feeding time into the small-diameter opening mold should be as brief as possible, ideally within a minute, particularly when working with formulations containing a high PCL ratio, as the blend tends to solidify rapidly within time in the mold opening. Consequently, a series of extensive preliminary experiments were conducted to determine the appropriate melting time, choice of solvent, and feeding time into the mold.

Figure 4.4 depicts the successful fabrication of the EPHCD device characterized by average dimensions of 30 mm in length, 4 mm in diameter, and 1.5 mm in inner diameter. The fabrication process involved solvent-assisted melting techniques, resulting in a device with a smooth and uniform surface.

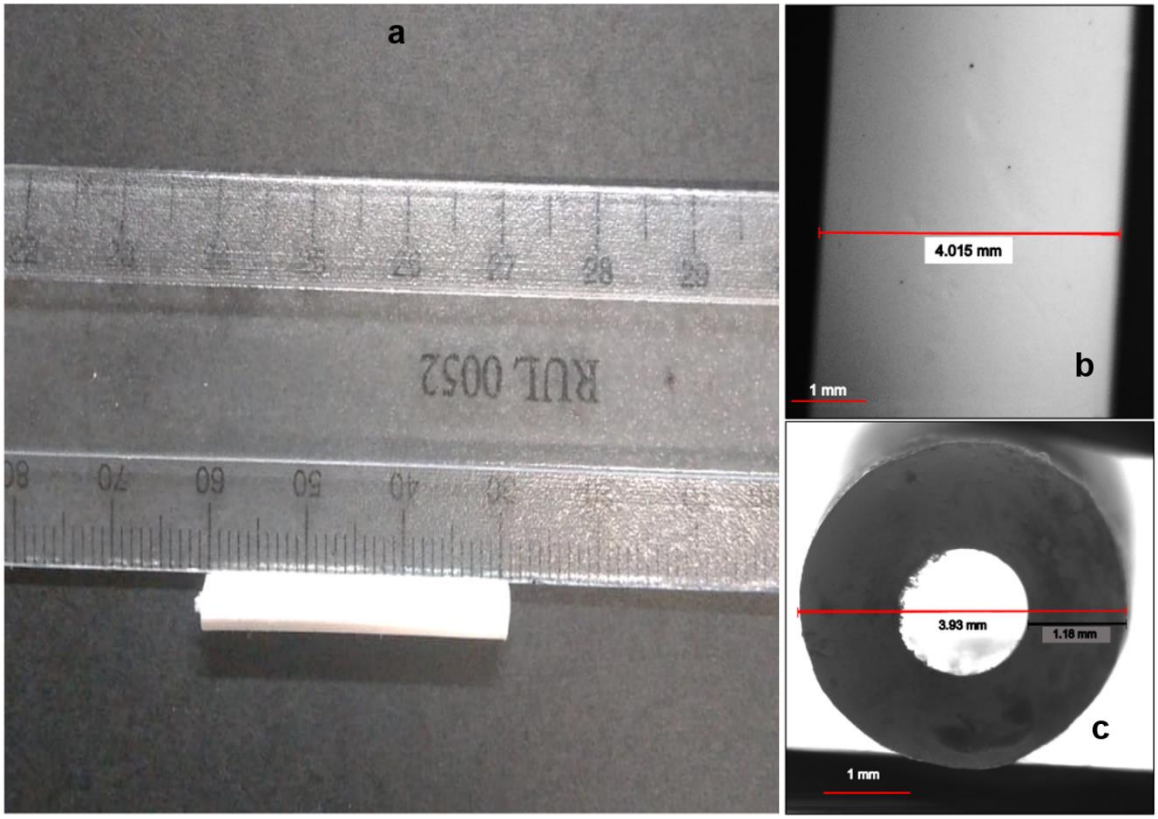

Figure 4.4: Photograph of the EPHCD PCL/EC hollow cylindrical device (a) front view in mm, (b) side view, and (c) cross-section view.

4.3.2 Evaluation of the Experimental Design

4.3.2.1 Determination of diameter and drug content uniformity

The evaluation of drug content uniformity provides crucial insights into the homogeneity of drug loads across different batches and the spatial distribution within the individual devices. Elucidated in Table 4.3 are the average diameter and drug content of the EPHCD. The results demonstrate that the E2 content in it is respective formulations closely conforms to the initial feed ratios across the various batches, exhibiting a minimal standard deviation (SD), less than the pharmacopoeial specification (15%) (Solano et al. 2013). This observation indicates a consistent and uniform distribution of E2 within the polymer matrices, with negligible evidence of drug decomposition during the fabrication process. Additionally, the drug content analysis revealed a direct correlation between the quantity of drug utilized in the device preparation and the resulting loaded drug content. However, formulations EH1, EH2, EH3, and EH6 showed relatively low incorporation efficiency which may indicate inadequate mixing processing in these formulations. Furthermore, the hydrophobic nature of the drug is observed to facilitate its effective incorporation within the matrix of the corresponding hydrophobic polymer blend. Moreover, the fabricated devices display marginal diameter variation, with values ≤ 2%. This slight variability is likely ascribed to disparities in the density and viscosity of blends employed throughout various formulations. Consequently, in light of outcomes pertaining to diameter and content uniformity, it can be deduced that the employed fabrication methodology and processing conditions adhere to criteria indicative of reproducibility, rendering them suitable and acceptable for consistent manufacturing practices (Li et al. 2010, Liu Xi et al. 2011).

Table 4.3: Diameter and drug content in the fabricated EPHCD (n=3).

Formulation Code	Diameter (mm)	Theoretical loading%	Drug content (%±SD)	Incorporation efficiency (%±SD)
EH1	3.76±0.076	5	4.56±0.34	91.24±6.70
EH2	4.07±0.006	10	9.17±0.50	91.69±5.04
EH3	4.07±0.010	5	4.46±0.46	89.15±9.10
EH4	4.13±0.035	10	9.97±0.02	99.73±0.21
EH5	4.09±0.015	7.5	7.26±0.34	96.79±4.55
EH6	4.10±0.010	7.5	7.01±0.17	93.41±2.20
EH7	4.07±0.006	7.5	7.14±0.34	95.23±4.53
EH8	3.85±0.025	3.96	3.89±0.09	98.33±2.22
EH9	4.04±0.051	11.04	10.79±0.24	97.77±2.13
EH10	3.97±0.030	7.5	7.29±0.12	97.18±1.60
EH11	4.07±0.045	7.5	7.34±0.10	97.91±1.37
EH12	4.06±0.035	7.5	7.16±0.12	95.39±1.62
EH13	4.05±0.050	7.5	7.31±0.09	97.49±1.24
EH14	4.10±0.010	7.5	7.09±0.22	94.49±2.92

4.3.2.2 Degradation study

The matrix erosion in SUF could potentially affect the release patterns of the E2 from the devices. Thus, it is vital to monitor *in vitro* erosion by assessing the percentage of weight loss over time. The percentage weight loss of formulations (EH1 to EH14) ranged from 1.66±0.35 to 3.06±0.38 as shown in Figure 4.5. Notably, formulations with a low drug load (5%), such as EH1 and EH3, showed a significant decrease in weight loss percentage with increasing EC content from 10% to 50%. Conversely, formulations with a high drug load (10%), such as EH2 and EH4, an increment in EC content led to an observable increase in the percentage of weight loss. Additionally, at 10% EC, a shift from a 5% to 10% drug load resulted in a decrease in weight loss percentage, observed in formulations EH1 and EH2. In contrast, at 50% EC, an increase in drug load from 5% to 10% led to an increase in weight loss percentage, as seen in formulations EH3 and EH4. Interestingly, combinations of intermediate levels for both independent variables resulted in the most significant reduction in weight loss.

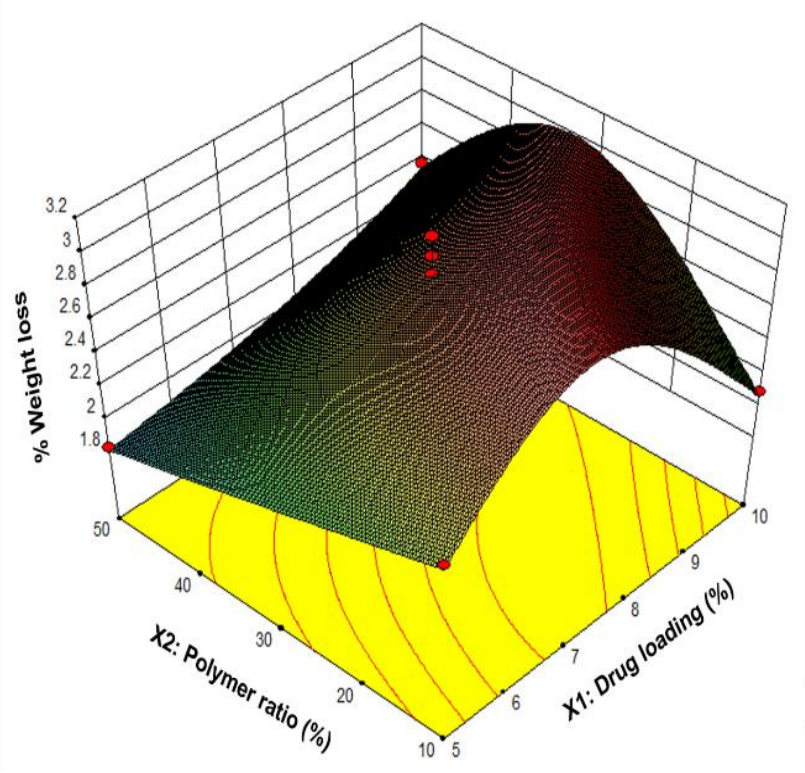

Figure 4.5: 3D plot portraying the influence of E2 load (%) and EC-to-PCL (%) on the weight loss percentage of the EPHCD.

Assisted alkaline degradation offers a more physiologically relevant simulation compared to alternative methods like temperature-based acceleration (Lam et al. 2008). The impact of E2 load and polymers ratio on the degradation EPHCD, as well as impact of polymer ratio on the degradation of the drug-free (DF) devices were analyzed under high pH conditions employing 5 M NaOH (Figure 4.6). The findings underscore a decrease in weight loss degree with an increase in EC percentage, as notable when comparing DF7 and EH10 versus DF8 and EH4, respectively. In addition, a discernible pattern emerged when comparing the degradation of formulations with 10% EC-to-PCL. Specifically, EH1 and EH2 showed a significant increase in weight loss percentage compared to drug-free counterparts DF1 and DF2 ($p < 0.05$, ANOVA followed by Tukey HSD). Conversely, when comparing the DF formulation with 50% EC-to-PCL (DF4) to its counterpart with both high EC content and 10% E2 load (EH4), no significant differences in weight loss percentage were observed after 96 hours ($p > 0.05$, ANOVA followed by Tukey HSD). From these findings, it can be deduced that the EC content employed in the fabrication of the devices play a pivotal role in shaping the erosion behaviours. EC, known for its hydrophobic properties and structural rigidity. With an increase in EC content within the matrix, a corresponding

escalation in hydrophobicity is expected. Furthermore, the escalation of EC content enhances the interfacial adhesion between the device components. The collective impact of heightened hydrophobicity and enhanced interfacial adhesion is formation of a protective barrier, impeding the ingress of water into the matrix, as well as growing a denser and even structural arrangement, minimizing the presence of micro-voids, and consequently sites for water penetration, thereby obstructing the initiation and progression of degradation processes.

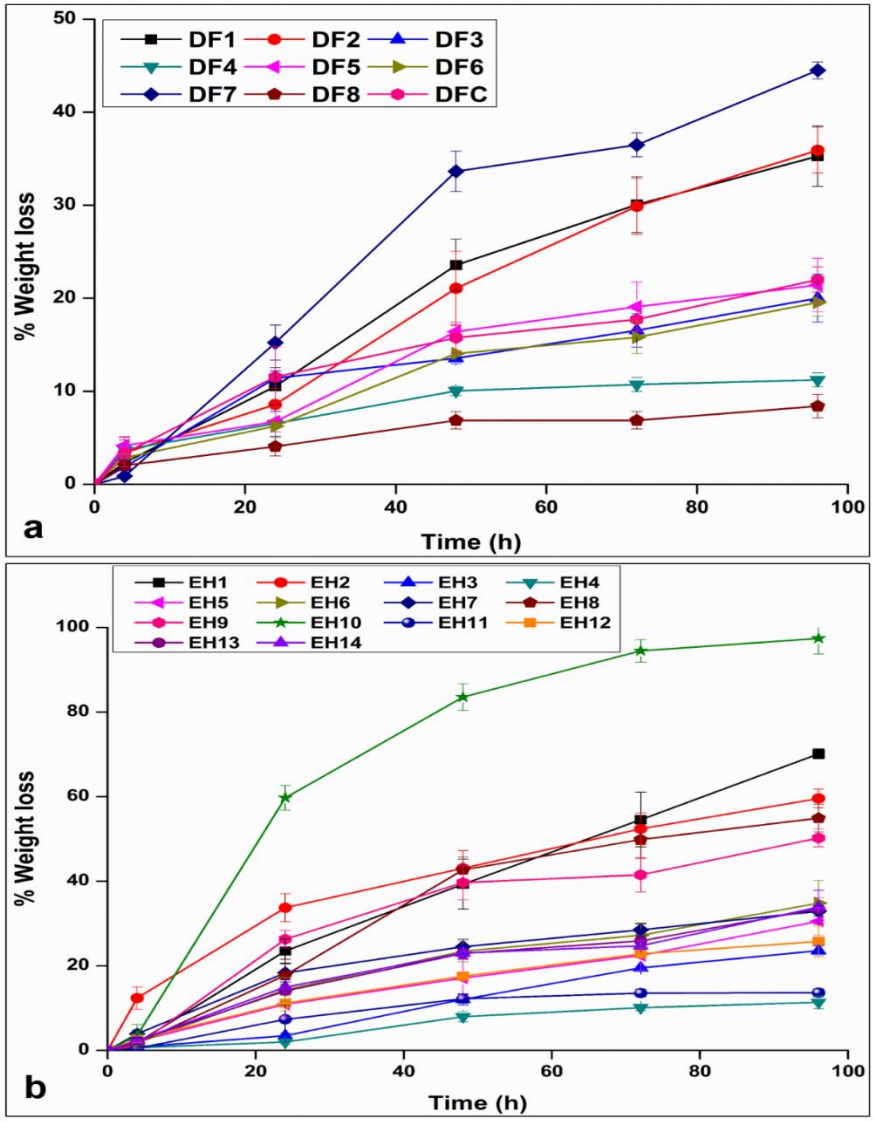

Figure 4.6: Accelerated weight loss % in alkaline media as a function of time (a) Drug-free device and (b) EPHCD.

4.3.2.3 Textural analysis

The results from the drug-free devices show a statistically significant impact of increasing EC levels on the force required to penetrate the polymeric matrices by 0.3 mm (Figure 4.7a). This effect is evident when comparing formulations DF4 and DF8, representing 50% and 58.28% EC-to-PCL, respectively, with those containing medium (30%) and low (10%) levels of EC, as well as an extra-low level (1.72%) ($p < 0.05$, ANOVA followed by Games-Howell post hoc test). Additionally, formulation DF9C, with a medium level of EC (30%), showed a slight, although not significant, increase in force compared to DF1 and DF2 (low level of EC) ($p > 0.05$, ANOVA followed by Games-Howell post hoc test), a significant increase in force compared to DF7 (extra-low level of EC), and a significantly lower force compared to DF4 (high level of EC) ($p < 0.05$, ANOVA followed by Games-Howell post hoc test).

In EPHCD (Figure 4.7b), the resulted force values exhibited a significant increase with the escalation of ethyl cellulose (EC) content. Formulations EH11 (58.28%), EH4 (50%), and EH3 (50%), featuring high content of EC, displayed substantial differences in the indentation force compared to formulations with lower EC content (EH1, EH2, and EH10 of 10%, 10%, and 1.72% EC-to-PCL percentages, respectively), as well as those with a medium level of EC (center point formulations of 30% EC-to-PCL). An increase in drug content resulted in a slight, albeit non-significant, rise in force, evident in the comparisons between EH1 and EH3 versus EH2 and EH4 (5% and 10% E2 levels, respectively). However, a significant impact on the force became apparent when transitioning from low and medium drug loads to the highest levels, accompanied by a decrease in EC from medium to the lowest level, as seen in the comparison between formulations EH9 and EH10 ($p < 0.05$, ANOVA followed by Tukey HSD). An interesting observation emerged when comparing formulations EH3, EH4, and EH11, representing 50% (EH3 and 4) and 58.28% (EH11) levels of EC. The change in drug load from the low level (EH3) to the medium level (EH11) and the high level (EH4) did not significantly affect the force. However, a significant influence on force was observed when transitioning from the medium level (EH11) to the high level (EH4) ($p = 0.019$, ANOVA followed by Tukey HSD). This result suggests a potential interaction effect between the two dependent variables as they fluctuate across upper and lower levels. The elevated resistance to indentation observed in the aforementioned results is likely a consequence of the uniform dispersion of the drug and EC within the PCL matrix. This uniform dispersion is presumed to enhance the interfacial adhesion between the polymers and drugs, particularly owing to their hydrophobic characteristics. Consequently, there is a reduction in micro-voids within the interphase region, thereby contributing to the observed effect.

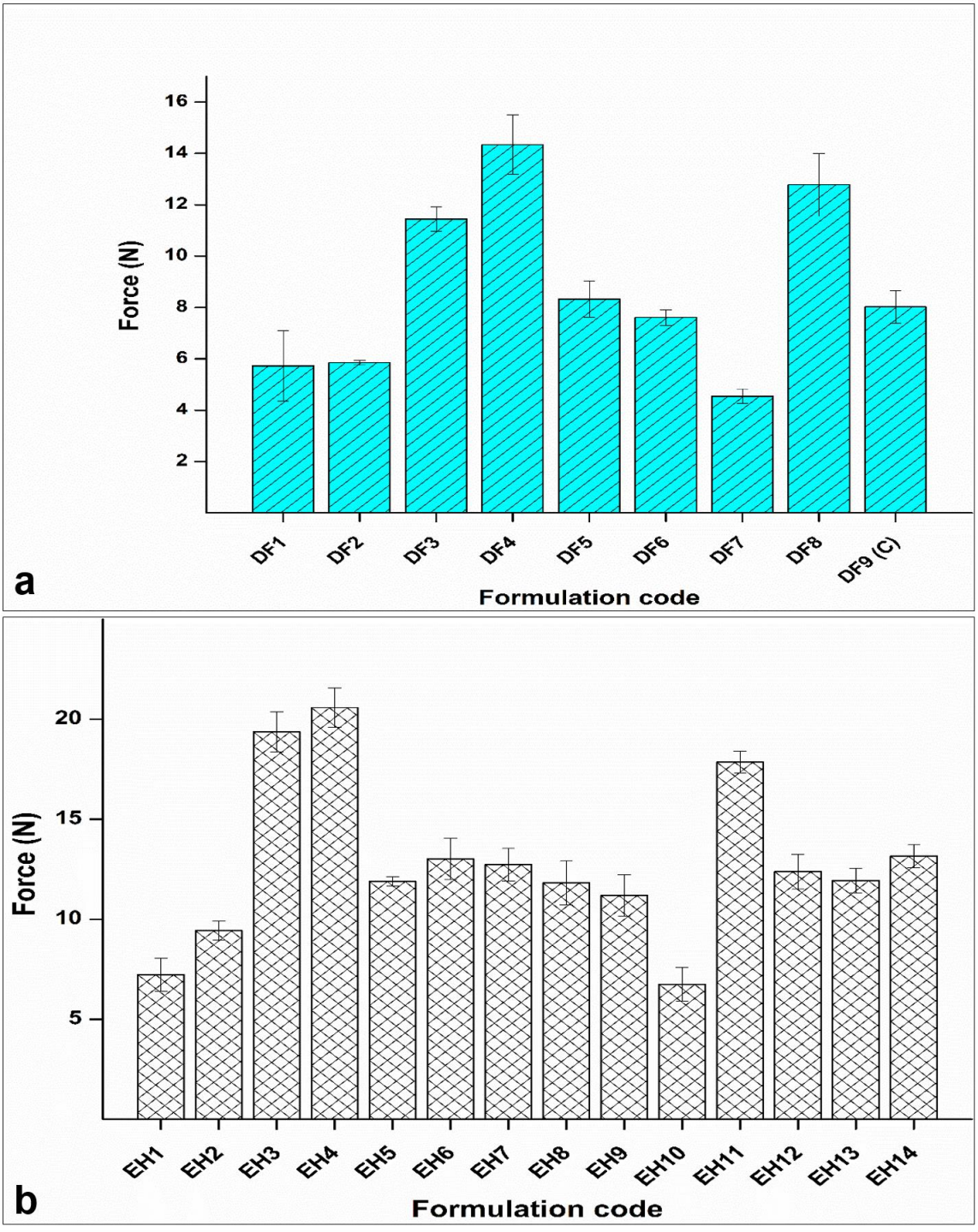

Figure 4.7: Analysis of indentation force of drug-free devices (a), EPHCDs (b).

4.3.2.4 In vitro drug release

The cumulative percentages of drug release from EPHCD formulations (EH1 to EH14) over a 4-week period (Y4) displayed a notable range, varying from 23.78±0.84 to 92.37±2.91. Particularly,

formulations EH2 and EH4, characterized by high drug loads (10%) combined with low (10%) and high EC (50%) ratios, respectively, demonstrated relatively lower release percentages. Conversely, formulation EH8, with the lowest E2 load (3.96%) and a medium EC ratio (30%), exhibited the highest release percentage. Additionally, a discernible trend surfaced when scrutinizing formulations with a 5% drug load, showing an increase in the percentage of drug release from 51.29±1.03 (EH3) to 65.65±2.29 (EH1) with a corresponding shift in the EC percentage from 50 to 10%. Furthermore, formulations with medium levels of both independent variables revealed intermediate release percentages, as observed in formulations EH5, EH6, EH7, EH12, EH13, and EH14. These results highlight the significant impact of variations in both independent variables on the percentage of drug release. Generally, EPHCD formulations featuring low E2 loads exhibited higher release rates compared to formulations with high E2 loading, consistent with prior findings (Muhindo et al. 2022). The hydrophobic nature of E2 contributes to this trend, as increasing drug concentration enhances the hydrophobicity of the E2-polymer matrix. Consequently, this heightened hydrophobicity may impede the influx of release medium, thereby retarding drug release. Figure 4.8 depicts the main effects of drug load and EC ratio on the cumulative E2 release percentage throughout a 4-week assessment period.

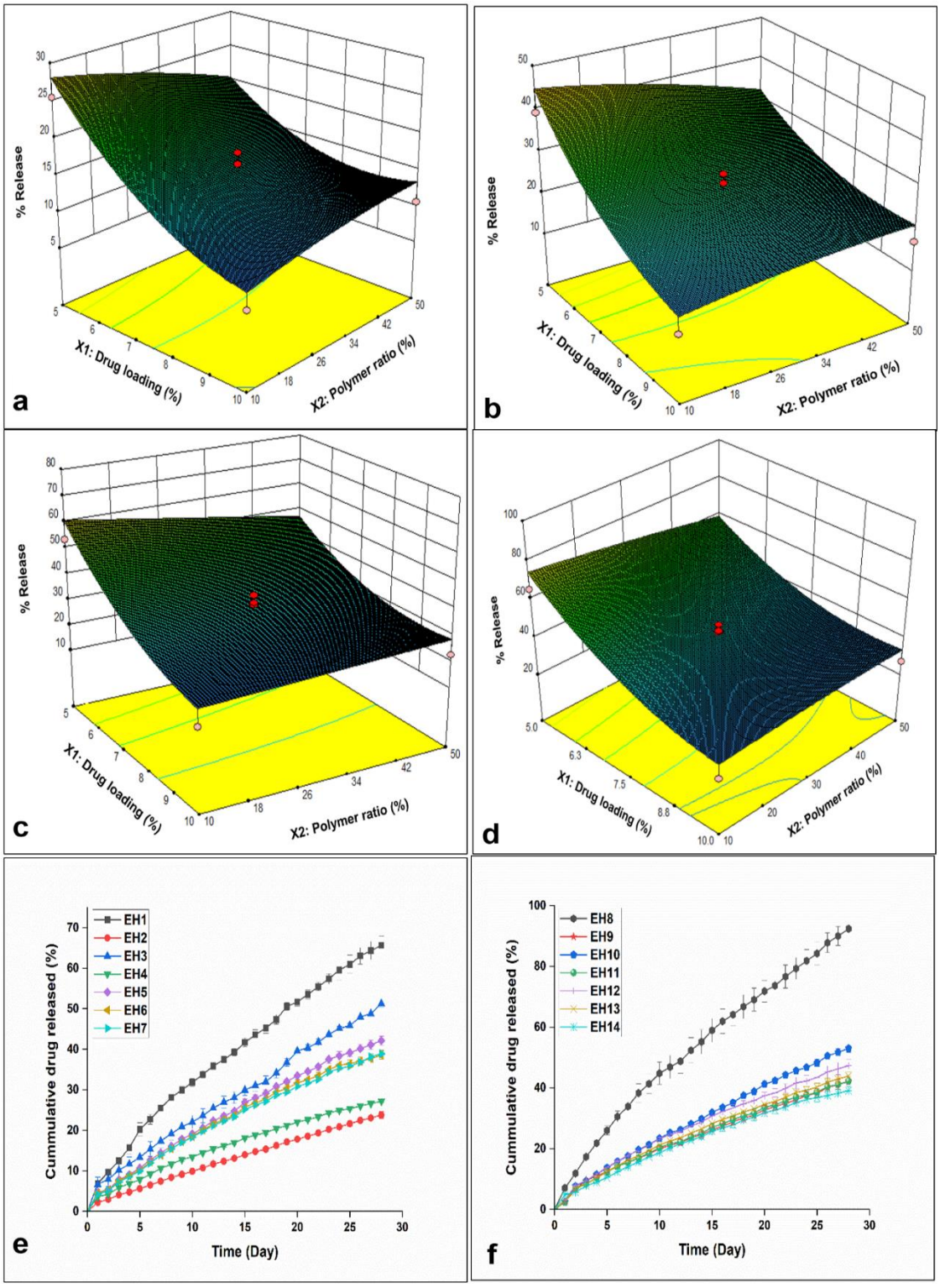

Figure 4.8: 3D Surface plots depicting the influence of E2 load (%) and EC-to-PCL (%) on the cumulative drug release at (a) week 1, (b) week 2, (c) week 3, and (d) week 4, with (e and f) displaying the release profiles of the EPHCD formulations.

4.3.2.5 Data analysis of the experimental design

Table 4.4 presents a summary of the outcomes derived from the CCD. The findings revealed that the 1, 2, 3, and 4-week percentage released of drug (Y1, Y2, Y3, and Y4) ranged from 7.43% to 33.89%, 13.09% to 55.18%, 18.54% to 73.66%, and 23.78% to 92.36%, respectively, while the 8-week weight loss percentage (Y5) ranged from 1.66% to 3.06%. This suggests that the chosen upper and lower levels for the factors were effective in generating a broad experimental domain. Both of the independent variables were encoded within the range of -1 to 1. To meet the validity requirements of ANOVA, the experimental data pertaining to Y2, Y4, and Y5 responses underwent transformations, specifically, the square root transformation for Y2 and Y4, while the inverse transformation for Y5. The fitting of the multi-linear regression models to the acquired CCD results was conducted, guided by the ANOVA results presented in Table 4.5. The remarkable low probability values (p-value < 0.0001 for Y1, Y3, Y4, Y5, and < 0.0003 for Y2) underscore the robust significance of the models developed for both responses, validated at a 95% confidence interval (where p-values below 0.05 denote significance). The absence of a significant lack-of-fit further emphasizes the high predictive capability of the model. Specifically, the Lack of Fit p-values of 0.2569, 0.1064, 0.0895, 0.1506, and 0.7573 for Y1, Y2, Y3, Y4, and Y5, respectively, strongly suggest their minimal influence in comparison to pure error. The findings demonstrate that the drug loading (X_1) significantly influences both drug release (Y1, Y2, Y3, and Y4) and weight loss (Y5) percentages. Conversely, the EC-to-PCL percentage (X_2) lack statistically significant effects on drug release (%) throughout the 4 weeks, while the interaction term between drug loading and EC-to-PCL percentage (X_1X_2) significantly influence the drug release (%) during the first 3 weeks and lack the influence in the week 4. On other hand, both X_2 and X_1X_2 do exert a significant influence on weight loss (%). Additionally, several quadratic terms displayed significant influences on the selected responses, with X_1^2 impacting all responses, and X_2^2, $X_1^2X_2$, and $X_1X_2^2$ affecting Y2 significantly.

The predicted and experimental responses demonstrated a good fit, with R^2 measuring more than 0.94. Furthermore, all responses exhibited adequate precision values exceeding 4, and the predicted R^2 values closely aligned with the adjusted R^2 values, with differences of less than 0.2. Additionally, the coefficient of variations were less than 10, and model selection prioritized minimizing PRESS values. Moreover, the analysis of CCD results led to the derivation of the following second-order polynomial equations, expressed in terms of coded factors:

$$Y1 = +15.04 - 6.36\,X_1 - 0.99\,X_2 + 2.83\,X_1X_2 + 3.47\,X_1^2 - 0.6\,X_2^2 \qquad \textit{Equation 4.3}$$

$$Sqrt\ (Y2) = +5.01 - 0.92\ X_1 - 0.14\ X_2 + 0.37\ X_1X_2 + 0.37\ X_1^2 - 0.11\ X_2^2$$ *Equation 4.4*

$$Y3 = +33.61 - 13.64\ X_1 - 2.54\ X_2 + 4.31\ X_1X_2 + 6.76\ X_1^2$$ *Equation 4.5*

$$Sqrt\ (Y4) = +6.41 - 1.2\ X_1 - 0.21\ X_2 + 0.32\ X_1X_2 + 0.52\ X_1^2$$ *Equation 4.6*

$$^1/_{Y5} = +0.35 - 0.069\ X_1 + 0.084\ X_2 - 0.051\ X_1X_2 + 0.052\ X_1^2 + 0.064\ X_2^2 - 0.062\ X_1^2\ X_2 + 0.055\ X_1X_2^2$$ *Equation 4.7*

The polynomial equations were employed to draw conclusions based on the magnitude and mathematical sign of the coefficients. In Equations 4.3, 4.4, 4.5, and 4.6, both the main effect terms X_1 and X_2 displayed a negative effect on the responses (Y1, Sqrt (Y2), Y3, and Sqrt(Y4)), with the drug load exerting a significant dominant influence. Conversely, the interaction terms X_1X_2 and the quadratic term X_1^2 had positive impact on the responses, with the X_1^2 term demonstrating a significant dominant effect. Furthermore, the quadratic term X_2^2 displayed slight non-significant positive effects on the Y1 and Sqrt (Y2). In Equation 4.7, It appears that inverse of weight loss percentage has a negative relationship with the X_1, X_1X_2, and $X_1^2X_2$ as main effect, interaction and quadratic terms, respectively. On the contrary, the X_2, X_{12}, X_{22}, and X_1X_{22} exhibited a significant positive impact on the inverse of the weight loss percentage.

Figure 4.9, the plot of the measured and model-predicted values of the 5 responses, illustrate a close alignment between the predicted values derived from the models and the actual experimental data, indicating the validity and robustness of the regression models. Also, the visual inspection of the normal probability plots, depicted in Figure 4.10, reveals that the data points closely align with a linear pattern. This observation not only indicates the constructed equations' viability to predict drug release and weight loss percentage but also implies their effectiveness in estimating the individual interactions between the responses and the independent variables, substantiating their adequacy.

Table 4.4: CCD experimental design matrix and results (n=3, ±SD).

F. Code*	1-week drug release (%)	2-week drug release (%)	3-week drug release (%)	4-week drug release (%)	8-week weight loss (%)
EH1	25.49±0.95	39.28±0.88	53.53±1.11	65.65±2.29	2.48±0.44
EH2	7.43±0.03	13.09±0.17	18.54±0.16	23.78±0.84	2.09±0.21
EH3	17.34±1.72	28.07±1.45	40.39±0.81	51.29±1.03	1.82±0.44
EH4	10.58±0.48	16.91±0.41	22.63±0.38	27.17±0.27	2.38±0.52
EH5	14.39±0.26	24.72±0.67	34.52±1.02	42.10±1.12	2.73±0.41
EH6	13.84±0.20	23.68±0.50	32.53±0.76	38.55±1.04	2.95±0.08
EH7	13.93±0.46	23.35±0.16	31.66±0.27	38.89±0.87	3.06±0.38
EH8	33.89±2.54	55.18±4.04	73.66±3.89	92.37±2.91	1.80±0.14
EH9	15.49±0.55	24.58±0.90	33.82±1.26	42.07±1.61	2.76±0.41
EH10	17.56±0.63	29.81±0.23	42.36±0.82	53.03±1.33	2.74±0.38
EH11	15.51±0.58	25.03±1.02	34.39±1.51	42.26±1.76	1.66±0.35
EH12	17.80±0.42	28.82±0.64	38.35±1.38	47.33±2.00	2.85±0.18
EH13	16.22±0.08	26.49±0.25	35.55±0.84	43.91±1.38	2.75±0.11
EH14	14.06±0.49	23.95±0.78	32.71±1.34	39.09±1.30	2.76±0.07

* Formulation Code

Table 4.5: Analysis of variance (ANOVA) for different responses of EPHCD formulations.

	Y1	Y2	Y3	Y4	Y5
Source	P-value	P-value	P-value	P-value	P-value
Model	< 0.0001	0.0003	< 0.0001	< 0.0001	<0.0001
X_1	< 0.0001	< 0.0001	< 0.0001	< 0.0001	0.0002
X_2	0.1258	0.1800	0.0881	0.1268	<0.0001
X_1X_2	0.0097	0.0284	0.0483	0.1097	0.0007
X_1^2	0.0006	0.0071	0.0011	0.0039	0.0002
X_2^2	0.3417	0.2862			<0.0001
$X_1^2X_2$					0.0015
$X_1X_2^2$					0.0025
Lack of Fit	0.2569	0.1064	0.0895	0.1506	0.7573

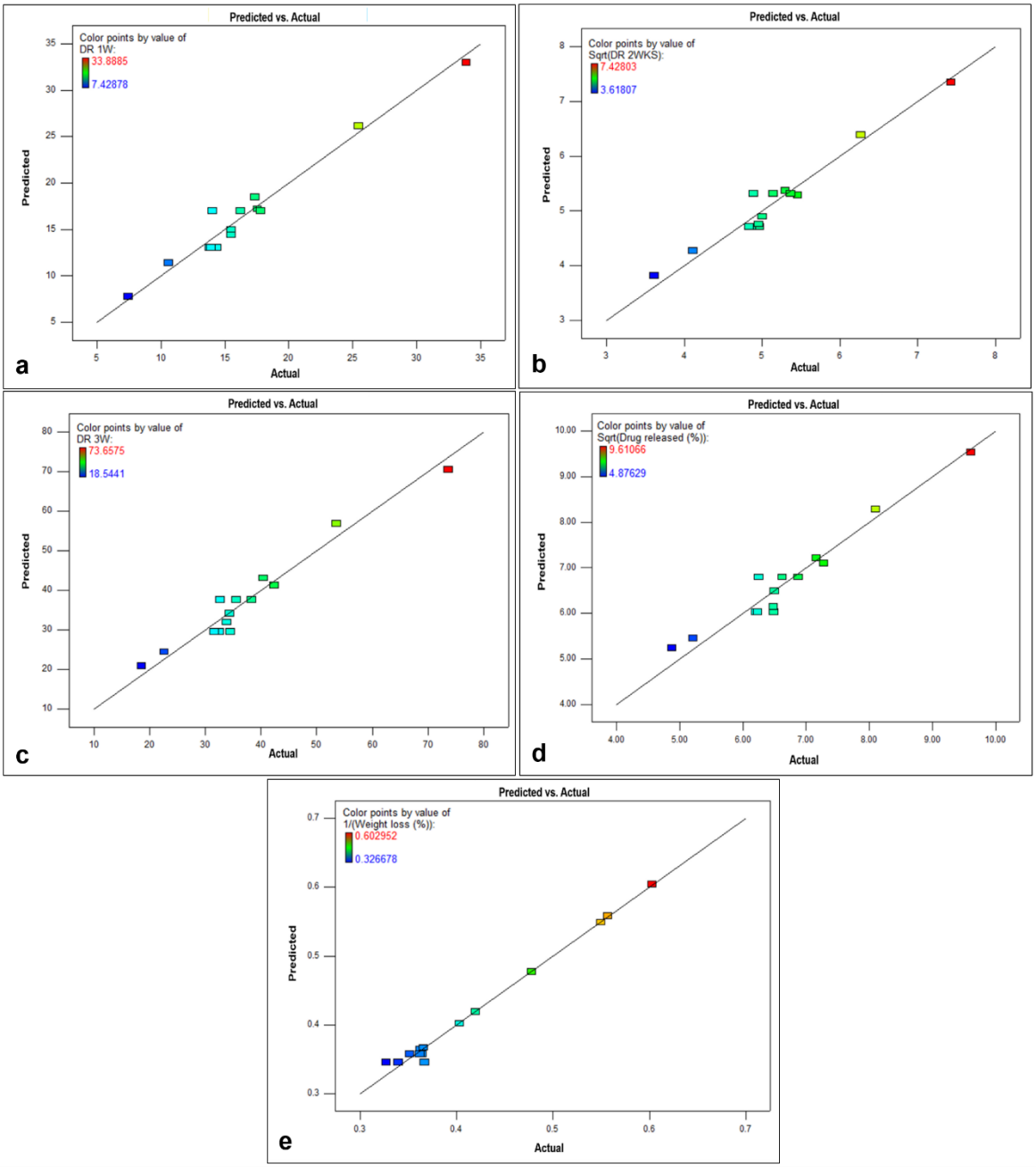

Figure 4.9: Plot of the measured and model-predicted values of the response (a) Y1, (b) Y2, (Y3), (Y4), and (Y5) of EPHCDs.

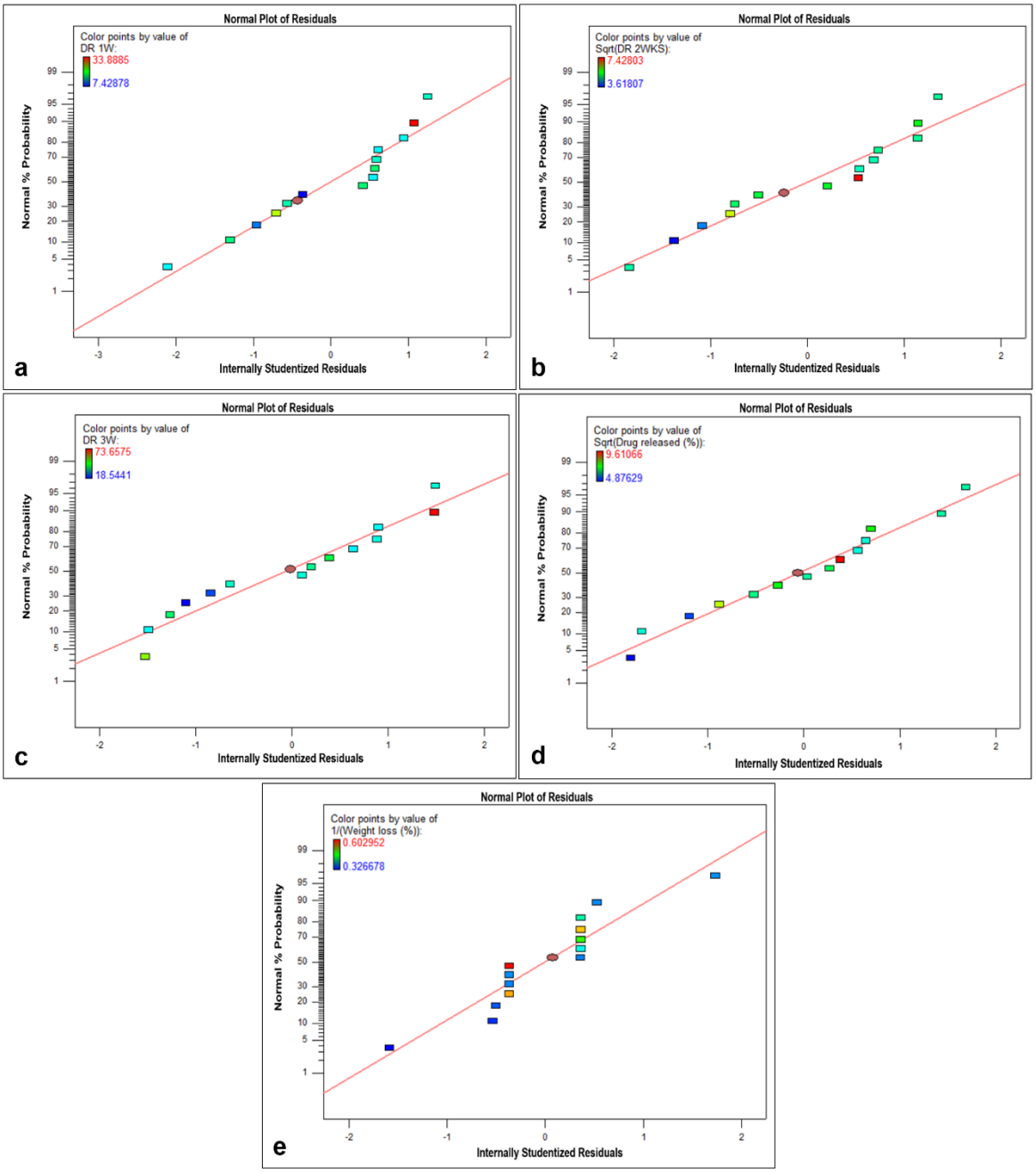

Figure 4.10: The normal plot of residuals for (a) Y1, (b) Y2, (c), Y3 (d) Y4, and (e) Y5 of EPHCDs.

4.3.2.6 Constrained statistical Optimization of the EPHCD

The primary aim of employing the CCD-based optimization approach was to derive the optimal formulation parameters required for the preparation of the estradiol-loaded segment. To achieve this goal, constraints were imposed on both the dependent and independent variables. A constraint referred to as 'in-range' was applied to independent variables, while the constraints

imposed on the dependent variables, namely drug release and weight loss%, were set as to (minimize).

Table 4.6 showcasing the chosen numerical optimization solution. The table provides a comprehensive insight into the specific values and conditions that were identified as optimal for the study. Figure 4.11a represents the contour plot of the numerical optimization illustrating the selected optimum solution. Moreover, Figure 4.11b portraying the constructed desirability landscape, an optimal design space, achieved by superimposing contour plots and main effect plots derived by using graphical optimization module of the implemented CCD. This graphical representation elucidated regions in the design space aligning to the specified optimization criteria, distinct in bright yellow. Consequently, the CCD model generated an optimized formulation, indicating that the formulation comprised a drug load of 10% and 10% ratio of EC to PCL. This optimized formulation was projected to yield the optimum results for both the 4-week percentage drug release and weight loss, achieving values of 31.7% and 2.07%, respectively.

Table 4.6: The selected optimal configuration from numerical optimization.

No	Drug load (%)	EC to PCL ratio (%)	Drug released W1 (%)	Drug released W2 (%)	Drug released W3 (%)	Drug released W4 (%)	Weight loss (%)	Desirability
1	10	10	9.71629	17.0243	24.9693	31.6712	2.07283	0.855

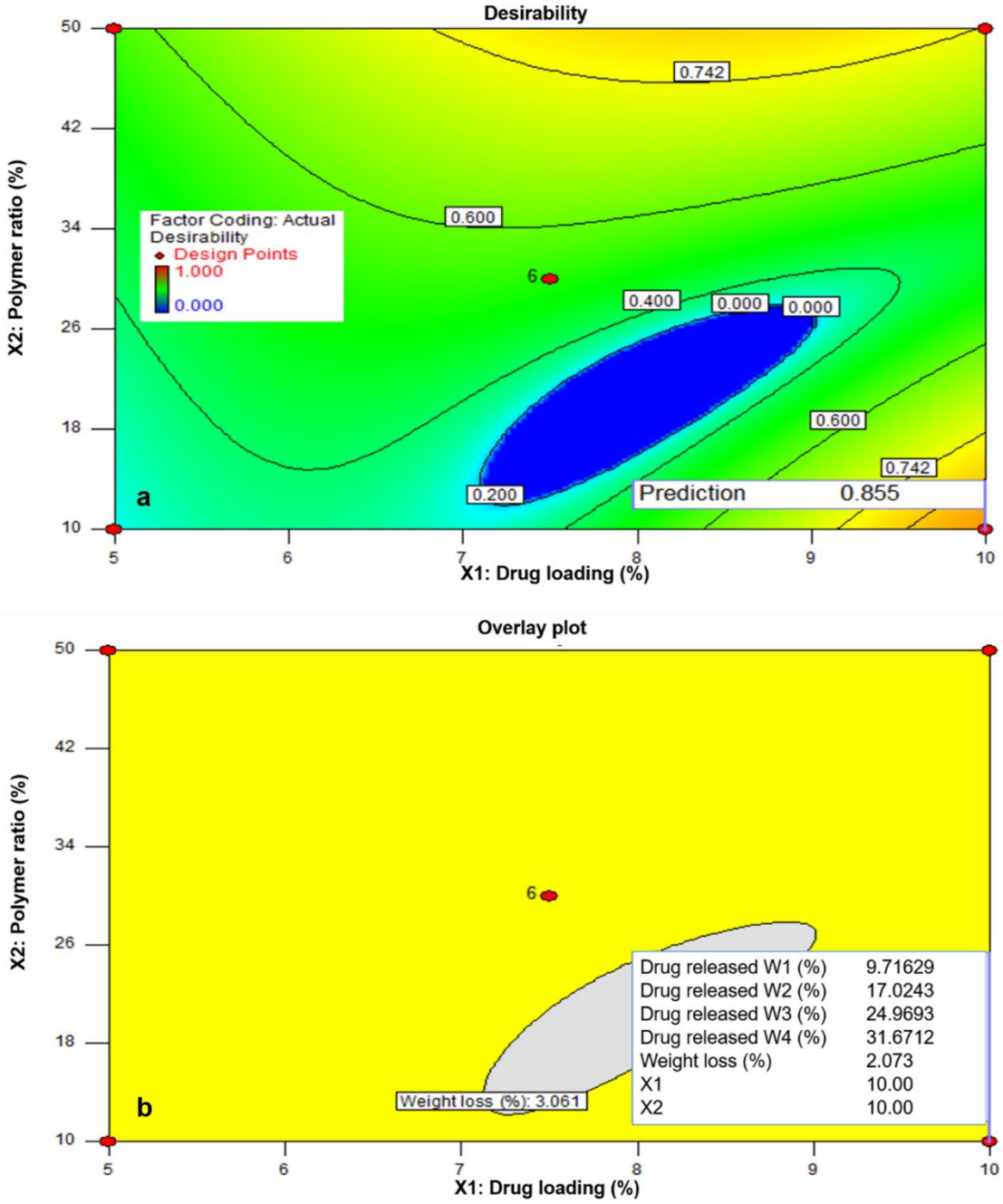

Figure 4.11: Contour plot of numerical optimization (a) and overlay plot of graphical optimization (b).

4.3.3 Characterization of the Optimized EPHCD formulation

4.3.3.1 Fourier transform infrared (FTIR) spectroscopy analysis

To ascertain the compatibility of the constituents within the fabricated EPHCD formulations, FTIR spectra of the EPHCD samples were analyzed with respect to their individual components, encompassing E2, PCL, and EC (Figure 4.12).

The E2 spectrum displayed broad bands at 3435 and 3194 cm^{-1}, signifying OH stretching near the C-17 and C-3 positions. The broadness suggests hydrogen bonding with entrapped water. Additionally, peaks at 1609 and 1586 cm^{-1} indicate absorption by a mixture of tautomeric keto and enol forms. All other observed peaks of PCL and EC are as detailed in Chapter 3, Section 3.3.2.2.

The FTIR analysis of the EPHCD displayed the primary peaks associated with pure constituents, although with reduced intensities. Concurrently, characteristic peaks corresponding to the PCL and EC structures were observed. The consistent presence of identical characteristic peaks and the absence of discernible new peaks in the prepared device, compared to the pure drug and polymers, indicate a homogeneous blending of the device components. These findings underscore physical interaction, support the absence of strong chemical interaction, and consequently affirm the compatibility of the device-forming polymers with the loaded drug.

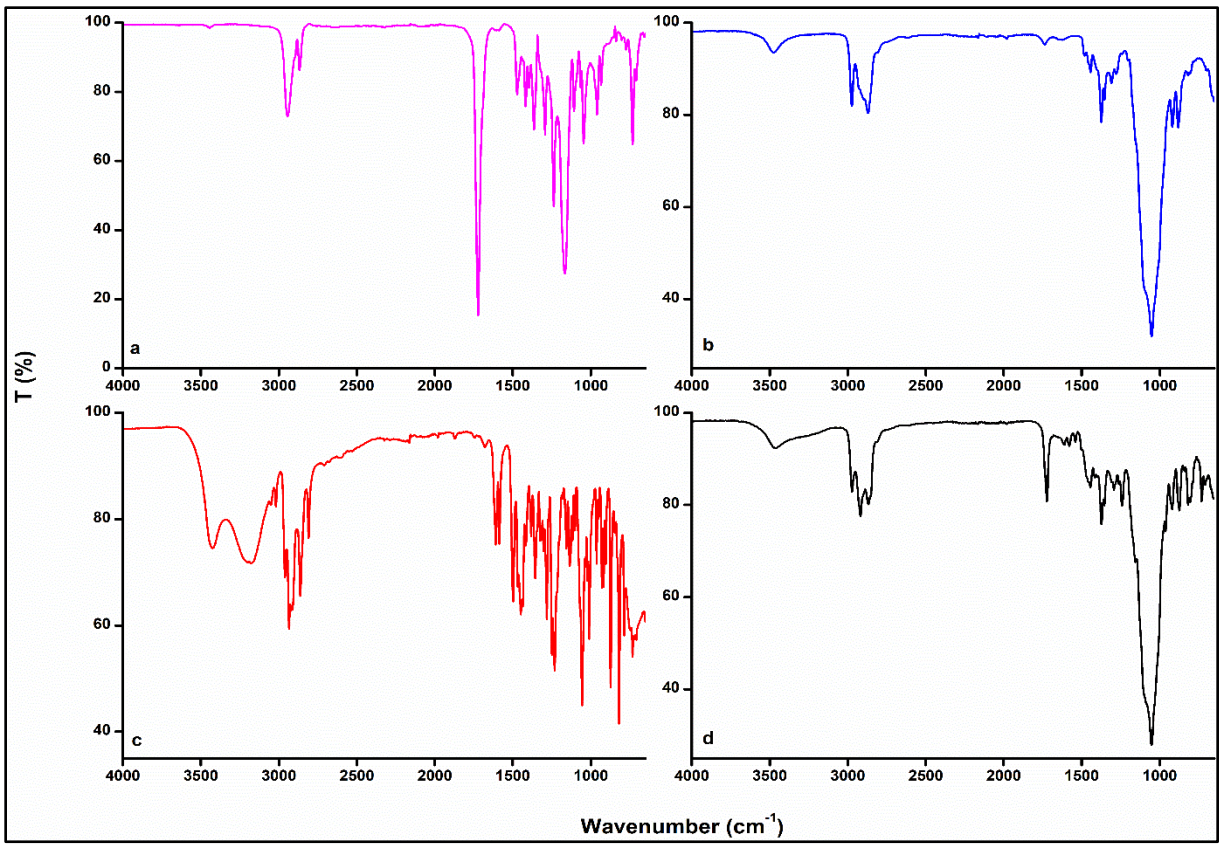

Figure 4.12: FTIR spectra of PCL (a), EC (b), E2 (c), and EPHCD (d).

4.3.3.2 Morphological analysis

SEM imaging was used to assess the surface morphological structures of optimized EPHCD as well as the alterations observed due to the erosion during an 8-week incubation in SUF. The results are illustrated in Figure 4.13. SEM analysis of EPHCD unveiled minimal surface irregularities in both the surface and cross-section, with fewer cavities and pores, along with evident drug crystals on the surface (Figure 4.13a1 and a2). However, subsequent to an 8-week degradation period in SUF, SEM (Figure 4.13b1 and b2) exhibited cracked and rough surfaces, concomitant with a notable cavities and the obliteration of pores, which may impede the diffusion of the dissolution medium into the matrix of the device.

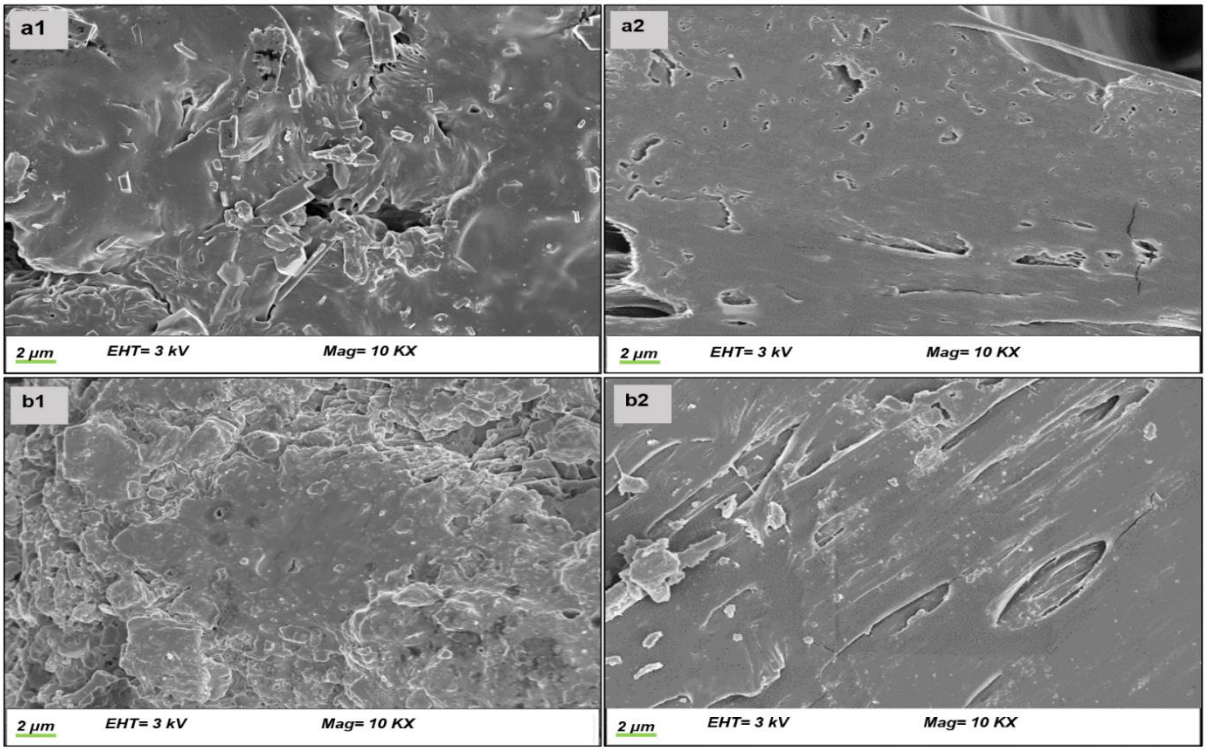

Figure 4.13: SEM analysis of surface and cross-sectional views for (a1 and a2) EPHCD and (b1 and b2) 2-month degraded EPHCD.

4.3.3.3 Water retention capacity

In vitro hydration investigations of the optimized drug-free and EPHCD formulations in water were carried out over a 24-hour period. The drug-free formulation exhibited a significantly higher hydration percentage in comparison to the drug-loaded formulation (43.99% ± 1.44 vs. 26.23% ± 1.58, respectively; $p < 0.05$). This discrepancy may be attributed to increased hydrophobicity, reduced porosity (Amini et al. 2021), and impeded water diffusion caused by drug depositions on micro-voids and the surface of the EPHCD. These findings provide additional insights into the observed low drug release in the optimized EPHCD formulation, highlighting the complex interplay between formulation characteristics and hydration behavior.

4.3.3.4 Drug release and release kinetics

The precise control of drug release stands as a paramount challenge in drug delivery, profoundly impacting treatment efficacy. Ensuring drug dosages align within a predefined range is imperative, with the lower threshold surpassing the therapeutic level and the upper limit remaining below toxic concentrations (Lei et al. 2011). Prior research underscores that the kinetics of drug release from polymeric systems are governed by a multitude of factors, including polymer characteristics,

environmental variables, and drug attributes. Furthermore, structural attributes of the system such as shape and size as well as drug loading of polymeric matrices exert notable influences on the release kinetics (Freire et al. 2017, Li et al. 2010). Polymeric systems mediate the drug release primarily through diffusion, erosion, and swelling mechanisms. Hydrophilic matrices facilitate drug release via water penetration and consequently the swelling and diffusion mechanisms are dominant. On the contrary, hydrophobic matrices predominantly rely on diffusion or erosion mechanisms, dictated by drug and excipient characteristics (Freire et al. 2017).

Formulation EH2 exhibits a favorable sustained drug release profile, marked by a cumulative release percentage of approximately 23% over the 4-week evaluation period. Notably, an initial burst release is observed on day 1, totaling 80.73 µg, followed by a rapid decline in daily drug release over the first 3 days, transitioning into a much slower release rate over the subsequent 3 weeks, dropping below 30 µg after 21 days (Figure 4.14a). The observed burst release may stem from the release of surface-bound drug, which could be attributable to various chemical, physical, and processing parameters. Factors such as drug migration towards the matrix surface during the cooling and drying processes likely promote burst release. Additionally, the emergence of surface cracks could facilitate surface erosion, further contributing to the burst release (Unagolla and Jayasuriya 2018). Analysis SEM images of the EH2 formulations reveal the presence of drug crystals on the EPHCD surface, along with low surface irregularities. These factors likely contribute to the observed burst release on the first day. The initial burst release, succeeded by a more gradual release may be ascribed to a decrease in the concentration gradient of the drug in the outer layers of the EC/PCL matrix. Furthermore, the decline in E2 release during diffusion from the inner layers could result from the longer path length for diffusion of aqueous release medium into deeper layers due to the decreased concentration gradient of the drug in the outer polymer layers.

To delineate the mechanism of E2 release from the optimal EPHCD, the release kinetics were assessed by fitting the experimental data to various release kinetic models, including zero-order, first-order, Higuchi, Korsmeyer-Peppas, Hixson-Crowell, and Peppas-Sahlin models. Table 4.7 presents the goodness-of-fit outcomes, comprising R^2, adjusted R^2, RMSE, AIC, and MSC values, applied to the averaged release profiles. Parameters derived from the nonlinear regression of the dataset fit to the models are also presented. Amongst the mathematical models applied to describe the drug release behavior of the optimal EPHCD, the Peppas-Sahlin model emerged as the most fitting, followed by the Korsmeyer–Peppas mode, as indicated by R^2 and adjst-R^2 values exceeding 0.999, as well as AIC values below 8.41. Moreover, the models exhibited MSC values

higher than 6.76, further highlighting their suitability for describing the release kinetics of the E2. Figures 4.14b and 4.14c illustrates the appropriateness of the best-fit models, Peppas-Sahlin and Korsmeyer-Peppas models, respectively, for accurately describing drug release profiles. In each of the figures, the time is represented on the horizontal axis, while the vertical axis represents the cumulative percentage of drug released over time. The chosen best-fit models closely align the predicted values with the actual experimental data, indicating their suitability for describing the drug release profiles.

In exploring the relation between the Peppas-Sahlin model and the dominant release mechanism, associations have been proposed between its parameters and the Korsmeyer-Peppas parameters. The release exponent "n" of the Korsmeyer–Peppas model for drug release from cylindrical polymeric delivery systems serves as a marker for the release mechanism. Values of 0.45, 0.45 < n < 0.89, and 0.89 signify Fickian diffusion, anomalous transport, and polymer Case II transport, respectively, with super Case II transport indicated by n greater than 0.89 (Ainurofiq and Choiri 2015, Solano et al. 2013). The equality of the "n" value in the Korsmeyer-Peppas model and the "m" value in the Peppas-Sahlin model is anticipated when the relaxation mechanism is insignificant (Unagolla and Jayasuriya 2018). Thus, the dissimilarity between the n exponent (0.835) and the "m" exponent (0.55) highlights the co-dependence of diffusion and Case II relaxation in governing E2 release. Additionally, the obtained release exponent "n" from the Korsmeyer–Peppas model was 0.835, corroborating that the mechanism of E2 release exhibits anomalous behavior or non-Fickian transport. This suggests that the release kinetics entail a degree of complexity with several internal collective processes possibly interplaying alongside the diffusional mechanism, including polymer erosion and relaxation. Furthermore, the high value of the Korsmeyer–Peppas kKP parameter (1.464) suggests a burst release during the initial phase of the release, with approximately 80 µg of E2 released on Day 1.

The ratio of relaxational to Fickian contribution, denoted as R/F, can be calculated using the formula (Equation 4.8):

$$\frac{Relaxation\ contribution}{Fickian\ contribution} = \frac{k_2}{k_1}\ t^m \qquad \text{Equation 4.8}$$

An R/F ratio of 1 denotes an equilibrium between the relaxation and diffusion processes within the release mechanism. A ratio values below 1 indicate that the diffusion plays the major role, whereas for ratio exceeding 1 signifies that the relaxation mechanism takes precedence (Unagolla

and Jayasuriya 2018). The calculation of the R/F ratio was based on the parameters provided in Table 4.7, and the temporal variation of the R/F ratio is graphically represented in Figure 4.14d. The low R/F values initially, indicate the prevalent influence of Fickian diffusion on drug release from the segment. The gradual increase in R/F ratio values over time signifies a growing role of relaxational contribution. Beyond day 12, when the R/F ratio surpasses 1, this marks the point at which the relaxation mechanism becomes the primary contributor.

Table 4.7: Statistical assessment and parameters for the best-fitting kinetic models to release data for optimal EPHCD.

Model	**R^2**	**Adj-R^2**	**RMSE**	**AIC**	**MSC**	**Parameter**	
Zero-order	0.9816	0.9816	0.892	87.90	3.924	k_0	0.892
First-order	0.9926	0.9926	0.567	62.55	4.829	k_1	0.010
Higuchi	0.8938	0.8938	2.144	136.99	2.171	kH	3.855
Korsmeyer-Peppas	0.9990	0.9990	0.212	8.41	6.763	kKP	1.464
						N	0.835
Hixson-Crowell	0.9898	0.9898	0.665	71.46	4.511	kHC	0.003
Peppas-Sahlin	0.9997	0.9997	0.111	-27.15	8.033	k_1	1.466
						k_2	0.376
						M	0.55

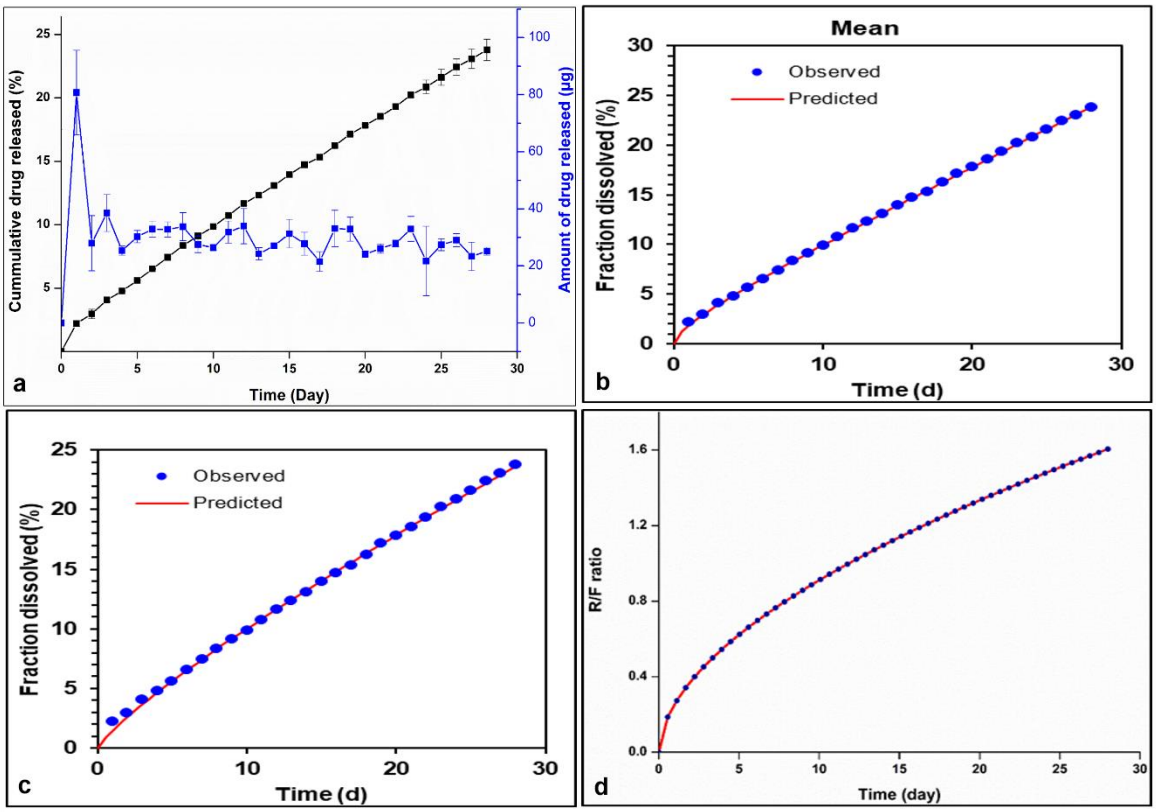

Figure 4.14: (a) E2 release profile from the optimized EPHCD formulation, EH2; Fitting curve and modeling of E2 release from the optimal formulation; (b) Peppas-Sahlin and (c) Korsmeyer-Peppas models; (d) the ratio of relaxational to Fickian contribution as function of time.

4.3.4 Evaluation of the Experimental Design for IND-LPM

4.3.4.1 Determination of diameter and drug content uniformity

Table 4.8 depict the average diameter and drug content of IND-LPM. The results demonstrate that both of diameter and content display marginal variation within the specification range (Solano et al. 2013). This observation indicates a consistent and uniform distribution of IND within the polymer matrices.

Table 4.8: Diameter and drug content in the fabricated IND-LPM (n=3).

Formulation Code	Diameter (mm)	Theoretical loading%	Drug content (%±SD)	Incorporation efficiency (%±SD)
IND1	4.17±0.017	7.69	7.93±0.45	103.07±5.86
IND2	4.06±0.012	14.29	13.63±0.29	95.39±2.04
IND3	4.13±0.058	6.7	5.70±0.15	85.14±2.24
IND4	4.19±0.020	12.5	11.78±0.26	94.23±2.07
IND5	4.11±0.006	10.35	9.86±0.23	95.23±2.21
IND6	4.02±0.052	10.35	9.64±0.36	93.12±3.45
IND7	4.05±0.042	10.35	9.46±0.44	91.36±4.23

4.3.4.2 Degradation study

The percentage weight loss of IND-LPM formulations ranged from 27.4±0.18 to 39.74±2.9 as shown in Figure 4.15. Notably, formulations with a high PEG content (IND3 and IND4, 38.86±0.65 and 39.74±2.9, respectively) showed higher weight loss compared to that with low PEG (IND1 and IND2, 28.34±0.18 and 27.4±0.18, respectively). These findings elucidate the significant effect of PEG variation on the weight loss percentages. Furthermore, the variation in drug content has no significant effect on the weight loss percentage.

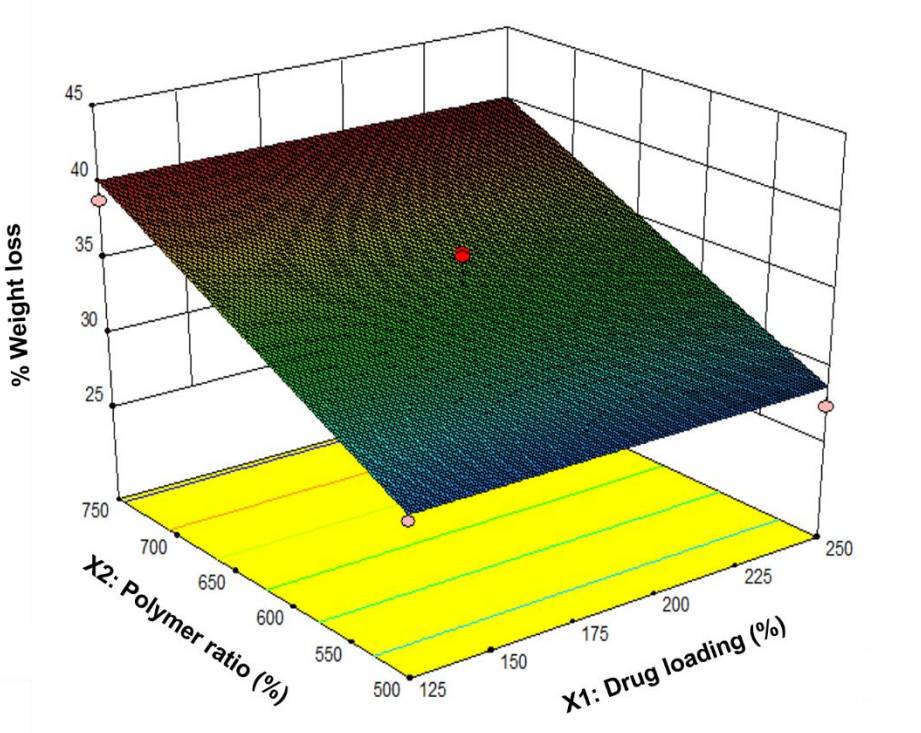

Figure 4.15: 3D plot portraying the influence of IND load (mg) and PEG content (mg) on the weight loss percentage of the IND-LPM.

4.3.4.3 Textural analysis

Figure 4.16 depicts the indentation resistance of IND-LPM. The findings reveal that both the drug and PEG demonstrated a significant impact on the force. Notably, there was a significant increase in force when comparing IND1 to the other formulations. Among these, the IND2 formulation, characterized by high drug content and a low PEG ratio, displayed the highest force. Furthermore, an increase in PEG content in formulations with high drug content resulted in a significant reduction in force, evident in the comparison between formulation IND2 and IND4 ($p < 0.05$, ANOVA followed by Tukey HSD).

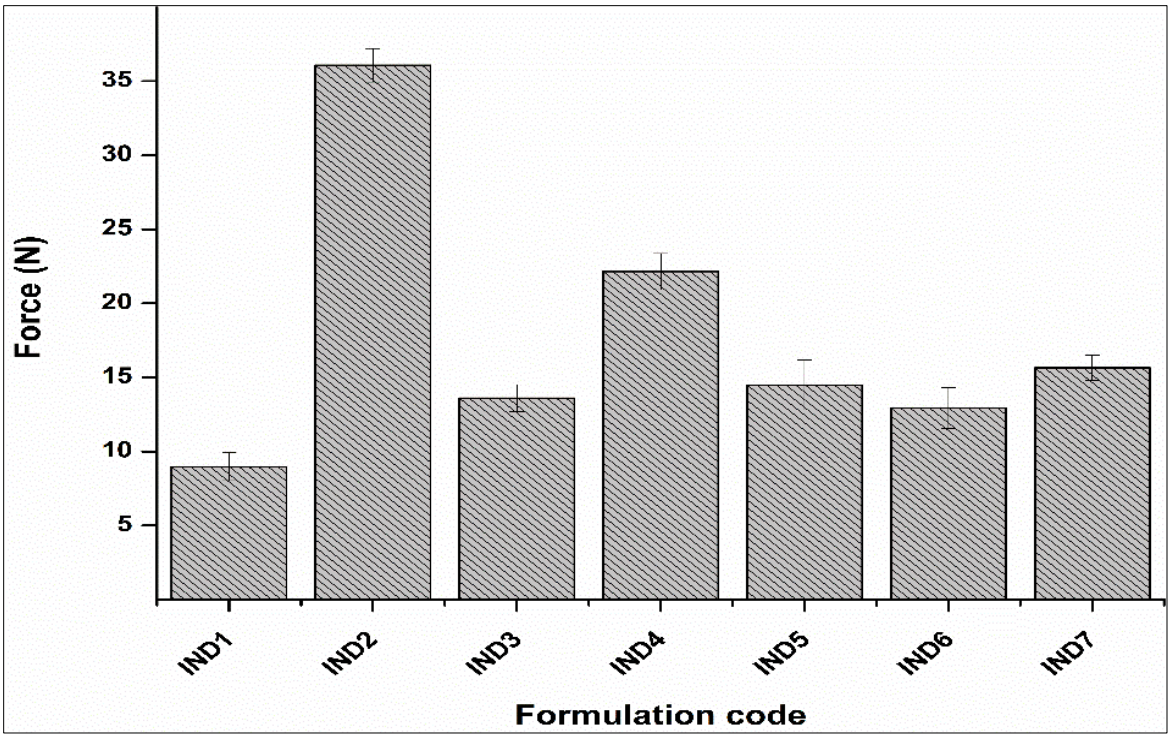

Figure 4.16: Analysis of indentation force of IND-LPM.

4.3.4.4 In vitro drug release

The cumulative percentages of drug release from IND-LPM formulations over a 2-week period (Y2) displayed a notable range, varying from 73.04±2.16 to 91.86±3.1 (Figure 4.17). Particularly, formulations IND2, with high drug load and low PEG content showed the lowest release percentage. Contrary, IND3 featured low drug content and high PEG load exhibited the higher release percentage. These findings signify the positive effect of augmentation of PEG on the percentage of drug release.

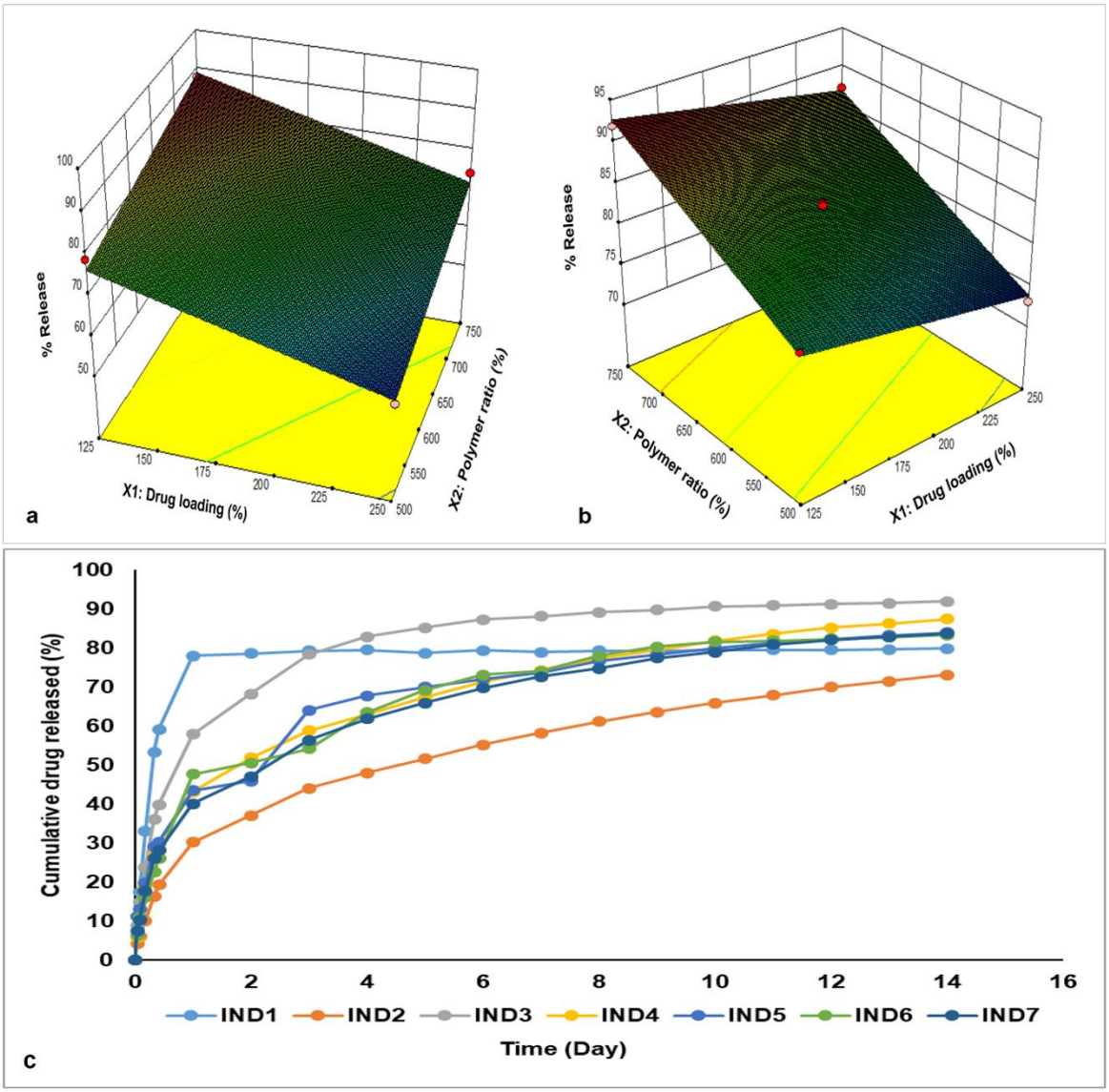

Figure 4.17: 3D plots depicting the influence of IND load (%) and PEG (%) on the cumulative drug release at (a) week 1, (b) week 2 (c) release profiles of the IND-LPM formulations.

4.3.5 Preparation and Characterization of the Optimized IND-LPM formulation

The Optimized IND-LPM formulation through the DOE was determined to be IND3 which characterized by low drug amount (125 mg) and PEG amount of 750 mg.

4.3.5.1 Fourier transform infrared (FTIR) spectroscopy analysis

The spectrum of IND (Figure 4.18) exhibits distinct peaks associated with its gamma-phases. Notably, characteristic peaks are observed at 2972 cm^{-1}, attributed to aromatic CH stretching, 2966 cm^{-1}, indicating C-H stretching vibrations, 1714 cm^{-1}, denoting C=O stretching vibrations, 1261 cm^{-1}, representing asymmetric aromatic O–C stretching, and 1089 cm^{-1}, signifying

symmetric aromatic O–H stretching. The PEG spectrum revealed various peaks signify the distinct molecular features. The 2878 cm^{-1} peak arises from aliphatic C–H stretching, while the 1463 and 1340 cm^{-1} peaks are attributed to C–H bending vibrations. Peaks at 1276 and 1094 cm^{-1} correspond to O–H and C–O–H stretching vibrations, respectively. The presence of C–O–C is indicated by the 1089 cm^{-1} peak, and the functional group CH2 is characterized by strong peaks at 2878 cm^{-1} and 954 cm^{-1}. All other observed peaks of PCL are as detailed in Chapter 3, Section 3.3.2.2.

The FTIR analysis of the IND-LPM displayed the primary peaks associated with pure constituents, in addition to the absence of discernible new peaks in the prepared device, indicate the absence of strong chemical interaction, and consequently affirm the compatibility of the device-forming polymers with the loaded drug.

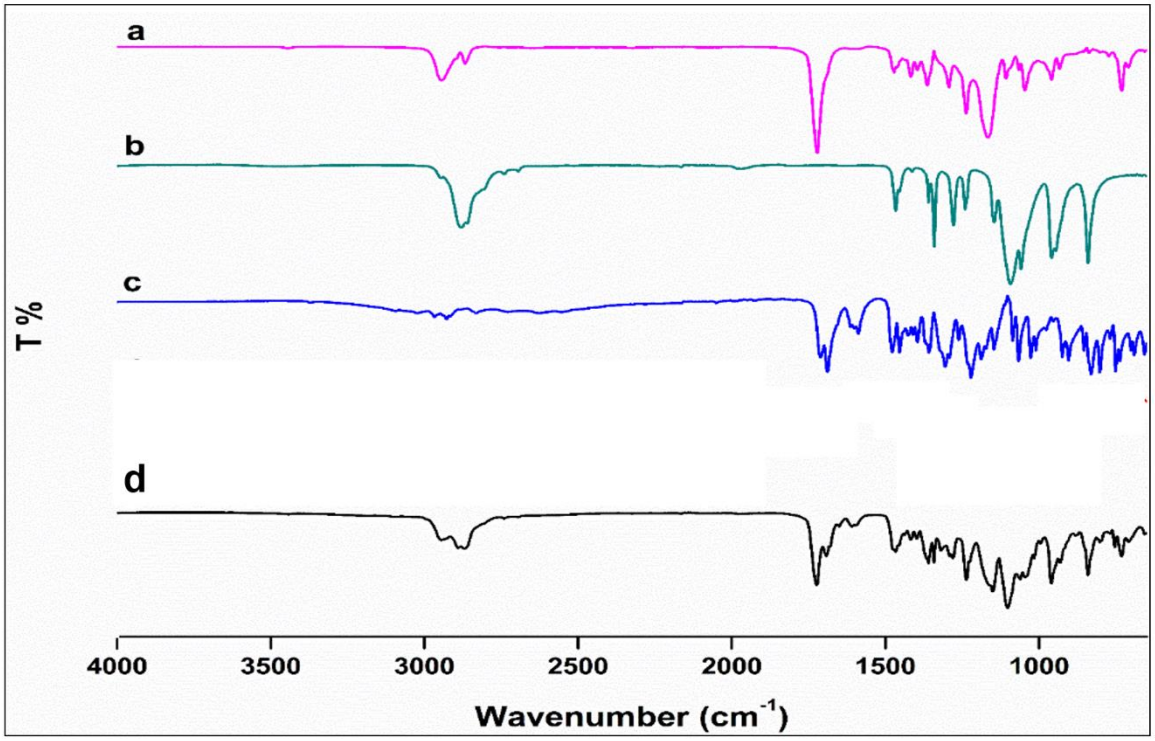

Figure 4.18: FTIR spectra of PCL (a), PEG (b), IND (c), IND-LPM (d).

4.3.5.2 Morphological analysis

SEM imaging was used to assess the surface morphological structures of optimal IND-LPM. The drug-free PCL/PEG matrix displayed smooth surfaces with minimal cavities, voids, and the

absence of aggregates (Figure 4.19a1 and a2). These surface irregularities and cavities become more less in IND-LPM without any apparent signs of drug migration on the surface. Additionally, there were no fractures observed in the IND-LPM (Figure 4.19b1 and b2). Following 2-week degradation period in SUF, the IND-LPM exhibited cracked and rough surfaces, accompanied by a notable degree of micro-porosities (Figure 4.19c1 and c2). The growth of these voids with incubations in SUF may contribute to facilitating the drug release from the polymeric matrix.

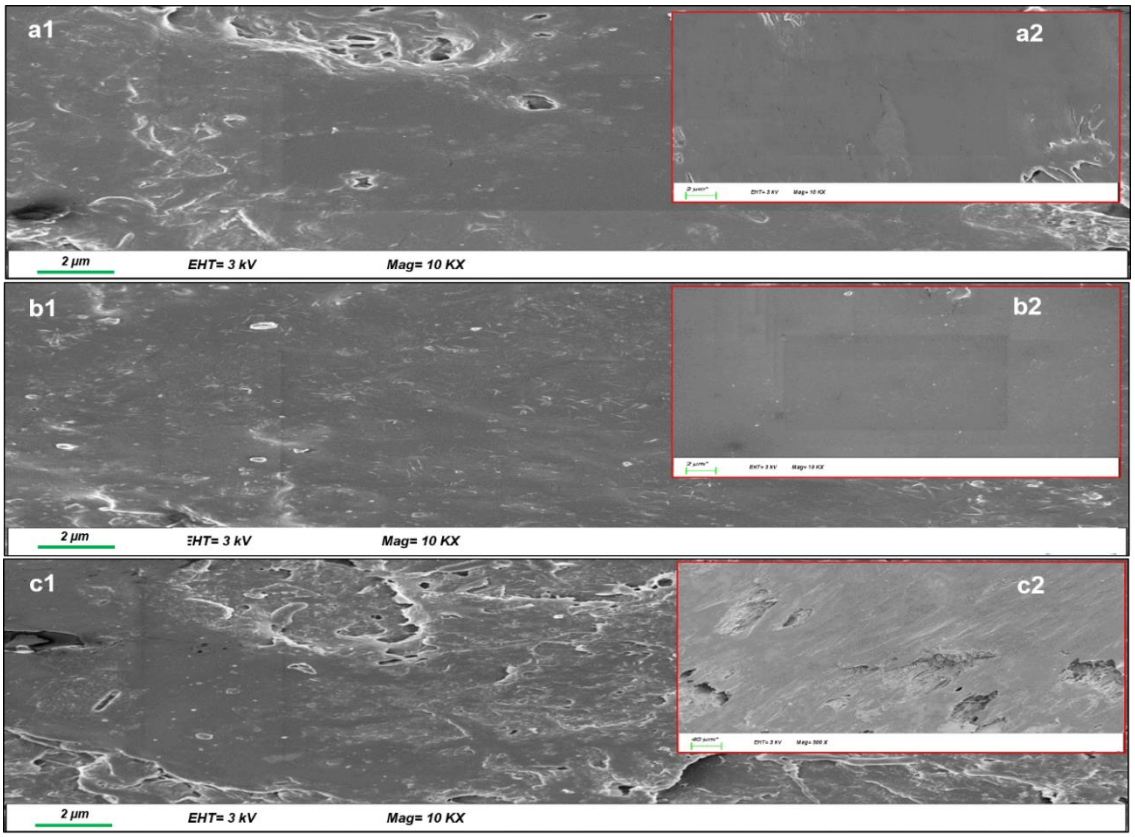

Figure 4.19: SEM analysis of surface and cross-sectional views for (a1 and a2) PCL-PEG drug-free matrix; (b1 and b2) IND-LPM; and (c1 and c2) 2-week degraded IND-LPM.

4.3.6 Assembly and release kinetics of MUPP variant one

Figure 4.20 illustrates the assembled MUPP variant one, showcasing the arrangement with the optimized IND-LPM positioned at the top, NLPM in the middle, and EPHCD in the lower segment of the T-shaped plastic frame of the intrauterine device. Moreover, the release profiles portray the sustained release of IND for 2 weeks, NETA and E2 for 4 weeks. Extrapolating the release profiles of NETA and E2 using the Korsmeyer-Peppas Equation 4.9, along with the model parameters in Table 3.6 and 4.7, respectively, reveals the platform's capability to sustain the release of NETA

for up to 19 weeks and E2 for up to 22 weeks (Figure 4.21). The Peppas-Sahlin equation was not used herein because it resulted in negative values for NETA released percentages after day 28.

$$Fraction\,released = kKP \times t^{n}$$ Equation 4.9

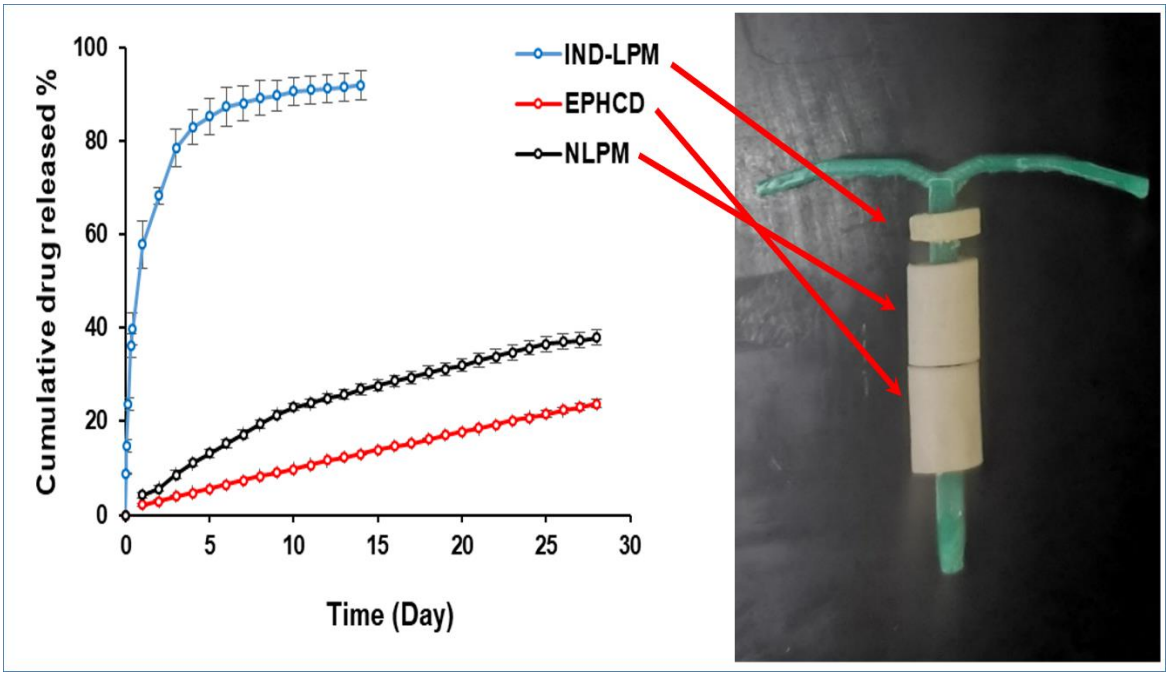

Figure 4.20: Assembly and release profile of MUPP variant one.

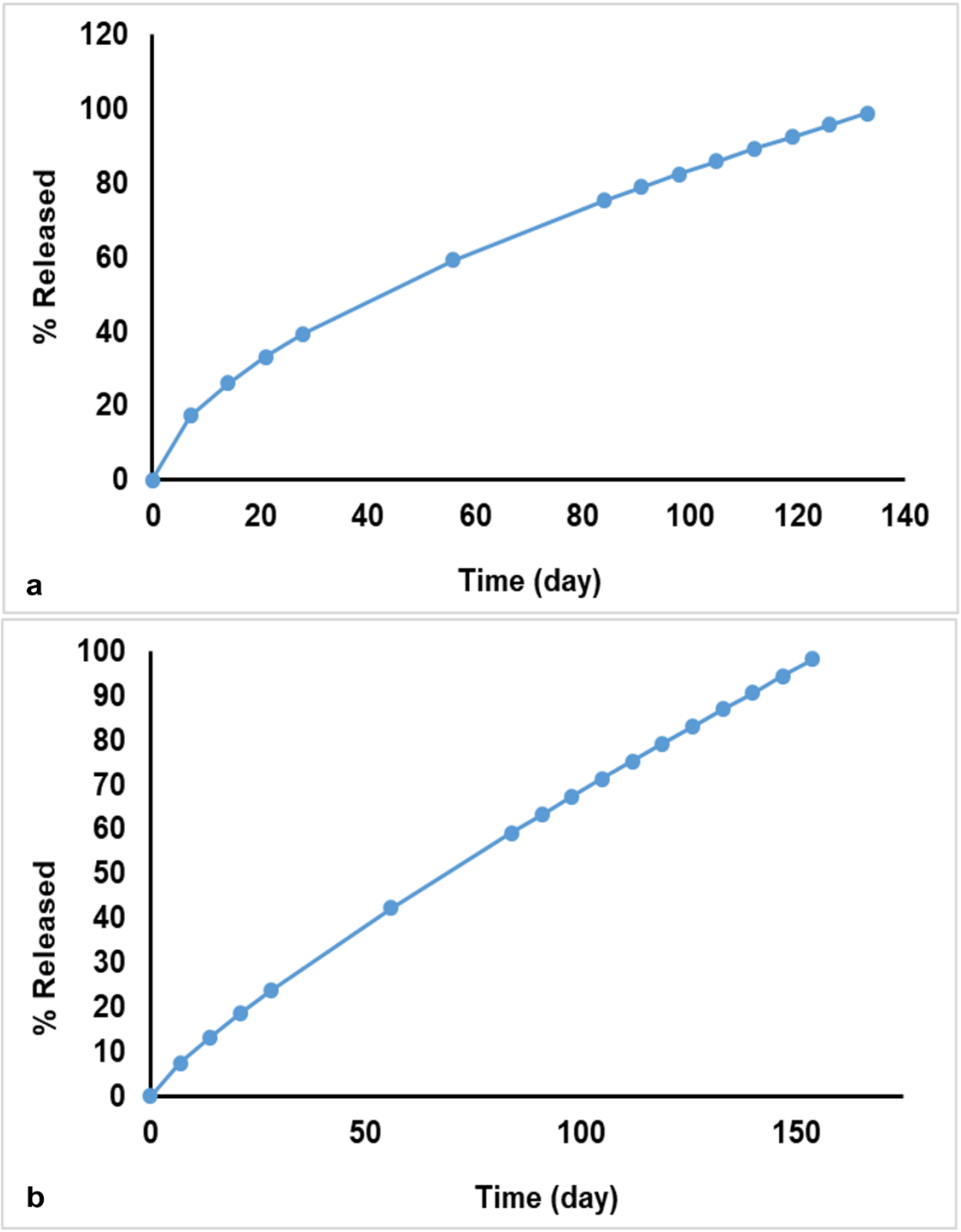

Figure 4.21: Expected release for (a) NETA and (b) E2 from the MUPP variant one device.

Post-assembly of MUPP variant one, an *in vitro* drug release study was conducted in SUF at pH 7 over a period of one week. The release profiles of E2 and NETA were analyzed using HPLC method. The objectives were to evaluate the feasibility of co-delivering two active pharmaceutical ingredients (APIs) within a single platform, to assess the sustained release characteristics of the MUPP, and to identify potential drug-drug interactions that could influence release patterns. Comparative analysis was performed between the release profiles of the combined MUPP and those of the individual units (NLPM and EPHCD).

A representative chromatogram for E2 and NETA obtained using a C18 column with a mobile phase of ACN and water at a flow rate of 0.8 mL/min is depicted in Figure (4.22a). Calibration curves were generated through linear regression analysis, with the area under the curve (AUC) of E2 and NETA as the dependent variables and drug concentrations as the independent variables. The coefficient of determination (R^2) was computed to assess the linearity and goodness of fit for each calibration curve (Figure 4.22b and 4.22c).

The results demonstrated that the release of both drugs from the MUPP was sustained over the one-week period, with release profiles comparable to the release from each unit tested independently. Additionally, after one week release study using HPLC analysis, the cumulative drugs released from the MUPP (7.90±0.10% and 15.11±0.33% for E2 and NETA, respectively) were consistent and comparable to that released from EPHCD and NLPM (7.43±0.03% and 17.26±0.90% for E2 and NETA, respectively) when tested alone and analyzed using UV spectrophotometer (Figure 4.23), demonstrating absence of *in vitro* drug-drug interactions in the MUPP.

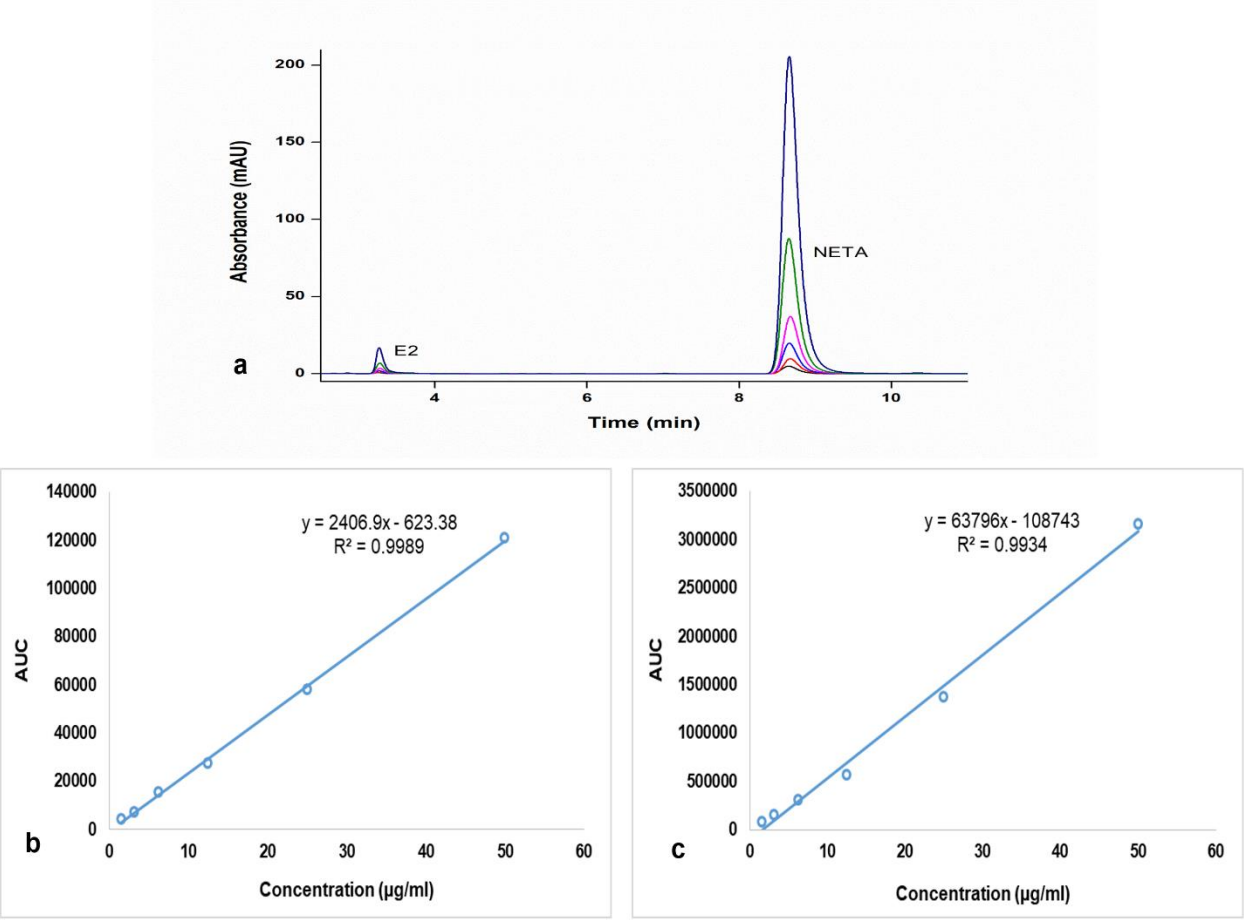

Figure 4.22: (a) HPLC chromatogram of E2 and NETA, (b) standard curve of E2, and (c) standard curve of NETA.

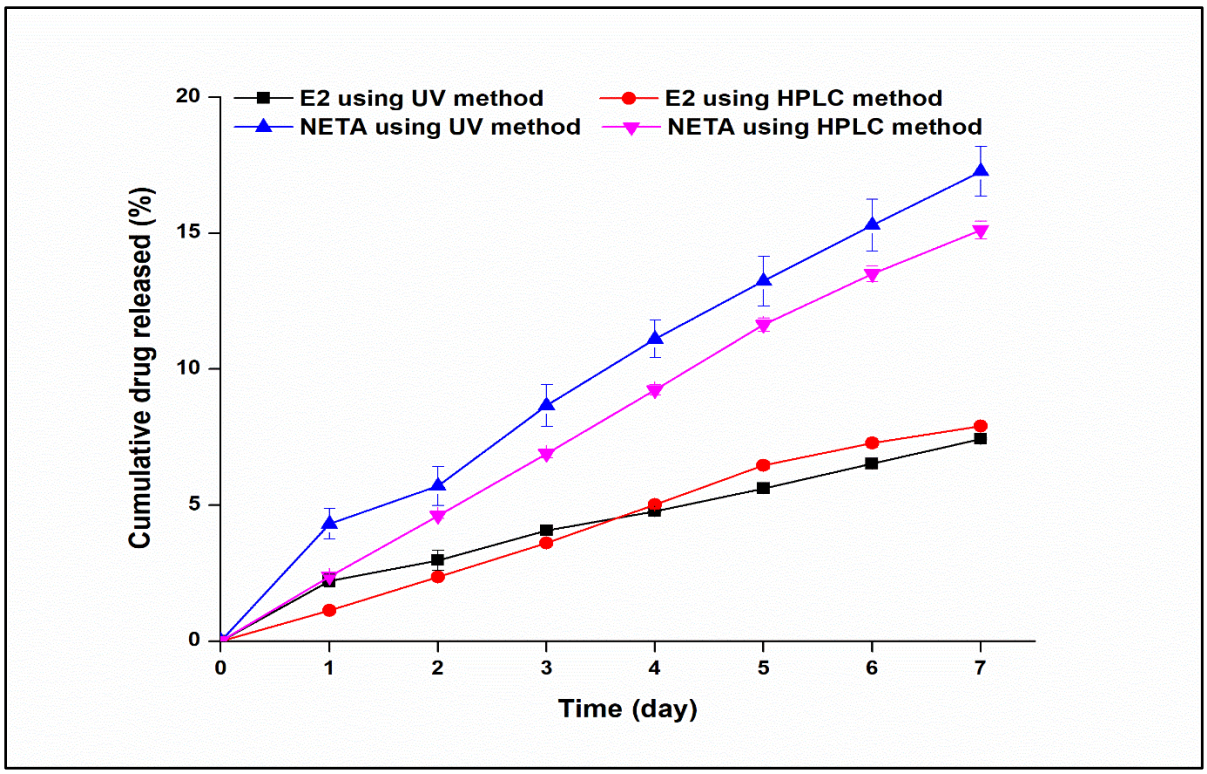

Figure 4.23: Release profiles of E2 and NETA for one week using UV spectrophotometer for EPHCD and NLPM and using HPLC analysis for MUPP variant one.

4.3.7 *Ex vivo* permeation studies

The transport of a drug molecule across a biological membrane is significantly influenced by several crucial parameters. These include the molecule's size, charge, lipophilicity, and hydrogen-bonding capacity. Physicochemical and structural attributes, such as molecular size, charge distribution, lipophilicity, and hydrogen-bonding capacity, play pivotal roles in determining the diffusional behavior of molecules across biological membranes (Lei et al. 2010). As the accumulation of E2 and NETA in genitourinary tissues is crucial for exerting pharmacological effects and controlling the GSM in safe manner, their adequate accumulation was assessed by determining the flux of E2 and NETA released from the EPHCD and NLPM, respectively, through the uterine membrane. The flux of both hormones across porcine uterine tissue over 8 hours is depicted in Figure 4.24. The results indicate an initial increase in the rate of E2 flux up to (0.054±0.009 mg cm^{-2} h^{-1}) during the first 2 h and NETA flux up to (0.092± 0.001 mg cm^{-2} h^{-1}) during the first hour, followed by a subsequent decrease in drug flux. This suggests that the mechanism of drug transport across the porcine tissue is hindered by binding and accumulation of E2 and NETA onto the membrane after 2 and 1 h, respectively. Therefore, it can be proposed that the majority of the drug was adsorbed onto the surface of the tissue, enabling localized effects

in the uterus and potential washing out through uterine fluid to translocate and exert therapeutic effects in the vaginal tissue.

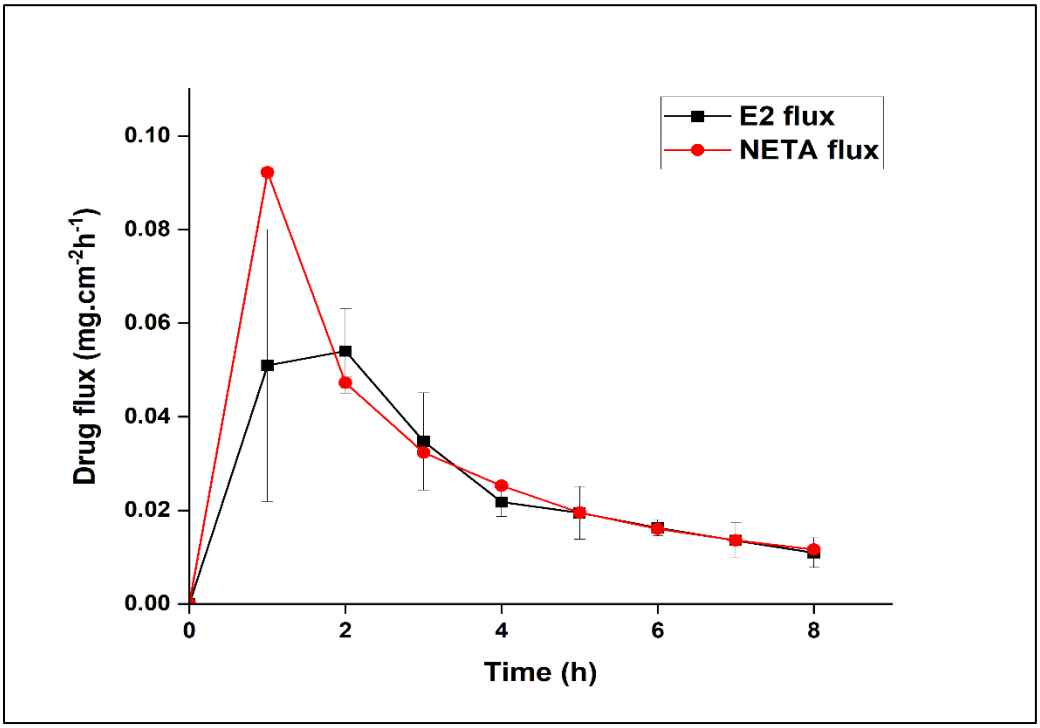

Figure 4.24: E2 and NETA flux through the uterine membrane as function of time.

4.3.8 Cytocompatibility Studies

Cytotoxicity studies stand as pivotal and extensively employed protocols for evaluating cyto-compatibility, recognized for their rapidity, sensitivity, and methodological simplicity (Prasadh et al. 2022b). The *in vitro* cytocompatibility of the optimized EPHCD and its respective drug-free counterpart was evaluated by assessing the cell viability of NIH/3T3 cells. The negative control comprised the cell culture medium, with the resultant cell viability normalized to a value of 100% for comparison with the test samples. Figure 4.25 depicts the results of an *in vitro* cell study using the MTT assay over a 7-day period, with both EPHCD and drug-free device demonstrated cell viability exceeding 70%, indicating the non-toxic and cyto-compatible nature of the prepared formulations in this investigation (Arany et al. 2021, Prasadh et al. 2022a, Wu et al. 2014). Evaluation 1 and 7 days post treatment, both treatments exhibited non-significant impact on the cellular viability, when compared to the negative control, [p=0.095, p=0.561 (Day 1) and p=0.925, p=0.968 (Day 7) for EPHCD and drug-free device, respectively]. On Day 3, both devices exhibited significant differences compared to the negative control (p=0.001, p=0.043, for EPHCD and drug-

free device, respectively). On Day 5, EPHCD-treated cells exhibited more significant cellular viability compared to the drug-free device and to the negative control [p=0.009, p=0.003], respectively. Figure 4.26 displays photomicrographs captured on Day 7 after treatment for the negative control, EPHCD extract, and drug-free device extract, further affirming the cytocompatibility of the optimal EPHCD formulation.

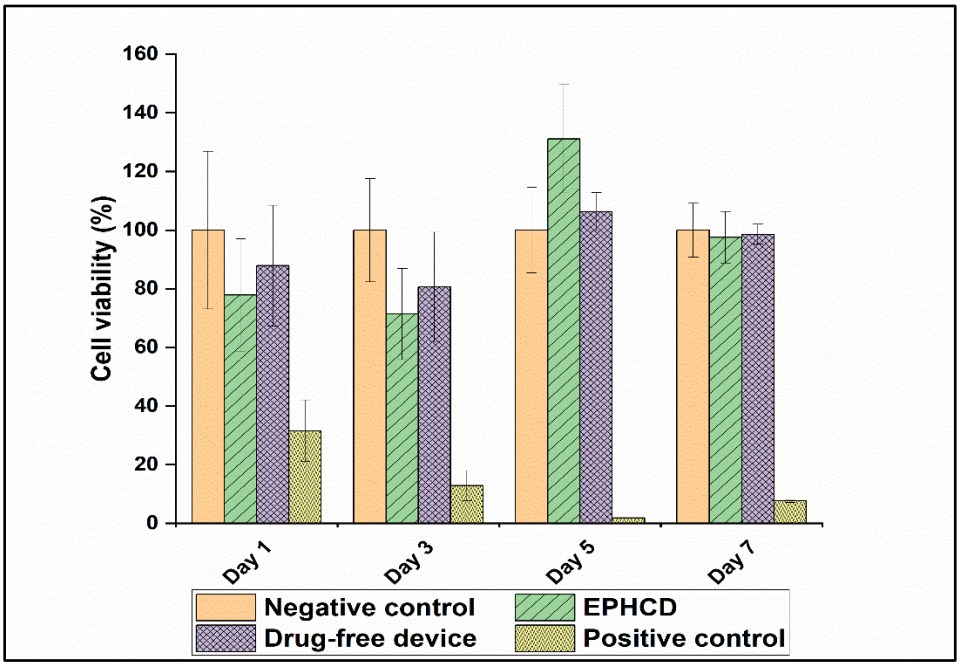

Figure 4.25: Cellular viability of NIH/3T3 by MTT assay in the presence of the optimal drug-free and EPHCD formulations.

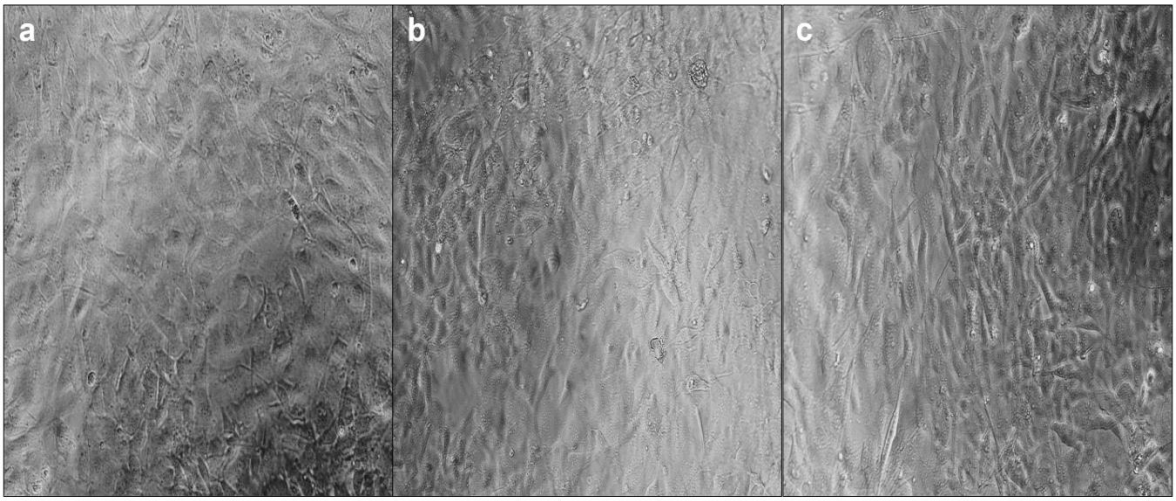

Figure 4.26: Micrographs of NIH/3T3 cells after 7 days treatment at 20X for (a) the negative control in cell culture media, (b) the drug-free device extract, and (c) EPHCD extract (scale: 1 cm = 100 µm).

Figure 4.27 illustrates the cellular viability of NIH/3T3 cells following treatment with extracts obtained from the mixture of the three drug-loaded units for 5 days and 4 weeks. Assessment at 3 and 7 days post-treatment revealed that the 5-day mixture extract showed cell viability above 70%, indicative of the non-toxic and cyto-compatible nature of the prepared formulations. Conversely, the 4-week mixture extract exhibited cellular viability of 68.9±4.27% and 67.53±6.76% post-incubation for 3 and 7 days with NIH/3T3 cells, respectively. This cellular viability, below the 70% threshold, could be attributed to high cumulative drug concentrations following the 4-week extraction period, which may not accurately mimic the *in vivo* conditions of the genitourinary tract's self-washing mechanism. The results of this study however note that in combination, the NETA-, E2- and IND-loaded devices did not significantly impact cellular viability at low concentrations. As *in vivo*, low concentrations of the individual drugs will be maintained through the genitourinary tract’s self-washing mechanism, the use of the MUPP device for the potential treatment of GSM still exists.

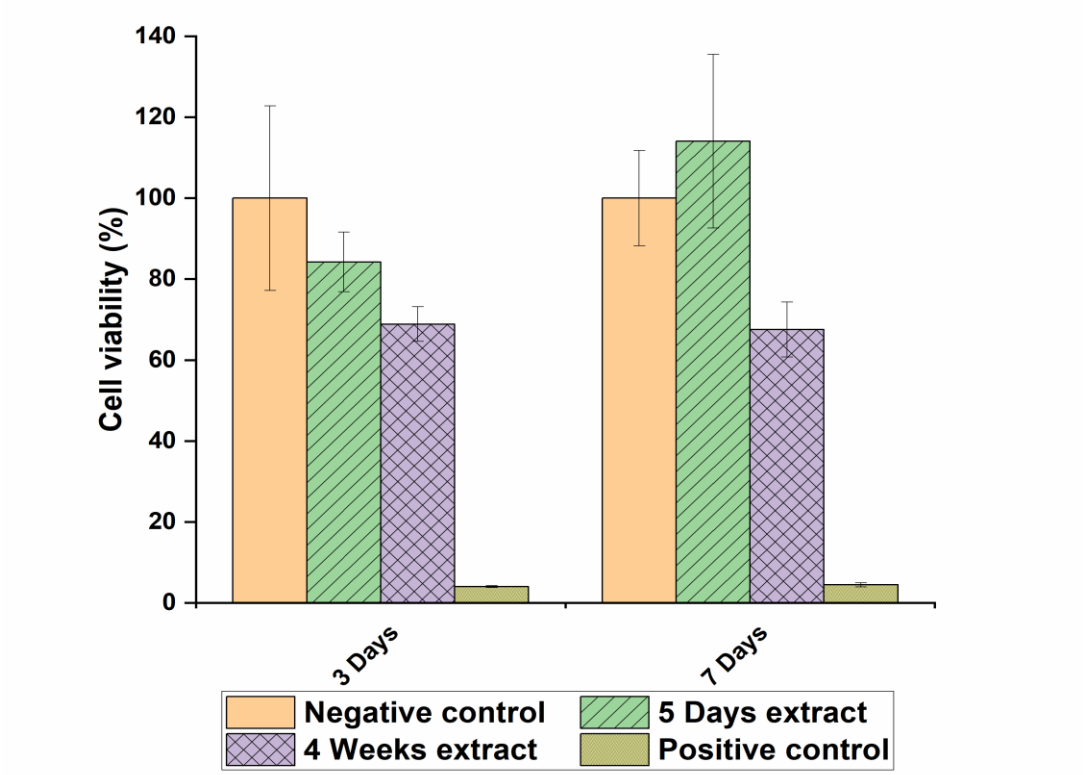

Figure 4.27: Cellular viability of NIH/3T3 by MTT assay in the presence of the (1:1:1) mixture of 5 Days and 4 Weeks extracts of the EPHCD, NLPM, and IND-LPM.

4.4 Concluding remarks

In this chapter, a polymeric hollow cylindrical device loaded with E2 was designed and prepared using a blend of PCL and EC, aiming for a continuous and sustained release of E2, as an estrogenic intervention, to address GSM. The study underscored the crucial roles of drug loading and the composition of matrix-forming polymers in modulating drug release kinetics and device integrity. The study employed the more statistically robust CCD for the exploration and parameters optimization of the prepared EPHCD. The CCD analysis unveiled notable differences in device properties arising from variations in the levels of drug load and the EC-to-PCL ratio. These properties were evaluated in terms of percentage drug release and weight loss, with ANOVA and response surface plots affirming the significant influence ($p < 0.05$) of factor levels on the measured parameters. The close alignment between experimental and fitted values underscored the precision and reliability of the used statistical design. The optimization process targeted both percentage drug release and weight loss, particular emphasis on the latter due to its considerable impact on matrix integrity and drug release kinetics. The release kinetics of E2 from optimal EPHCD adhered to Peppas-Sahlin kinetics, indicative of an intricate interplay

between diffusion and polymer relaxation behaviors. Furthermore, the developed optimized device demonstrated commendable cytocompatibility, indicating its potential as a biocompatible and implantable intrauterine device for managing GSM. Similarly, an IND-loaded polymeric hollow cylindrical device was fabricated from PCL and PEG, optimized using a 2^2 FD and evaluated for its structural and morphological properties. The MUPP variant one device was further prepared in this chapter with the cytocompatibility studies using leachates of NETA, E2 and IND noting that at low concentration of the drug, which will be maintained *in vivo* through natural self-washing processes, the MUPP device is suitable for the long-term treatment of GSM. Overall, the outcomes of this study firmly position the developed platform as a promising candidate for the sustained release of drugs within the uterine cavity, a feature that can be finely modulated by choice of drug load and polymer ratio. This functionality presents a viable intervention for addressing GSM, with potential implications for advanced biomedical applications such as contraception.

In continuation of the methodologies and findings outlined in chapters 3 and 4, which focused on the development and optimization of a multi-unit platform tailored for the uterine cavity implantation, the following chapter extends into an expanded investigation across two anatomically distinct body compartments, the vagina and uterus cavities. Hence, Chapter 5 explores the physicochemical and physicomechanical performance of the multi-unit platform in two distinct body compartments, it details the development, evaluation, and optimization of an intravaginal unit designed to be coupled with the intrauterine unit for the sustained release of E2.

CHAPTER 5

5 Fabrication and *In Vitro Evaluation* of a Novel Estradiol-Loaded Intrauterine-Intravaginal Delivery System: A Promising Approach for the Treatment of the Genitourinary Syndrome of Menopause

5.1 Introduction

Localized implants are crucial for achieving sustained and targeted drug delivery, ensuring elevated drug concentrations at specific sites while minimizing systemic exposure, thereby optimizing therapeutic outcomes and reducing systemic adverse effects. Various drug delivery devices, including doughnut-shaped tablets, multilayer tablets, and microparticles, have been investigated to achieve controlled and zero-order drug release rates (Wu et al. 2014). The zero-order kinetics is characterized by a constant drug release rate from the formulation, which can be demonstrated by plotting the fraction of drug released over time, resulting in a linear relationship (Abdelgader et al. 2024).

The human vagina serves as an advantageous route for drug delivery due to its accessibility and potential for tailored carrier systems to address both local and systemic conditions. Intravaginal drug delivery is especially relevant for medications addressing women's health concerns and holds potential for broader applications in female healthcare. It stands out as an ideal route for administering drugs such as contraceptive steroids, metronidazole, anti-retroviral. The implementation of an intra-vaginal controlled-release drug delivery system proves effective in ensuring continuous therapeutic agent delivery, catering to both systemically active drugs and locally acting drugs (Sahoo et al. 2013). Vaginal administration offers several advantages over the oral route, including dose reduction, less frequent dosing, diminished side effects, and the absence of hepatic first-pass effects. Nevertheless, challenges such as dilution by vaginal fluid and peristaltic activity of the vaginal wall need to be addressed for optimal efficacy (Osmałek et al. 2021). In addition, the design of a vaginal formulation demands consideration of the dynamic and variable conditions within the vaginal cavity. These conditions, encompassing acidity, temperature, vaginal fluid production, and epithelial thickness, are intricately influenced by factors such as the menstrual cycle phase, sexual activity, patient age, and concurrent medical conditions (Osmałek et al. 2021).

This chapter details the development and fabrication of a doughnut-shaped vaginal delivery system (DVDS) based on EC and PCL for incorporation into an intrauterine-intravaginal device

(MUPP variant two) for the treatment of GSM. Physicochemical and physicomechanical attributes including degradability, *in vitro* drug release kinetics, morphology, and texture, as well as biological properties including cytotoxicity, were thoroughly scrutinized. To address the challenge of limited residence time within the vaginal cavity due to its self-cleansing mechanism, the DVDS was engineered to affix to a thread protruding from an IUD. This integration facilitates the protracted release of its E2 payload over an extended period. The IUD, loaded with NETA and IND, as discussed in previous chapters, serves to counter the estrogenic effects of E2 on uterine tissue while also providing beneficial anti-inflammatory effects. The biodegradable nature of the system obviates the necessity for removal once the entire E2 load is released. Furthermore, the process of DVDS manufacturing is easy and reproducible, since it involves direct compression processing using tableting press. Figure 5.1 portrays a schematic representation of the DVDS within the human vaginal cavity, affixed to the IUD.

The doughnut-shaped form has been chosen over the hollow cylindrical shape for delivering the E2 into the vaginal cavity due to several key advantages. Firstly, the doughnut shape offers greater ease of application and comfort, minimizing irritation compared to the cylindrical design. Additionally, the central hole in the doughnut shape allows for easy attachment to the thread protruding from an IUD, which enhances retention within the vaginal cavity, reduces the risk of expulsion, and improves stability by keeping the DVDS more securely in place. The central void also promotes more even release of the drug over the surface area and thereby enhancing overall efficacy. From a manufacturing perspective, the DVDS is advantageous because it can be produced more consistently and efficiently at scale, which is essential for commercial production. Moreover, this shape facilitates innovative design possibilities, such as a multi-layer DVDS, which can support incorporation of multiple active ingredients. Collectively, these factors position the DVDS as a superior choice over the hollow cylindrical shape, for optimizing therapeutic effectiveness and patient experience in terms of vaginal drug delivery.

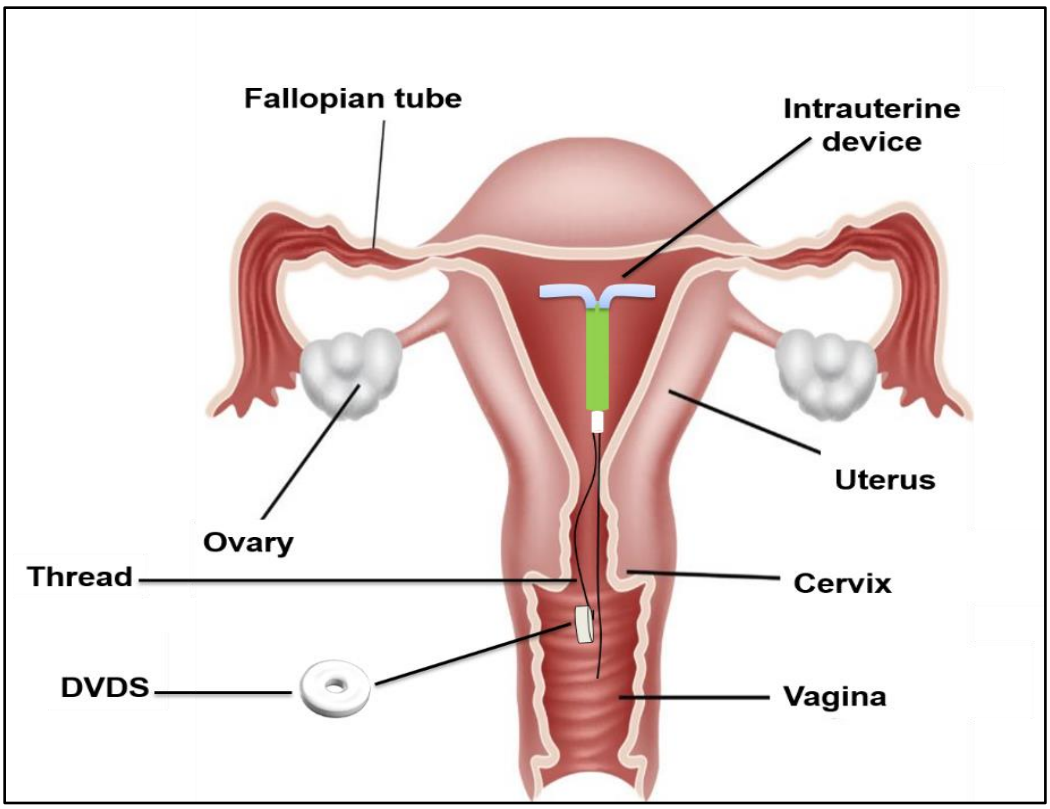

Figure 5.1: Schematic representation of the DVDS within the vaginal cavity.

5.2 Materials and Methods

5.2.1 Materials

Ethyl Cellulose was purchased from Sigma-Aldrich Chemie GmbH (St Louis, MI, USA), PCL Mn = 10,000 was purchased from Sigma-Aldrich (Tokyo, Japan), Estradiol hemihydrate purchased from Leap Chem (Hong Kong, China), and sodium hydroxide pellets from Merck Chemicals (Modderfontein, South Africa). NIH/3T3 mouse fibroblast cells (ATCC CRL-1658) were obtained from the ATCC (American Type Culture Collection, Manassas, VA, USA), Dulbecco's Modified Eagle Medium (DMEM) from Life Technologies Limited “Gibco” (Paisley, UK), Fetal bovine serum from PAN Biotech (Aidenbach, Germany), and MTT solution and solubilizing buffer from Roche Diagnostic GmbH (Mannheim, Germany). All other chemicals were of analytical grade and used without further purification.

5.2.2 Methods

5.2.2.1 Structure design, statistical design of experiment, and fabrication of the polymer-based DVDS

In this study, the intravaginal drug delivery system was designed with specific structural features. The device was designed as a doughnut-shaped tablet structure with an outer diameter of 7 mm and a height of 3.5 mm. Furthermore, the center of the device featured a 2 mm diameter hole. Figure 5.2 depicts the detailed schematic diagram of the device structure, highlighting the available volume for drug loading and the surface area for drug release. This device's structural design and specific features may offer potential advantages in drug delivery for vaginal applications.

A factorial design of experiments was implemented to systematically analyze and assess the impact of two factors at two levels using Design Expert® version 10 (Stat Ease, Inc, Minneapolis MN 55413, USA). The objective was to identify the optimal combination of independent variables, represented by the percentage of PCL-to-EC and compression force (X_1 and X_2, respectively), in relation to critical dependent variables, namely cumulative % drug release at week 2 and 4 (Y1 and Y2, respectively), weight loss percentage after 4 weeks of incubation in SVF (Y3), and DVDS hardness in term of force generated due to the matrix indentation (Y4). The experimental design included 7 runs, comprising 4 factorial formulations at low (−1) and high (+1) levels (F1–F4), along with 3 central points (F5–F7), as outlined in Table 5.1.

To prepare various formulations consisting of E2 in combination with biodegradable polymers (EC and PCL), the drugs and polymers were thoroughly blended according to specified ratios outlined in experimental design matrix Table 5.1. This blending process was carried out using a cube blender (Erweka® GmbH, Heusenstamm, Germany) for 10 minutes. Prior to blending, all powders underwent screening through a 500 µm mesh. The PCL granules were initially powdered using domestic blender after being subjected to cooling in liquid nitrogen. Subsequently, the powder blends, each of 130 mg weight, were compressed using a single punch tableting press (Manesty F3, Manesty, England) equipped with a specialized die and punch tooling set (Figure 5.3). The tooling tips were lubricated using a suspension of magnesium stearate in acetone (5% w/v) prior to compaction processing. The devices were prepared through manual die-filling of powder blends and compressed at compression forces of 28, 30, and 32 KN. The filling volume was maintained constant; therefore, the thickness of the prepared DVDS varied depending on the compression force applied and powders density. In-process validation tests were conducted to verify that the

produced devices adhered to the desired quality attributes such as matrix hardness and weight uniformity.

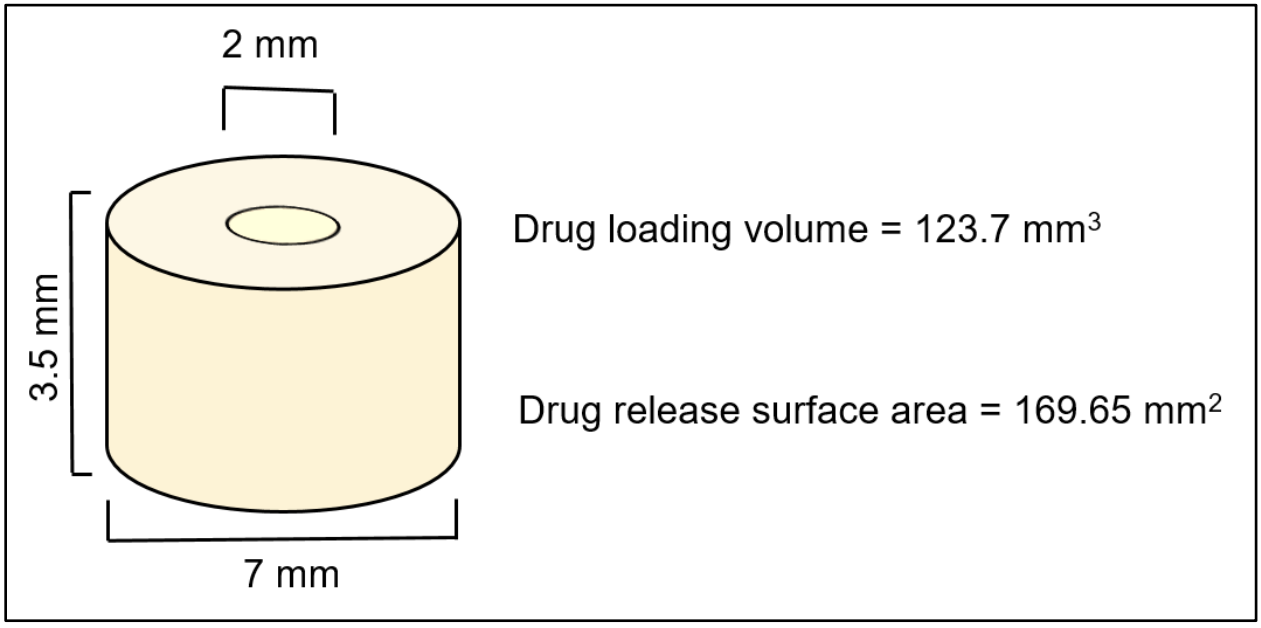

Figure 5.2: Ideograph of DVDS structure and it is common features.

Table 5.1: Experimental design domain of the 2^2 FD.

Formulation code	PCL-to-EC (%)	Compression force (KN)
F1	10 (-1)	28 (-1)
F2	50 (+1)	28 (-1)
F3	10 (-1)	32 (+1)
F4	50 (+1)	32 (+1)
F5	30 (0)	30 (0)
F6	30 (0)	30 (0)
F7	30 (0)	30 (0)

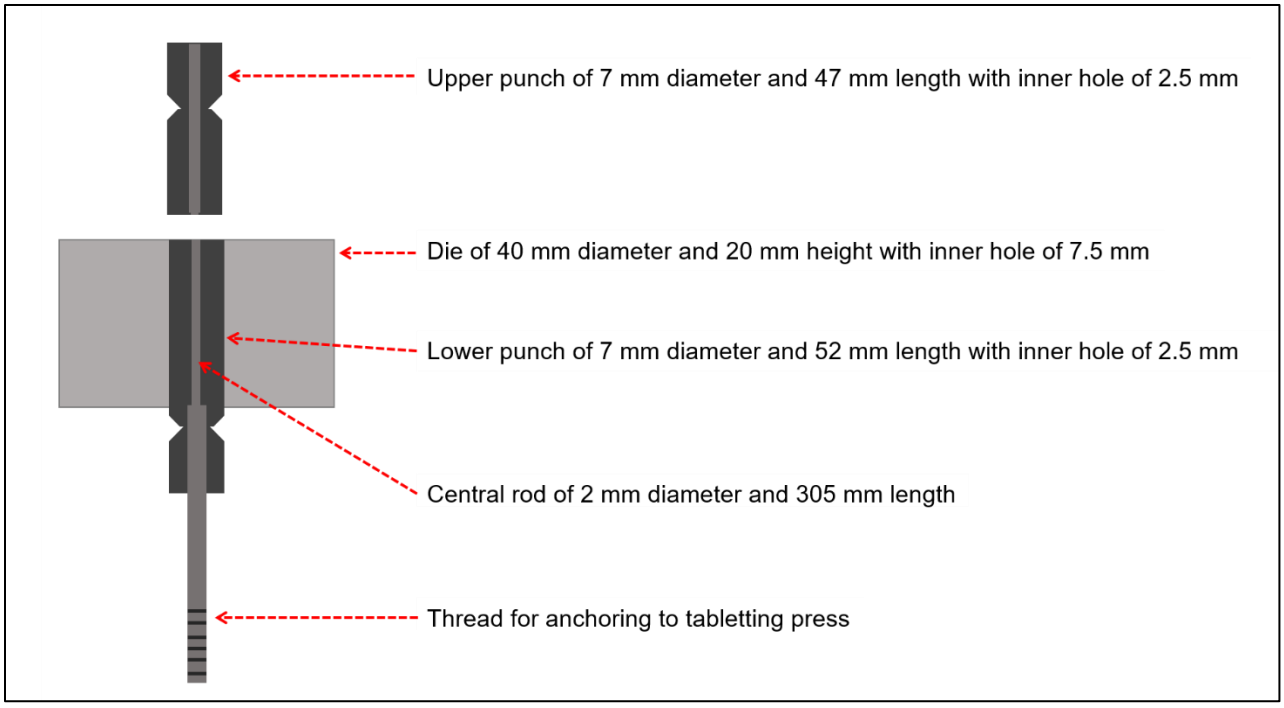

Figure 5.3: Schematic representation of tableting press tools used to compress the DVDS.

5.2.2.2 Experimental design evaluation and optimization of DVDS

5.2.2.2.1 DVDS dimension, weight variation, and drug content uniformity analysis

Following compression, the fabricated DVDS underwent a period of 24 h under ambient conditions to allow for stress relaxation within the devices. The diameter and thickness as well as the weight of 10 units of each DVDS formulation were obtained utilizing a digital vernier caliper and electronic balance. Thereafter, the average and standard deviation for each parameter was determined. To determine the E2 content in the prepared devices, three units from each formulation were precisely weighed, crushed, and dissolved separately in 100 mL of methanol. The solutions were stirred with a magnetic stirrer for 24 h at room temperature before centrifugation at 12,000 rpm for 10 min. The supernatant was then filtered using 0.45 mm syringe filters before being analyzed at 280 nm using an Implen nano-photometer. The drug content was represented as mean ± standard deviation.

5.2.2.2.2 Erosion studies of DVDS

The bio-erosion assessments of the fabricated devices were conducted gravimetrically using samples incubated for 4 weeks in SVF. The SVF was prepared by dissolving 3.51 g NaCl, 2 g lactic acid, 1.4 g KOH, 1 g acetic acid, 0.22 g Ca $(OH)_2$, 0.16 g glycerol, 0.4 g urea, and 5 g glucose in 1 L of distilled water. The pH of the solution was adjusted accordingly to pH 6 or 4.5

using 0.1 M HCl acid and 1 N NaOH solution (Owen and Katz 1999). After removal from the release medium, the samples underwent rinsing with double distilled water to remove any residual solutes adhering to the device surface, and subsequently air-dried for 72 hours in a fume hood before being weighed. The bio-erosion was then quantified as the percentage weight loss using Equation 3.1. All experiments were conducted in triplicate, and the results are presented as the mean ± standard deviation.

5.2.2.2.3 Determination of the physicomechanical properties

To elucidate the physicomechanical properties of the DVDS, both dry and hydrated samples were analyzed to assess textural changes associated with matrix hydration dynamics. The dry samples of DVDS were presented as compacts approximately 7 mm in diameter and 3.5 mm in thickness. Subsequently, the corresponding hydrated samples were immersed in 10 mL of SVF at pH 4.5 for 24 hours to achieve hydration. A calibrated Texture Analyzer (TA XTplus; Stable Micro Systems, Surrey, UK) equipped with a steel ball probe (5 mm diameter) was employed for analysis. The maximum force generated from matrix indentation to a depth of 0.3 mm was determined and regarded as the hardness or indentation resistance. Data were captured via Texture Exponent Software (Version 3.2). The experimental conditions, including parameter settings, are detailed in Chapter 3, Table 3.2. All analyses were conducted at room temperature (22°C) (Kolawole et al. 2007).

5.2.2.2.4 E2 saturation solubility in SVF

The shake-flask method is a common method for solubility determination in which an excess amount of solute is added to a certain solvent and after reaching the equilibrium condition by shaking at a constant temperature, the solute's concentration in the saturated solution is determined by a valid analytical method (Shayanfar 2020). The method of Woolfson *et al.* (Woolfson et al. 1999) was employed for determination of solubility of E2 in SVF. Briefly, an excess amount of drug was shaken in a predetermined volume of SVF at pH value of 4.5, 6, and 7.4 (Owen and Katz 1999). The stoppered glass vials were shaken on an orbital shaker incubator with 25 rpm and at 37±0.5 ºC for 96 h. The pH of saturated solutions was determined immediately after addition of the drug to the SVF and after 96 h shaking in the orbital shaker using Mettler Toledo pH meter (Mettler Toledo, Switzerland). Following equilibration, the samples were filtered using 0.45 µm syringe filter. The concentration of drug solubilized in each sample was determined after measuring its absorbance value at 280 nm using a nano-photometer NP80 (Implen GmbH, USA). The data of the solubility was taken as the average of three experimental results.

5.2.2.2.5 Drug release studies of DVDS

The E2 release profiles from the DVDS devices were assessed over a period of 4 weeks. Each formulation (n=3) was immersed in 15 mL of SVF (Figure 5.4) and maintained at 37°C in a water bath shaker operating at 25 rpm. Sampling was conducted at predetermined time intervals, with 80% (12 mL) of the release medium refreshed during each sampling point. To emulate the clinical setting and simulate pH fluctuations in SVF post-application of estrogenic medications, drug release was examined at pH 6 for the initial 2 weeks followed by pH 4.5 for the subsequent 2 weeks.

Figure 5.4: Photographs of different DVDS formulations suspended in the release medium (SVF, pH 6).

5.2.2.2.6 Statistical optimization of DVDS

The optimization of DVDS was accomplished by leveraging the data obtained from the evaluation of experimental design formulations. The parameters utilized for optimization included maintaining the PCL-to-EC percentage and the compression force within the specified experimental range. The goal was set to minimize the percentage of the release and weight loss while maximizing resistance to indentation. Statistical optimization of DoE led to the identification of an optimal formulation with a PCL-to-EC ratio of 10% and a 28 KN compression force. Subsequently, the optimal formulation underwent hydration studies, structural profiling, morphological analysis, release kinetic modeling, and cytocompatibility studies as outlined below.

5.2.2.3 In vitro characterization of the optimal EPHCDs

5.2.2.3.1 Determination of chemical integrity using FTIR spectroscopy analysis

FTIR spectroscopy was acquired for E2, pure polymers, and optimal formulation, as detailed in Chapter 3, Section 3.2.2.3.2, in order to assess whether any constituents within the formulation interacted as a result of polymers and drug blending and compression processing of the device.

5.2.2.3.2 Water retention capacity

The hydration characteristics of optimal DVDS formulations were evaluated gravimetrically as per method outlined in Chapter 3, Section 3.2.2.3.1.

5.2.2.3.3 Mathematical modeling of the release kinetics

The mechanism of drug release of optimal DVDS was elucidated through the application of mathematical models, encompassing zero-order, first-order, Higuchi, Korsmeyer-Peppas, and Peppas-Sahlin models.

5.2.3 Preparation of and analysis of MUPP variant two

The MUPP variant two was assembled by envelopment of the optimized NLPM and IND-LPM on the 3D printed T-shaped plastic frame of IUD and attaching the DVDS through a string, which was thereafter characterized for its drug release kinetics. Further cytotoxicity studies have been undertaken on the MUPP variant two and have been described in Section 5.2.5.

5.2.4 *Ex vivo* Drug Permeation Studies

Porcine vaginal tissues were procured from the Wits Research Animal Facility (WRAF, School of Health Sciences, University of the Witwatersrand, Johannesburg, South Africa) under the approved waiver from the Animal Research Ethics Committee, University of the Witwatersrand (Waiver 16-11-2023-O). The tissues were sourced immediately after the sacrifice of pigs and transported to the laboratory in phosphate-buffered saline (PBS). Upon arrival, the tissues were preserved in PBS and the drug permeation across porcine vaginal membrane was assessed using the FDC as detailed in Chapter 4, Section 4.2.2.3.2 with SVF (pH 6) in donor compartment.

5.2.5 Cytocompatibility Studies

The cytocompatibility over 7 days period of the optimal DVDS and its corresponding drug-free formulation was assessed on the NIH/3T3 cells (mouse fibroblast cells) as described in Chapter 3, Section 3.2.3. Furthermore, the cells viability in the presence of a mixture of extracts of DVDS, NLPM, and IND-LPM was evaluated as described in Chapter 4, Section 4.2.6.

5.2.6 Statistical Analysis

Design Expert® 8 software was employed to generate the 2^2 FD matrix, aimed at elucidating the influence of PCL-to-EC ratio and the compression force on selected response parameters of the fabricated DVDS and performing optimization strategies. All other statistical analyses were executed as detailed in Chapter 3, Section 3.2.4.

5.3 Results and Discussion

5.3.1 Fabrication of the DVDS

Direct compression is a widely adopted method in the pharmaceutical industry for the development of extended-release formulations due to its simplicity, cost-effectiveness, and time efficiency. The process involves only two main steps, blending of the active pharmaceutical ingredient with excipients and subsequent compression into the intended delivery system. This simplified approach reduces the number of processing steps, making it an attractive option for large-scale production. However, successful implementation of direct compression requires an understanding of the physical and chemical properties of both the API and excipients as well as the interplay between raw materials, formulation, and processing parameters, as these influence the flowability, compressibility, and uniformity of the final product. In addition, despite the challenges such as segregation and poor hardness, when properly managed, direct compression offers a highly feasible and efficient method for industrial-scale production of extended-release drug formulations (Sun et al. 2017).

The polymeric DVDS were successfully fabricated via direct compression, utilizing a specialized die and punch set as depicted in Figure 5.5. Upon characterization, these devices exhibited average dimensions of 3.5 mm in thickness, 7 mm in diameter, and 2 mm in inner diameter.

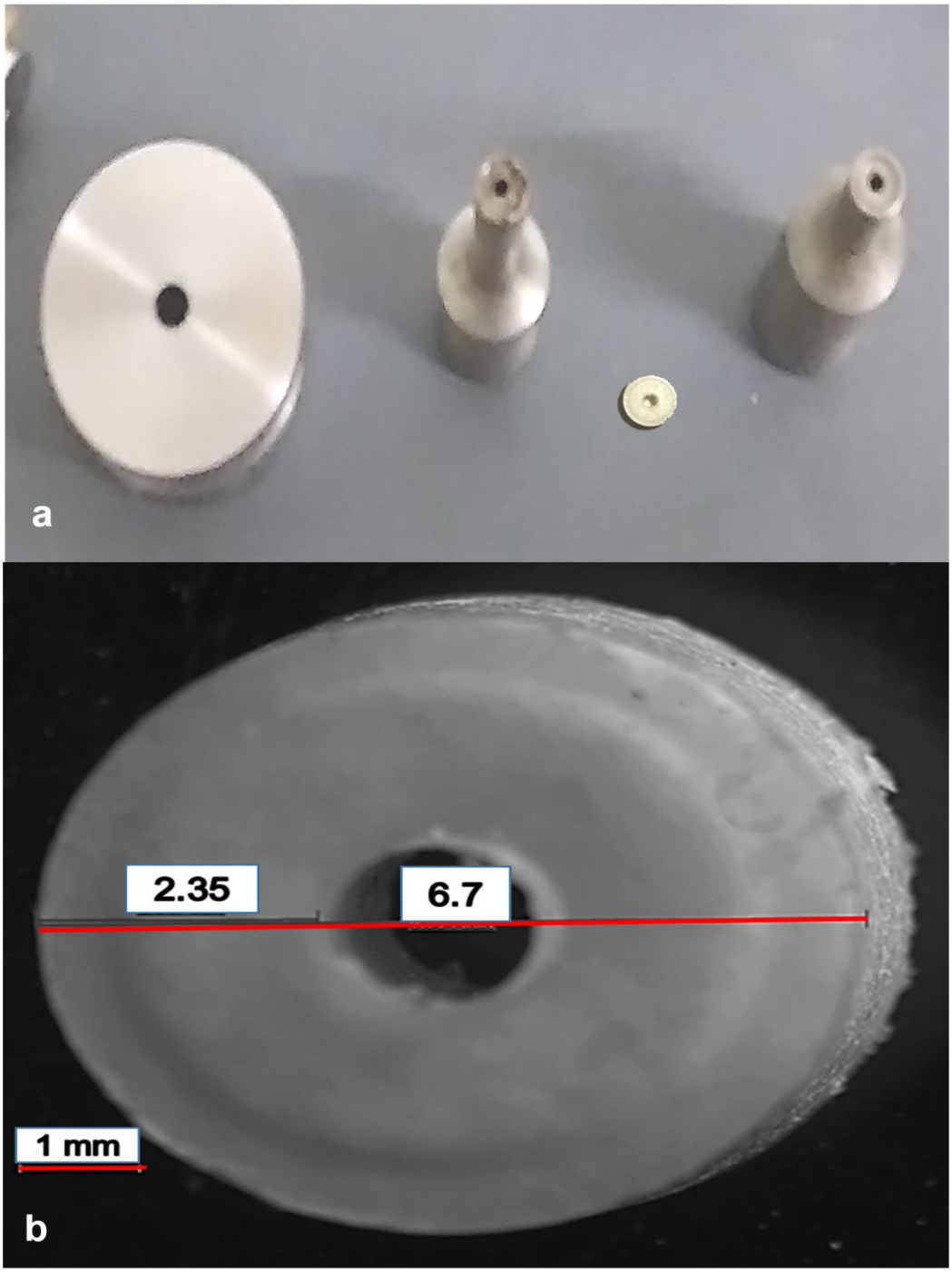

Figure 5.5: Photographic images of (a) the specialized die and punch set and (b) the DVDS fabricated using the set.

5.3.2 Experimental design evaluation and optimization

5.3.2.1 DVDS dimension, weight variation, and drug content uniformity analysis

The findings detailed in Table 5.2 provide an overview of the thickness and diameter measurements for the various DVDS formulations. The fabricated devices demonstrate minimal variability in both thickness and diameter, as evidenced by relative standard deviation (RSD) below 1.2% and 0.5% for thickness and diameter, respectively. This slight deviation is likely attributed to inherent differences in the density of powder blends and the application of varying compression forces during the fabrication process across different formulations.

Ensuring the drug content of each unit falls within acceptable limits around the label strength is crucial for maintaining therapeutic efficacy and safety (Križman et al. 2021b). Both content uniformity and the simple weight uniformity tests considered as viable tests to evaluate the consistency of drug content across individual delivery units (Zaid et al. 2012).

According to the European Pharmacopeia (Ph. Eur.), adherence to batch acceptance standards dictates that individual unit content measurements should fall within the range of 85% to 115% of the average content (Bendicho-Lavilla et al. 2024, Rastpeiman et al. 2024). Throughout this study, all formulations successfully met these criteria (Table 5.2), affirming that each formulation contained the specified quantity of E2.

To assess the weight variation of the prepared DVDS formulations, their mean and standard SD were calculated, and RSD was subsequently determined (Table 5.2). The RSD percentage, found to be less than 1%, signifies adherence to USP standards, which stipulate an acceptance range of 5 (Karami et al. 2024, Rastpeiman et al. 2024). It's pertinent to note that an increase in tableting speed can potentially lead to higher weight variation, given its direct correlation with fill time for volumetric die filling (Goodwin et al. 2018). Nonetheless, for these formulations, the risk was estimated low, as manual powder feed to the die alongside the similar tableting speed ensured precise die filling.

Table 5.2: Diameter, thickness and drug content of the DVDS formulations (mean ± SD).

F. Code*	Diameter (mm)	Thickness (mm)	Weight uniformity (mg)		Drug content (%±SD)
			Mean ± SD	**RSD**	
F1	7.02±0.020	3.51±0.040	129.54±0.934	0.72	104.12±4.400
F2	7.02±0.012	3.50±0.015	128.39±0.603	0.47	99.27±2.024
F3	7.01±0.006	3.58±0.006	128.99±0.603	0.47	99.78±1.415
F4	7.02±0.015	3.40±0.025	128.98±1.097	0.85	97.42±4.764
F5	7.04±0.010	3.50±0.015	130.48±0.843	0.65	106.36±4.401
F6	7.05±0.012	3.48±0.012	130.30±0.234	0.18	104.27±1.265
F7	7.04±0.006	3.50±0.005	130.22±0.201	0.15	103.99±1.312

*Formulation code.

5.3.2.2 Erosion studies of DVDS

The matrix erosion of the prepared DVDS formulations has the potential to impact the release patterns of the loaded E2. To correlate the erosion and release profiles of the DVDS formulations, the weight loss percentage over time was determined after a 4-week incubation period in SVF, as illustrated in Figure 5.6. The formulated DVDS exhibited relatively low weight loss profiles, ranging from 0.34% ± 0.022% to 1.3% ± 0.348%. Notably, formulations with a higher PCL-to-EC ratio (50%), such as F2 and F4, and those with a lower PCL-to-EC ratio (10%) demonstrated significant decrease in weight loss percentage with increasing of compression force from 28 to 32 KN. Conversely, formulations compressed at similar forces exhibited significant increase in weight loss percentage with escalating PCL-to-EC ratios, as observed in the comparison between F1 and F2 (compressed at 28 KN) and F3 and F4 (compressed at 32 KN). Moreover, formulation with intermediate levels of both independent variables resulted in an intermediate reduction in weight loss.

The observed increase in weight loss with higher PCL content may be attributed to the low molecular weight of the PCL used (Mn 10000), which reduces polymer entanglement and consequently enhances SVF ingress into the matrix (Bartnikowski et al. 2019). Conversely, the reduced weight loss with increased compression force may be due to decreased void volume and porosity under higher applied forces, thereby enhancing resistance to SVF ingress into the matrix (Diab et al. 2021).

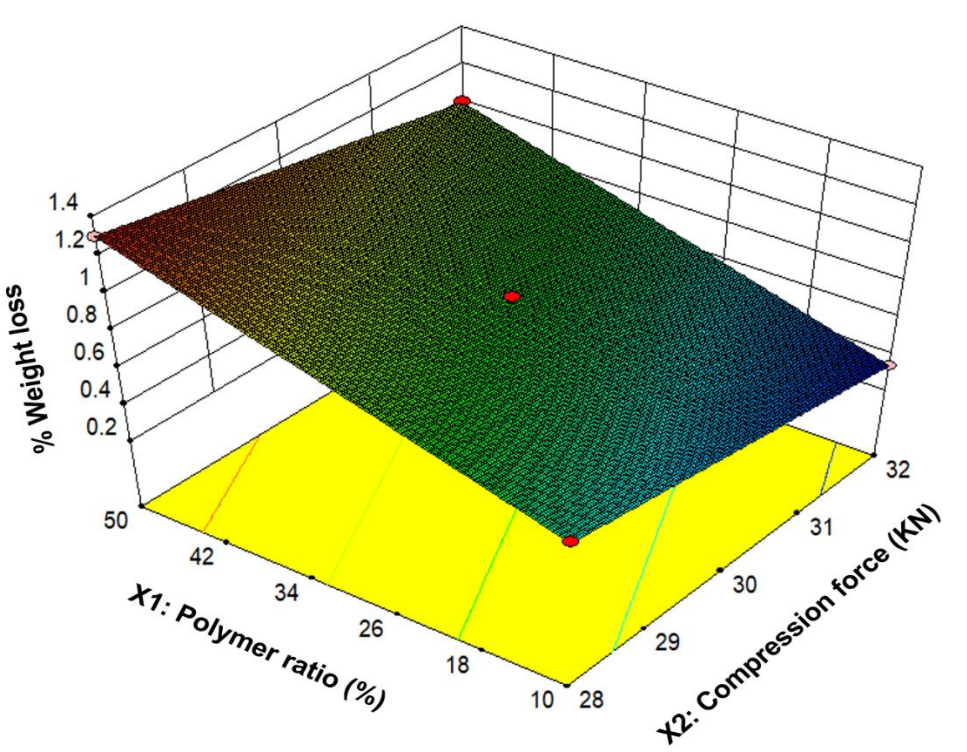

Figure 5.6: 3D plot portraying the influence of PCL-to-EC (%) and the compression force (KN) on the weight loss percentage of the DVDS formulations.

5.3.2.3 Determination of the physicomechanical properties

The mechanical characteristics of vaginal devices are pivotal for their functionality, encompassing aspects such as application simplicity, biocompatibility, and retention capability. A device that is excessively rigid may lead to discomfort and abrasion, as it interacts with the contractile forces of the vaginal tract. This susceptibility to abrasion can be further exacerbated by chemical and hormonal factors, potentially leading to an inflammatory reaction (Kaur et al. 2011).

The hardness of the prepared devices, both in dry and wet states, was assessed by measuring their resistance to indentation force. This assessment was conducted using a Texture Analyzer equipped with a 50 kg load-cell and a 5 mm ball probe. The dry DVDS formulations displayed varying indentation forces, ranging from 21.21±1.137 to 47.25± 5.12 N. Figure 5.7 illustrates the force (N) required to indent the device to a depth of 0.3 mm. A notable, statistically significant, inversely proportional relationship was observed between the increasing PCL content and the indentation force. This trend was particularly evident when comparing formulations F2 and F4 with those containing 30% and 10% PCL-to-EC ($p < 0.05$). In formulations with low PCL content (10%), increasing the compression force from 28 to 32 KN led to a significant increase in force,

as observed in the comparison between F1 and F3. The decrease in indentation force associated with higher PCL content may be attributed to the low molecular weight of the PCL used, which reduces polymer entanglement within the polymeric matrix.

Furthermore, upon 24 h of incubation in SVF, all formulations exhibited a statistically significant reduction in force compared to their dry counterparts. In the wet state, the energy required to compress the amorphous domains may be minimized due to the plasticizing effect of water within these regions and at the interface of the amorphous and crystalline domains (Kaur et al. 2011).

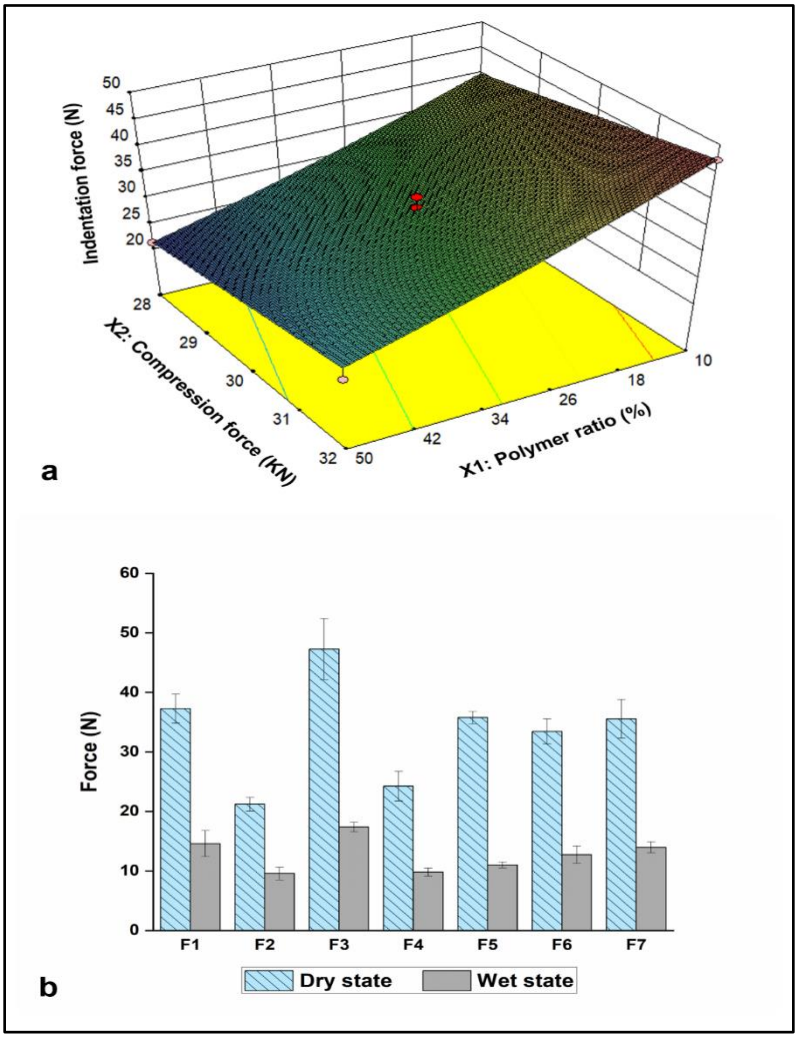

Figure 5.7: 3D plot portraying the influence of PCL-to-EC (%) and the compression force (KN) on the indention force of the dry DVDS formulations (a); and the effect of hydration on the indentation force (b).

5.3.2.4 Saturation solubility of E2 in SVF

The impact of drug solubility in the release medium on drug kinetic and pattern is apparent. Heightened drug solubility induces increased osmotic stress, expediting water ingress into the matrix. This effect results in greater polymer swelling, This leads to intensified polymer swelling, micro-pores formation, and accelerated polymer erosion at interfaces with the release medium, and consequently, intensified drug release (Yang Libo and Fassihi 1997). The experimentally ascertained solubility data at 37°C are presented in Table 5.3. Notably, E2 exhibited low solubility in SVF with pH 4.5 compared to more alkaline SVF. To ensure the integrity of the solubility determinations, pH measurements were conducted both at the commencement and end of the experiments. It is important to note that in all instances, the observed pH shift during the experiments remained within the acceptable limits, consistently measuring less than 0.5.

Table 5.3: Saturation solubility values for E2 in SVF.

pH of SVF	pH after addition of the E2	Final pH after 96 h shaking	Solubility µg/ml
4.5	4.40±0.033	4.39±0.038	1.84
6	5.97±0.087	6.35±0.215	5.52
7.4	7.10±0.035	6.93±0.150	3.88

5.3.2.5 Drug release studies of DVDS

The cumulative percentages of drug release from DVDS formulations over a 4-week period (Y2) exhibited a narrow range, ranging from 5.84 ± 0.239 to 7.82 ± 0.374 (Figure 5.8). Notably, formulation F1, characterized by a low PCL content (10%), demonstrated relatively lower release percentages, while formulation F2, with a high PCL content (50%), exhibited the highest release percentage. These results underscore the significant influence of PCL variations on E2 release from the polymeric matrix, consistent with findings from erosion and physicomechanical studies.

The decreased PCL content in F1 results in higher EC content and consequently a tighter, non-porous matrix, leading to slower drug release compared to F2, which exhibited greater weight loss and lower resistance to indentation. Additionally, high levels of EC have been reported to decrease drug release rates due to the formation of a strong, less porous matrix, increasing diffusional path length and reducing water penetration through micro-pores (Chandran et al. 2008).

Furthermore, analysis of Figure 5.8b reveals that variation in compression force had no significant effect on cumulative release percentage over the 4-week period. Moreover, intermediate levels of both independent variables (center point formulations) showed drug release comparable to F4, suggesting that interaction effects significantly influenced drug release. These findings are consistent with the results of the experimental design analysis in Section 5.3.2.6.

It is noteworthy that the DVDS formulations exhibited greater release in basic SVF (pH 6) during the first two weeks of the study, with release significantly decreasing in acidic SVF (pH 4.5) (Figures 5.8a and 5.8b). This observation aligns with increased E2 saturation solubility in SVF with pH 6 compared to its solubility in acidic pH environments, elucidated in Section 5.3.2.4.

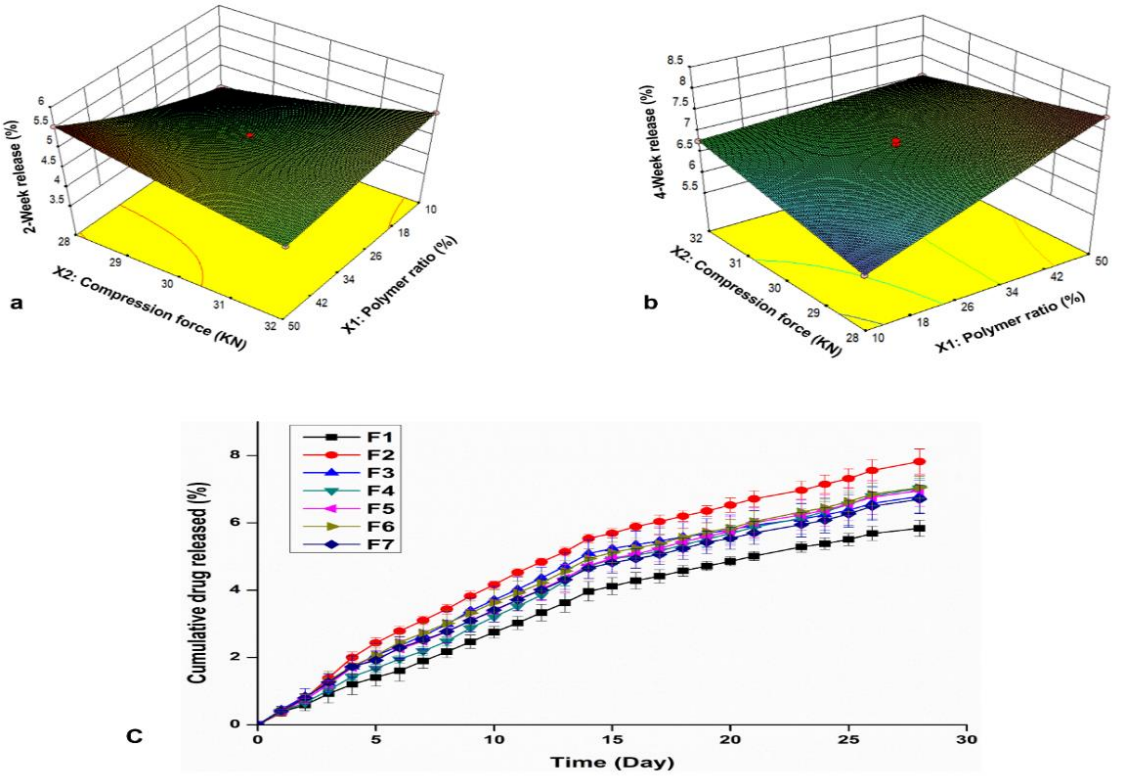

Figure 5.8: 3D Surface plots depicting the influence of PCL-to-EC (%) and compression force (KN) on the cumulative drug release at (a) 2-Week, (b) 4-Week, and (c) displaying the release profiles of the DVDS formulations.

5.3.2.6 Data analysis of the experimental design

In order to ascertain optimal conditions for DVDS formulations, 2^2 FD was employed to assess the impact of critical formulation and process attributes on DVDS development, using Design Expert software.

The experimental results are detailed in Table 5.4, with the corresponding ANOVA results summarized in Table 5.5. Models with a p-value less than 0.05 were considered statistically significant. Furthermore, suitability of models was assessed by ensuring that the p-value of the lack of fit was greater than 0.05. Based on the ANOVA results, all models exhibited p-values less than 0.05, while the lack-of-fit p-values were greater than 0.05.

The findings presented in Table 5.5 reveal that the PCL-to-EC ratio (X_1) significantly influences all studied responses. Additionally, while the compression force does not significantly impact drug release (Y1 and Y2), it does exhibit a significant influence over weight loss and indentation force (Y1 and Y4, respectively). Interestingly, the interaction term between compression force and PCL-to-EC percentage (X_1X_2) significantly affects drug release (%) during both the first 2 weeks (Y1) and the 4-week period (Y2)

The Pareto chart, a recognized statistical tool, serves to visually elucidate the most influential factors, with each bar's length representing the absolute value of the estimated effect (Modi and Bharadia 2023). The Pareto charts, depicted in Figure 5.9, delineate both the positive and negative effects of the factors on the studied responses. Statistical parameters such as R2, adjusted R2, predicted R2, adequate precision, CV, and PRESS indicate a robust fit for all generated models, as detailed in. Furthermore, contour plots (Figure 5.10) were generated to depict how each factor influences the responses.

The analysis of the design results yielded first-order equations expressed in terms of coded factors, providing further insight into the relationships between variables:

$$\frac{1}{Y1} = +0.21 - 0.014\,X_1 - 0.005967\,X_2 + 0.022\,X_1X_2 \qquad \textit{Equation 5.1}$$

$$Y2 = +6.88 + 0.56\,X_1 + 0.039\,X_2 - 0.43\,X_1X_2 \qquad \textit{Equation 5.2}$$

$$Y3 = +0.82 + 0.33\,X_1 - 0.15\,X_2$$ *Equation 5.3*

$$Sqrt(Y4) = +5.75 - 0.86\,X_1 + 0.27\,X_2$$ *Equation 5.4*

In Equations 5.1 and 5.4, the main effect term X_1 displayed significant negative effect on the inverse of the release during the first 2 weeks ($\frac{1}{Y1}$) and Sqrt (square root) of the indentation force ($Sqrt(Y4)$), while the X_2 demonstrate non-significant negative effect on ($\frac{1}{Y1}$) and significant positive effect on the $\left(Sqrt(Y4)\right)$. On other hand, X_1 exert significant positive effect on both the drug release during the 4 weeks (Y2) and weight loss percentage (Y3), as depicted in Equations 5.2 and 5.3, respectively. Furthermore, the interaction term X_1X_2, displayed significant negative effect on the drug release during 2 and 4 weeks as illustrated in Equations 5.1 and 5.2.

The evaluation of plots comparing the measured and model-predicted values for the four responses demonstrated a strong agreement between the predicted values from the models and the experimental data. Additionally, examination of the normal plots of residuals reveals a linear pattern in the data points, indicating the reliability of the regression models and the ability of the constructed equations to accurately predict the responses.

Table 5.4: 2^2 Factorial design results (n=3, ±SD).

Formulation code	2-week drug release (%)	4-week drug release (%)	Weight loss (%)	Indentation force (N)
F1	3.97±0.288	5.84±0.239	0.65±0.108	37.27±2.462
F2	5.54±0.126	7.82±0.374	1.30±0.348	21.21±1.137
F3	5.09±0.411	6.79±0.486	0.34±0.022	47.25±5.128
F4	4.71±0.161	7.03±0.289	1.01±0.063	24.24±2.484
F5	4.74±0.395	6.96±0.462	0.86±0.149	35.77±1.032
F6	4.94±0.298	7.05±0.334	0.78±0.087	33.44±2.103
F7	4.65±0.308	6.70±0.427	0.82±0.138	35.53±3.245

Table 5.5: Analysis of variance (ANOVA) for different responses of DVDS formulations.

	Y1	**Y2**	**Y3**	**Y4**
Source	P-value	P-value	P-value	P-value
Model	0.0077	0.01	< 0.0001	0.0037
X_1	0.0125	0.0051	< 0.0001	0.0017
X_2	0.1047	0.6371	0.0006	0.0077
X_1X_2	0.0035	0.0103		
Lack of Fit	0.8749	0.8328	0.9779	0.1135

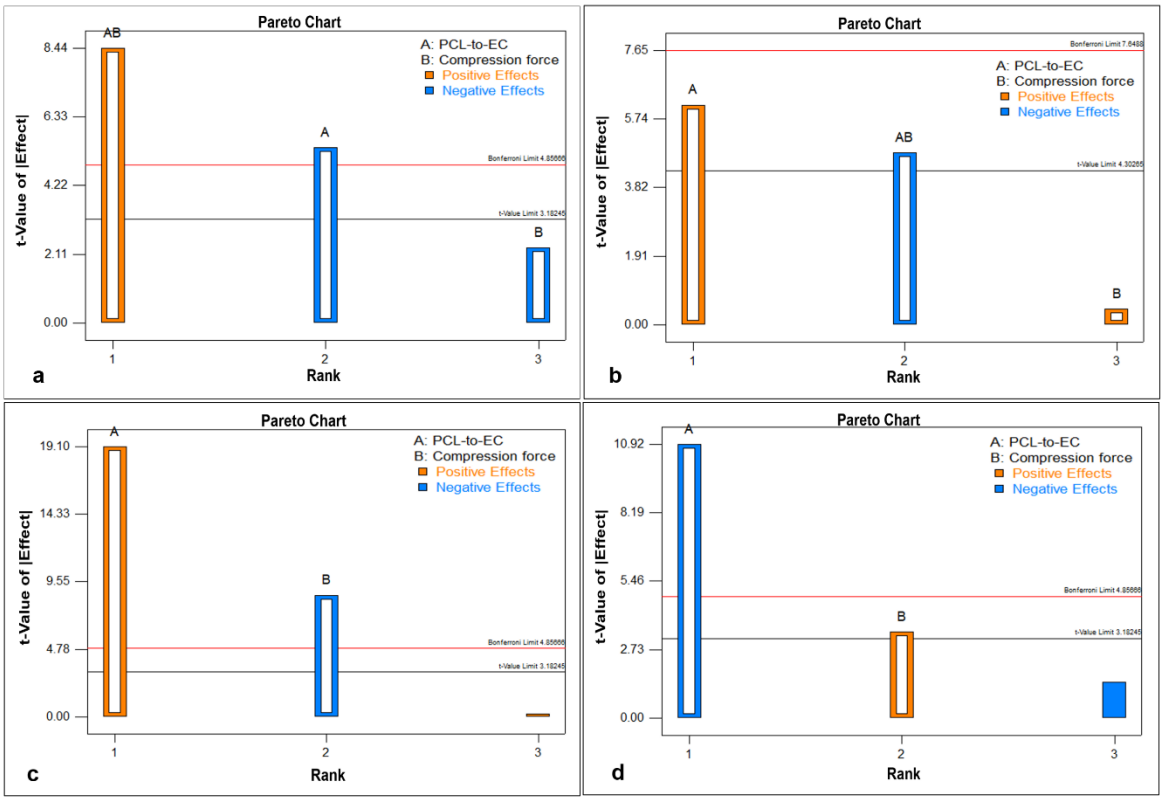

Figure 5.9: Pareto Charts showing the t-Value |effect| of the dependent variables on (a) 2-Week release%, (b) 4-Week release %, (c) weight loss%, and (d) resistance to indentation force of DVDS formulations.

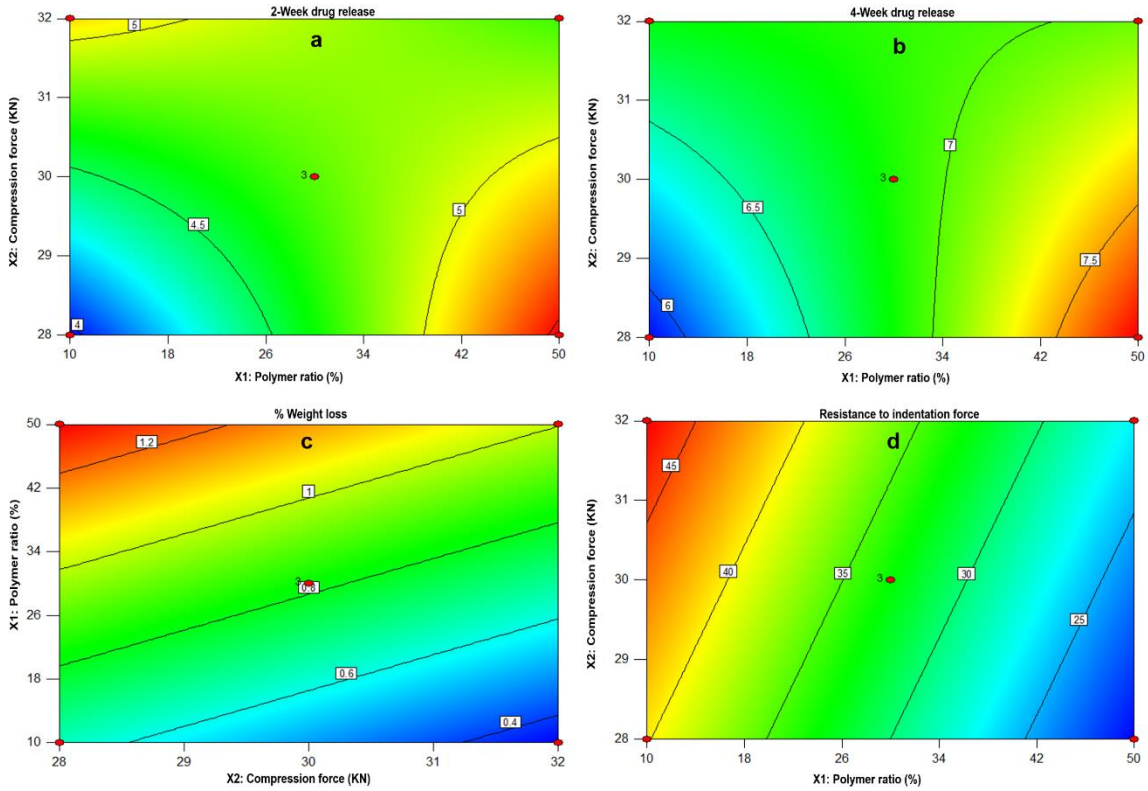

Figure 5.10: Contour plot portraying the influence of PCL-to-EC (%) and the compression force (KN) on (a) 2-Week drug release%, (b) 4-Week release %, (c) weight loss%, and (d) resistance to indentation force of DVDS formulations.

5.3.2.7 Statistical optimization of DVDS

Formulation optimization of the DVDS was achieved employing the desirability function and utilizing the data generated in the evaluation of design formulations. The parameters utilized for the optimization were the "in range" for PCL-to-EC ratio and compression force. In addition, the release and weight loss were set as to be minimized, while the indentation force was set to be maximized. The desirability function predicts the ideal values for the independent variables by combining all the results into one variable. Statistic optimization generated an optimal formulation of low PCL content (10%) and compression force of 28 KN with desirability of 0.84, as depicted in Figure 5.11. The optimal formulation was thereafter subjected to *ex vivo* Drug Permeation Studies, structural profiling, with hydration studies, release kinetic modeling and cytocompatibility studies undertaken as described below.

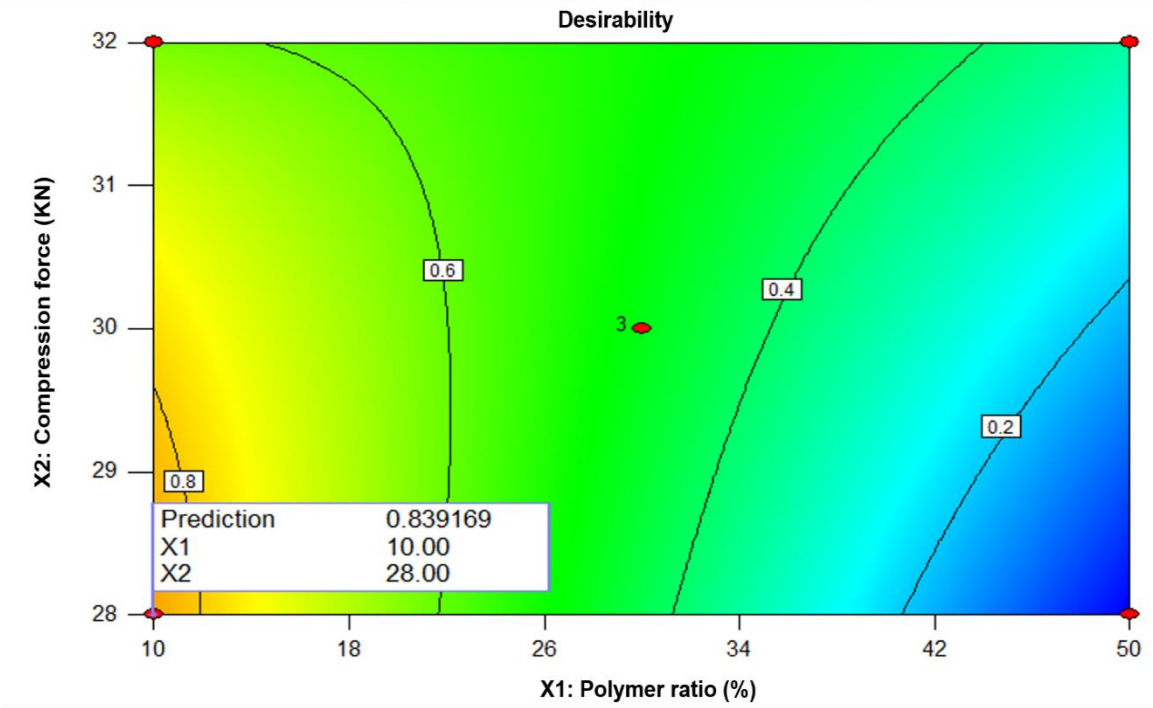

Figure 5.11: Contour plot of DVDS numerical optimization.

5.3.3 *In vitro* characterization of the optimal DVDS

5.3.3.1 Determination of chemical integrity using FTIR spectroscopy analysis

FTIR studies were performed to determine any interactions that could be occurred between the drugs and polymers. The characteristics peaks of pristine E2, PCL, and EC as well as the peaks of their combinations are detailed in Chapter 3, Section 3.3.2.2, and Chapter 4, Section 4.3.3.1. The findings emphasize the absence of significant chemical interaction, thus confirming the compatibility of the device-forming polymers with the loaded drug.

5.3.3.2 Water retention capacity

The *in vitro* hydration of the optimal DVDS formulation was examined in SVF over 24 h. The devices displayed a minimal percentage of hydration capacity equivalent to 15.31% ± 0.636. This reduced hydration percentage could be due to heightened hydrophobicity of the matrix imparted by the employed polymers. In addition, the low hydration capacity likely contributed to the low release percentage achieved by the optimal DVDS.

5.3.3.3 Mathematical modeling of the release kinetics

To elucidate the mechanism governing the release of E2 from the optimal DVDS, the release kinetics were scrutinized by fitting the experimental data to several release kinetic models. These

models included zero-order, first-order, Higuchi, Korsmeyer-Peppas, Hixson-Crowell, and Peppas-Sahlin models. Table 5.6 summarizes the goodness-of-fit results, including R^2, adjusted R^2, RMSE, AIC, and MSC values, which were applied to the averaged release profiles. The parameters obtained from the nonlinear regression of the dataset fitted to the models are also presented.

The Peppas-Sahlin model demonstrated superior fitting to the experimental data, with R2 and adjusted R2 values surpassing 0.99, and an AIC value of -6.7, indicating its robustness in describing the release kinetics of E2. Furthermore, the model displayed an MSC value of 4.56, emphasizing its suitability for characterizing the drug release profiles accurately. Figures 5.12 depict the appropriateness of the Peppas-Sahlin model in capturing the observed drug release patterns. The alignment of the experimental release data with the Peppas-Sahlin model indicate the drug transport mechanism was governed by both Fickian diffusion and case II relaxations.

Table 5.6: Statistical assessment and parameters for the best-fitting kinetic models to release data for optimal DVDS.

Model	**R^2**	**Adj-R^2**	**RMSE**	**AIC**	**MSC**	**Parameter**	
Zero-order	0.9499	0.9499	0.385	36.06	2.916	k_0	0.240
First-order	0.9564	0.9564	0.359	32.46	3.055	k_1	0.002
Higuchi	0.9003	0.9003	0.543	53.93	2.229	kH	1.020
Korsmeyer-Peppas	0.9870	0.9865	0.2000	2.93	4.191	kKP	0.461
						n	0.780
Hixson-Crowell	0.9543	0.9543	0.3678	33.67	3.008	kHC	0.001
Peppas-Sahlin	0.9917	0.9910	0.163	-6.70	4.561	k_1	-1.586
						k_2	1.702
						m	0.264

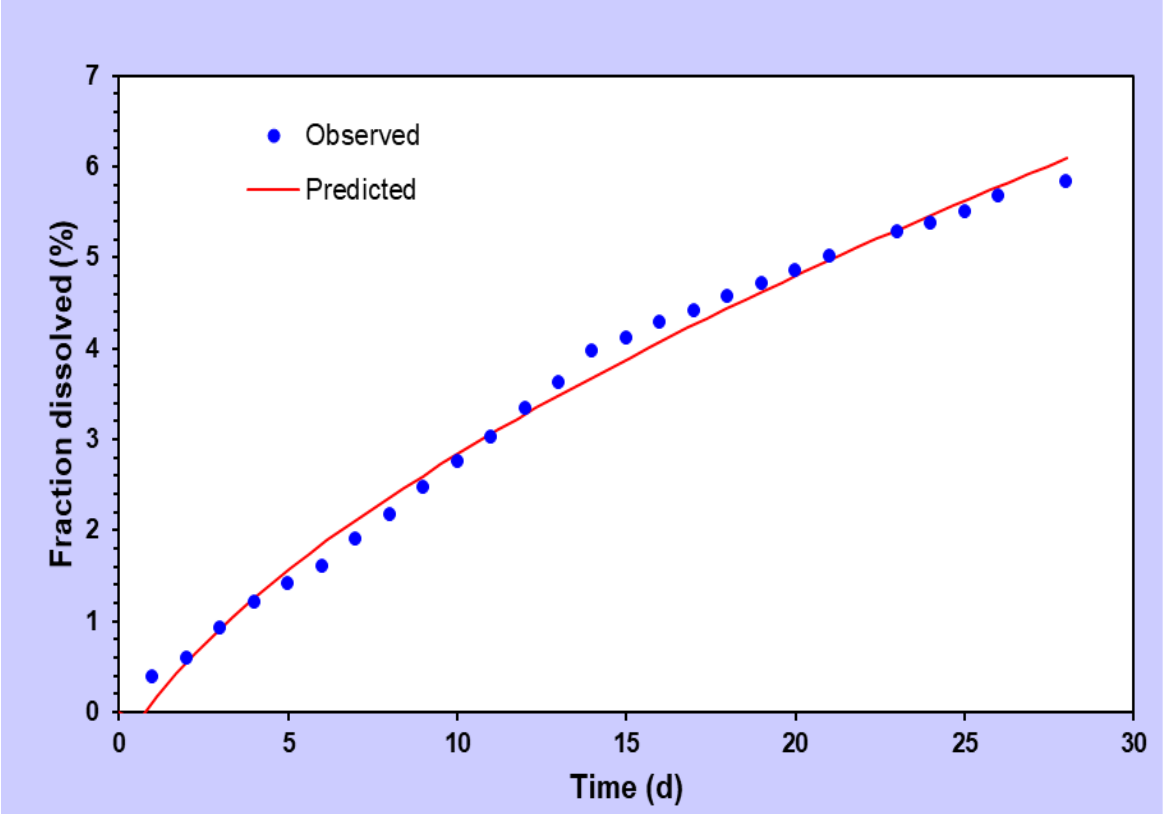

Figure 5.12: Fitting curve and modeling of E2 release from the optimal formulation, F1; to Peppas-Sahlin model.

5.3.4 Assembly and release kinetics of MUPP variant two

Figure 5.13 depicts the assembled MUPP variant two, demonstrating the arrangement with IND-LPM and NLPM encased to the top and lower segment of the T-shaped plastic frame of the intrauterine device, respectively, and DVDS attaching to the IUD through a protruding string. Furthermore, the release profiles reveal the sustained release of E2 for 4 weeks. Extrapolating the release profiles of E2 using the Korsmeyer-Peppas Equation (4.9), along with the model parameters in Table 5.6, unveils the DVDS capability to sustain the release of E2 for more than 140 weeks (Figure 5.13c). This findings with the result of extrapolating of NETA release discussed in Chapter 4, Section 4.3.6, suggest that to increase the percentages of NETA loaded and EC-to-PCL to the NLPM with aim of extending the release of NETA to correspond the predicted duration for E2 release from DVDS. Furthermore, the DVDS could be attached to the currently available Mirena®, which now is approved to be used for 5 years.

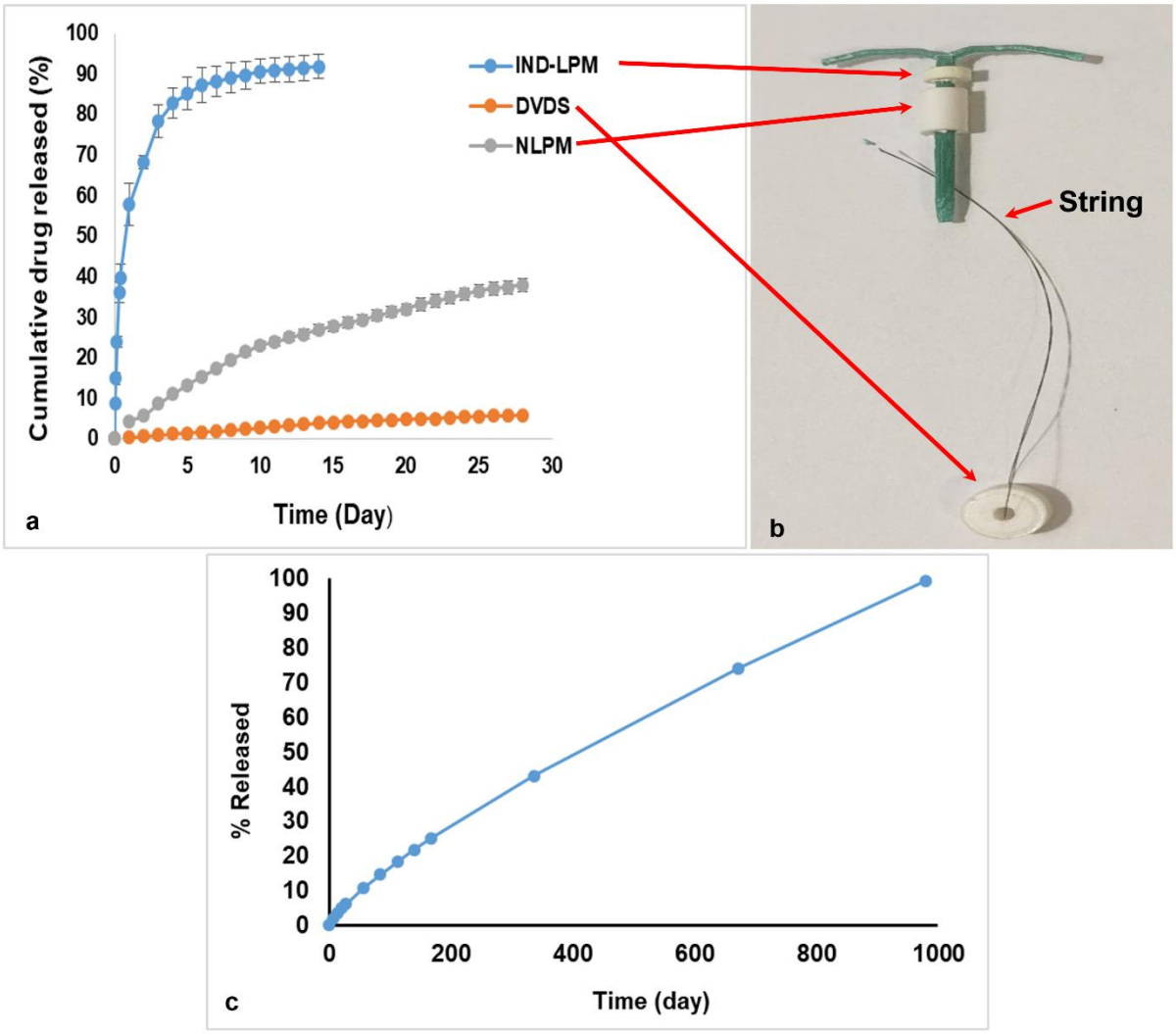

Figure 5.13: (a) Release profile of MUPP variant two; (b) Assembly of variant two; and (c) expected release of DVDS.

5.3.5 *Ex vivo* Drug Permeation Studies

Figure 5.14 presents the flux of E2 through porcine vaginal tissue as function of time. Initially, there is an upward in the flux rate, reaching a peak of (0.18±0.047 mg cm^{-2} h^{-1}) within the first hour, followed by a subsequent decline in drug flux. This indicates a delayed drug transport mechanism through the porcine tissue, likely due to drug binding and accumulation on the vaginal membrane after 1 h. Consequently, it is inferred that most of the drug is retained on the surface of the vaginal membrane, facilitating localized effects.

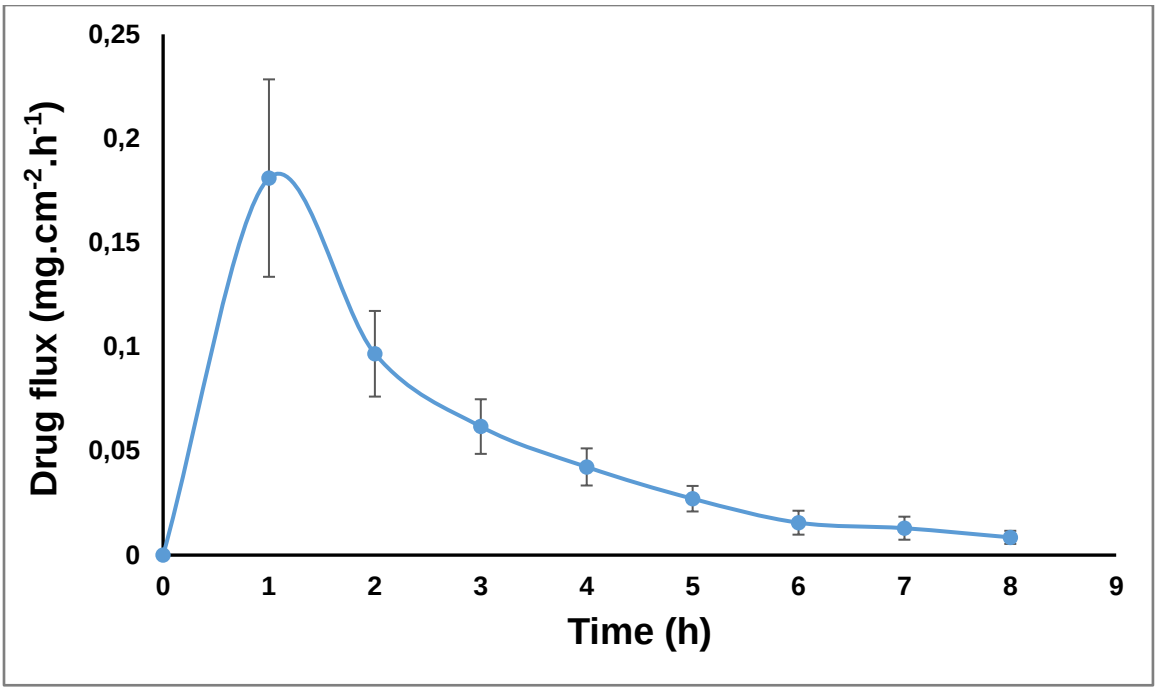

Figure 5.14: E2 flux through the vaginal membrane as function of time.

5.3.6 Cytocompatibility Studies

Figure 5.15 depicts the results of an *in vitro* cell study spanning a 7-day period. Both the DVDS and the drug-free device exhibited an average cell viability surpassing 70%, suggesting the non-toxic and cyto-compatible characteristics of the formulations prepared in this study (Arany et al. 2021, Prasadh et al. 2022a, Wu et al. 2014).

At evaluation points 1 and 5 days post-treatment, both the DVDS and the drug-free device showed no significant impact on cellular viability compared to the negative control ($p=0.214$, $p=0.96$ for DVDS and $p=0.176$, $p=0.348$ for drug-free device on Day 1 and Day 5, respectively). However, on Day 3 and Day 7, the DVDS exhibited average cellular viability of 69.9% and 82%, respectively, with significant differences compared to the negative control ($p=0.002$, $p<0.0001$, respectively). Photomicrographs captured on Day 3, 5, and 7 after treatment for the negative control, DVDS extract, and drug-free device extract are depicted in Figure 5.16, further confirming the cytocompatibility of the optimal DVDS formulation.

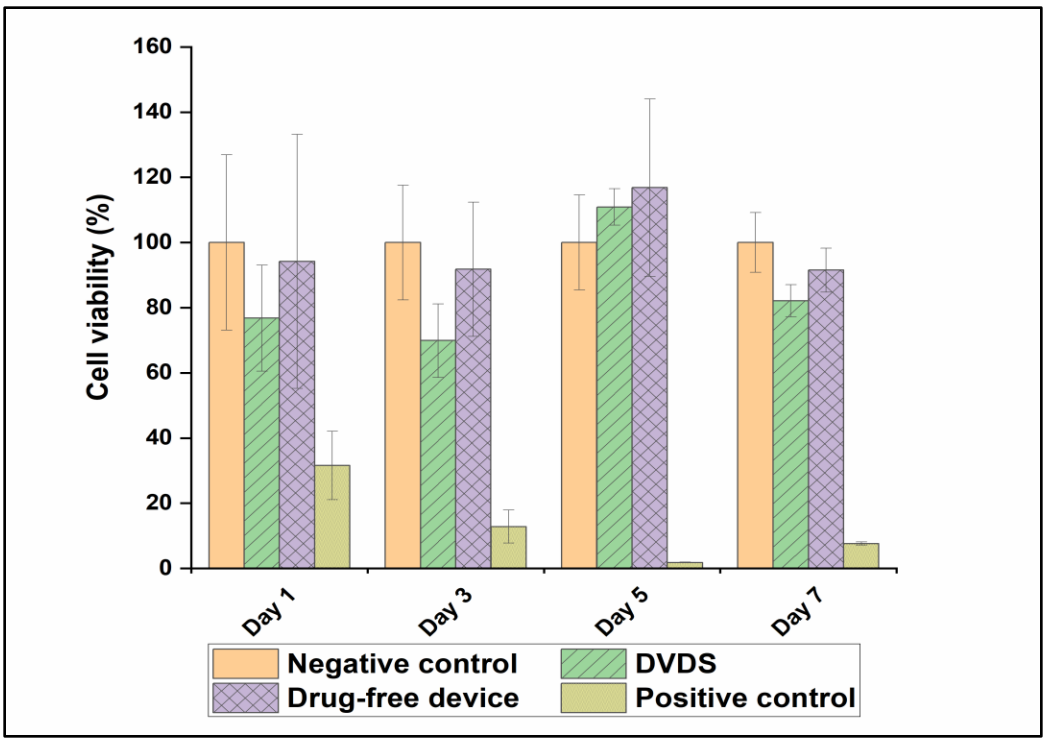

Figure 5.15: Cellular viability of NIH/3T3 by MTT assay in the presence of the optimal DVDS and corresponding drug-free formulations.

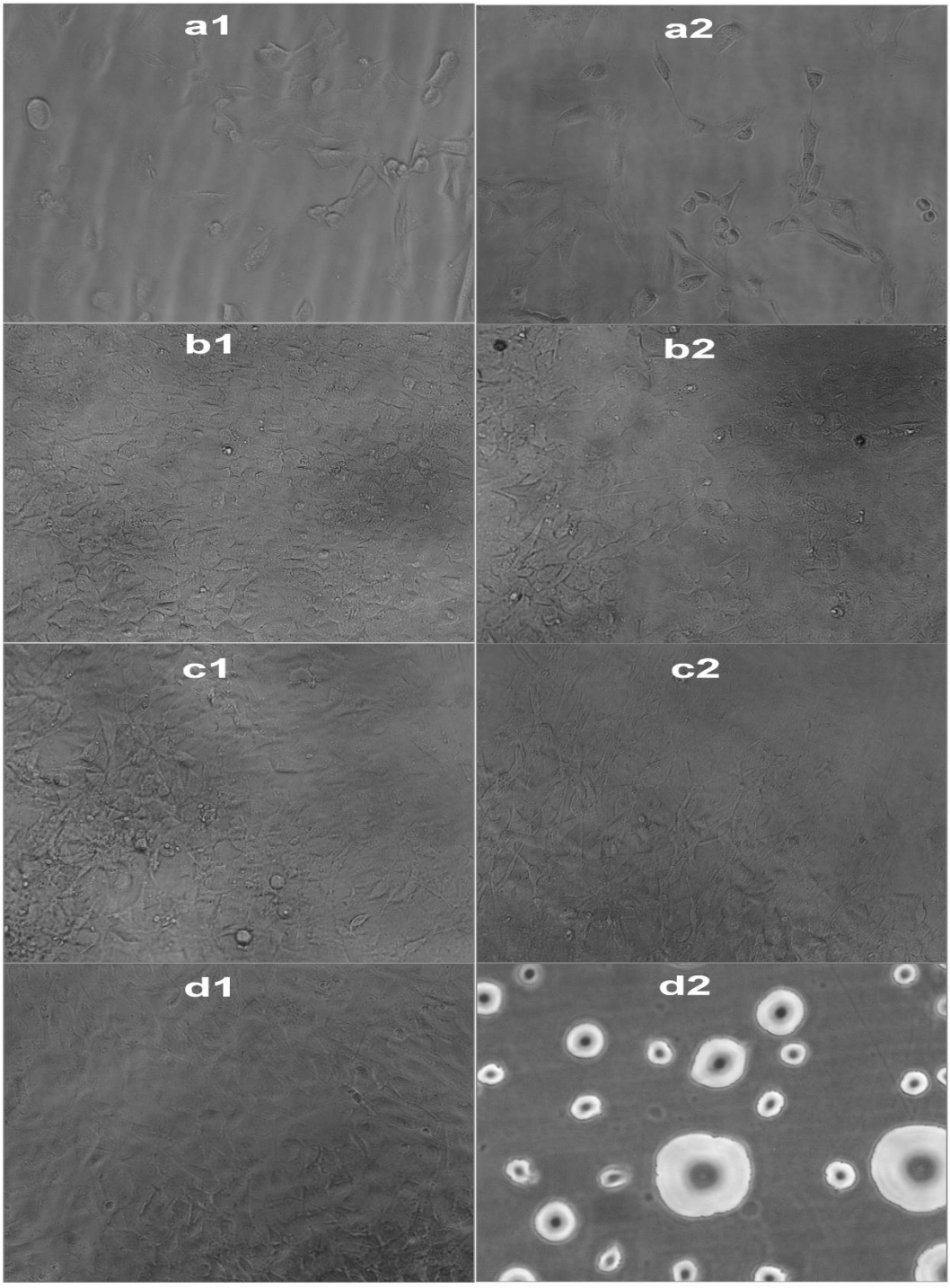

Figure 5.16: Micrographs of NIH/3T3 cells at 20X after 3 days treatment for (a1) drug-free DVDS and (a2) DVDS; after 5 days treatment for (b1) drug-free DVDS and (b2) DVDS; after 7 days treatment for (c1) drug-free DVDS and (c2) DVDS; and after 7 days treatment for (d1) the negative control in cell culture media, (d2) the positive control using DMSO, (in all cases scale: 1 cm = 100 μm).

Figure 5.17 depicts the cellular viability of NIH/3T3 cells following treatment with extracts obtained from the mixture of the hormonal-loaded units for 4 weeks alongside IND-LPM for 2 weeks. Evaluation at 3 and 7 days post-treatment revealed that the mixture extract displayed average cell viability of more than 72% in day 3, which improved up to more than 82% in day 7. These results are suggestive of the non-toxic and cyto-compatible nature of the prepared MUPP variant two formulation.

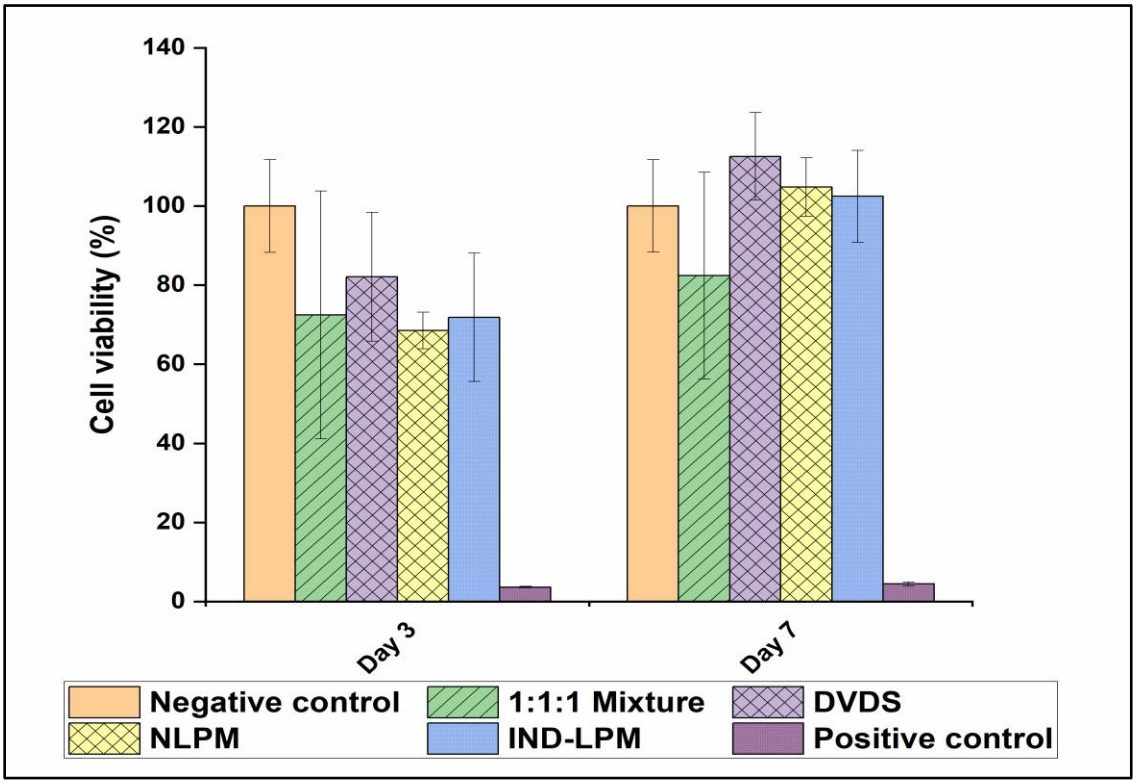

Figure 5.17: Cellular viability of NIH/3T3 by MTT assay in the presence of the (1:1:1) mixture of 4 Weeks extracts of (DVDS, NLPM, and IND-LPM); DVDS 4 Weeks extracts; NLPM 4 Weeks extracts; and IND-LPM 2 Weeks extracts.

5.4 Concluding remarks

In this chapter, a novel polymeric delivery system, formed as a donut-shaped tablet and loaded with E2, was successfully developed for vaginal administration as an estrogenic intervention in treating GSM. Utilizing factorial experimental design, the formulation was optimized through direct compression, with the compression force and polymer proportions being key factors influencing drug release kinetics, hardness, and weight loss profile. Notably, the cumulative drug release over 4 weeks for the optimal formulation was 5.84%±0.24 in SVF and the release kinetics of E2 were

best described by the Peppas-Sahlin model, suggesting a complex interplay between diffusion and polymer relaxation behaviors. Moreover, the fabricated optimal delivery system demonstrated excellent cytocompatibility, highlighting its potential as a biocompatible and implantable intravaginal device for GSM management. Evaluation of the MUPP variant two extracts further revealed a favorable biocompatibility with these promising findings position the developed system as a viable candidate for providing sustained release of NETA and IND in the uterine cavity and E2 within the vaginal cavity to address GSM and potentially other biomedical applications.

Traditionally, two dimensional (2D) cell culture systems (in flask) have dominated in *in vitro* studies, however, they often fail to mimic the complex three-dimensional (3D) microenvironments found within human tissues. This limitation has driven the evolution of 3D *in vitro* models, offering improved biomimicry and functionality, essential for evaluating drug delivery systems and therapeutic interventions. In this context, the next chapter explores the development and characterization of an engineered uterine-vaginal cellular model (EUVM). This model utilizes 3D bio-printing technology to construct cell-laden hydrogel structures that simulate the uterine and vaginal environments, providing a novel platform for biocompatibility studies.

CHAPTER 6

6 Engineered Uterine-Vaginal Cellular Model for *In Vitro* Biocompatibility Assessment

6.1 Introduction

Assessing the biocompatibility of a material stands as a crucial prerequisite for its acceptance, alongside the evaluation of its physical characteristics. Over recent years, the assessment of biomaterials and medical devices has seen a rise in global standardization, paralleling the release of ISO 10993, a standard dedicated to biomaterial and medical device testing. Biocompatibility assessments entail the examination of either the material itself or its extract, depending on the intended application. Typically, *in vitro* cell culture studies serve as the initial phase in biocompatibility assessment. Subsequent *in vivo* biological reactivity tests aim to elucidate the response of animals to materials or medical devices, whether through direct or indirect contact or via the administration of specific extracts derived from the material under examination (Hu et al. 2013).

In vitro safety studies serves as efficient and cost-effective alternatives for evaluating formulation safety profiles, circumventing the significant logistical and economical challenges often associated with *in vivo* animal studies (Kaur et al. 2011). Comparative studies have systematically examined the behavior of human cells in both two-dimensional (2D) and three-dimensional (3D) culture environments to assess their correlation with *in vivo* cellular behavior. Numerous studies have demonstrated the superiority of 3D models over 2D cultures in plastic flasks, although preclinical research remains predominantly employs monolayer cell cultures (Kimlin et al. 2013).

Research on the human uterine wall through *in vivo* studies remains limited, constrained by ethical and technical challenges (Kuperman et al. 2020). Nonetheless, a range of *in vitro* culture models have been developed to simulate the uterine endometrium's biological functions and responses. These models typically involve co-cultures composed of endometrial epithelial cells, smooth muscle cells, and endometrial stromal cells. They can be organized either in single layers on rigid substrates or within 3D scaffolds or gels. The primary objectives of these models include gaining insights into various biological aspects of uterine development and remodeling, inter-cellular interactions, cancer invasion mechanisms, as well as the expression of genes and hormones involved in uterine physiology and pathology (Kuperman et al. 2020).

Extrusion-based 3D printing represents a widely utilized additive manufacturing techniques, attributed to its cost-effectiveness and broad material compatibility. This method involves the deposition of material, typically referred to as ink, which is loaded into a syringe and extruded through a nozzle under pneumatic or mechanical forces (Rastin et al. 2020, Tytgat et al. 2019). The spatial resolution of the resultant structures is governed by parameters such as nozzle diameter, deposition speed, and applied extrusion pressure (Tytgat et al. 2019). In addition, this technology enables the rapid construction of cell-laden structures by depositing cell-encapsulating hydrogels (bioink) in predetermined location through a layer-by-layer approach, thus offering precise control over geometry, architecture, and composition, facilitating the study of cellular interactions within 3D microenvironment and effectively addressing the constraints associated with conventional 2D cell culture systems (Kim et al. 2019, Lim et al. 2020, Ouyang et al. 2016, Rastin et al. 2020).

Hydrogels are polymeric materials extensively employed in tissue engineering due to their minimal cytotoxicity and their structural resemblance to the extracellular matrix (ECM). These materials can encapsulate therapeutic agents, cells, and bio-macromolecules (Chung et al. 2013, Tavakoli et al. 2019). Their highly hydrated network architecture facilitates gas exchange and nutrient diffusion, rendering them highly suitable for the development of bioinks (Chung et al. 2013). The bioink-forming material must meet several essential criteria, including biocompatibility, support for cell viability, and appropriate mechanical and rheological properties. While numerous biocompatible materials have been investigated as potential bioinks, only a limited number, such as alginate (Alg) and gelatin (GEL), have been successfully optimized for use in 3D bioprinting (Lim et al. 2020). Furthermore, the blending of hydrogels offers a promising strategy to combine the distinct properties of individual components, enabling the customization of the hydrogel to meet specific requirements (Chung et al. 2013).

Gelatin derived by the partial hydrolysis of collagen, is extensively employed in tissue engineering, wound healing, and various surgical applications due to its favorable properties (Chung et al. 2013, Tytgat et al. 2019). This bioresorbable polymer is cost-effective, FDA approved, and can be enzymatically degraded. Above its gelation temperature, GEL exhibits a sol-like state, transitioning into a gel-like hydrogel upon cooling, driven by the formation of conformational cross-bonds (Panouillé and Larreta-Garde 2009). This simple thermo-reversible crosslinking mechanism has led to its widespread use as a fundamental component in cell printing technologies for over a decade (Imani et al. 2012, Yan et al. 2005, Yao et al. 2009, Zehnder et al. 2015). However, the inherent reversibility of thermal crosslinking limits the stability of GEL under

physiological conditions, necessitating chemical crosslinking to ensure structural integrity at body temperature (Tytgat et al. 2019).

Alginate, a polymer derived from brown algae, is extensively utilized in tissue engineering as a matrix material as well as in controlled drug delivery systems (Augst et al. 2006). The gelation of Alg is rapidly induced by its interaction with divalent cations, resulting in a stable gel that demonstrates superior structural integrity under physiological conditions compared to thermally cross-linked GEL (Jeon et al. 2012). The combination of GEL and Alg in bioink formulations combines the thermo-responsive properties of GEL with the rapid ionic crosslinking capability of Alg, ensuring long-term structural stability in culture environments (Ouyang et al. 2015, Zhao et al. 2014), This GEL/Alg composite bioink is widely adopted in cell printing practices due to its synergistic properties (Chung et al. 2013, Liu et al. 2011, Zehnder et al. 2015).

The primary aim of this chapter is to develop an engineered uterine-vaginal cellular model (EUVM) that emulates the anatomical architecture observed *in vivo*. This model is constructed using a polylactic acid-based custom architecture (PLA-CA), designed with two distinct chambers that simulate the uterine and vaginal cavities. These chambers provide a suitable substrate onto which a bioink composed of GEL/Alg/Cells can be precisely extruded. This engineered model has been purposefully invented to facilitate the biocompatibility assessment of the prepared dual-compartment MUPP (Variant two). Moreover, the structural and functional attributes of the PLA-CA design offer substantial versatility, rendering this innovative model highly adaptable for a wide range of physiological and mechanobiological investigations. This versatility enables in-depth exploration of cellular behavior, tissue interactions, and material properties under controlled conditions, closely resembling the *in vivo* environment, and serves as a valuable platform for advancing research in tissue engineering and regenerative medicine.

6.2 Materials and Methods

6.2.1 Materials

Gelatin type A from porcine skin and alginate sodium chloride were purchased from (Sigma-Aldrich, USA). Calcium chloride were purchased from (Rochelle Chemicals, SA). NIH/3T3 mouse fibroblast cells (ATCC CRL-1658) were obtained from the ATCC (American Type Culture Collection, Manassas, VA, USA), Dulbecco's Modified Eagle Medium (DMEM) from Life Technologies Limited “Gibco” (Paisley, UK), Fetal bovine serum (FBS) from PAN Biotech (Aidenbach, Germany), and MTT solution and solubilizing buffer from Roche Diagnostic GmbH

(Mannheim, Germany). All other chemicals were of analytical grade and used without further purification.

6.2.2 Methods

6.2.2.1 Overview of the engineered uterine-vaginal cellular model (EUVM)

For this study, a cellular model simulating the anatomy of the uterine/vaginal environment was engineered. The model was NIH/3T3-embeded GEL/Alg hydrogel laden PLA-based custom-designed construct (Figure 6.1). The rectangular model features two distinct chambers, each enclosed by double walls with an interstitial cavity. The structure is equipped with apertures at the top and bottom, as well as between the chambers, to facilitate nutrient supplementation and fluid circulation and exchange. In addition to the inter-chamber openings, the double-walled architecture with an intervening cavity likely serve to mimic physiological conditions by allowing controlled flow and diffusion of nutrients and other factors throughout the model. The inner length, width, and high were respectively as 30 mm, 30 mm, and 10 mm of the vaginal chamber and as 37 mm, 30 mm, and 10 mm of the uterine chamber, while the area available for the extruded GEL/Alg/cells bioink in the vaginal and uterine chambers were 3000 mm^2 and 3560 mm^2, respectively. This setup was suitable for *in vitro* studies focused on drug delivery and toxicity assessment, providing a controlled and reproducible environment for the exploration of various biological processes.

6.2.2.2 Design and printing of the PLA-based custom-designed architecture (PLA-CA)

The 3D printed PLA-CA was designed using Autodesk Tinkercad, a 3D computer-aided design (CAD) software (Figure 6.1). The design was generated and exported as a Stereolithography (STL) file, which was then imported into EnvisionTEC Perfactory RP Software and thereafter sliced and converted to a Borland Package Library (BPL) file. The PLA-CA was printed using an EnvisionTEC® 3D Bioplotter (EnvisionTEC® GmbH, Gladbeck, Germany) equipped with both high- and low-temperature printing heads. PLA filament was cut into small pieces and then introduced into the high-temperature print head, which was heated to 230 °C and allowed to equilibrate for 20 min prior to printing. The structure was printed with a needle tip diameter of 0.7 mm, under a pressure of 4 bar, at a printing speed of 20 mm/s. Pre-flow and post-flow timings, as well as the time between layers, were set to 0 seconds to ensure precise layer deposition according to the design specifications (Figure 6.2).

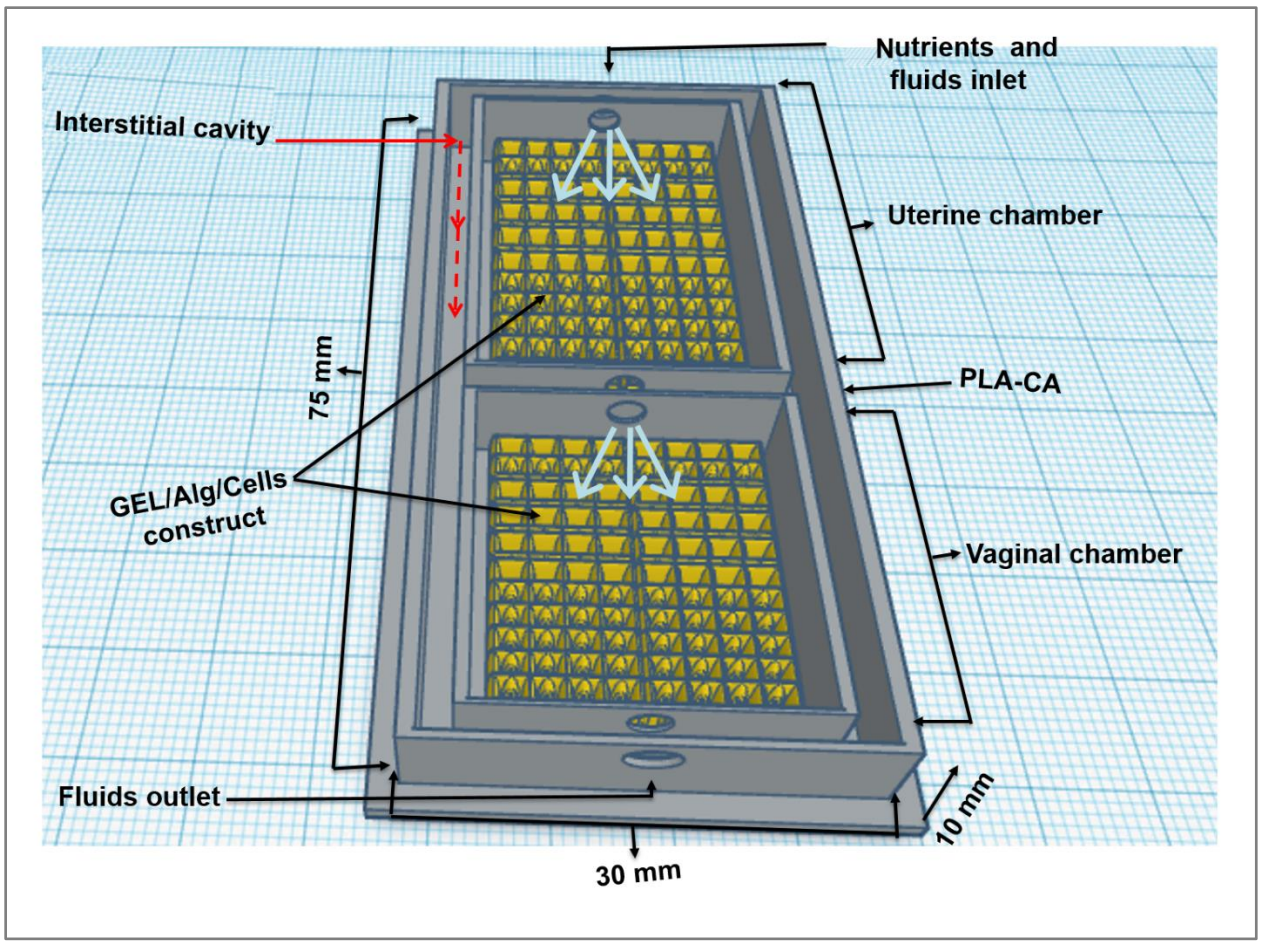

Figure 6.1: Computer-aided design specifications of the 3D printed PLA-CA.

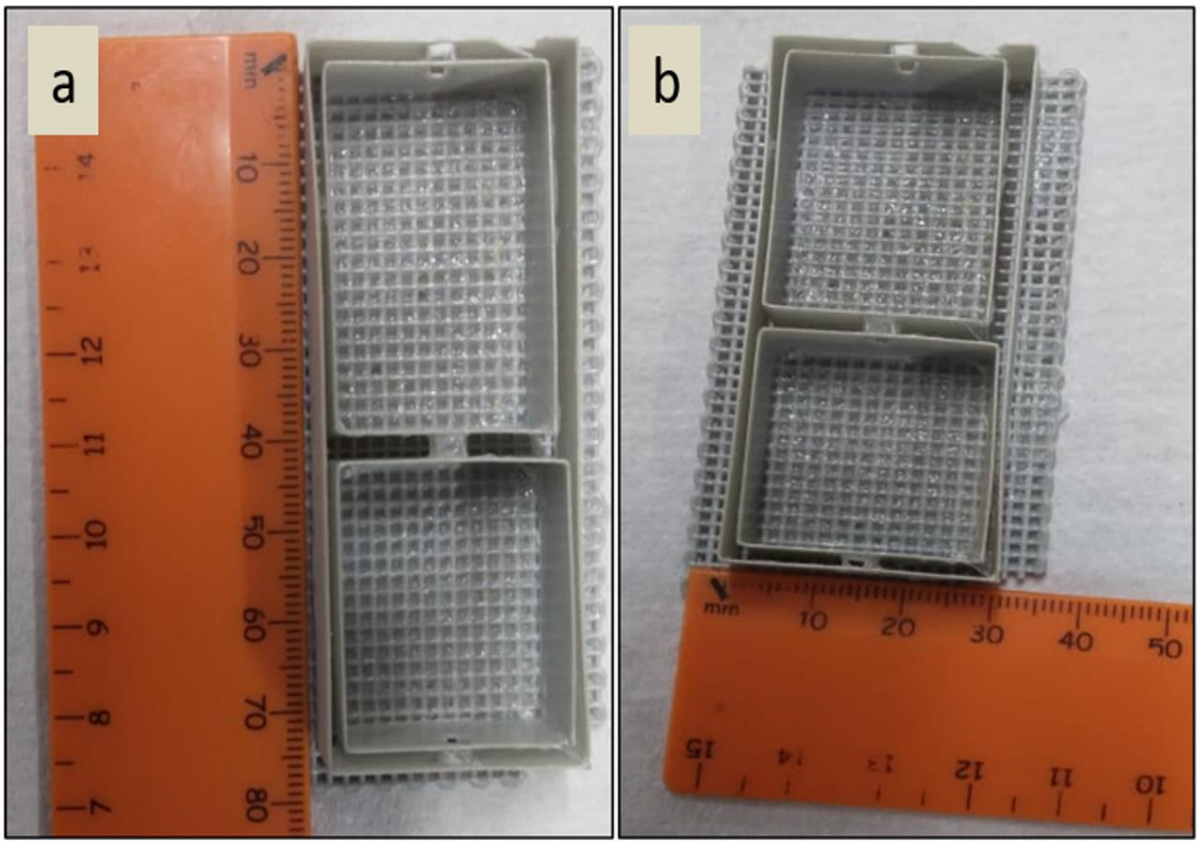

Figure 6.2: Digital images of the 3D printed PLA-CA (a) and (b).

6.2.2.3 Cell culture

NIH/3T3 mouse fibroblast cells (ATCC CRL-1658) were cultured in DMEM supplemented with 10% FBS and 1% penicillin/streptomycin. The cells were maintained in a humidified incubator at 37°C with 5% CO_2, with the culture medium being refreshed every 2 days. Upon reaching approximately 90% confluence in the T-flask, the adherent cells were detached, re-suspended in fresh culture medium, and centrifuged at 1500 rpm for 5 min to remove the culture medium.

6.2.2.4 Bioink preparation

The bioink formulation was developed using a GEL/Alg hydrogel mixture, selected based on its rapid gelation and cytocompatibility (Yao et al. 2012). Gelatin and Alg powders were each dissolved in a 0.5% (w/v) sodium chloride solution to generate stock bioink solutions. Sterilization was achieved by subjecting the solutions to a heating protocol of 70°C for 30 minutes, repeated over three cycles, and subsequently stored at 4°C until further use. Prior to bioink preparation, the solutions were incubated at 37°C for 30 minutes to facilitate the mixing processing. The GEL and Alg solutions were then mixed to achieve a final volume of 30 mL, with concentrations of 5%

(w/v) GEL and 1% (w/v) Alg. Subsequently, 3 mL with a density of a 1.5×10^6 cell suspension was added into the GEL/Alg solution, and the mixture was gently mixed to ensure uniform distribution of the cells. The resulting bioink was allowed to undergo gelation at 4°C for 5 minutes before being extruded for subsequent applications (Ouyang et al. 2016). All the bioink preparation processing was performed under aseptic conditions in a Class II biological safety cabinet.

6.2.2.5 Bioink extrusion process

An extrusion-based technique was employed to fabricate cell-laden constructs featuring interconnected channels, which promote efficient diffusion of oxygen and nutrients. The bioink was extruded through a sterile 21G stainless steel needle connected to a 10 mL sterile plastic syringe. The extrusion process was conducted at ambient temperature (22°C) to promote immediate GEL crosslinking and the structural formation of the 3D constructs. A six-layered grid constructs were built up with manual pressure extrusion flux through the stainless steel needle. Post-extrusion, the cell-laden constructs were immersed in a 4% calcium chloride solution for 3 minutes to induce Alg crosslinking, followed by three washes with PBS. The constructs were subsequently cultured in DMEM, with medium changes occurring every 48 hours to maintain optimal culture conditions (Ouyang et al. 2016). Thereafter, the GEL/Alg/cells constructs were integrated into the uterine and vaginal chambers of the PLA-CA to assemble the EUVM. Prior to use, the PLA-CA and all related apparatus were disinfected using a 70% (w/v) ethanol solution to ensure aseptic conditions and minimize the risk of contamination.

6.2.2.6 Cell viability assay

The EUVM was employed to evaluate the cytotoxicity induced by drug-loaded formulations. The experimental setup included the exposure of models to the optimal MUPP Variant two (n=3), DMSO as a toxic control (n=3), and an untreated control group. Figure 6.2 represents the schematic description of the treatment protocol. Prior to the study, the MUPP were sterilized by exposure to UV light for 5 minutes, followed by immersion in a 70% ethanol solution for 15 seconds, and subsequent air drying in a laminar flow hood for 24 hours. Pre-warmed cell culture medium (5 ml) was added to the MUPP and allowed to equilibrate overnight in a humidified, 37°C, and 5% CO_2 incubator. The following day, the MUPP were gently placed into the apical surface of the EUVM, NLPM and DVDS were placed into uterine and vaginal chamber, respectively, as illustrated in Figure 6.3. To assess cellular viability post-treatment, the models were subjected to the MTT assay on day 3. The treated and untreated samples were incubated with MTT reagent (0.5 g/ml) for 4 hours to facilitate the formation of formazan crystals. Subsequently, an MTT solubilizing buffer was added to dissolve the formazan crystals (Tavakoli et al. 2019). A volume

of 100 µl from each sample was transferred to a 96-well plate. The optical absorbance was measured using a VICTOR™ X3 Multilabel Plate Reader (PerkinElmer, USA) at a wavelength of 570 nm, with 690 nm used as the background reference. The cells viability of the treated model was determined by normalizing absorbance values of the treated samples to that of the untreated controls, and the data were expressed as a percentage of cell viability.

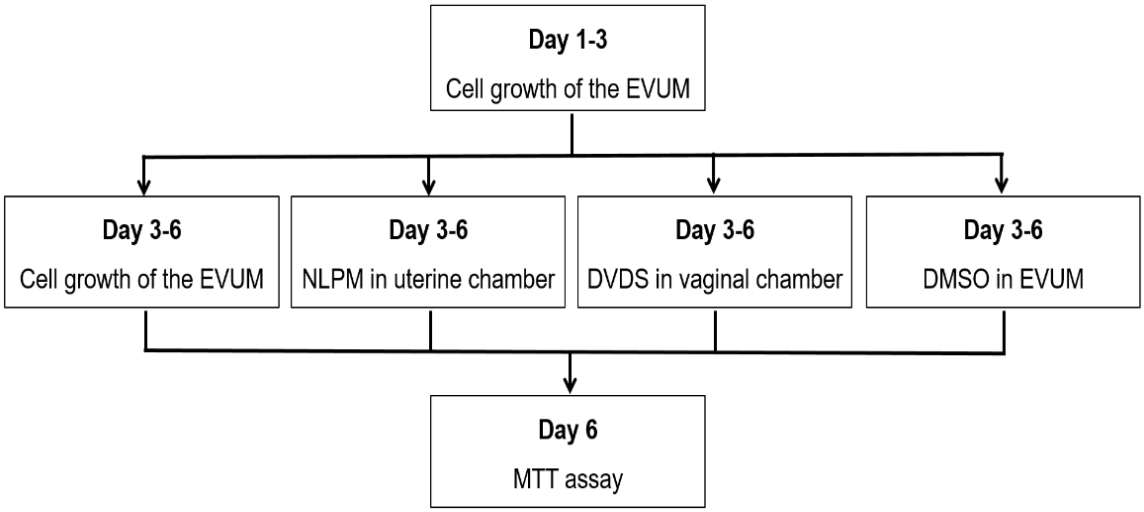

Figure 6.3: Schematic illustration of the *in vitro* treatment protocol.

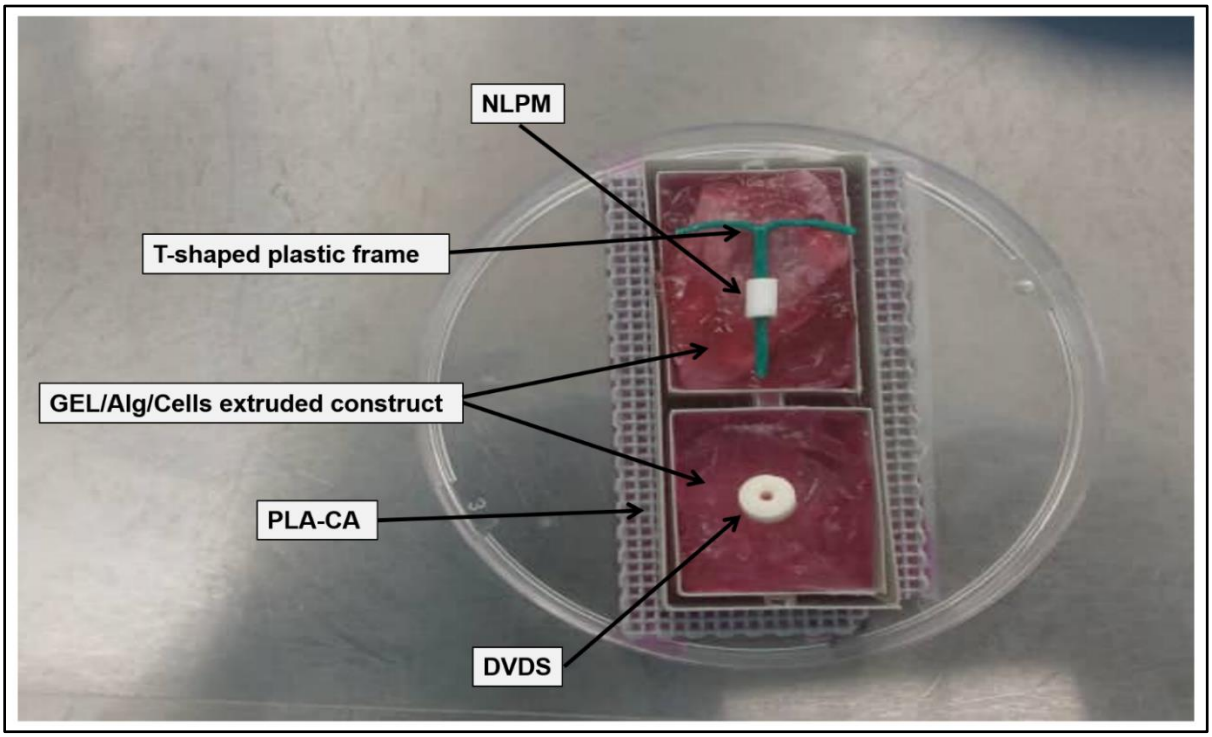

Figure 6.4: Digital image of the EUVM treated with MUPP.

6.2.3 Statistical analysis

All results were expressed as the mean ± SD. Statistical analyses were conducted using SPSS software as detailed in Chapter 3, Section 3.2.4.

6.3 Results and discussion

The PLA-CA were successfully fabricated via 3D printing technique as depicted in Figure 6.1. The fabrication process resulted in a construct with uniform and smooth surfaces and characterized by average dimensions designated in the CAD model which are 30 mm, 30 mm width and 10 mm high for both chambers as well as 30 and 37 mm of length for vaginal and uterine chamber, respectively. On the other hand, the obtained GEL/Alg/Cells constructs resulted from the manual extrusion-based technique are characterized by rough surfaces morphology, with a dimensions fitting the available surface area of the PLA-CA chambers as seen in Figure 6.3.

The extrusion of viscous bioinks, in conjunction with the post-extrusion solidification processes, presents significant challenge for ensuring the successful deposition of living cells while preserving their viability. This challenge arises by the need to maintain cellular viability while ensuring that the bioink undergoes proper gelation. Additionally, the time-dependent rheological properties of GEL/Alg mixtures further complicate the process, as prolonged holding times are associated with increased cell death. Although rapid processing can mitigate some of these effects, it is critical to establish an acceptable minimum threshold for cell viability over the entire fabrication period, taking into account the time-sensitive behavior of the bioink (Ouyang et al. 2016). In this study, a 30-minute time window was designated for the entire fabrication process to optimize the balance between bioink gelation and cellular viability. Figure 6.4a presents the outcomes of an *in vitro* cellular viability assay conducted over a 3-day period. Both MUPP units, NLPM and DVDS, demonstrated an average cell viability exceeding 70% relative to the negative control, indicating the non-toxic and cyto-compatible nature of the MUPP units developed in this study (Arany et al. 2021). Representative photomicrographs taken on Day 3 post-treatment, displayed in Figure 6.4b, 6.4c, and 6.4d, depict the morphological features of the negative control, as well as the NLPM and DVDS-treated GEL/Alg/Cells constructs for both the uterine and vaginal chambers. These images reveal a smooth surface morphology, further substantiates the cytocompatibility and non-cytotoxic profile of the optimized MUPP variant one.

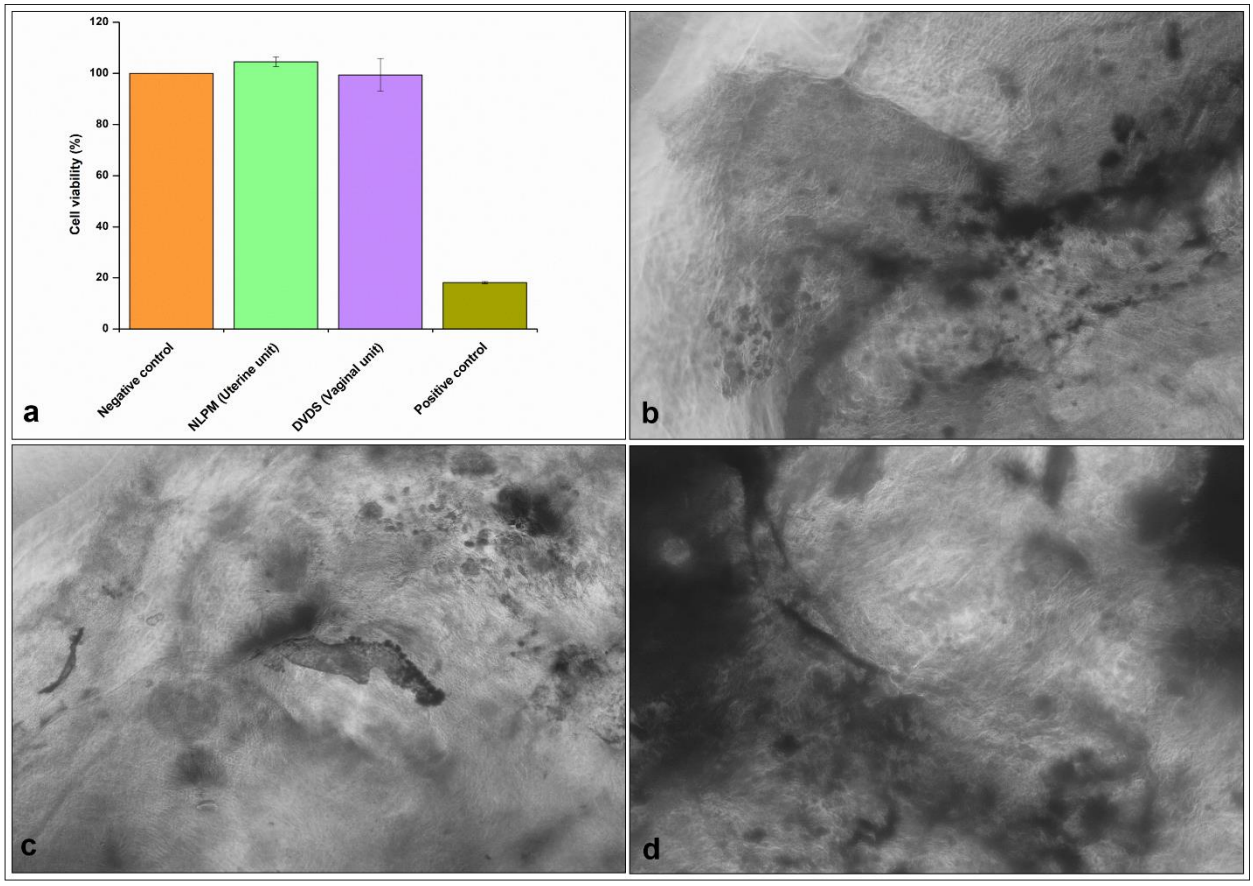

Figure 6.5: (a) Cell viability by MTT assay in the presence of the optimal MUPP variant two, NLPM in the uterine chamber and DVDS in the vaginal chamber, and surface morphology of the GEL/Alg/Cells extruded construct after 3-days treatment for (b) negative control, (c) uterine chamber or NLPM treated, and (d) vaginal chamber or DVDS treated (in all cases scale: 1 cm = 50 µm).

6.4 Concluding remarks

This chapter has successfully established an EUVM that effectively emulate the anatomical and functional aspects of the uterine and vaginal environments *in vitro*. By utilizing a 3D-printed PLA-CA and a bioink comprising GEL, Alg, and NIH/3T3 mouse fibroblast cells, the EUVM demonstrates substantial utility as a platform for biocompatibility assessments. The model displayed an average cell viability exceeding 70% after three days of treatment, indicating the non-cytotoxic and cytocompatible nature of the MUPP variant two. The smooth surface morphology of the GEL/Alg/Cells constructs further validated the structural integrity and biocompatibility of the system. The EUVM provides a novel and efficient alternative to traditional 2D culture methods, offering improved biomimetic characteristics, including more accurate simulations of *in vivo* tissue architecture and cellular microenvironments. By incorporating cell-

laden hydrogels and precision 3D printing technology, this platform addresses key limitations associated with conventional cell culture systems, particularly for the evaluation of drug delivery systems. This innovative approach provides controlled and reproducible conditions for examining tissue-biomaterial interactions and offers a versatile tool for a wide range of tissue engineering and regenerative medicine applications.

In term of future prospects, the model's ability to mimic *in vivo* physiological conditions can be enhanced by incorporating a perfusion system to simulate the natural secretion of uterine and vaginal fluids, as well as fluid exchange within the uterine and vaginal chambers. Applying this strategy permits for more accurate assessments of drug delivery interactions with the mucosal tissues. In addition, expanding the scope of the model to include assessments of inflammatory responses is crucial. Measuring cytokine release and other biomarkers of inflammation will provide insight into the model's ability to predict inflammatory responses in mucosal tissues. This would be especially valuable in preclinical testing of delivery systems designed for use in the reproductive system. Furthermore, Investigating long-term cell viability and differentiation within the EUVM will facilitate optimize the model for various applications, such as testing the sustained effects of drugs over and extended period of time. Also, future research could explore the integration of multiple cell types, including epithelial, stromal, and smooth muscle cells, to more closely emulate the complex tissue structure of the uterus and vagina. Constructing multi-layered tissue models with distinct cellular compositions would improve the model applicability in studies related to efficacy and cyto-toxcicity of delivery systems, tissue development, and disease modeling. Moreover, using advanced imaging and analytical techniques such as live-cell microscopy and biomechanical testing will provide deeper insights into cellular behavior and material properties within the EUVM. This will further elucidate the effects of therapeutic interventions on tissue architecture and function.

CHAPTER 7

7 CONCLUSIONS AND RECOMMENDATIONS

7.1 Conclusions

The landscape of drug delivery is rapidly evolving, prompting numerous advances that enhance the safety, effectiveness, and patient acceptance of contemporary drug therapies. Over time, various innovative modalities of drug administration have emerged and undergone improvement. Nevertheless, a growing trend of the global drug delivery market is dedicated to enhancing the performance of drugs administered via the genitourinary tract routes. Vaginal and uterine drug delivery offers benefits in terms of bypassing the first hepatic effect and offering viable routes for *in-situ* drug delivery, with associated limitations mainly related to patient acceptability, which can be readily addressable. Moreover, while the physiology of the genitourinary tract varies among individuals and according to factors such as age and menstrual cycle, the distinctive characteristics of the genitourinary tract presents opportunities for targeted and long-term site-specific drug delivery. This can be achieved by employing polymers capable of degradation in the surrounding environment.

Patient compliance represents a substantial challenge in the effective management of various diseases, including GSM. Poor compliance with conventional drug delivery systems is often identified as a primary reason for low patient adherence with treatment regimens. The complexity of dosing schedules represented in multiple doses administered at different times and limitations associated with these delivery systems such as messiness and leakage, and invasive insertion procedures pose significant barriers to standard treatment regimens, making it difficult for patients, and eventually compromising therapeutic outcomes.

The current thesis endeavored to a MUPP to address the limitations of current delivery systems for treating the GSM and enhance patient compliance through extended and site-specific delivery of multiple drugs in a controlled manner. The MUPP was designed in two configurations, each comprising three units. The first design involved an IUD consisting of three intrauterine units composed of PCL and EC for E2- and NETA-loaded units, alongside PCL and PEG for the unit loaded with IND. The second design was formulated as a combined device comprising NETA- and IND-loaded intrauterine units and an E2-loaded donut-shaped intravaginal unit. The development of the MUPP followed a logical step-wise approach, with each unit being developed and optimized separately following comprehensive preliminary studies that identified the

appropriate method, drug load, and polymer blends ratio necessary to attain the desired properties.

Extensive *in vitro* analysis led to the identification of formulation variables for the respective intrauterine and intravaginal units which comprised the MUPP. A 2^2 factorial design was employed to generate 7 formulations for each of NLPM, IND-LPM, and DVDS, while the rotatable central composite design was employed to generate 14 formulations for EPHCD. The influences of formulations and processes variables on the key attributes of the formulations were evaluated and subsequently the optimal formulations closely met the desired prolonged release and low weight loss profiles for each unit were identified. Thereafter, the optimal formulations underwent further *in vitro* analysis to determine their hydration capacity, structural integrity, *ex vivo* permeation, and release kinetics analysis as well as an extensive cytocompatibility studies using 2D cell cultures.

After individual optimization and evaluation of the optimal formulations, the units were assembled to form the two configurations of the MUPP. Subsequent *in vitro* assessments demonstrated the system's ability to deliver drugs in a sustained and prolonged manner alongside favorable physicomechanical attributes with maximum release expected to be after 22 weeks for variant one (both NETA and E2), increasing to 140 weeks for E2 through variant two.

The successful incorporation of two hormonal drugs and an analgesic anti-inflammatory drug, each with distinct properties, within the system underscores its adaptability. Through adjustments and optimization to the formulation and processing parameters, the system achieved the desired properties, highlighting its versatility.

Without loss of generality, the MUPP exhibited the capacity to address many limitations inherent in current delivery systems used for treating GSM. Moreover, its capability for site-specific sustained delivery of multiple drugs within a single platform holds potential for augmenting treatment and therapeutic outcomes.

To this end, the overall aim was achieved, as evidenced by the successful development and optimization of the MUPP, the demonstration of its sustained release capabilities, and its favorable physicochemical and biocompatibility profiles. Moreover, this study effectively addressed the limitations of current delivery systems, offering a promising platform for the effective management of GSM.

7.2 Limitations and Recommendations

The undertaken research has identified a few limitations which may be considered for future research. These include the composition and volume of the SUF and SVF used for drug release and weight loss assessments, which may not precisely mimic the complexity and protein content of real fluids, which contains multiple proteins such as γ-globulin and hemoglobin. Additionally, the presence of proteins in the release medium could serve as a nutritional source for microorganisms, potentially leading to bio-fouling of the prepared platform and influencing the release and weight loss profiles. Furthermore, the stability of prepared platform over a prolonged period of time under different environmental conditions, including storage, was not undertaken in this research. Nevertheless, further investigations to assess the performance of the optimal formulations under varying conditions, including alterations in simulated uterine and vaginal fluids compositions through the use of more biorelevant media, volume, pH values, and agitation speeds, in addition to stability studies over time could offer valuable insights into the broader applicability and robustness of the findings presented in the current research.

Following the successful evaluation of the developed MUPP and its constituent units through a comprehensive array of *in vitro*, *ex vivo*, and cyto-compatibility assessments outlined in this thesis, it is recommended to conduct further cyto-compatibility studies employing cell lines derived from the genitourinary tract to deepen our understanding of regional-specific responses. Additionally, further analyzes are recommended to ascertain the drugs' release kinetics, mechanical attributes, safety profile, and overall efficacy of the MUPP in animal models and subsequently in human subjects. Additionally, liquid chromatographic methods, such as through High-performance liquid chromatography, can be developed to separate and individually quantify the drug molecules used in the preparation of the MUPP.

For comparative purposes, analyzing currently marketed formulations for treating the GSM, using similar techniques would enable the identification of superior products in terms of drug release, textural properties, and cytocompatibility.

Furthermore, the system developed herein holds potential for application with various bio-actives, particularly those necessitating controlled sustained release over extended durations, bio-actives required for systemic effects while circumventing the gastrointestinal milieu and hepatic first-pass effect. These potential applications include, but are not limited to, utilization of the MUPP platform for long-term hormonal replacement therapy, employment of the platform to deliver hormones at concentrations within the contraceptive window, delivering of E2 into the uterine cavity with aim of addressing the uterine adhesions, employment of the vaginal unit of the platform to deliver

antifungal and antibacterial agents, as well as for personal hygiene purposes, and adapting the optimal polymer blend matrix for use in other anatomical sites requiring biodegradation and prolonged drug delivery.

Regarding scale-up considerations, further pre-formulation studies for intravaginal unit components are recommended to determine starting material attributes such as particle size distribution, densities, and flowability properties, which are critical for die filling and achieving final device characteristics such as weight and content uniformity. Additionally, there is a need to establish industrial-scale fabrication processes for the intrauterine units. This approach would involve the production of large "long" hollow cylinders, which can then be trimmed to the required sizes, obviating the need for individual unit fabrication.

REFERENCES

Abbaspoor S, Ashrafi A, Salehi M. 2018. Synthesis and characterization of ethyl cellulose micro/nanocapsules using solvent evaporation method. Colloid and Polymer Science 296: 1509-1514.

Abdelgader A, Govender M, Kumar P, Choonara YE. 2023. Intravaginal Drug Delivery Systems to Treat the Genitourinary Syndrome of Menopause: Towards the Design of Safe and Efficacious Estrogen-Loaded Prototypes. Journal of Pharmaceutical Sciences 112: 1566-1585.

Abdelgader A, Govender M, Kumar P, Choonara YE. 2024. A Novel Intrauterine Device for the Spatio-Temporal Release of Norethindrone Acetate as a Counter-Estrogenic Intervention in the Genitourinary Syndrome of Menopause. Pharmaceutics 16: 587.

Abdelrazek E, Hezma A, El-Khodary A, Elzayat A. 2016. Spectroscopic studies and thermal properties of PCL/PMMA biopolymer blend. Egyptian Journal of basic and applied sciences 3: 10-15.

Abidin IZ, Rezoagli E, Simonassi-Paiva B, Fehrenbach GW, Masterson K, Pogue R, Cao Z, Rowan N, Murphy EJ, Major I. 2020. A bilayer vaginal tablet for the localized delivery of disulfiram and 5-fluorouracil to the cervix. Pharmaceutics 12: 1185.

Abilova GK, Kaldybekov DB, Irmukhametova GS, Kazybayeva DS, Iskakbayeva ZA, Kudaibergenov SE, Khutoryanskiy VV. 2020. Chitosan/poly (2-ethyl-2-oxazoline) films with ciprofloxacin for application in vaginal drug delivery. Materials 13: 1709.

Abramowicz M, Zuccotti G, Pflomm J-M. 2019. Imvexxy-Another Estradiol Vaginal Insert for Dyspareunia (Reprinted from Medical Letter on Drugs and Therapeutics, vol 60, pg 147-148, 2018). JAMA-JOURNAL OF THE AMERICAN MEDICAL ASSOCIATION 321: 506-507.

Acharya G, Lee CH, Lee Y. 2012. Optimization of cardiovascular stent against restenosis: factorial design-based statistical analysis of polymer coating conditions.

Águas F, Pargana L, Faustino F, Matos A, Filipe T, da Silva DP. 2020. Satisfaction on the use of a transdermal spray containing 1.53 mg estradiol for the treatment of symptoms associated with menopause. Gynecological and Reproductive Endocrinology and Metabolism 1: 248-253.

Ahmed MM, Fatima F, Anwer MK, Ansari MJ, Das SS, Alshahrani SM. 2020. Development and characterization of ethyl cellulose nanosponges for sustained release of brigatinib for the treatment of non-small cell lung cancer. Journal of Polymer Engineering 40: 823-832.

Ahmed RK, Saad EM, Fahmy HM, El Nashar RM. 2022. Multivariate experimental design: towards more reliable electrochemical detection. Current Opinion in Electrochemistry 31: 100880.

Ainurofiq A, Choiri S. 2015. Drug release model and kinetics of natural polymers-based sustained release tablet. Lat. Am. J. Pharm 34: 1328-1337.

Al-Azzawi, Buckler H. 2003. Comparison of a novel vaginal ring delivering estradiol acetate versus oral estradiol for relief of vasomotor menopausal symptoms. Climacteric 6: 118-127.

Al-Azzawi, Lees B, Thompson J, Stevenson JC. 2005. Bone mineral density in postmenopausal women treated with a vaginal ring delivering systemic doses of estradiol acetate. Menopause 12: 331-339.

Al-Baghdadi O, Ewies A. 2009. Topical estrogen therapy in the management of postmenopausal vaginal atrophy: an up-to-date overview. Climacteric 12: 91-105.

Al-Nimry SS, Altaani BM, Haddad RH. 2019. RP-HPLC method for determination of norethindrone in dissolution media and application to study release from a controlled release nanoparticulate liquid medicated formulation. Journal of Applied Pharmaceutical Science 9: 079-086.

Albertini B, Passerini N, Di Sabatino M, Vitali B, Brigidi P, Rodriguez L. 2009. Polymer–lipid based mucoadhesive microspheres prepared by spray-congealing for the vaginal delivery of econazole nitrate. European journal of pharmaceutical sciences 36: 591-601.

Amini MM, Di Martino A, Šopík T, Fei H, Císař J, Pummerová M, Sedlařík V. 2021. Polylactide/polyvinylalcohol-based porous bioscaffold loaded with gentamicin for wound dressing applications. Polymers 13: 921.

Angelou K, Grigoriadis T, Diakosavvas M, Zacharakis D, Athanasiou S. 2020. The genitourinary syndrome of menopause: an overview of the recent data. Cureus 12.

Annuryanti F, Domínguez-Robles J, Anjani QK, Adrianto MF, Larrañeta E, Thakur RRS. 2023. Fabrication and Characterisation of 3D-Printed Triamcinolone Acetonide-Loaded Polycaprolactone-Based Ocular Implants. Pharmaceutics 15: 243.

Antoniou G, Kalogirou D, Karakitsos P, Antoniou D, Kalogirou O, Giannikos L. 1997. Transdermal estrogen with a levonorgestrel-releasing intrauterine device for climacteric complaints versus estradiol-releasing vaginal ring with a vaginal progesterone suppository: clinical and endometrial responses. Maturitas 26: 103-111.

Arany P, Papp I, Zichar M, Regdon Jr G, Béres M, Szalóki M, Kovács R, Fehér P, Ujhelyi Z, Vecsernyés M. 2021. Manufacturing and examination of vaginal drug delivery system by FDM 3D printing. Pharmaceutics 13: 1714.

Archer DF, Kimble TD, Lin FY, Battucci S, Sniukiene V, Liu JH. 2018. A randomized, multicenter, double-blind, study to evaluate the safety and efficacy of estradiol vaginal cream 0.003% in postmenopausal women with vaginal dryness as the most bothersome symptom. Journal of Women's Health 27: 231-237.

Archer DF, Constantine GD, Simon JA, Kushner H, Mayer P, Bernick B, Graham S, Mirkin S. 2017. TX-004HR vaginal estradiol has negligible to very low systemic absorption of estradiol. Menopause (New York, NY) 24: 510.

Asvadi NH, Dang NT, Davis-Poynter N, Coombes AG. 2013a. Evaluation of microporous polycaprolactone matrices for controlled delivery of antiviral microbicides to the female genital tract. Journal of Materials Science: Materials in Medicine 24: 2719-2727.

Augst AD, Kong HJ, Mooney DJ. 2006. Alginate hydrogels as biomaterials. Macromolecular bioscience 6: 623-633.

Ayton RA, Darling GM, Murkies AL, Farrell EA, Weisberg E, Selinus I, Fraser IS. 1996. A comparative study of low dose oestradiol safety and efficacy of continuous released from a vaginal ring compared with conjugated equine oestrogen vaginal cream in the treatment of postmenopausal urogenital atrophy. British Journal of Obstetrics and Gynaecology 103: 351-358.

Azhdari E, Emami A, Ferreira JA. 2020. Drug release from a surface erosion biodegradable viscoelastic polymeric platform: Analysis and numerical simulation. Computers & Mathematics with Applications 80: 3004-3026.

Bachmann GA. 1998. The clinical platform for the 17β-estradiol vaginal releasing ring. American Journal of Obstetrics and Gynecology 178: 257-260.

Ballagh SA. 2004. Vaginal rings for menopausal symptom relief. Drugs & aging 21: 757-766.

Bansal SS, Vadhanam MV, Gupta RC. 2011. Development and *in vitro-in vivo* evaluation of polymeric implants for continuous systemic delivery of curcumin. Pharmaceutical research 28: 1121-1130.

Bao Q, Zou Y, Wang Y, Choi S, Burgess DJ. 2020. Impact of product design parameters on *in vitro* release from intrauterine systems. International journal of pharmaceutics 578: 119135.

Barentsen R, Weijer PHMvd, Schram JHN. 1997. Continuous low dose estradiol released from a vaginal ring versus estriol vaginal cream for urogenital atrophy. European Journal of Obstetrics & Gynecology and Reproductive Biology 71: 73-80.

Barmpalexis P, Kanaze FI, Kachrimanis K, Georgarakis E. 2010. Artificial neural networks in the optimization of a nimodipine controlled release tablet formulation. European journal of pharmaceutics and biopharmaceutics 74: 316-323.

Bartnikowski M, Dargaville TR, Ivanovski S, Hutmacher DW. 2019. Degradation mechanisms of polycaprolactone in the context of chemistry, geometry and environment. Progress in Polymer Science 96: 1-20.

Bassand C, Benabed L, Charlon S, Verin J, Freitag J, Siepmann F, Soulestin J, Siepmann J. 2023. 3D printed PLGA implants: APF DDM vs. FDM. Journal of controlled release 353: 864-874.

Beikzadeh S, Hosseini SM, Mofid V, Ramezani S, Ghorbani M, Ehsani A, Mortazavian AM. 2021. Electrospun ethyl cellulose/poly caprolactone/gelatin nanofibers: The investigation of mechanical, antioxidant, and antifungal properties for food packaging. International journal of biological macromolecules 191: 457-464.

Bendicho-Lavilla C, Rodríguez-Pombo L, Januskaite P, Rial C, Alvarez-Lorenzo C, Basit AW, Goyanes A. 2024. Ensuring the quality of 3D printed medicines: Integrating a balance into a pharmaceutical printer for in-line uniformity of mass testing. Journal of Drug Delivery Science and Technology 92: 105337.

Bernkop-Schnürch A, Hornof M. 2003. Intravaginal drug delivery systems. American journal of drug delivery 1: 241-254.

Bhat SR, Shivakumar H. 2010. Bioadhesive Controlled Release Clotrimazole Vaginal Tablets. Tropical Journal of Pharmaceutical Research 9: 339-346.

Boia R, Dias PA, Martins JM, Galindo-Romero C, Aires ID, Vidal-Sanz M, Agudo-Barriuso M, de Sousa HC, Ambrósio AF, Braga ME. 2019. Porous poly (ε-caprolactone) implants: A novel strategy for efficient intraocular drug delivery. Journal of controlled release 316: 331-348.

Boyd P, Variano B, Spence P, McCoy CF, Murphy DJ, Bashi YHD, Malcolm RK. 2019. *In vitro* release testing methods for drug-releasing vaginal rings. Journal of controlled release 313: 54-69.

Brunner H, Theodor RA. 2020. Multiple use applicator for vaginal tablets/vaginal inserts: compliance verification and suitability studies. BMC Women's Health 20: 1-9.

Buckler H, Al-Azzawi F, Group UVMT. 2003. The effect of a novel vaginal ring delivering oestradiol acetate on climacteric symptoms in postmenopausal women. BJOG: an international journal of obstetrics and gynaecology 110: 753-759.

Buster JE. 2009. Low-dose estradiol spray: a novel treatment for vasomotor instability in postmenopausal women. Women's Health 5: 23-28.

Calvo NL, Svetaz LA, Alvarez VA, Quiroga AD, Lamas MC, Leonardi D. 2019. Chitosan-hydroxypropyl methylcellulose tioconazole films: A promising alternative dosage form for the treatment of vaginal candidiasis. International journal of pharmaceutics 556: 181-191.

Carson L, Merkatz R, Martinelli E, Boyd P, Variano B, Sallent T, Malcolm RK. 2021. The vaginal microbiota, bacterial biofilms and polymeric drug-releasing vaginal rings. Pharmaceutics 13: 751.

Carter JE, Sluss PM. 2013. Estradiol solubility in aqueous systems: effect of ionic concentrations, pH, and organic solvents. Journal of Hormones 2013.

Casper F, Petri E, Group tVRS. 1999. Local Treatment of Urogenital Atrophy with an Estradiol-Releasing Vaginal Ring: A Comparative and a Placebo-Controlled Multicenter Study. International Urogynecology Journal 10: 171–176.

Caufriez A. 2007. Hormonal replacement therapy (HRT) in postmenopause: a reappraisal. Pages 241-250. Annales d'endocrinologie: Elsevier.

Chandran S, Asghar LF, Mantha N. 2008. Design and evaluation of ethyl cellulose based matrix tablets of ibuprofen with pH modulated release kinetics. Indian journal of pharmaceutical sciences 70: 596.

Chang H-I, Williamson M, Perrie Y, Coombes AG. 2005. Precipitation casting of drug-loaded microporous PCL matrices: incorporation of progesterone by co-dissolution. Journal of controlled release 106: 263-272.

Cheng L, Guo S, Wu W. 2009. Characterization and *in vitro* release of praziquantel from poly (ε-caprolactone) implants. International journal of pharmaceutics 377: 112-119.

Chism LA. 2012. Overcoming resistance and barriers to the use of local estrogen therapy for the treatment of vaginal atrophy. International journal of women's health 4: 551.

Chollet JA. 2011. Efficacy and safety of ultra-low-dose Vagifem (10 mcg). Patient preference and adherence 5: 571-574.

Chompootaweep S, Nunthapisud P, Trivijitsilp P, Sentrakul P, Dusitsin N. 1998. The use of two estrogen preparations (a combined contraceptive pill versus conjugated estrogen cream) intravaginally to treat urogenital symptoms in postmenopausal Thai women: a comparative study. Clinical Pharmacology & Therapeutics 64: 204-210.

Chung JH, Naficy S, Yue Z, Kapsa R, Quigley A, Moulton SE, Wallace GG. 2013. Bio-ink properties and printability for extrusion printing living cells. Biomaterials Science 1: 763-773.

Cicinelli E. 2008. Intravaginal oestrogen and progestin administration: advantages and disadvantages. Best Practice & Research Clinical Obstetrics & Gynaecology 22: 391-405.

ClinicalTrials.gov. To Study Generic Estradiol 10 mcg Vaginal Tablets in the Treatment of Vulvar and Vaginal Atrophy in Post Menopausal Women. (4-August 2022; https://clinicaltrials.gov/ct2/show/NCT02668796).

ClinicalTrials.gov. Study to Evaluate the Safety and Bioequivalence of Estradiol Vaginal Inserts, 10 mcg and Vagifem® 10 mcg and Compare to Placebo. (20. July 2022; https://clinicaltrials.gov/ct2/show/NCT01779947).

ClinicalTrials.gov. Study to Evaluate the Equivalence of Estradiol Vaginal Cream to Reference Standard in the Treatment of Vaginal Atrophy. (31-July 2022; https://clinicaltrials.gov/ct2/show/results/NCT03332303).

ClinicalTrials.gov. Study to Evaluate Equivalence of Estradiol Vaginal Cream 0.01% to Estrace® Cream 0.01% in Atrophic Vaginitis. (20-July 2022; https://clinicaltrials.gov/ct2/show/study/NCT03294538)

ClinicalTrials.gov. A Study Comparing Estradiol Vaginal Cream to Estrace® Cream in Females With Atrophic Vaginitis. (31-July 2022; https://clinicaltrials.gov/ct2/show/study/NCT02995694).

ClinicalTrials.gov. A Comparison of Estradiol Vaginal Cream to Estrace® Cream in 350 Postmenopausal Females With Atrophic Vaginitis. (31-July 2022; https://clinicaltrials.gov/ct2/show/NCT02195986).

Constantine GD, Bouchard C, Pickar JH, Archer DF, Graham S, Bernick B, Mirkin S. 2017a. Consistency of effect with a low-dose, estradiol vaginal capsule (TX-004HR): evaluating

improvement in vaginal physiology and moderate-to-severe dyspareunia in subgroups of postmenopausal women. Journal of Women's Health 26: 616-623.

Constantine GD, Simon JA, Pickar JH, Archer DF, Bernick B, Graham S, Mirkin S. 2018. Estradiol vaginal inserts (4 µg and 10 µg) for treating moderate to severe vulvar and vaginal atrophy: a review of phase 3 safety, efficacy and pharmacokinetic data. Current medical research and opinion 34: 2131-2136.

Constantine GD, Simon JA, Pickar JH, Archer DF, Kushner H, Bernick B, Gasper G, Graham S, Mirkin S. 2017b. The REJOICE trial: a phase 3 randomized, controlled trial evaluating the safety and efficacy of a novel vaginal estradiol soft-gel capsule for symptomatic vulvar and vaginal atrophy. Menopause (New York, NY) 24: 409.

Da Silva AS, Baines G, Araklitis G, Robinson D, Cardozo L. 2021. Modern management of genitourinary syndrome of menopause. Faculty Reviews 10.

Daneshmand F, Hosseinzadeh P, Ghahiri A, Ghasemi M. 2014. A comparative study of vaginal estrogen cream and sustained-released estradiol vaginal tablet (vagifem) in the treatment of atrophic vaginitis among postmenopausal women. International Journal of Reproductive BioMedicine 12: 12.

Dang NT, Turner MS, Coombes AG. 2013. Development of intra-vaginal matrices from polycaprolactone for sustained release of antimicrobial agents. Journal of biomaterials applications 28: 74-83.

Das Neves J, Notario-Pérez F, Sarmento B. 2021. Women-specific routes of administration for drugs: a critical overview. Advanced Drug Delivery Reviews: 113865.

De Araújo PR, Calixto GMF, da Silva IC, de Paula Zago LH, Junior JAO, Pavan FR, Ribeiro AO, Fontana CR, Chorilli M. 2019. Mucoadhesive in situ gelling liquid crystalline precursor system to improve the vaginal administration of drugs. AAPS PharmSciTech 20: 1-12.

Derzko CM, Röhrich S, Panay N. 2021. Does age at the start of treatment for vaginal atrophy predict response to vaginal estrogen therapy? Post hoc analysis of data from a randomized clinical trial involving 205 women treated with 10 µg estradiol vaginal tablets. Menopause 28: 113-118.

Desai J, Alexander K, Riga A. 2006. Characterization of polymeric dispersions of dimenhydrinate in ethyl cellulose for controlled release. International journal of pharmaceutics 308: 115-123.

Diab S, Bano G, Dhenge RM, Taylor J. 2021. Impact of process parameters and formulation properties on dissolution performance of an extended release tablet: a multivariate analysis. Journal of Pharmaceutical Innovation: 1-19.

Diem SJ, Guthrie KA, Mitchell CM, Reed SD, Larson JC, Ensrud KE, LaCroix AZ. 2018. Effects of vaginal estradiol tablets and moisturizer on menopause-specific quality of life and mood in healthy post-menopausal women with vaginal symptoms: a randomized clinical trial. Menopause (New York, NY) 25: 1086-1093.

Dorantes, A. and S. Stavchansky, Modification of the USP dissolution method for the analysis of norethindrone and ethinyl estradiol tablets. Journal of pharmaceutical sciences, 1994. 83(3): p. 379-381.

Dugal R, Hesla K, Sørdal T, Aase KH, Lilleeidet O, Wickstrøm E. 2000. Comparison of usefulness of estradiol vaginal tablets and estriol vagitories for treatment of vaginal atrophy. Acta Obstetricia et Gynecologica Scandinavica 79: 293-297.

Dupeyrón D, Kawakami M, Ferreira AM, Cáceres-Vélez PR, Rieumont J, Azevedo RB, Carvalho JCT. 2013. Design of indomethacin-loaded nanoparticles: effect of polymer matrix and surfactant. International journal of nanomedicine: 3467-3477.

Ekin M, Yaşar L, Savan K, Temur M, Uhri M, Gencer I, Kıvanç E. 2011. The comparison of hyaluronic acid vaginal tablets with estradiol vaginal tablets in the treatment of atrophic vaginitis: a randomized controlled trial. Archives of gynecology and obstetrics 283: 539-543.

Elbjorn M, Provencio J, Phillips P, Sainz J, Harrison N, Rocco DD, Jaramillo A, Jain P, Lozano A, Hood RL. 2023. An Innovative Polymeric Platform for Controlled and Localized Drug Delivery. Pharmaceutics 15: 1795.

Ellington DR, Szychowski JM, Malek JM, Gerten KA, Burgio KL, Richter HE. 2016. Combined tolterodine and vaginal estradiol cream for overactive bladder symptoms after randomized single-therapy treatment. Female pelvic medicine & reconstructive surgery 22: 254.

Elsokkary M, Shafik A, Nader S. 2016. The Role of Endometrial Volume in the Prediction of Endometrial Hyperplasia. Obstet Gynecol Int J 4: 00136.

Enayati M, Stride E, Edirisinghe M, Bonfild W. 2012. Modifiation of the release characteristics of estradiol encapsulated in PLGA particles via surface coating. Therapeutic Delivery 3: 209–226.

Eriksen BC. 1999. A randomized, open, parallel-group study on the preventive effect of an estradiol-releasing vaginal ring (Estring) on recurrent urinary tract infections in postmenopausal women. American journal of obstetrics and gynecology 180: 1072-1079.

Eriksen PS, Rasmussen H. 1992. Low-dose 17β-estradiol vaginal tablets in the treatment of atrophic vaginitis: a double-blind placebo controlled study. European Journal of Obstetrics & Gynecology and Reproductive Biology 44: 137-144.

Estrace Cream. estradiol vaginal cream, USP, 0.01% [package insert]. Rockaway, NJ: Warner Chilcott, Inc.

Estring. estradiol vaginal ring, [prescribing information] New York, NY: Pharmacia and Upjohn Company, Division of Pfizer Inc.

European Medicines Agency. 16.January.2020. Estradiol-containing (0.01% w/w) medicinal products for topical use. (20.July 2022; https://www.ema.europa.eu/en/medicines/human/referrals/estradiol-containing-001-ww-medicinal-products-topical-use).

Farmer Z-L, Utomo E, Domínguez-Robles J, Mancinelli C, Mathew E, Larrañeta E, Lamprou DA. 2021. 3D printed estradiol-eluting urogynecological mesh implants: Influence of material and mesh geometry on their mechanical properties. International journal of pharmaceutics 593: 120145.

Femring. estradiol acetate vaginal ring, [prescribing information]. East Hanover, NJ: Millicent Pharma Ltd.

Fernando HV, Chan LL, Dang N, Santhanes D, Banneheke H, Nalliah S, Coombes AG. 2019. Controlled delivery of the antiprotozoal agent (tinidazole) from intravaginal polymer matrices for treatment of the sexually transmitted infection, trichomoniasis. Pharmaceutical development and technology 24: 348-356.

Frank A, Rath SK, Venkatraman SS. 2005. Controlled release from bioerodible polymers: effect of drug type and polymer composition. Journal of controlled release 102: 333-344.

Freire MCLC, Alexandrino F, Marcelino HR, Picciani PHdS, Silva KGdHe, Genre J, Oliveira AGd, Egito ESTd. 2017. Understanding drug release data through thermodynamic analysis. Materials 10: 651.

Gandhi J, Chen A, Dagur G, Suh Y, Smith N, Cali B, Khan SA. 2016. Genitourinary syndrome of menopause: an overview of clinical manifestations, pathophysiology, etiology, evaluation, and management. American journal of obstetrics and gynecology 215: 704-711.

Gavini E, Sanna V, Juliano C, Bonferoni MC, Giunchedi P. 2002. Mucoadhesive vaginal tablets as veterinary delivery system for the controlled release of an antimicrobial drug, acriflavine. AAPS PharmSciTech 3: 32-38.

Goodwin DJ, Van Den Ban S, Denham M, Barylski I. 2018. Real time release testing of tablet content and content uniformity. International journal of pharmaceutics 537: 183-192.

Hamada AL, Maruo T, Samoto T, Yoshida S, Nash H, Spitz I, Johansson E. 2003. Estradiol/progesterone-releasing vaginal rings for hormone replacement therapy in postmenopausal women. Gynecological Endocrinology 17: 247-254.

Hariharan S, Bhardwaj V, Bala I, Sitterberg J, Bakowsky U, Kumar MR. 2006. Design of estradiol loaded PLGA nanoparticulate formulations: a potential oral delivery system for hormone therapy. Pharmaceutical research 23: 184-195.

Hassan AS, Soliman GM, Ali MF, El-Mahdy MM, El-Gindy GE-DA. 2018. Mucoadhesive tablets for the vaginal delivery of progesterone: *In vitro* evaluation and pharmacokinetics/pharmacodynamics in female rabbits. Drug development and industrial pharmacy 44: 224-232.

Henriksson L, Sgemquist M, Boquist L, Mander U, Selinus I. 1994. A comparative multicenter study of the effects of continuous low-dose estradiol released from a new vaginal ring versus estriol vaginal pessaries in postmenopausal women with symptoms and signs of urogenital atrophy. AM J OBSTET GVNECOL 171: 624-632.

Henriksson L, Stjernquist M, Boquist L, Cedergren I, Selinus I. 1996. A one-year multicenter study of efficacy and safety of a continuous, low-dose, estradiol-releasing vaginal ring (Estring) in postmenopausal women with symptoms and signs of urogenital aging. American journal of obstetrics and gynecology 174: 85-92.

Hill DA, Crider M, Hill SR. 2016. Hormone therapy and other treatments for symptoms of menopause. American family physician 94: 884-889.

Hiorth M, Nilsen S, Tho I. 2014. Bioadhesive mini-tablets for vaginal drug delivery. Pharmaceutics 6: 494-511.

Hirschberg AL, Bitzer J, Cano A, Ceausu I, Chedraui P, Durmusoglu F, Erkkola R, Goulis DG, Kiesel L, Lopes P. 2021. Topical estrogens and non-hormonal preparations for postmenopausal vulvovaginal atrophy: An EMAS clinical guide. Maturitas 148: 55-61.

Holländer J, Genina N, Jukarainen H, Khajeheian M, Rosling A, Mäkilä E, Sandler N. 2016. Three-dimensional printed PCL-based implantable prototypes of medical devices for controlled drug delivery. Journal of pharmaceutical sciences 105: 2665-2676.

Holmgren PA, Lindskog M, Schoultz Bv. 1989. Vaginal rings for continuous low-dose release of oestradiol in the treatment of urogenital atrophy. Moturitas 11: 55-63.

Horvat G, Žvab K, Knez Ž, Novak Z. 2022. Simple, One-Pot Method for Preparing Transparent Ethyl Cellulose Films with Good Mechanical Properties. Polymers 14: 2399.

Hosseinzadeh P, Ghahiri A, Daneshmand F, Ghasemi M. 2015. A comparative study of vaginal estrogen cream and sustained-release estradiol vaginal tablet (Vagifem) in the treatment of atrophic vaginitis in Isfahan, Iran in 2010-2012. Journal of research in medical sciences: the official journal of Isfahan University of Medical Sciences 20: 1160.

Hu L-Xi, He J, Hou L, Wang H, Li J, Xie C, Duan Z, Sun L-K, Wang X, Zhu C. 2013. Biological Evaluation of the Copper/Low –density Polyethylene Nanocomposite Intrauterine Device. PLOS ONE 8.

Hussain A, Ahsan F. 2005. The vagina as a route for systemic drug delivery. Journal of controlled release 103: 301-313.

Ilhan G, Aslan MM, Cevrioglu AS, Yıldırım M, Erkorkmaz U. 2021. Clinical efficacy of hormonal and nonhormonal agents in the treatment of vulvovaginal atrophy. Journal of Menopausal Medicine 27: 15.

Imani R, Emami SH, Moshtagh PR, Baheiraei N, Sharifi AM. 2012. Preparation and characterization of agarose-gelatin blend hydrogels as a cell encapsulation matrix: An *in-vitro* study. Journal of Macromolecular Science, Part B 51: 1606-1616.

Jana SK, Chakravarty B, Chaudhury K. 2014. Letrozole and curcumin loaded-PLGA nanoparticles: a therapeutic strategy for endometriosis. J. Nanomed. Biotherap. Discov 4: 10.4172.

Javaid S, Ahmad NM, Mahmood A, Nasir H, Iqbal M, Ahmad N, Irshad S. 2021. Cefotaxime loaded polycaprolactone based polymeric nanoparticles with antifouling properties for *in-vitro* drug release applications. Polymers 13: 2180.

Jeon O, Alt DS, Ahmed SM, Alsberg E. 2012. The effect of oxidation on the degradation of photocrosslinkable alginate hydrogels. Biomaterials 33: 3503-3514.

Jiang X, Bossert A, Parthasarathy KN, Leaman K, Minassian SS, Schnatz PF, Woodland MB. 2021. Safety assessment of compounded non-FDA-approved hormonal therapy versus FDA-approved hormonal therapy in treating postmenopausal women. Menopause 28: 867-874.

Jinying L, Ying L, Xuan G, Yanli G, Jianping L. 2008. Investigation of the release behavior of cupric ion for three types of Cu-IUDs and indomethacin for medicated Cu-IUD in simulated uterine fluid. Contraception 77: 299-302.

Jonasson AF, Bixo M, Poromaa IS, Åstrom M. 2020. Safety and Effiacy of an Oxytocin Gel and an Equivalent Gel but Without Hormonal Ingredients (Vagivital® Gel) in Postmenopausal Women with Symptoms of Vulvovaginal Atrophy: A Randomized, Double-Blind Controlled Study. Medical Devices: Evidence and Research: 339–347.

Kagan R, Kellogg-Spadt S, Parish SJ. 2019. Practical treatment considerations in the management of genitourinary syndrome of menopause. Drugs & aging 36: 897-908.

Kaluzynski K, Pretula J, Lewinski P, Kaźmierski S, Penczek S. 2022. Synthesis and Properties of Functionalized Poly (ε-caprolactone); Chain Polymerization Followed by Polycondensation in One Pot with Initiator and Catalyst in One Molecule. Synthesis and Molecular Structures. Macromolecules 55: 2210-2221.

Kalva SN, Dalvi YB, Khanam N, Varghese R, Ahammed I, Augustine R, Hasan A. 2023. Air-jet spun PHBV/PCL blend tissue engineering scaffolds exhibit improved mechanical properties and cell proliferation. Results in Materials: 100415.

Karami T, Ghobadi E, Akrami M, Haririan I. 2024. Fabrication of a Controlled-Release Core-Shell Floating Tablet of Ketamine Hydrochloride Using a 3D Printing Technique for Management of Refractory Depressions and Chronic Pain. Polymers 16: 746.

Karunakaran D, Simpson SM, Su JT, Bryndza-Tfaily E, Hope TJ, Veazey R, Dobek G, Qiu J, Watrous D, Sung S. 2021. Design and testing of a cabotegravir implant for HIV prevention. Journal of controlled release 330: 658-668.

Kaur K, Kaur SP, Kaur P, Bedi GK, Kaur H, Kaur A. 2019. Correlation of vaginal pH with FSH levels in menopause. Int J Clin Obstet Gynecol 3: 107-110.

Kaur M, Gupta KM, Poursaid AE, Karra P, Mahalingam A, Aliyar HA, Kiser PF. 2011. Engineering a degradable polyurethane intravaginal ring for sustained delivery of dapivirine. Drug Delivery and Translational Research 1: 223-237.

Kemala T, Budianto E, Soegiyono B. 2012. Preparation and characterization of microspheres based on blend of poly(lactic acid) and poly(e-caprolactone) with poly(vinyl alcohol) as emulsifier. Arabian Journal of Chemistry 5: 103–108.

Kendall A, Dowsett M, Folkerd E, Smith I. 2006. Caution: vaginal estradiol appears to be contraindicated in postmenopausal women on adjuvant aromatase inhibitors. Annals of Oncology 17: 584-587.

Khalili M, Khalili A, Bokov DO, Golmirzaei M, Oleneva MS, Naghiaei N, Radmehr M, Esmaeili E. 2022. Preparation and characterization of bi-layered polycaprolactone/polyurethane nanofibrous scaffold loaded with titanium oxide and curcumin for wound dressing applications. Applied Physics A 128: 497.

Kim MH, Lee YW, Jung W-K, Oh J, Nam SY. 2019. Enhanced rheological behaviors of alginate hydrogels with carrageenan for extrusion-based bioprinting. Journal of the mechanical behavior of biomedical materials 98: 187-194.

Kimlin LC, Casagrande G, Virador VM. 2013. *In vitro* three-dimensional (3D) models in cancer research: an update. Molecular carcinogenesis 52: 167-182.

Kingsberg SA, Kroll R, Goldstein I, Kushner H, Bernick B, Graham S, Mirkin S, Constantine GD. 2017. Patient acceptability and satisfaction with a low-dose solubilized vaginal estradiol softgel capsule, TX-004HR. Menopause 24: 894-899.

Kireç O, Alacabey İ, Erol K, Alkan H. 2021. Removal of 17 β -estradiol from aqueous systems with hydrophobic microspheres. J Polym Eng 41: 226–234.

Kolawole OA, Pillay V, Choonara YE. 2007. Novel polyamide 6, 10 variants synthesized by modified interfacial polymerization for application as a rate-modulated monolithic drug delivery system. Journal of bioactive and compatible polymers 22: 281-313.

Korelidou A, Domínguez-Robles J, Magill ER, Eleftheriadou M, Cornelius VA, Donnelly RF, Margariti A, Larrañeta E. 2022. 3D-printed reservoir-type implants containing poly (lactic

acid)/poly (caprolactone) porous membranes for sustained drug delivery. Biomaterials Advances 139: 213024.

Kovachev SM, Kovachev MS. 2022. Genitourinary syndrome, local oestrogen therapy and endometrial pathology: a single-centre, randomised study. Journal of Obstetrics and Gynaecology: 1-4.

Krause M, Wheeler II TL, Snyder TE, Richter HE. 2009. Local effects of vaginally administered estrogen therapy: a review. Journal of pelvic medicine & surgery 15: 105.

Križman K, Novak S, Kristl J, Majdič G, Drnovšek N. 2021a. Long-acting silk fibroin xerogel delivery systems for controlled release of estradiol. Journal of Drug Delivery Science and Technology: 102701.

Kroll R, Archer DF, Lin Y, Sniukiene V, Liu JH. 2018. A randomized, multicenter, double-blind study to evaluate the safety and efficacy of estradiol vaginal cream 0.003% in postmenopausal women with dyspareunia as the most bothersome symptom. Menopause (New York, NY) 25: 133-138.

Kumar G, Virmani T, Pathak K, Kamaly OA, Saleh A. 2022. Central Composite Design Implemented Azilsartan Medoxomil Loaded Nanoemulsion to Improve Its Aqueous Solubility and Intestinal Permeability: *In Vitro* and *Ex Vivo* Evaluation. Pharmaceuticals 15: 1343.

Kuperman T, Gavriel M, Gotlib R, Zhang Y, Jafa A, Elad D, Grisaru D. 2020. Tissue-engineered multi-cellular models of the uterine wall. Biomechanics and Modeling in Mechanobiology 19: 1629–1639.

Labrie F, Cusan L, Gomez J-L, Côté I, Bérubé R, Bélanger P, Martel C, Labrie C. 2009. Effect of one-week treatment with vaginal estrogen preparations on serum estrogen levels in postmenopausal women. Menopause 16: 30-36.

Lam CX, Savalani MM, Teoh S-H, Hutmacher DW. 2008. Dynamics of *in vitro* polymer degradation of polycaprolactone-based scaffolds: accelerated versus simulated physiological conditions. Biomedical Materials 3: 034108.

Lebourg M, Sabater Serra R, Más Estellés J, Hernández Sánchez F, Gómez Ribelles J, Suay Antón J. 2008. Biodegradable polycaprolactone scaffold with controlled porosity obtained by modified particle-leaching technique. Journal of Materials Science: Materials in Medicine 19: 2047-2053.

Lei L, Liu X, Guo S, Tang M, Cheng L, Tian L. 2010. 5-Fluorouracil-loaded multilayered fi lms for drug controlled releasing stent application: Drug release, microstructure, and *ex vivo* permeation behaviors. Journal of Controlled Release 146: 45-53.

Lei L, Liu X, Shen Y-Y, Liu J-Y, Tang M-F, Wang Z-M, Guo S-R, Cheng L. 2011. Zero-order release of 5-fluorouracil from PCL-based films featuring trilayered structures for stent application. European Journal of Pharmaceutics and Biopharmaceutics 78: 49-57.

Li, Cheng L, Zhang Y, Guo S, Wu W. 2010. Effects of implant diameter, drug loading and end-capping on praziquantel release from PCL implants. International journal of pharmaceutics 386: 23-29.

Li S, Culkin A, Jones DS, Andrews GP. 2021. Development of Polycaprolactone-Based metronidazole matrices for intravaginal extended drug delivery using a mechanochemically prepared therapeutic deep eutectic system. International journal of pharmaceutics 593: 120071.

Lim W, Kim GJ, Kim HW, Lee J, Zhang X, Kang MG, Seo JW, Cha JM, Park HJ, Lee M-Y. 2020. Kappa-carrageenan-based dual crosslinkable bioink for extrusion type bioprinting. Polymers 12: 2377.

Lindahl SH. 2014. Reviewing the options for local estrogen treatment of vaginal atrophy. International journal of women's health 6: 307-312.

Liu H, Zhang L, Shi P, Zou Q, Zuo Y, Li Y. 2010. Hydroxyapatite/polyurethane scaffold incorporated with drug-loaded ethyl cellulose microspheres for bone regeneration. Journal of Biomedical Materials Research Part B: Applied Biomaterials 95: 36-46.

Liu HX, Li SJ, Yan YN. 2011. Cell direct assembly technology adopting hybrid of gelatin-based hydrogels. Advanced Materials Research 189: 2986-2992.

Liu JH, Bernick B, Mirkin S. 2020. Estradiol softgel inserts for the treatment of VVA symptoms: an expert opinion. Expert Opinion on Drug Delivery 17: 1573-1581.

Liu X, Lei L, Hou J-W, Tang M-F, Guo S-R, Wang Z-M, Chen K-M. 2011. Evaluation of two polymeric blends (EVA/PLA and EVA/PEG) as coating film materials for paclitaxel-eluting stent application. Journal of Materials Science: Materials in Medicine 22: 327-337.

Lu F, Shen Y-Y, Shen Y-Q, Hou J-W, Wang Z-M, Guo S-R. 2012. Treatments of paclitaxel with poly(vinyl pyrrolidone) to improve drug release from poly(ε-caprolactone) matrix for film-based stent. International Journal of Pharmaceutics 434: 161–168.

Luo Y, Chen A, Xu M, Chen D, Tang J, Ma D, Zhang H. 2021. Preparation, characterization, and *in vitro/vivo* evaluation of dexamethasone/poly (ε-caprolactone)-based electrode coatings for cochlear implants. Drug Delivery 28: 1673-1684.

Lykke MR, Becher N, Haahr T, Boedtkjer E, Jensen JS, Uldbjerg N. 2021. Vaginal, cervical and uterine ph in women with normal and abnormal vaginal microbiota. Pathogens 10: 90.

Lynch C. 2009. Vaginal estrogen therapy for the treatment of atrophic vaginitis. Journal of Women's Health 18: 1595-1606.

Lyons JG, Blackie P, Higginbotham CL. 2008. The significance of variation in extrusion speeds and temperatures on a PEO/PCL blend based matrix for oral drug delivery. International journal of pharmaceutics 351: 201-208.

Ma G, Song C, Sun H, Yang J, Leng X. 2006. A biodegradable levonorgestrel-releasing implant made of PCL/F68 compound as tested in rats and dogs. Contraception 74: 141-147.

Maderuelo C, Zarzuelo A, Lanao JM. 2011. Critical factors in the release of drugs from sustained release hydrophilic matrices. Journal of controlled release 154: 2-19.

Maji R, Ray S, Das B, Nayak AK. 2012. Ethyl cellulose microparticles containing metformin HCl by emulsification-solvent evaporation technique: effect of formulation variables. International Scholarly Research Notices 2012.

Malcolm K, Woolfson D, Russell J, Tallon P, McAuley L, Craig D. 2003. Influence of silicone elastomer solubility and diffusivity on the *in vitro* release of drugs from intravaginal rings. Journal of controlled release 90: 217-225.

Malcolm RK, McCullagh S, Woolfson AD, Catney M, Tallon P. 2002. A dynamic mechanical method for determining the silicone elastomer solubility of drugs and pharmaceutical excipients in silicone intravaginal drug delivery rings. Biomaterials 23: 3589–3594.

Manini G, Deldime M, Benali S, Raquez J-M, Goole J. 2021. Long-acting implantable dosage forms containing paliperidone palmitate obtained by 3D printing. International journal of pharmaceutics 603: 120702.

Marino JM. 2021. Genitourinary Syndrome of Menopause. Journal of Midwifery & Women's Health 66: 729-739.

Martin PL, Yen SS, Burnier AM, Hermann H. 1979. Systemic absorption and sustained effects of vaginal estrogen creams. Jama 242: 2699-2700.

Maruo T, Mishell Jr DR, Ben-Chetrit A, Hochner-Celnikier D, Hamada AL, Nash HA. 2002. Vaginal rings delivering progesterone and estradiol may be a new method of hormone replacement therapy. Fertility and sterility 78: 1010-1016.

Mashingaidze F. 2014. Design of an intravaginal composite polymeric system for the reduction and prevention of STI and HIV transmissionDepartment of Pharmacy and Pharmacology, University of the Witwatersrand.

Mettler L, Olsen PG. 1991. Long-term treatment of atrophic vaginitis with low-dose oestradiol vaginal tablets. Maturitas 14: 23-31.

Minkin MJ, Maamari R, Reiter S. 2013. Improved compliance and patient satisfaction with estradiol vaginal tablets in postmenopausal women previously treated with another local estrogen therapy. International journal of women's health 5: 133.

Mirkin S, Simon JA, Liu JH, Archer DF, Castro PD, Graham S, Bernick B, Komm B. 2021. Evaluation of endometrial progesterone receptor expression after 12 weeks of exposure to a low-dose vaginal estradiol insert. Menopause (New York, NY) 28: 998-1003.

Mittal G, Sahana D, Bhardwaj V, Kumar MR. 2007. Estradiol loaded PLGA nanoparticles for oral administration: effect of polymer molecular weight and copolymer composition on release behavior *in vitro* and *in vivo*. Journal of controlled release 119: 77-85.

Modi C, Bharadia P. 2023. Pareto chart-enabled screening of influential factors in designing transfersomes. Separation Science Plus 6: 2200082.

Mohammad F, Arfin T, Al-Lohedan HA. 2017. Sustained drug release and electrochemical performance of ethyl cellulose-magnesium hydrogen phosphate composite. Materials Science and Engineering: C 71: 735-743.

Mohebian Z, Tajmohammadi I, Yavari Maroufi L, Ramezani S, Ghorbani M. 2022. A novel aloe vera-loaded ethylcellulose/hydroxypropyl methylcellulose nanofibrous mat designed for wound healing application. Journal of Polymers and the Environment: 1-11.

Mora N, Cano E, Mora E, Bastidas J. 2002. Influence of pH and oxygen on copper corrosion in simulated uterine fluid. Biomaterials 23: 667-671.

Muhindo D, Ashour EA, Almutairi M, Repka MA. 2022. Development and evaluation of raloxifene hydrochloride-loaded subdermal implants using hot-melt extrusion technology. International journal of pharmaceutics 622: 121834.

Nappi RE, Di Carlo C, Cucinella L, Gambacciani M. 2020. Viewing symptoms associated with Vulvovaginal Atrophy (VVA)/Genitourinary syndrome of menopause (GSM) through the estro-androgenic lens–Cluster analysis of a web-based Italian survey among women over 40. Maturitas 140: 72-79.

Nash HA, Brache V, Alvarez-Sanchez F, Jackanicz TM, Harmon TM. 1997. Estradiol delivery by vaginal rings: potential for hormone replacement therapy. Maturitas 26: 27-33.

Nash HA, Alvarez-Sanchez F, Mishell DR, Fraser IS, Maruo T, Harmon TM. 1999. Estradiol-delivering vaginal rings for hormone replacement therapy. Am J Obstet Gynecol 1999;: 181: 1400-1406.

Naunton M, Al Hadithy AFY, Brouwers JRBJ, Archer DF. 2006. Estradiol gel: review of the pharmacology, pharmacokinetics, efficacy, and safety in menopausal women. Menopause 13: 517-527.

Ndesendo VM, Pillay V, Choonara YE, Buchmann E, Bayever DN, Meyer LC. 2008. A review of current intravaginal drug delivery approaches employed for the prophylaxis of HIV/AIDS and prevention of sexually transmitted infections. AAPS PharmSciTech 9: 505-520.

Nelson AL, Massoudi N. 2016. New developments in intrauterine device use: focus on the US. Open access journal of contraception 7: 127.

Nilsson K, Heimer G. 1992. Low-dose oestradiol in the treatment of urogenital oestrogen deficiency—a pharmacokinetic and pharmacodynamic study. Maturitas 15: 121-127.

Nilsson K, Heimer G. 1995. Low-dose 17β-oestradiol during maintenance therapy—a pharmacokinetic and pharmacodynamic study. Maturitas 21: 33-38.

Nilsson K, Risberg B, Heimer G. 1995. The vaginal epithelium in the postmenopause—cytology, histology and pH as methods of assessment. Maturitas 21: 51-56.

Notelovitz M, Funk S, Nanavati N, Mazzeo M. 2002. Estradiol Absorption From Vaginal Tablets in Postmenopausal Women. Obstetrics & Gynecology 99: 556-562.

Nygaard L, Kilde HD, Andersen SG, Henriksen L, Overby V. 2004. Development and validation of a reversed-phase liquid chromatographic method for analysis of degradation products of estradiol in Vagifem® tablets. Journal of pharmaceutical and biomedical analysis 34: 265-276.

Osmałek T, Froelich A, Jadach B, Tatarek A, Gadziński P, Falana A, Gralińska K, Ekert M, Puri V, Wrotyńska-Barczyńska J. 2021. Recent advances in polymer-based vaginal drug delivery systems. Pharmaceutics 13: 884.

Ostad SN, Malhi JS, Gard PR. 1998. *In vitro* cytotoxicity and teratogenicity of norethisterone and levonorgestrel released from hollow nylon monofilaments. Journal of controlled release 50: 179-186.

Ouyang L, Yao R, Zhao Y, Sun W. 2016. Effect of bioink properties on printability and cell viability for 3D bioplotting of embryonic stem cells. Biofabrication 8: 035020.

Ouyang L, Yao R, Chen X, Na J, Sun W. 2015. 3D printing of HEK 293FT cell-laden hydrogel into macroporous constructs with high cell viability and normal biological functions. Biofabrication 7: 015010.

Owen DH, Katz DF. 1999. A vaginal fluid simulant. Contraception 59: 91-95.

Pacheco-Quito E-M, Ruiz-Caro R, Rubio J, Tamayo A, Veiga M-D. 2020. Carrageenan-Based Acyclovir Mucoadhesive Vaginal Tablets for Prevention of Genital Herpes. Marine drugs 18: 249.

Palacios S, Mejía A. 2016. Progestogen safety and tolerance in hormonal replacement therapy. Expert Opinion on Drug Safety 15: 1515-1525.

Palacios S, Castelo-Branco C, Currie H, Mijatovic V, Nappi RE, Simon J, Rees M. 2015. Update on management of genitourinary syndrome of menopause: a practical guide. Maturitas 82: 308-313.

Pan C-T, Hwang Y-M, Lin Y-M, Zeng S-W, Wang S-Y, Kuo S-W, Ju S-P, Liang S-S, Liu Z-H, Yen C-K. 2019. Development of polycaprolactone microspheres with controllable and uniform particle size by uniform design experiment in emulsion progress. Sensors and Materials 31: 311-318.

Panay N, Maamari R. 2012. Treatment of postmenopausal vaginal atrophy with 10-µg estradiol vaginal tablets. Menopause International 18: 15-19.

Panouillé M, Larreta-Garde V. 2009. Gelation behaviour of gelatin and alginate mixtures. Food hydrocolloids 23: 1074-1080.

Paolini MS, Fenton OS, Bhattacharya C, Andresen JL, Langer R. 2019. Polymers for extended-release administration. Biomedical Microdevices 21: 1-24.

Parhi R, Jena GK. 2022. An updated review on application of 3D printing in fabricating pharmaceutical dosage forms. Drug Delivery and Translational Research: 1-35.

Pathak M, Turner M, Palmer C, Coombes AG. 2014. Evaluation of polycaprolactone matrices for the intravaginal delivery of metronidazole in the treatment of bacterial vaginosis. Journal of biomaterials applications 29: 354-363.

Pathak M, Coombes AG, Ryu B, Cabot PJ, Turner MS, Palmer C, Wang D, Steadman KJ. 2018. Sustained simultaneous delivery of metronidazole and doxycycline from polycaprolactone matrices designed for intravaginal treatment of pelvic inflammatory disease. Journal of pharmaceutical sciences 107: 863-869.

Paton DM. 2018. Estradiol vaginal inserts (Imvexxy): effective in genitourinary syndrome of menopause without increasing systemic estrogen levels. Drugs Today (Barc) 54: 667-677.

Penhasi A, Gertler A, Baluashvili I, Elzinaty O, Shalev DE. 2020. High modulus thermoplastic segmented polyurethane/poly (L-lactide) blends as potential candidates for structural implantable drug delivery systems: I. Structure-properties relationship study. Journal of Applied Polymer Science 137: 49517.

Phadke KV, Manjeshwar LS, Aminabhavi TM. 2014. Microspheres of gelatin and poly (ethylene glycol) coated with ethyl cellulose for controlled release of metronidazole. Industrial & Engineering Chemistry Research 53: 6575-6584.

Pickar J, Amadio J, Bernick B, Mirkin S. 2016a. Pharmacokinetic studies of solubilized estradiol given vaginally in a novel softgel capsule. Climacteric 19: 181-187.

Pickar JH, Amadio JM, Hill JM, Bernick BA, Mirkin S. 2016b. A randomized, double-blind, placebo-controlled phase 2 pilot trial evaluating a novel, vaginal softgel capsule containing solubilized estradiol. Menopause (New York, NY) 23: 506.

Pinkerton JV, Kaunitz AM, Manson JE. 2017. Vaginal estrogen in the treatment of genitourinary syndrome of menopause and risk of endometrial cancer: an assessment of recent studies provides reassurance. Menopause 24: 1329-1332.

Poletaev G, Bebikhov Y, Semenov A. 2023. Molecular dynamics study of the formation of the nanocrystalline structure in nickel nanoparticles during rapid cooling from the melt. Materials Chemistry and Physics 309: 128358.

Portman D, Shulman L, Yeaw J, Zeng S, Uzoigwe C, Maamari R, Iyer NN. 2015. One-year treatment persistence with local estrogen therapy in postmenopausal women diagnosed as having vaginal atrophy. Menopause 22: 1197-1203.

Prakapenka AV, Bimonte-Nelson HA, Sirianni RW. 2017. Engineering poly (lactic-co-glycolic acid)(PLGA) micro-and nano-carriers for controlled delivery of 17β-estradiol. Annals of biomedical engineering 45: 1697-1709.

Prakapenka AV, Quihuis AM, Carson CG, Patel S, Bimonte-Nelson HA, Sirianni RW. 2020. Poly (lactic-co-glycolic acid) nanoparticle encapsulated 17β-estradiol improves spatial memory and increases uterine stimulation in middle-aged ovariectomized rats. Frontiers in Behavioral Neuroscience 14: 235.

Prasadh S, Gupta M, Wong R. 2022a. *In vitro* cytotoxicity and osteogenic potential of quaternary Mg-2Zn-1Ca/X-Mn alloys for craniofacial reconstruction. Scientific Reports 12: 8259.

Prasadh S, Gupta M, Wong R. 2022b. *In vitro* cytotoxicity and osteogenic potential of quaternary Mg-2Zn-1Ca/X-Mn alloys for craniofacial reconstruction. Scientifc Reports 12: 8259.

Puga AM, Rey-Rico A, Magariños B, Alvarez-Lorenzo C, Concheiro A. 2012. Hot melt poly-ε-caprolactone/poloxamine implantable matrices for sustained delivery of ciprofloxacin. Acta Biomaterialia 8: 1507-1518.

Qi C, Xia X, Zhang W, Xie C, Cai S. 2012. Indomethacin/Cu/LDPE porous composite for medicated copper intrauterine devices with controlled release performances. Composites science and technology 72: 428-434.

Racles C. 2013. Polydimethylsiloxane–Indomethacin blends and nanoparticles. AAPS PharmSciTech 14: 968-976.

Rafiei F, Tabesh H, Farzad S, Farzaneh F, Rezaei M, Hosseinzade F, Mottaghy K. 2021. Development of Hormonal Intravaginal Rings: Technology and Challenges. Geburtshilfe und Frauenheilkunde 81: 789-806.

Rahman SS, Ahmed AB. 2016. Vaginal Drug Delivery System a Promising Approach for Antiretroviral Drug in the Prevention of HIV Infection: A Review. Journal of Pharmaceutical Sciences and Research 8: 1330-1338.

Rastin H, Zhang B, Bi J, Hassan K, Tung TT, Losic D. 2020. 3D printing of cell-laden electroconductive bioinks for tissue engineering applications. Journal of Materials Chemistry B 8: 5862-5876.

Rastpeiman S, Panahi Z, Akrami M, Haririan I, Asadi M. 2024. Facile fabrication of an extended-release tablet of ticagrelor using three dimensional printing technology. Journal of Biomedical Materials Research Part A 112: 20-30.

Ridgeway K, Montgomery ET, Smith K, Torjesen K, Straten Avd, Achilles SL, Griffin JB. 2022. Vaginal ring acceptability: A systematic review and meta-analysis of vaginal ring experiences from around the world. Contraception 106: 16–33.

Rigg LA, Hermann H, Yen SSC. 1978. Absroption of estrogens from vaginal creams. The New England Journal of Medicine 298: 195-197.

Rioux JE, Devlin MC, Gelfand MM, Steinberg WM, Hepburn DS. 2018. 17β-estradiol vaginal tablet versus conjugated equine estrogen vaginal cream to relieve menopausal atrophic vaginitis. Menopause 25: 1208-1213.

Rose S, Chaudhari A, Peterson CM. 2009. Mirena®(Levonorgestrel intrauterine system): A successful novel drug delivery option in contraception. Advanced Drug Delivery Reviews 61: 808-812.

Rosenblum N. 2020. Update in Female Hormonal Therapy: What the Urologist Should Know: NYU Case of the Month, December 2020. Reviews in Urology 22: 182.

Sahoo CK, Nayak PK, Sarangi DK, Sahoo TK. 2013. Intra vaginal drug delivery system: an overview. Am. J. Adv. Drug Deliv 1: 43-55.

Saini P, Arora M, Kumar MR. 2016. Poly (lactic acid) blends in biomedical applications. Advanced Drug Delivery Reviews 107: 47-59.

Saleh SI, Khidr SH, Ahmed SM, Jackanicz TM, Nash HA. 2003. Estradiol–progesterone interaction during the preparation of vaginal rings. Journal of pharmaceutical sciences 92: 258-265.

Samsioe B. 1998. Urogenital aging—a hidden problem. American journal of obstetrics and gynecology 178: S245-S249.

Santen R. 2015. Vaginal administration of estradiol: effects of dose, preparation and timing on plasma estradiol levels. Climacteric 18: 121-134.

Santen RJ, Pinkerton JV, Conaway M, Ropka M, Wisniewski L, Demers L, Klein KO. 2002. Treatment of urogenital atrophy with low-dose estradiol: preliminary results. Menopause 9: 179-187.

Santoro N, Komi J. 2009. Prevalence and impact of vaginal symptoms among postmenopausal women. The journal of sexual medicine 6: 2133-2142.

Sarkar NN. 2003. Low-dose intravaginal estradiol delivery using a Silastic vaginal ring for estrogen replacement therapy in postmenopausal women: a review. The European Journal of Contraception and Reproductive Health Care: 217–224.

Shayanfar A. 2020. Comments on “Measurement and correlation of the solubility of estradiol and estradiol-urea co-crystal in fourteen pure solvents at temperatures from 273.15 K to 318.15 K”. Journal of Molecular Liquids 309: 113161.

Shim S, Park K-M, Chung Y-J, Kim M-R. 2021. Updates on Therapeutic Alternatives for Genitourinary Syndrome of Menopause: Hormonal and Non-Hormonal Managements. Journal of Menopausal Medicine 27: 1.

Shulman LP, Portman DJ, Lee WC, Balu S, Joshi AV, Cobden D, Wang Q, Pashos CL. 2008. A Retrospective Managed Care Claims Data Analysis of Medication Adherence to Vaginal Estrogen Therapy: Implications for Clinical Practice. Journal of Women’s Health 17: 569-578.

Siddiqa AJ, Shrivastava NK, Mohsin MA, Abidi MH, Shaikh TA, El-Meligy MA. 2019. Preparation of letrozole dispersed pHEMA/AAm-g-LDPE drug release system: *In-vitro* release kinetics for the treatment of endometriosis. Colloids and Surfaces B: Biointerfaces 179: 445-452.

Siddiqa AJ, Shrivastava NK, Ali Mohsin M, Abidi MH, Sharaf MAF, Shaikh TA. 2021. *In vitro* release and degradation study of letrozole-loaded poly (lactic-co-glycolic acid) microparticles. JOM 73: 450-459.

Simon, Kagan R, Archer D, Constantine G, Bernick B, Graham S, Mirkin S. 2019. TX-004HR clinically improves symptoms of vulvar and vaginal atrophy in postmenopausal women. Climacteric 22: 412-418.

Simon, Pickar JH, Shadiack AM, Warrier B, Graham S, Bernick B, Mirkin S. 2020. Physical characteristics and properties of estradiol softgel vaginal inserts. Menopause (New York, NY) 27: 150.

Simon, Archer DF, Constantine GD, Pickar JH, Amadio JM, Bernick B, Graham S, Mirkin S. 2017a. A vaginal estradiol softgel capsule, TX-004HR, has negligible to very low systemic absorption of estradiol: efficacy and pharmacokinetic data review. Maturitas 99: 51-58.

Simon J, Nachtigall L, Ulrich LG, Eugster-Hausmann M, Gut R. 2010. Endometrial safety of ultra-low-dose estradiol vaginal tablets. Obstetrics & Gynecology 116: 876-883.

Simon JA, Maamari R. 2013. Ultra-low-dose vaginal estrogen tablets for the treatment of postmenopausal vaginal atrophy. Climacteric 16: 37-43.

Simon JA, Archer DF, Kagan R, Bernick B, Graham S, Constantine GD, Mirkin S. 2017b. Visual improvements in vaginal mucosa correlate with symptoms of VVA: data from a double-blind, placebo-controlled trial. Menopause (New York, NY) 24: 1003.

Smith P, Heimer G, Lindskog M, Ulmsten U. 1993. Oestradiol-releasing vaginal ring for treatment of postmenopausal urogenital atrophy. Maturitas 16: 145-154.

Solano AGR, de Fátima Pereira A, Pinto FCH, Ferreira LGR, de Oliveira Barbosa LA, Fialho SL, de Oliveira Patricio PS, da Silva Cunha A, da Silva GR, Pianetti GA. 2013. Development and evaluation of sustained-release etoposide-loaded poly (ε-caprolactone) implants. AAPS PharmSciTech 14: 890-900.

Somboonporn W, Panna S, Temtanakitpaisan Tr, Kaewrudee S, Soontrapa S. 2011. Effects of the levonorgestrel-releasing intrauterine system plus estrogen therapy in perimenopausal and postmenopausal women: systematic review and meta-analysis. Menopause 18: pp. 1060/1066.

Speroff L, Group USVI. 2003. Efficacy and tolerability of a novel estradiol vaginal ring for relief of menopausal symptoms. Obstetrics & Gynecology 102: 823-834.

Srikrishna S, Cardozo L. 2013. The vagina as a route for drug delivery: a review. International urogynecology journal 24: 537-543.

Sritonchai C, Manonai J, Sophonsritsuk A, Cherdshewasart W. 2020. Comparison of the effects of Pueraria mirifica gel and of placebo gel on the vaginal microenvironment of postmenopausal women with Genitourinary Syndrome of Menopause (GSM). Maturitas 140: 49-54.

Stamatialis DF, Papenburg BJ, Gironés M, Saiful S, Bettahalli SN, Schmitmeier S, Wessling M. 2008. Medical applications of membranes: Drug delivery, artificial organs and tissue engineering. Journal of membrane Science 308: 1-34.

Steele NM, Ledbetter CA. 2016. Genitourinary Syndrome Of Menopause and Vaginal Estrogen Use. Urologic Nursing 36: 59-65.

Steffi C, Wang D, Kong CH, Wang Z, Lim PN, Shi Z, San Thian E, Wang W. 2018. Estradiol-loaded poly (ε-caprolactone)/silk fibroin electrospun microfibers decrease osteoclast activity and retain osteoblast function. ACS applied materials & interfaces 10: 9988-9998.

Stewart SA, Domínguez-Robles J, McIlorum VJ, Mancuso E, Lamprou DA, Donnelly RF, Larrañeta E. 2020. Development of a biodegradable subcutaneous implant for prolonged drug delivery using 3D printing. Pharmaceutics 12: 105.

Stumpf PG, Maruca J, Santen RJ, Demers LM. 1982. Development of a vaginal ring for achieving physiologic levels of 17β-estradi0l in hypoestrogenic women1. The Journal of Clinical Endocrinology & Metabolism 54: 208-210.

Sun W-J, Aburub A, Sun CC. 2017. Particle engineering for enabling a formulation platform suitable for manufacturing low-dose tablets by direct compression. Journal of pharmaceutical sciences 106: 1772-1777.

Tanmahasamut P, Jirasawas T, Laiwejpithaya S, Areeswate C, Dangrat C, Silprasit K. 2020. Effect of estradiol vaginal gel on vaginal atrophy in postmenopausal women: A randomized double-blind controlled trial. Journal of Obstetrics and Gynaecology Research 46: 1425-1435.

Tavakoli S, Kharaziha M, Kermanpur A, Mokhtari H. 2019. Sprayable and injectable visible-light Kappa-carrageenan hydrogel for in-situ soft tissue engineering. International journal of biological macromolecules 138: 590-601.

Thapa R, Gurung S, Parat M-O, Parekh HS, Pandey P. 2022. Application of Sol–Gels for Treatment of Gynaecological Conditions—Physiological Perspectives and Emerging Concepts in Intravaginal Drug Delivery. Gels 8: 99.

Tian K, Xie C, Xia X. 2013. Chitosan/alginate multilayer film for controlled release of IDM on Cu/LDPE composite intrauterine devices. Colloids and Surfaces B: Biointerfaces 109: 82-89.

Tietz K, Klein S. 2018. Simulated genital tract fluids and their applicability in drug release/dissolution testing of vaginal dosage forms. Dissolut. Technol 25: 40-51.

Tosca EM, Rocchetti M, Pérez E, Nieto C, Bettica P, Moscoso del Prado J, Magni P, De Nicolao G. 2021. *In Vitro–In Vivo* Correlation (IVIVC) Population Modeling for the In Silico Bioequivalence of a Long-Acting Release Formulation of Progesterone. Pharmaceutics 13: 255.

Tuğcu-Demiröz F, Saar S, Kara AA, Yıldız A, Tunçel E, Acartürk F. 2021. Development and characterization of chitosan nanoparticles loaded nanofiber hybrid system for vaginal controlled release of benzydamine. European journal of pharmaceutical sciences 161: 105801.

Turcan N, Gradinaru-Fometescu D, Baros A, Coravu V, Turcan G, Cirstoiu MM. 2022. Vulvovaginal atrophy–the impact on the quality of life and self-regard. Review of literature. Romanian Journal of Military Medicine 125: 50-55.

Turek A, Olakowska E, Borecka A, Janeczek H, Sobota M, Jaworska J, Kaczmarczyk B, Jarząbek B, Gruchlik A, Libera M. 2016. Shape-memory terpolymer rods with 17-β-estradiol for the treatment of neurodegenerative diseases: an *in vitro* and *in vivo* study. Pharmaceutical research 33: 2967-2978.

Tytgat L, Van Damme L, Arevalo MdPO, Declercq H, Thienpont H, Otteveare H, Blondeel P, Dubruel P, Van Vlierberghe S. 2019. Extrusion-based 3D printing of photo-crosslinkable gelatin and κ-carrageenan hydrogel blends for adipose tissue regeneration. International journal of biological macromolecules 140: 929-938.

Unagolla JM, Jayasuriya AC. 2018. Drug transport mechanisms and *in vitro* release kinetics of vancomycin encapsulated chitosan-alginate polyelectrolyte microparticles as a controlled drug delivery system. European Journal of Pharmaceutical Sciences 114: 199-209.

Vagifem Tablet. estradiol vaginal tablets, [prescribing information]. Princeton, NJ: Novo Nordisk Inc.

Varela-Fernández R, Lema-Gesto MI, González-Barcia M, Otero-Espinar FJ. 2021. Design, development, and characterization of an idebenone-loaded poly-ε-caprolactone intravitreal implant as a new therapeutic approach for LHON treatment. European journal of pharmaceutics and biopharmaceutics 168: 195-207.

Vermani K, Garg S. 2000. The scope and potential of vaginal drug delivery. Pharmaceutical science & technology today 3: 359-364.

Wang J, Ben-Jebria A, Edwards DA. 1999. Inhalation of Estradiol for Sustained Systemic Delivery. JOURNAL OF AEROSOL MEDICINE 12: 27-36.

Wang Y-Y, Hu S-F, Rao M, Xia X-P, Xia W, Zhu C-H. 2019. Antifertility effectiveness of a novel polymer matrix composite and its influence on the endometrium in rhesus macaques (Macaca mulatta). Contraception 100: 132-136.

Weber M, Limpens J, Roovers J. 2015. Assessment of vaginal atrophy: a review. International urogynecology journal 26: 15-28.

Weisberg E, Ayton R, Darling G, Farrell E, Murkies A, O'Neill S, Kirkegard Y, Fraser I. 2005. Endometrial and vaginal effects of low-dose estradiol delivered by vaginal ring or vaginal tablet. Climacteric 8: 83-93.

Weiss H, Martell B, Constantine GD, Davis SM, Vidal JD, Mayer PR, Doorbar M, Friend DR. 2019. Pharmacokinetics and tolerability of a novel 17β-Estradiol and progesterone intravaginal ring in sheep. Journal of pharmaceutical sciences 108: 2677-2684.

Willhite LA, O'Connell MB. 2001. Urogenital atrophy: prevention and treatment. Pharmacotherapy: The Journal of Human Pharmacology and Drug Therapy 21: 464-480.

Woodruff MA, Hutmacher DW. 2010. The return of a forgotten polymer—Polycaprolactone in the 21st century. Progress in polymer science 35: 1217-1256.

Woods NF. 2012. An overview of chronic vaginal atrophy and options for symptom management. Nursing for women's health 16: 482-494.

Woolfson A, Elliott G, Gilligan CA, Passmore CM. 1999. Design of an intravaginal ring for the controlled delivery of 17β-estradiol as its 3-acetate ester. Journal of controlled release 61: 319-328.

Wsoo MA, Razak S, Shahir S, Al-Moalemi HAA, Kadir MRA, Nayan NHM. 2021. Development of prolonged drug delivery system using electrospun cellulose acetate/polycaprolactone nanofibers: Future subcutaneous implantation. Polym. Adv. Technol 32: 3664-3678.

Wu G, Wu W, Zheng Q, Li J, Zhou J, Hu Z. 2014. Experimental study of PLLA/INH slow release implant fabricated by three dimensional printing technique and drug release characteristics *in vitro*. BioMedical Engineering OnLine 2014, 13:97 13: 97.

Xiong H, Fu J, Sun H, Wang E, Ding Y, Ren G, Jing Q, Ren F. 2017. The Physicochemical Investigation of 17 β -Estradiol Crystalline Prepared by In Situ pH-Dependent Solubility Technique with Polyvinylpyrrolidone. AAPS PharmSciTech.

Yan Y, Wang X, Pan Y, Liu H, Cheng J, Xiong Z, Lin F, Wu R, Zhang R, Lu Q. 2005. Fabrication of viable tissue-engineered constructs with 3D cell-assembly technique. Biomaterials 26: 5864-5871.

Yang, Xie C, Xiang H, Feng J, Xia X, Cai S. 2009. IDM release behavior and surface characteristics of the novel Cu/IDM/LDPE nanocomposite for intrauterine device. Colloids and Surfaces B: Biointerfaces 69: 276-280.

Yang, Lin I-E, Chen T-C, Chen Z-Y, Kuan C-Y, Lin J-N, Chou Y-C, Lin F-H. 2021. Synthesis, characterization, and evaluation of BDDE crosslinked chitosan-TGA hydrogel encapsulated with genistein for vaginal atrophy. Carbohydrate Polymers 260: 117832.

Yang L, Fassihi R. 1997. Examination of drug solubility, polymer types, hydrodynamics and loading dose on drug release behavior from a triple-layer asymmetric configuration delivery system. International journal of pharmaceutics 155: 219-229.

Yao R, Zhang R, Yan Y, Wang X. 2009. *In vitro* angiogenesis of 3D tissue engineered adipose tissue. Journal of Bioactive and Compatible Polymers 24: 5-24.

Yao R, Zhang R, Luan J, Lin F. 2012. Alginate and alginate/gelatin microspheres for human adipose-derived stem cell encapsulation and differentiation. Biofabrication 4: 025007.

Zaghloul AA, Mustafa F, Siddiqu A, Khan M. 2005. Biodegradable microparticulates of beta-estradiol: preparation and *in vitro* characterization. Drug development and industrial pharmacy 31: 803-811.

Zaghloul AA, Mustafa F, Siddiqui A, Khan M. 2006. Response surface methodology to obtain β-estradiol biodegradable microspheres for long-term therapy of osteoporosis. Pharmaceutical development and technology 11: 377-387.

Zaid AN, Al-Ramahi R, Ghoush AA, Malkieh N, Kharoaf M. 2012. Influence of physical factors on tablet splitting, weight and content uniformity of atenolol tablets. Journal of Pharmaceutical Investigation 42: 229-234.

Zehnder T, Sarker B, Boccaccini AR, Detsch R. 2015. Evaluation of an alginate–gelatine crosslinked hydrogel for bioplotting. Biofabrication 7: 025001.

Zhang C, Xu N, Yang B. 1996. The corrosion behaviour of copper in simulated uterine fluid. Corrosion science 38: 635-641.

Zhang Z. 2021. Application of Biorelevant Dissolution Method for Intrauterine DevicesUniversity of Pittsburgh.

Zhao X, Milford C, Smit J, Zulu B, Boyd P, Malcolm RK, Beksinska M. 2022. Color, Scent and Size: Exploring Women's Preferences Around Design Characteristics of Drug-Releasing Vaginal Rings. AIDS and Behavior: 1-15.

Zhao Y, Yao R, Ouyang L, Ding H, Zhang T, Zhang K, Cheng S, Sun W. 2014. Three-dimensional printing of Hela cells for cervical tumor model *in vitro*. Biofabrication 6: 035001.

Zhou H, Hernandez C, Goss M, Gawlik A, A Exner A. 2015. Biomedical imaging in implantable drug delivery systems. Current drug targets 16: 672-682.

Zolghadri J, Haghbin H, Dadras N, Behdin S. 2014. Vagifem is superior to vaginal Premarin in induction of endometrial thickness in the frozen-thawed cycle patients with refractory endometria: A randomized clinical trial. Iranian Journal of Reproductive Medicine 12: 415.

APPENDICES

APPENDIX A

Abstracts of Papers Published/Submitted/Under Preparation

APPENDIX A1

Journal of Pharmaceutical Sciences 112 (2023) 1566–1585

Contents lists available at ScienceDirect

Journal of Pharmaceutical Sciences

journal homepage: www.jpharmsci.org

Review

Intravaginal Drug Delivery Systems to Treat the Genitourinary Syndrome of Menopause: Towards the Design of Safe and Efficacious Estrogen-loaded Prototypes

Ahmed Abdelgader, Mershen Govender, Pradeep Kumar, Yahya E. Choonara*

Wits Advanced Drug Delivery Platform Research Unit, Department of Pharmacy and Pharmacology, School of Therapeutic Sciences, Faculty of Health Sciences, University of the Witwatersrand, Johannesburg, 7 York Road, Parktown, 2193, South Africa

ARTICLE INFO

Article history:
Received 7 February 2023
Revised 23 February 2023
Accepted 23 February 2023
Available online 1 March 2023

Keywords:
Estradiol
Drug delivery systems
Vaginal delivery
Menopause
Genitourinary syndrome of menopause

ABSTRACT

Estrogens locally delivered to the vagina by tablets, capsules, rings, pessaries, and creams are the most common and highly recommended platforms to treat the genitourinary syndrome of menopause (GSM). Estradiol, an essential estrogen, is routinely administered alone, or in combination with progestins, to effectively alleviate the symptoms associated with moderate to severe menopause when non-pharmacological interventions are not indicated. Since the risk and side effects of estradiol use depends on the administered amount and duration of use, the lowest effective dose of estradiol is recommended when long-term treatment is required. Although there is a wealth of data and literature comparing vaginally administered estrogen-containing products, there is a lack of information revealing the effect of the delivery system used and formulation constituent's attributes on the efficacy, safety, and patient acceptability of these dosage forms. This review therefore aims to classify and compare various designs of commercially available and non-commercial vaginal 17β-estradiol formulations and analyze their performance in terms of systemic absorption, efficacy, safety, and patient satisfaction and acceptance. The vaginal estrogenic platforms included in this review are the currently marketed and investigational 17β-estradiol tablets, softgel capsules, creams, and rings for the treatment of GSM, based on their different design specifications, estradiol loads, and materials used in their preparation. Additionally, the mechanisms of the effects of estradiol on GSM have been discussed, as well as their potential impact on treatment efficacy and patient compliance.

Introduction

The genitourinary symptoms experienced during menopause are broad and include a number of physiological processes that often result in dryness of the vagina, pain during intercourse, urinary inconsistency and hot flashes.[1] In 2014, the term of genitourinary syndrome of menopause (GSM) was introduced for the first time, replacing the terms vulvovaginal atrophy, vaginal atrophy, and urogenital atrophy, with both postmenopausal and premenopausal women affected by this condition. However, GSM has been noted to be more prevalent in postmenopausal women,[2,3] with more than 50% experiencing at least one of the above-mentioned symptoms.[4–7] Despite the high prevalence and availability of treatments for GSM, these conditions are often under-diagnosed and ineffectively treated for several reasons including: the unwillingness of women to discuss the symptoms with their healthcare provider, a lack of education regarding the condition and its treatments, women not recognizing that their experienced symptoms relate to estrogenic deficiency, and many healthcare practitioners not assessing their patients for GSM symptoms.[8–10]

The initial aim of treating GSM symptoms is to lessen and eliminate the experienced symptoms.[3] Numerous treatment options are available for GSM and can be classified into non-hormonal therapy and hormone replacement therapy. Non-hormonal therapy is considered the first-line treatment for mild symptoms and includes vaginal lubricants and moisturizers. Recently, ospemifene, laser therapy, and radio frequency-based therapy are also being used as new alternatives when estrogenic therapies are not recommended. It is routinely only when severe and persistent symptoms are experienced, and non-hormonal therapy is not as effective, that hormonal treatment, including estrogen-containing medications, are introduced. They are considered the "gold standard" pharmacological treatment and the most effective therapy since they act directly towards the cause of GSM; the lack of estrogen.[1,3,11]

Several routes of administration are used for delivering estrogen-containing medications, including the vaginal, oral or transdermal

* Corresponding author.
E-mail address: yahya.choonara@wits.ac.za (Y.E. Choonara).

https://doi.org/10.1016/j.xphs.2023.02.021
0022-3549/

APPENDIX A2

pharmaceutics

MDPI

Article

A Novel Intrauterine Device for the Spatio-Temporal Release of Norethindrone Acetate as a Counter-Estrogenic Intervention in the Genitourinary Syndrome of Menopause

Ahmed Abdelgader, Mershen Govender, Pradeep Kumar and Yahya E. Choonara *

Wits Advanced Drug Delivery Platform Research Unit, Department of Pharmacy and Pharmacology, School of Therapeutic Sciences, Faculty of Health Sciences, University of the Witwatersrand, Johannesburg, 7 York Road, Parktown 2193, South Africa

* Correspondence: yahya.choonara@wits.ac.za; Tel.: +27-11-717-2052

Abstract: The genitourinary syndrome of menopause (GSM) is a widely occurring condition affecting millions of women worldwide. The current treatment of GSM involves the use of orally or vaginally administered estrogens, often with the risk of endometrial hyperplasia. The utilization of progestogens offers a means to counteract the effects of estrogen on the endometrial tissue, decreasing unwanted side effects and improving therapeutic outcomes. In this study, a norethindrone acetate (NETA)-loaded, hollow, cylindrical, and sustained release platform has been designed, fabricated, and optimized for implantation in the uterine cavity as a counter-estrogenic intervention in the treatment of GSM. The developed system, which comprises ethyl cellulose (EC) and polycaprolactone (PCL), has been statistically optimized using a two-factor, two-level factorial design, with the mechanical properties, degradation, swelling, and in vitro drug release of NETA from the device evaluated. The morphological characteristics of the platform were further investigated through scanning electron microscopy in addition to cytocompatibility studies using NIH/3T3 cells. Results from the statistical design highlighted the platform with the highest NETA load and the EC-to-PCL ratio that exhibited favorable release and weight loss profiles. The drug release data for the optimal formulation were best fitted with the Peppas–Sahlin model, implicating both diffusion and polymer relaxation in the release mechanism, with cell viability results noting that the prepared platform demonstrated favorable cytocompatibility. The significant findings of this study firmly establish the developed platform as a promising candidate for the sustained release of NETA within the uterine cavity. This functionality serves as a counter-estrogenic intervention in the treatment of GSM, with the platform holding potential for further advanced biomedical applications.

Keywords: implantable devices; intrauterine delivery; controlled release; polycaprolactone; ethyl cellulose

Citation: Abdelgader, A.; Govender, M.; Kumar, P.; Choonara, Y.E. A Novel Intrauterine Device for the Spatio-Temporal Release of Norethindrone Acetate as a Counter-Estrogenic Intervention in the Genitourinary Syndrome of Menopause. *Pharmaceutics* **2024**, *16*, 587. https://doi.org/10.3390/pharmaceutics16050587

Academic Editors: Natasa Skalko-Basnet and Meredith Roberts

APPENDIX B

Waiver for Using Animal Tissues

APPENDIX B1

Waiver for Using Animal Tissues

ANIMAL RESEARCH ETHICS COMMITTEE
Registration number: AREC-101210-002

Date: 16/11/2023

Certificate reference: Waiver 16-11-2023-O

Category: O

Applicant: Ahmed Abdelgader

Department: Department of Pharmacy and Pharmacology (WITS)

Tel: 011 717 2552; **Email**: 2380064@students.wits.ac.za

Re: Waiver from the Animal Ethics Research Committee of the University of the Witwatersrand

This letter is to confirm that Ahmed Abdelgader (#2380064), PhD student under the supervision of Prof. Yahya E. Choonara, Prof. Pradeep Kumar, and Dr. Mershen Govender (Department of Pharmacy and Pharmacology), does not require full Animal Ethics Research Committee clearance to undertake the work titled **"*A multi-unit, polymer-based, prolonged-release, intrauterine device for the relief of the genitourinary syndrome of menopause*"**.

Reason for waiver

The project is using uterine and vaginal mucosal tissue obtained from pig (n=4) and sheep (n=4) already euthanized at WRAF.

Details of the study

The aim of the study is to develop an intrauterine platform, featured with prolonged-release for the loaded drugs. An *ex-vivo* study will be conducted to assess the drug permeation and influence

of drug carriers on permeation and diffusion across the uterine and vaginal membrane of euthanized pig and sheep.

Efficacy of drug delivery systems rely on their ability to promote adequate drug concentrations at the targeted site of action. When a systemic effect is the objective, drugs must be transported across the administration site membrane to access the systemic circulation. On the other hand, when a local effect is the goal, retention of the drug at the surface of the dosing site (vagina, uterus) is desirable with low grade of absorption. The interest in performing *ex vivo* permeability studies using biological membranes is evident due to it is similarities with the *in vivo* conditions and may provide information on bioavailability of the drug. Drug permeation studies are important for vaginal and uterine drug administration when systemic or local delivery is intended as well as important for safety characterization (enables histological analysis to assess differences before and after drug application/permeation). So permeability tests are important to provide comprehensiveness about mechanisms of permeation, absorption and also to characterize the drug delivery systems and the formulation ability to either promote or avoid permeation through the vagina and uterus.

The Franz diffusion cell will be used to assess the permeability studies. The uterine and vaginal membranes will be mounted and stabilized in Franz diffusion cell assembly which will contain 10 mL phosphate buffer having pH 6.8 in receptor compartment. After this, segment of the platform loaded with 10% estradiol hemihydrate or norethindrone acetate or 5%indomethacin will be placed in donor compartment containing 3 ml of either SUF or SVF for norethindrone/indomethacin loaded segments or estradiol loaded segment, respectively. At predetermined time interval, 1 ml samples from a receptor compartment will be withdrawn and to maintain the sink conditions equal volume of fresh phosphate buffer will be added. The concentration of drug permeated from fabricated platforms through to the receptor compartment will be analyzed and measured by spectrophotometer at 320, 280, and 240 nm for indomethacin, estradiol, and norethindrone, respectively, using Implen Nano Photometer. The cumulative amount of drug permeated will be then calculated.

Condition: The applicant should liaise with WRAF to obtain the tissue.

The individuals covered by the waiver are Ahmed Abdelgader, Yahya Choonara, Pradeep Kumar and Mershen Govender (Department of Pharmacy and Pharmacology, WITS).

Please contact me should you require further information. Yours sincerely

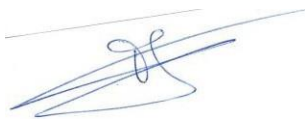

A/Prof Frederic Michel

Chair: Animal Research Ethics Committee University of the Witwatersrand